UNIVERSITY OF SHEFFIELD

Department of Civil and Structural Engineering

THE PERFORMANCE IN FIRE OF RESTRAINED COLUMNS IN STEEL-FRAMED CONSTRUCTION

by

Paul Shepherd

A thesis submitted in partial fulfilment of the requirements for the Degree of Doctor of Philosophy

July 1999

ABSTRACT

The University of Sheffield has a non-linear finite element analysis program called VULCAN which has been developed in-house over a number of years and has been thoroughly validated. A parametric study has been conducted using this software, which assesses the influence of such factors as load, geometric imperfection, material properties, temperature profile and axial and rotational restraint on the behaviour of isolated steel columns in fire. This study is then extended to investigate the behaviour of steel columns as part of a larger multi-storey frame, in which axial restraint to thermal expansion of the heated column is provided by the floors above. A method of modelling these effects in VULCAN using a linear spring element to provide axial restraint has been developed and validated.

An experimental partner project has been carried out at the University of Ulster, in which steel columns were furnace-tested with various levels of load, slenderness and axial restraint. These tests have been paralleled with analyses using VULCAN and a good correlation with test results has been shown. The VULCAN program was then used to examine the effects of parameters outside the range of the physical constraints imposed by the test facility.

A numerical model, capable of assessing the level of axial restraint imparted on a column by a general multi-storey framed structure has been developed, which has a number of levels of complexity, each giving a higher degree of accuracy. Once the level of restraint for a structure has been assessed, the parametric studies and test data can be applied, and conclusions drawn about the behaviour of the frame.

The applicability of different mathematical solution procedures to the analysis of these columns, which exhibit snap-through and snap-back behaviour, has been conducted. The arc-length method has been identified as applicable in such cases and a skeleton version of the procedure introduced into the VULCAN program.

The program structure of VULCAN has been improved and the format for data input and output has been developed to allow flexibility. A graphical file-viewer program has also been created. Details of these changes are shown in appendices.

CONTENTS

LIST OF FIGURES

LIST OF TABLES

NOTATION

(Only the general notations used during this thesis are presented here. Symbols which have only been used once and are of a more specific nature have been clearly explained where they arise in the text).

α	Relative restraint factor
ε	Strain
λ	Slenderness
σ	Stress
θ	Temperature
A_t, B_t, n_t	Temperature dependent Ramberg-Osgood parameters
E	Young's Modulus of the material
I_x, I_y	Second moment of area about minor / major axis
K	Stiffness
K_b	Beam stiffness
K_c	Column stiffness
K_r	Restraint stiffness
K_s	Spring stiffness
L	Member length

ACKNOWLEDGEMENT

The author expresses his thanks to Dr. Ian Burgess and Prof. Roger Plank for their supervision and support during this research project. The financial assistance of the Engineering and Physical Sciences Research Council and of British Steel Ltd. is gratefully acknowledged.

The work in this thesis is part of a joint project conducted between the Universities of Sheffield and Ulster. I would therefore like to thank Dr. Michael Randall, Dr. Faris Ali and Dr. David O'Connor of the University of Ulster for their assistance and hospitality.

I would also like to thank my colleagues, especially Dr. Colin Bailey and Paul Rose for their intellectual support; and my friends and family, especially Ian, Tony, Nigel, Dave, Roger, Emma, Philip, Markus, Klaus and Laura for their non-intellectual support. And Mrs. B for the sandwiches.

DECLARATION

Except where specific reference has been made to the work of others, this thesis is the result of my own work. No part of it has been submitted to any University for a degree, diploma or other qualification.

Paul Shepherd

1 Introduction and Literature Review

1.1 Fire

It is said that the discovery of fire was a major turning point in the development of human civilisation, as it was used for heating, lighting and cooking. Natural sources of fire such as volcanoes and lightning were exploited, and the resulting flames were controlled and fed to keep a constantly available resource. This need to store fire has been attributed to the change of human society from a nomadic lifestyle into settled communities. Later, man learned to create fire at will by the use of friction of suitable material, such as wood, and later by sparking flints.

However, even before this, uncontrolled fires were responsible for destroying countryside, property and life. Consequently, most animals have a developed sense of heat and are able to detect a fire and move away from it. This means that relatively little life is lost due to fire. In fact, according to the London Gazette of 8th September 1666, one of the most infamous fires, the so-called "Great Fire of London" burned four fifths of the city to the ground; however only sixteen people were thought to have been killed. To prevent a similar future catastrophe, the Rebuilding Act of 1667 was passed banning the use of timber and thatched roofs, and limiting the proximity of buildings within the city boundary. The buildings constructed in the aftermath of the Great Fire tended to be brick-walled in order to reduce flammability and this trend continued for many years. This legislation was an attempt to learn from the mistakes of the past and was the first real attempt at providing guidance for the fire-resistant design of buildings. In recent years this subject has been widely researched and has led to the concept of a global approach to fire safety of buildings[1].

1.1.1 Development Of A Fire

An uncontrolled fire passes through four definable stages of development as shown on Fig. 1. The initial ignition phase depends upon the surface flammability of the materials surrounding the source of the fire. It is during this phase that smoke detection is useful. The smouldering phase then develops as more material is burned locally and the temperature slowly rises. A large amount of smoke can be given off during this stage and since this is hazardous to life, occupants must have been

evacuated. The really critical point in fire development is known as *flashover*. This occurs when the temperature has risen to such a level that combustible gasses emitted by the burning organic materials in the fire spontaneously combust and the whole compartment is engulfed in flame. Thus the fire becomes fully developed within the compartment and fighting the fire is practically impossible; the only feasible course of action is to prevent the fire spreading to neighbouring compartments. The atmosphere temperature at which this occurs is dependent on the materials affected by the fire, but is typically around 400°C for the wood- and plastic-based fires which occur in offices and homes. A rapid heating phase of the fire then begins, controlled by the balance between the density of the fire load and the availability of oxygen, as well as the ability of the compartment to retain the heat generated. A typical fire of this type can reach temperatures of 1100°C. The temperature begins to decrease as the combustible material is used up, although the rate of cooling is also controlled by the ventilation.

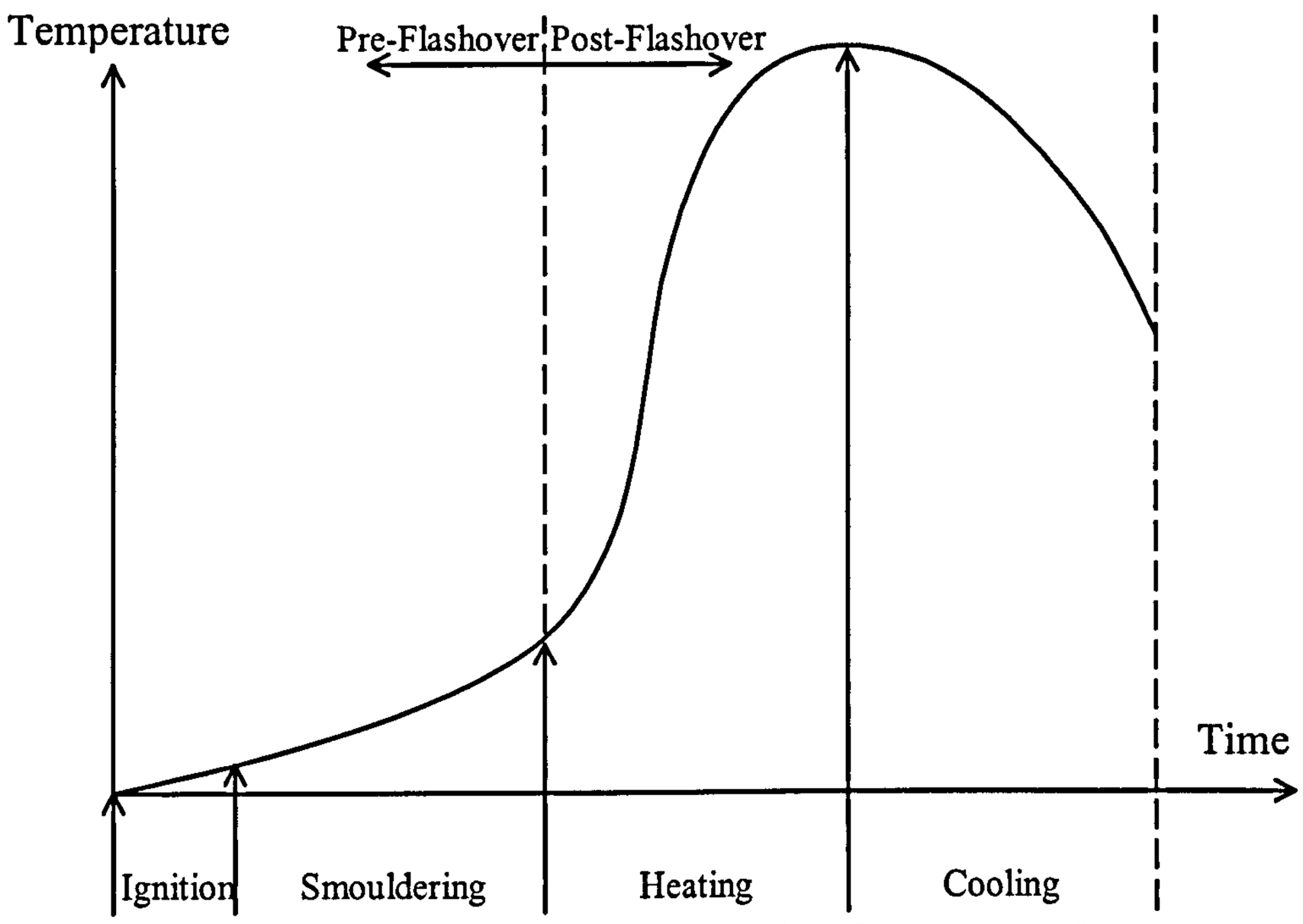

Fig. 1 Atmosphere temperatures during the development and decay of a fire

1.1.2 Fire Safety

The subject of fire safety within buildings has two main objectives, firstly to minimise loss of life, and secondly to minimise the resulting financial loss due to a fire. These objectives can be at least partially met by taking a number of preventative steps during building design.

Reduction of the probability of ignition of a fire is the most obvious step. This can be achieved by taking care in the choice of materials used within a building both within its basic structural makeup and in its finishes and furnishings. Effective building management also plays an important role by controlling the location of inflammable materials and sources of ignition such as cigarettes and electrical wiring.

The provision of means of escape is of importance in preventing loss of life. This is done at the design stage, when a building must have adequate fire escape routes in terms of number, capacity and escape distance for all envisaged usage. Much legislation has been developed[2] to provide strict rules on this subject. Venting of smoke can increase the time available to escape from a building. Building management is important in educating the occupants on the fire procedures and exits.

Prevention or control of fire development can be achieved by the use of sprinklers, after detection of fire and smoke. Recent technological advances have allowed the development of extremely reliable and effective systems. Fire-resistant boundary walls and compartmentation are also used to limit the spread of a fire.

Until recently, the philosophy of structural fire protection in steel-framed buildings has been confined to limitation of the growth of structural temperatures using passive fire protection. Materials such as steel have been protected from the effects of temperature growth by the application of insulating materials such as fibreboard or intumecent sprays. Modern fire-engineering techniques are currently being developed which allow an accurate estimation of the effect of a particular fire on a structural member. This information is then incorporated into the basic member design so that steel-framed structures can be safely designed, either without the need for passive protection or using combinations of strategies which produce more economical overall designs. This is discussed in more detail in section 1.1.4.

Each of these considerations, with the possible exception of provision of means of escape, can assist with both objectives of protecting life and property. However, escape routes for building occupants are often used by the fire brigade as means of entry. As such, providing ventilation and extra fire resistance in these areas can also minimise loss of building contents by allowing early fire fighting.

1.1.3 Risk

No matter how careful and detailed is the design and operation of any given building, not every eventuality can be catered for and some level of risk of fire has to be accepted. The level of risk for a particular building is a combination of the probability of occurrence of an uncontrolled fire and the probable resulting financial or human loss. The probability of occurrence can be estimated using statistics gathered over the years. It has been shown that this probability is highly dependent upon the use of the building and the number of active measures taken to restrict fire development. The probable loss is also dependent on the nature of the building's occupancy and financial losses include consequences of interruption to its use.

The acceptable degree of risk will vary from building to building, depending on the relative importance of preserving life and reducing financial loss. However, in a modern litigious society, loss of human life often incurs a heavy financial loss.

1.1.4 Fire Concepts

The main concept used during design to minimise the risk of unacceptable losses during a fire is the structural concept of passive protection. This accepts that a fire will flash-over and will then fully develop. The structure is then designed to withstand the high atmospheric temperatures by insulating the structural members from the heat. Since no amount of insulation will keep the temperature ambient, the structure is also designed so that it retains sufficient strength to support its load during a fire. Since it is accepted that a fire will fully develop, all property inside the fire compartment will be destroyed. Thus compartments are designed to retain integrity and may be kept small in order to minimise loss. So long as the loads are supported over the fire compartment to prevent excessive damage to external compartments, deflections that would normally be considered excessive are allowed. This can however result in a high repair cost after the fire. Therefore, the structural fire safety concept is more and more being combined with active protection methods such as the monitoring or extinguishing concepts to provide an integrated solution.

The monitoring concept makes use of modern automatic detection and alarm systems to detect the ignition of a fire and automatically alert the fire brigade. In this way, the fire brigade can extinguish a fire before flashover occurs. Financial loss is still incurred due to the fire and the damage caused by water used during the fire fighting

process. However, since flashover does not occur, structural damage is eliminated and repair bills are reduced. The reliance on the fire brigade reaching the fire before flashover means that this concept is only viable if there is a fire station close by. Large industrial complexes such as airports, where an on-site dedicated fire station is available, use this method very successfully.

A more generally applicable system is the extinguishing concept. This is similar to the monitoring concept, but incorporates the ability to fight the fire automatically. Sprinklers or extinguishers are triggered when a fire is detected, an alarm is sounded and the fire brigade is alerted. This early tackling of the fire can slow its development and give the fire brigade time to arrive. Since the fire is fought from an early stage in its development, when it is relatively small, this system can sometimes be enough to put out the fire completely. This reduces financial loss and clean-up costs, especially since a choice of extinguishing methods can be used depending upon the situation. For example, carbon dioxide gas can be utilised in computer areas where water damage to equipment in surrounding areas is undesirable.

Active protection methods require high levels of regular maintenance in order to be effective. However, this is usually offset against the financial savings made by preventing flashover and retaining structural integrity in the event of a fire. The material loss is usually negligible compared to the loss of business during refurbishment. As modern active protection systems become more developed, their reliability is increased and the chance of false alarms decreased. These modern systems allow the construction of architecturally pleasing bare steel structures to be economically viable.

1.2 Steel

During the mid-19th Century, ancient techniques for the refining of iron ore were adapted to combine it with specific quantities of carbon and produce steel on a large scale. Steel has a high strength-to-weight ratio, and its development facilitated easy construction of high and long-span structures.

Modern production and construction techniques favour steel since it allows speedy fabrication and erection of buildings. Its surface finish can be aesthetically pleasing and many cross-section shapes can be created, so that architecturally it is often the

first choice of structural material. However, at the high temperatures that may be expected in a post-flashover fire situation, the strength of steel is significantly reduced. This means that a structure may become unstable and collapse.

1.2.1 Stress-Strain Curves

If a steel specimen is slightly strained, for example in a tensile test machine, and its stress recorded, the stress will increase linearly with strain according to the simple equation *Stress = Young's modulus x Strain*. This behaviour continues until the stress approaches the so-called Yield Stress, when the stiffness of the steel begins to reduce. Thus, for a given increase in strain, there is less and less increase in force up until the yield stress is attained. From this point, the steel cannot support any more load and further straining occurs at a constant stress level. At higher strain levels, the stiffness may increase slightly due to Strain Hardening and a gradual increase in stress is seen. However, beyond the limiting strain, the stress begins to reduce until it reaches fracture, at which point there is no capacity to support any load as shown on Fig. 2. For design purposes, the complicated behaviour of steel has been simplified into a number of models by making various "engineer's" assumptions, a few of which are also shown on Fig. 2.

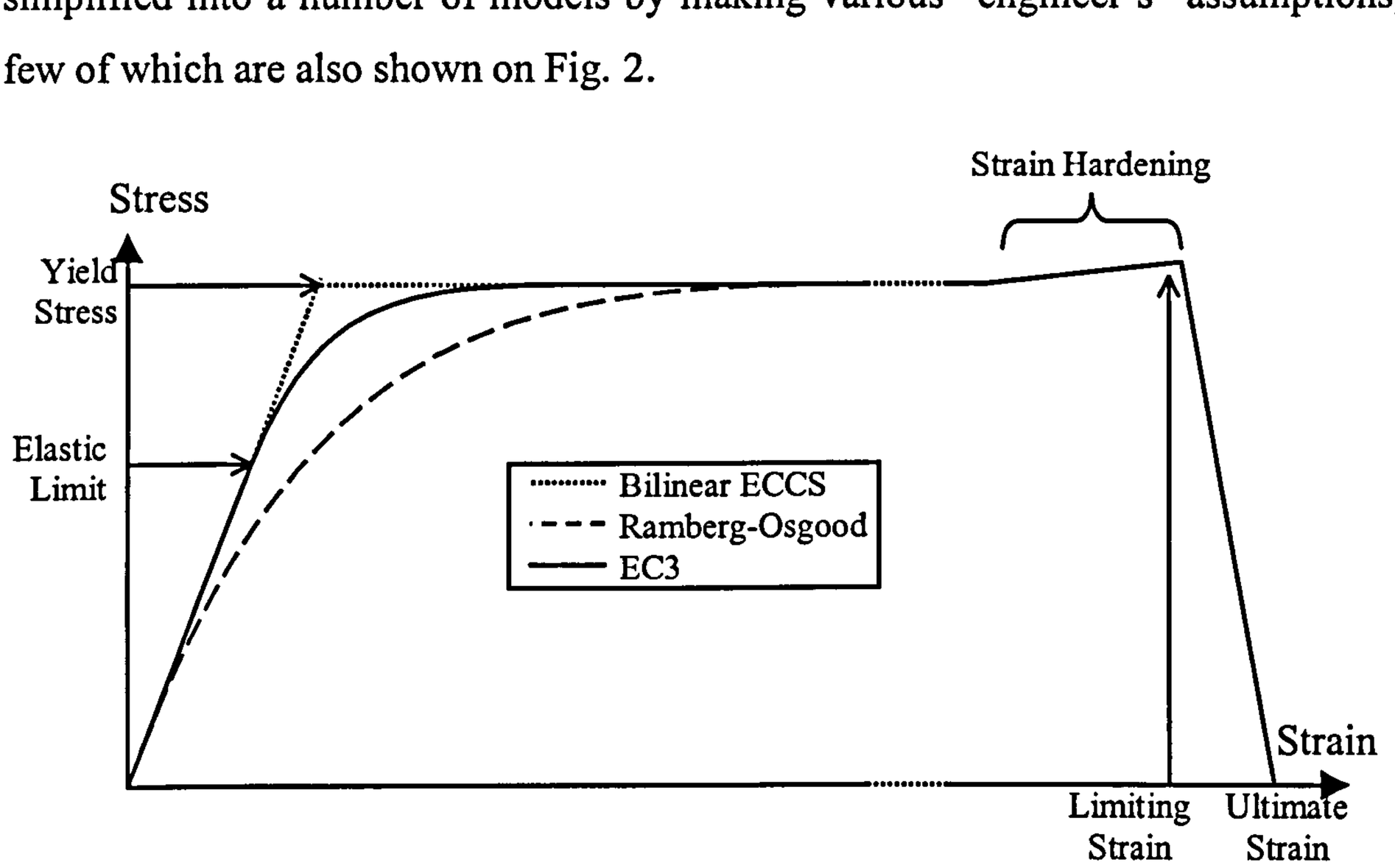

Fig. 2 Typical ambient temperature stress-strain curve for steel

One of the simplest constitutive models is the bilinear ECCS model[3]. This assumes linear behaviour of steel up until the yield stress, beyond which point a constant stress is maintained indefinitely. A more flexible assumption[4] is that the stress-strain

curve has the following single equation relating stress σ, and strain ε, as shown in eqn. (1).

$$\varepsilon = \left(\frac{\sigma}{A}\right) + \frac{1}{100}\left(\frac{\sigma}{B}\right)^{N} \tag{1}$$

Where A is the Young's modulus of the steel, B is the yield stress and N is a factor which controls the curvature of the pre-yield range.

The most complicated, and therefore the most accurate, representation of the stress-strain curve is the EC3[5] model. This splits the curve into three sections and defines a separate equation for each. The linear range of the curve is represented by a straight line, the gradient of which is dependent on the Young's modulus. There is a curved region prior to yield, which has a complicated elliptical representation as shown in eqn. (2). Once the yield stress has been attained, a horizontal region is specified until the limiting strain beyond which there is no further increase in stress.

$$\sigma = \sigma_l - c + \frac{b}{a}\sqrt{a^2 - (\varepsilon_y - \varepsilon)^2} \tag{2}$$

Where σ_l is the stress at the limit of the linear region and ε_y is the yield strain. A, b and c are specified constants dependent on the yield stress and Young's modulus.

The curves shown in Fig. 2 for these three models are only illustrative and their actual shapes are much more similar to each other. The curvature in the pre-yield region of the latter two models is very tight and so each quite accurately represents the true ambient-temperature behaviour of steel, which is very nearly bilinear. However, steel behaves in a non-linear fashion when it is at high temperatures, and this determines the suitability of each model for elevated temperature design.

1.2.2 Elevated Temperature Material Degradation

The yield strength and Young's modulus of steel both decrease as the temperature increases. The exact nature of this reduction in material properties depends on the chemical and crystalline structure of the steel in question, and on the manufacturing processes used in forming the structural sections. Much experimental research[6,7] has been conducted on general structural steels in order to determine their behaviour at elevated temperatures. The results from these studies have allowed modification of

the design models described above, so that they are more appropriate for elevated-temperature structural design. Each model uses a different system to decrease the yield strength and Young's modulus (and to modify the pre-yield curvature if appropriate) such that they have effectively reduced to zero at 1200°C. This is conservatively assumed for design purposes as the temperature at which the steel retains no strength or stiffness, although this does not actually occur until the steel melts at around 1550°C.

In the case of the bilinear ECCS material model[3], the ambient temperature yield strength and Young's modulus are decreased by polynomial functions based on the temperature. Two sets of polynomials are used; one set for temperatures below, and one for temperatures above 600°C. The Ramberg-Osgood model[4] divides the temperature range into five sections and specifies the way each of the parameters A, B and N from eqn. (2) decrease as either linear or quadratic equations. This is explained in detail in Section 2.2.1 and is shown on Fig. 2.4. The EC3 model[5] decreases the elastic limit, yield stress and Young's modulus in a multi-linear fashion within 100°C bands.

Special steels have been developed in Japan, which are alloys with chromium and molybdenum, and retain up to two-thirds of their ambient temperature yield stress up to 600°C[8,9]. Although these special steels are used in certain specialist applications, their cost usually prohibits their more general use.

An alternative way to allow steel structures to function at high temperature is to use steel with a higher yield stress, or larger cross-sectional area, than would otherwise be required for ambient temperature design. In this way, although the material properties degrade in a fire situation, sufficient strength remains to support the required load. Again, this results in a higher cost of steel for a given structure, but this can be offset against the cost saving generated by eliminating the need for passive fire protection and thus speeding the construction process. Usually, the most economical design solution involves a trade-off between over-design of steelwork and application of fire protection.

1.2.3 Thermal Expansion

Nearly all materials expand when heated, and in metals such as steel this is particularly noticeable. Again, the level of thermal expansion depends upon the

exact metallurgical composition of a given steel, but general guidelines are available for design purposes based on experimental results. For example, EC3[5] defines the thermally induced strain for steel, in terms of its temperature θ by eqns. (3). This is discussed in more detail in Section 4.2.3 and is shown graphically on Fig. 4.9.

$$\varepsilon_t = 0.4x10^{-8}\theta^2 + 1.2x10^{-5}\theta - 2.416x10^{-4} \quad 20°C \le \theta < 750°C \tag{3a}$$

$$\varepsilon_t = 1.1x10^{-1} \quad 750°C \le \theta \le 850°C \tag{3b}$$

$$\varepsilon_t = 2.0x10^{-5}\theta - 6.2x10^{-3} \quad 850°C < \theta < 1200°C \tag{3c}$$

The thermal expansion of a steel member can cause the stress in the member to increase, since in a typical building, any individual member is restrained from this expansion by the surrounding structure. Especially where concrete slabs are present and connected to the steel by shear studs, thermal expansion of the exposed steel is restrained causing the stress to increase. Similarly, in a multi-storey structure with a fire on one storey, steel columns are restrained from thermal expansion by the floors above and below. It is the study of this restraint to the thermal expansion of steel columns which forms the main part of this thesis.

1.3 Steel Columns

Steel is often used as the material of structural columns in low-rise industrial units where speed and ease of erection are important factors. It is also widely used in the construction of high-rise buildings, where its high strength-to-weight ratio allows the minimisation of dead-loads transmitted to the floors below. This section looks at the factors which are influential in the understanding of the behaviour and design of steel columns.

1.3.1 Slenderness And Euler Buckling

The slenderness ratio λ of a column is a measure of its affinity to buckling under compressive loads. It is defined as the effective length of the column L, divided by the radius of gyration of the cross-section r, about the buckling axis under consideration. A short, squat pin-ended column section has a low slenderness ratio and is unlikely to buckle under axial compression. The axial stress could be increased until its yield stress is attained, at which point the material would yield. A long, thin column section on the other hand, would be highly susceptible to buckling

and the yield stress could never be reached. In fact, the Euler buckling formula[10] gives the maximum axial force that can be supported by a theoretically perfect slender strut, and is shown in eqn. (4).

$$P_{cr} = \frac{\pi^2 EI}{L^2} \tag{4}$$

This Euler buckling load, and the yield stress, form two upper bounds on the compressive capacity of struts, as shown in Fig. 3. Practical steel struts have geometric imperfections such as an initial out-of-straightness and material imperfections such as residual stresses induced during the manufacturing process. Consequently, lower values for the critical stress of columns are used for design purposes. Four "strut curves" have been developed for use in BS5950[11] and EC3[5], each of which is conservative compared with Euler and yield by a different amount depending on section type, manufacturing tolerances and the design case. One such curve is illustrated on Fig. 3.

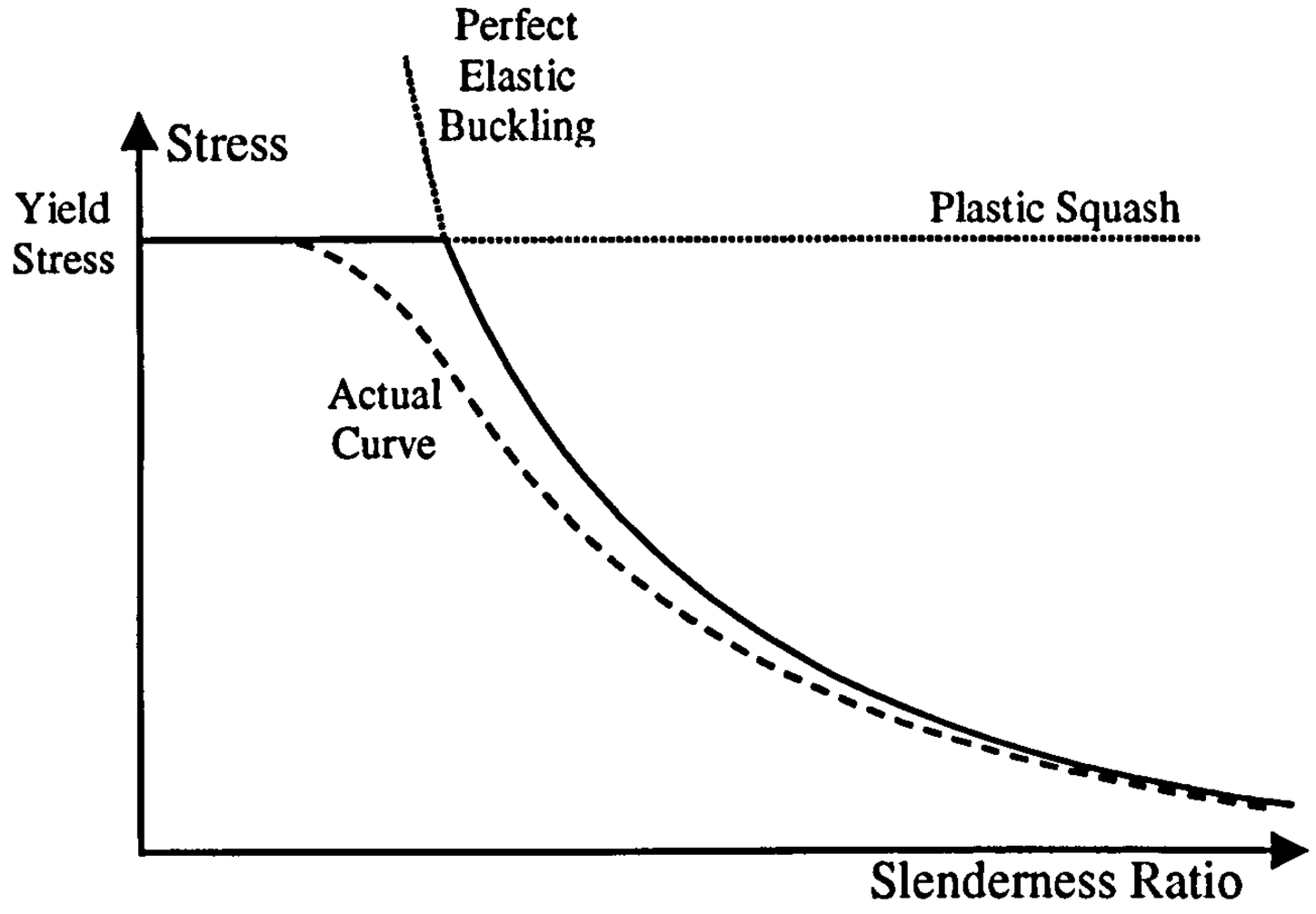

Fig. 3 Column buckling curve

1.3.2 EC3 Design Load

The design load according to EC3 Part 1.1[12], which covers general rules for the design of steel structures, is expressed as:

$$N_{b.Rd} = \frac{\chi \beta_A A f_y}{\gamma_{M1}} \tag{5}$$

Where γ_{M1} = material partial safety factor = 1.05

f_y = ambient temperature yield stress of the steel

A = cross-sectional area of the section

β_A = effective area factor; taken to be unity in the case of Class 1, 2 or 3 sections, in which local buckling is not a limiting factor, such as those studied in the following chapters.

χ = reduction factor for flexural buckling, which is the relevant buckling mode for hot-rolled steel column sections.

Since f_y is the stress required to cause the steel to begin to yield, Af_y is necessarily the force required to cause the steel to yield. This resulting force is then scaled down by the safety factor γ_{M1} such that it is sufficiently conservative. This is an accurate failure load for very squat columns, which fail by yielding of the steel. However, more slender columns will fail by flexural buckling at a lower force than that required for yielding. Thus χ is introduced to reduce the design force according to the column slenderness as defined in eqn. (6). This equation would permit χ to be greater than unity for very small levels of imperfection, which would give a design load for the column greater than the yield stress of the steel. This does not make physical sense and is just a product of the fact that the Euler buckling load increases to infinity as the slenderness decreases. Thus, a maximum value of χ=1 is allowed.

$$\chi = \frac{1}{\phi + \sqrt{\phi^2 - \lambda^{*2}}} \qquad \text{but } \chi \leq 1 \tag{6}$$

Where ϕ is defined as:

$$\phi = \frac{1 + \alpha(\lambda^* - 0.2) + \lambda^{*2}}{2} \tag{7}$$

In which:

α = An imperfection factor taken from tables to take into account the fact that the column will not be initially straight, which has the effect of amplifying the effects of slenderness.

λ^* = Non-dimensional slenderness defined by the following equation, which uses $N_{cr} = \pi^2 EA/\lambda^2$ to indicate the elastic critical force for the relevant buckling mode, where E is Young's modulus of steel.

$$\lambda^* = \sqrt{\frac{\beta_A A f_y}{N_{cr}}} = \frac{\lambda}{\pi}\sqrt{\frac{\beta_A f_y}{E}} \tag{8}$$

1.3.3 EC3 Design Imperfection

EC3 Part 1.1 gives a number of equations that can be used to calculate the maximum equivalent initial out-of-straightness for compression members, depending on the type of cross-section used, and the method of analysis. Since elasto-plastic analyses of non-linearly elastic I-sections will be performed, the equations for initial imperfection are thus:

$$\text{Minor Axis Imperfection } \delta_{minor} = \frac{\alpha(\lambda^* - 0.2)k_y W_{pl}}{A} \tag{9}$$

$$\text{Major Axis Imperfection } \delta_{major} = \frac{k_y e_{eff}}{\sqrt{\frac{235}{f_y}}} \tag{10}$$

Where: W_{pl} = plastic section modulus available from section tables.

e_{eff} = effective length factor dependent on the conditions of support at the ends of the member, and:

$$k_y = 1 - k_\delta + 2k_\delta \lambda^* \tag{11}$$

In which k_y is an imperfection factor which is dependent upon λ^*, thus slender columns are assumed to have an imperfection level greater than squat columns. The constant k_δ is dependent upon the buckling curve and the safety factor γ_{M1} and a value of 0.08 is taken from the relevant table and used for subsequent calculations.

These equations are complicated, and generating the information to set up the column data files for VULCAN would have been extremely time consuming. Therefore a computer program was written to automatically generate VULCAN input files for columns designed to the above specifications.

1.3.4 Axial Restraint

When columns are heated, their lengths increase due to thermal expansion of the steel[13]. In realistic situations, this elongation is restrained by parts of the adjoining structure. In a number of subsequent chapters, the effects of this restraint are studied.

The stiffness of this restraint is measured in units of force per unit displacement. When a column expands against restraint, an additional axial force is introduced in the column, together with a corresponding force in the restraint system. However, for the purpose of investigation of the effects of axial restraint, it is desired to have a measure of the severity of this additional force. For example, if a restraint of 10kN/mm is applied to a large column section, which expands by 1mm, an additional force of 10kN is introduced into the system. In a large section, this force may have a negligible effect upon the behaviour of the column. If a small section size were similarly heated, a similar additional axial force of 10kN would be introduced. This may cause the total force in the member to be comparable in size to the critical load of the section and thus cause failure. So 10kN/mm may be a relatively small level of restraint for a large section and a catastrophic level of restraint for a smaller section.

Therefore, a Relative Restraint Factor (α) is defined as the ratio of the restraint stiffness k_s to the column stiffness k_c:

$$\alpha = \frac{k_s}{k_c} = \frac{k_s}{EA/l} \tag{12}$$

Where E = Young's modulus of steel.

A = cross-sectional area of the column.

l = length of the column.

Thus, a higher value of α signifies a more severe restraint stiffness in that there is a greater increase in force for a given expansion.

1.4 VULCAN

Due to the relatively high cost of performing structural tests, particularly at elevated temperatures, computer simulations are often used. Once fully validated against test results, these programs can be used to perform parametric studies and investigate the

behaviour of structural systems so that an in-depth understanding can be gained of the mechanisms involved. This method of research has become particularly viable over recent years, as the power and speed of readily available computers has increased substantially.

Although there exist fully validated, commercially available pieces of software[14,15] capable of performing non-linear finite element analysis at elevated temperatures, these are often undesirable to researchers, since their source code cannot be examined or improved, and their basic assumptions fixed. The finite element model used for this research is the VULCAN program, and this section describes its theory, assumptions and formulation.

1.4.1 Program History

The VULCAN program is based on a piece of software called INSTAF, which was developed by El-Zanaty and Murray[16] at the University of Alberta in 1980. INSTAF was written in the FORTRAN programming language and was capable of analysing two-dimensional steel frames at ambient temperature, incorporating geometrical non-linearity and the spread of yield. By 1990, the program had been developed at the University of Sheffield by Saab[17,18] to include elevated temperature material properties. Najjar[19,20] then extended this work to allow three-dimensional behaviour to be analysed, including the effects of twisting and warping. Most recently, Bailey[21,22,23,24] has further extended the program's capabilities to take account of lateral-torsional buckling and strain reversal, and to include non-linear spring elements and elastic concrete-slab elements with composite action. It is this version which was used as the starting point for the research reported here, and the program has been renamed VULCAN to reflect the fact that it has been so extensively developed from the original version.

1.4.2 General Description

The VULCAN program could be described as a black-box program, in that it is not normally user-interactive. A textual input file is created, which precisely describes the structure to be modelled as a series of nodes connected by a number of beam-column, spring or shell elements, each with specified geometric and material properties. A heating regime and a series of temperature increments are also prescribed. The format of this input file has been reformulated by the author to make

it more user-friendly and to increase its flexibility for future program enhancements. This new format is fully documented in Appendix A. A user interface program known as the INSTAF Interface has been developed to aid the creation of these input files with the help of a translation program called MAKEDAT developed by the author. An interactive, graphical software tool called SHOWGRID has also been created by the author to facilitate the verification of both old- and new-style input files. The features of this program are described in Appendix B.

The VULCAN program itself takes an input file, performs the non-linear finite element analysis on the structure, and creates a corresponding textual output file of results. Many input files can be analysed in series by the use of batch files, allowing large parametric studies to be performed relatively easily.

This output file can then be interrogated with a text editor or spreadsheet program. Alternatively, the results can be plotted graphically, using the purpose-written program DATAMOD, or displayed pictorially with animation using SHOWGRID.

1.4.3 Capabilities And Limitations

Beam-column elements are represented in the program as two-noded line elements, each node having eight degrees of freedom in local co-ordinates. These degrees of freedom represent the displacements and strains in each of the three dimensions together with three selected derivatives of these degrees of freedom (which represent either direct- or shear-strains), along with twisting and warping. These eight local degrees of freedom are transformed into eleven in global co-ordinates. Thus at each node, at least three degrees of freedom must be constrained for the problem to be solvable, either naturally, by the application of external boundary conditions, or by being constrained by the interaction of other elements.

At present, only an I-shaped, symmetric cross-section can be defined for these line elements. The properties of other shapes can be approximated by defining an I-section with similar cross-sectional properties similar to those of the desired shape. Similarly, tapered elements can be approximated by dividing a long element along its length into a number of sub-elements, each with a progressively smaller cross-sectional area.

Spring elements have the same degrees of freedom as beam-column elements. However, they are normally used to represent semi-rigid connections, so that their

rotational stiffness properties are modified throughout an analysis to simulate the behaviour of a moment connection with a specific, temperature-dependent stiffness and capacity.

Included in the re-formulation of the input file format by the author was the ability to specify each spring element as one of a choice of pre-defined types. Pinned, rigid and semi-rigid elastic characteristics have been defined, along with two temperature-dependent characteristics representing generic full- and partial-depth end plate connections based on results from the Cardington tests. An in-depth study of elevated-temperature connection characteristics has been carried out by Leston-Jones[25,26] and Al-Jabri[27,28], and their inclusion in the VULCAN program is currently in progress.

Shell elements have only five degrees of freedom per node in local co-ordinates, displacements in the three dimensions, and rotations about the two bending axes. Since shell elements are required to conform with the eleven global degrees of freedom used by line elements, then at least six of them must be constrained where they meet at common nodes.

The current formulation of shell elements is simplistic, however it has been shown to be an adequate approximation for global analysis of composite steel-framed structures. The material is assumed elastic although a simplistic cracking model has been included to define failure. Considerable work was in progress by Rose[29,30,31], Huang[32,33,34] and Allam[35] during the period of this project to expand the program's capabilities to layered shell elements with more reasonable cracking criteria, shear-connection interaction and geometric non-linearity.

1.5 Ulster Test Programme

This research project has been conducted as part of a joint project with the University of Ulster who have performed a series of fire tests on steel columns at elevated temperatures, subject to axial restraint.

1.5.1 Motivation

Although a reasonable amount of test data is available for steel columns in fire, it was clear that further, specific tests were required. In an international review of column tests, Franssen et al.[36] found that out of over two hundred tests, only ninety-

three were reasonably well conducted and reported. The majority of elevated-temperature tests have been performed on supposedly pin-ended columns with no axial restraint. However, in a realistic fire scenario, columns form part of continuous steel frames, and are restrained rotationally by beams, floor-slabs and column continuity into adjacent storeys. The fire at Broadgate[37] showed that a potential benefit could be gained from axial and rotational restraint once the initial heating phase of a fire had been completed. This indicated that further, high quality research into the effects of axial restraint was needed.

1.5.2 History

A large number of steel column fire tests have been carried out by various organisations throughout the world with the aim of assisting with the production of design guides and, in more recent years, of validating computer models. These tests have mainly involved the investigation of isolated members, and their results have been collated into a compendium by Franssen[36].

It has recently become apparent that investigation is required of the behaviour of columns when restrained by a surrounding frame is required. More complex computer models have been developed, which have allowed inexpensive investigation of the effects of many different parameters. However, these models require independent validation against test results. As part of this validation, two series of tests on cruciform beam-column arrangements have been performed at B.R.E. by Leston-Jones[26] and Al-Jabri[28] in order to quantify rotational restraint. A series of large-scale fire tests has also been performed at B.R.E.'s Cardington facility[38,39]. Prior to the test programme on restrained columns which is described below, a pilot study was performed by Simms[40] into the effects of axial restraint on steel columns in fire. This identified a detrimental effect of axial restraint, and indicated the need for a further study using more realistic slenderness values.

1.5.3 Brief Description

A dedicated test facility has been constructed in the fire research laboratory at the University of Ulster. This test rig is capable of testing 1.8m long test specimens, and the effects of slenderness can be investigated by varying the section size. Three section sizes were chosen for this programme, representing slendernesses within the range typically found for the columns of steel framed buildings.

Heat was provided by two gas burners situated near the bottom of the furnace and the steel temperature was measured by thermocouples attached to the column at various points along its length and around the cross-section. Axial and minor-axis mid-span displacements were measured by transducers and all the data was logged by computer at sensible time increments. Prior to testing, the initial out-of-straightness and end-eccentricities were measured with a vernier gauge by placing the column in a specially constructed jig. In most cases, post-test deflected shapes were also recorded. These tests are described in more detail in Chapter 4 and in the associated thesis produced by Randall[41].

2 Initial Investigation Of Isolated Columns

A preliminary study into the behaviour of steel columns at elevated temperatures has been conducted by investigating the effects of geometric imperfection, load ratio, material model and thermal gradient on the failure temperatures of columns. For this study, all columns were 203x203x52UC sections designed to EC3 design rules[12]. The steel had a yield stress of 275 N/mm^2 and a Young's modulus of 210 kN/mm^2.

2.1 Uniformly Heated Columns Of Varying Slenderness

This section forms the basis of the study, by considering the effects of load ratio and geometric imperfection on uniformly heated columns.

2.1.1 Introduction

All columns were modelled with 8 elements (9 nodes). They were restrained from horizontal movement, twisting and warping at both ends, and from vertical movement at one end. A single load was applied axially at the other end. Pin-ended connections are simulated at both ends and the column is free to buckle about both major and minor axes. The slenderness ratio used to define a column in these studies is the slenderness ratio of the minor axis. The Ramberg-Osgood model[4] was used to define the stress-strain relationship of steel at elevated temperatures, and is shown on Fig. 4.

2.1.2 Results

For each slenderness ratio, columns with various multiples of the EC3 imperfection in both axes and with 60% of the EC3 design load capacity were modelled and the temperature at which the column failed was recorded. The results are shown on Fig. 5. For columns with the standard EC3 imperfection, different multiples of the critical load were applied and the failure temperature recorded. These results are shown on Fig. 6.

It can be seen that failure temperatures for squat columns are almost independent of the magnitude of the initial imperfection. The absolute calculated initial imperfection is very small at this level of slenderness. Therefore, taking 0.5 or 1.5

times the imperfection does not make very much difference to the failure of the column.

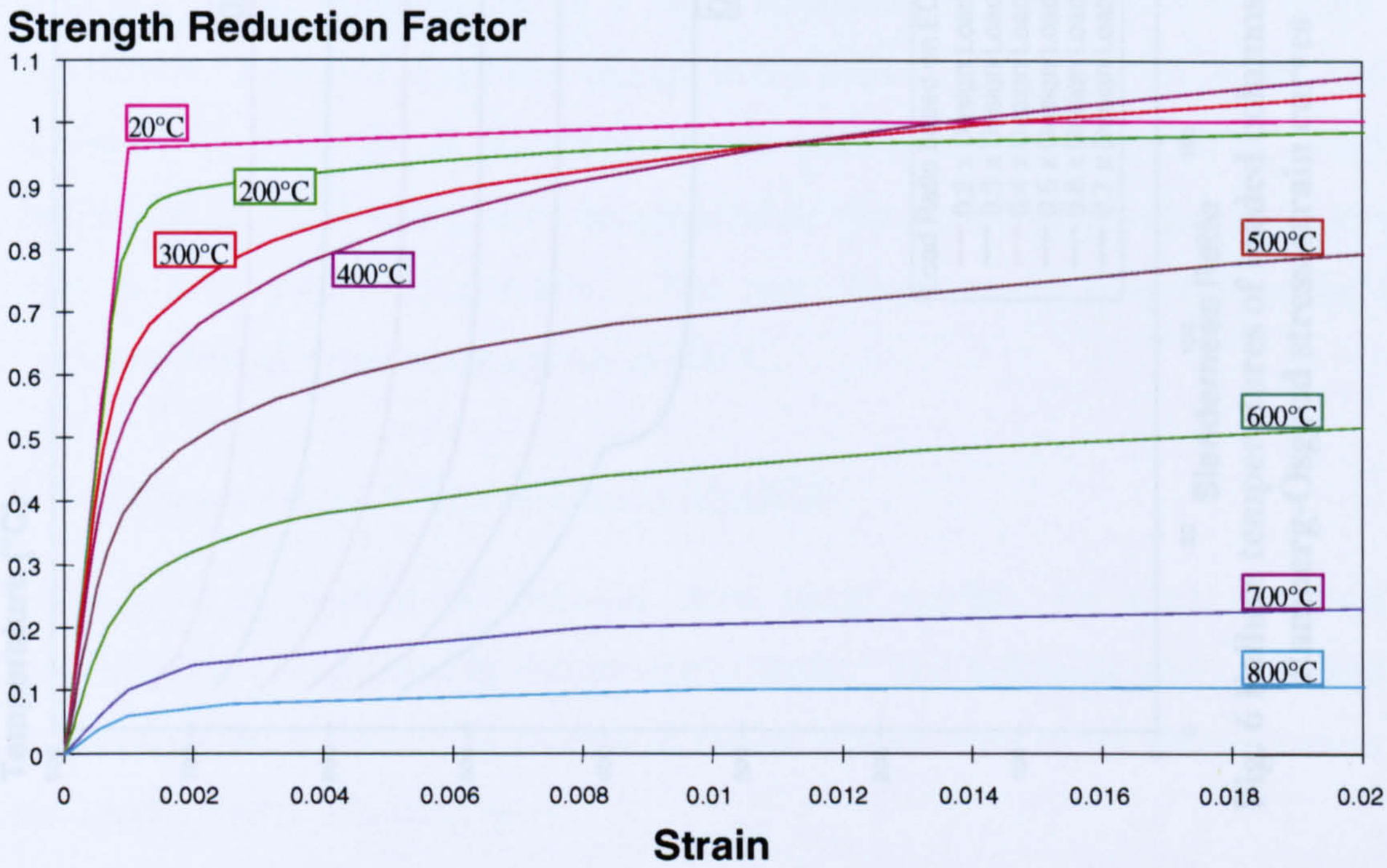

Fig. 4 Ramberg-Osgood stress-strain curves

A similar trend is seen as the level of load is varied, although the load level affects the failure of squat columns to a noticeable degree. These columns fail by squashing and this makes the imperfection unimportant compared to the load level. The failure temperature for slender columns on the other hand, is highly dependent upon the initial imperfection value. These columns fail by buckling and so the larger the initial imperfection the less is the temperature-induced bending required for failure. The same can be said about the columns in which the load level is varied. The larger the initial load, the less temperature-induced bending is required for failure.

On initial inspection, it seems that there is an actual benefit in selecting more slender columns at low imperfection levels. However, these curves are plotted at a constant load ratio, or proportion of the EC3 design load level. This design load is dependent on the column slenderness and so a constant load level does not imply a constant load value.

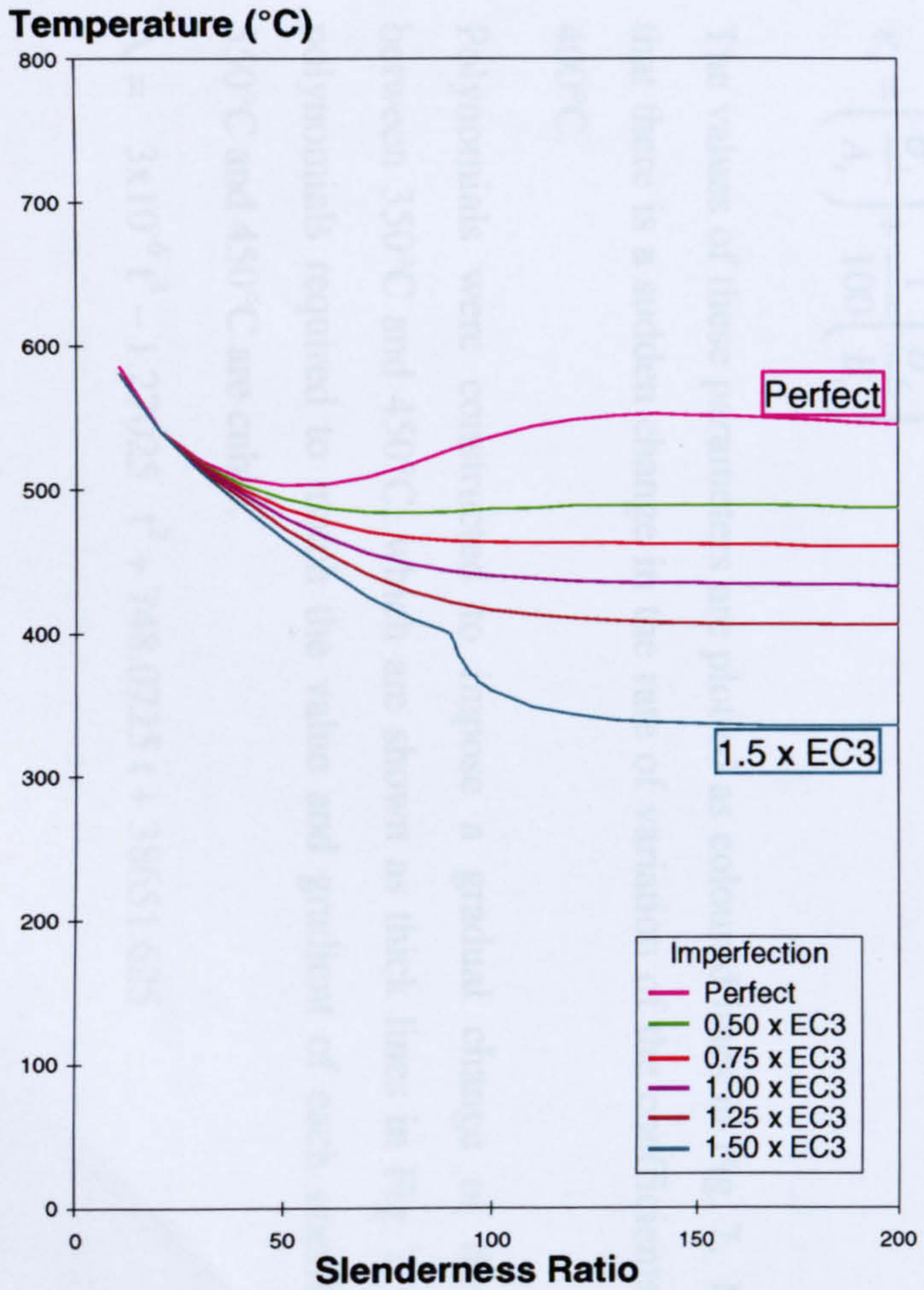

Fig. 5 Failure temperatures of imperfect columns using Ramberg-Osgood stress-strain curves

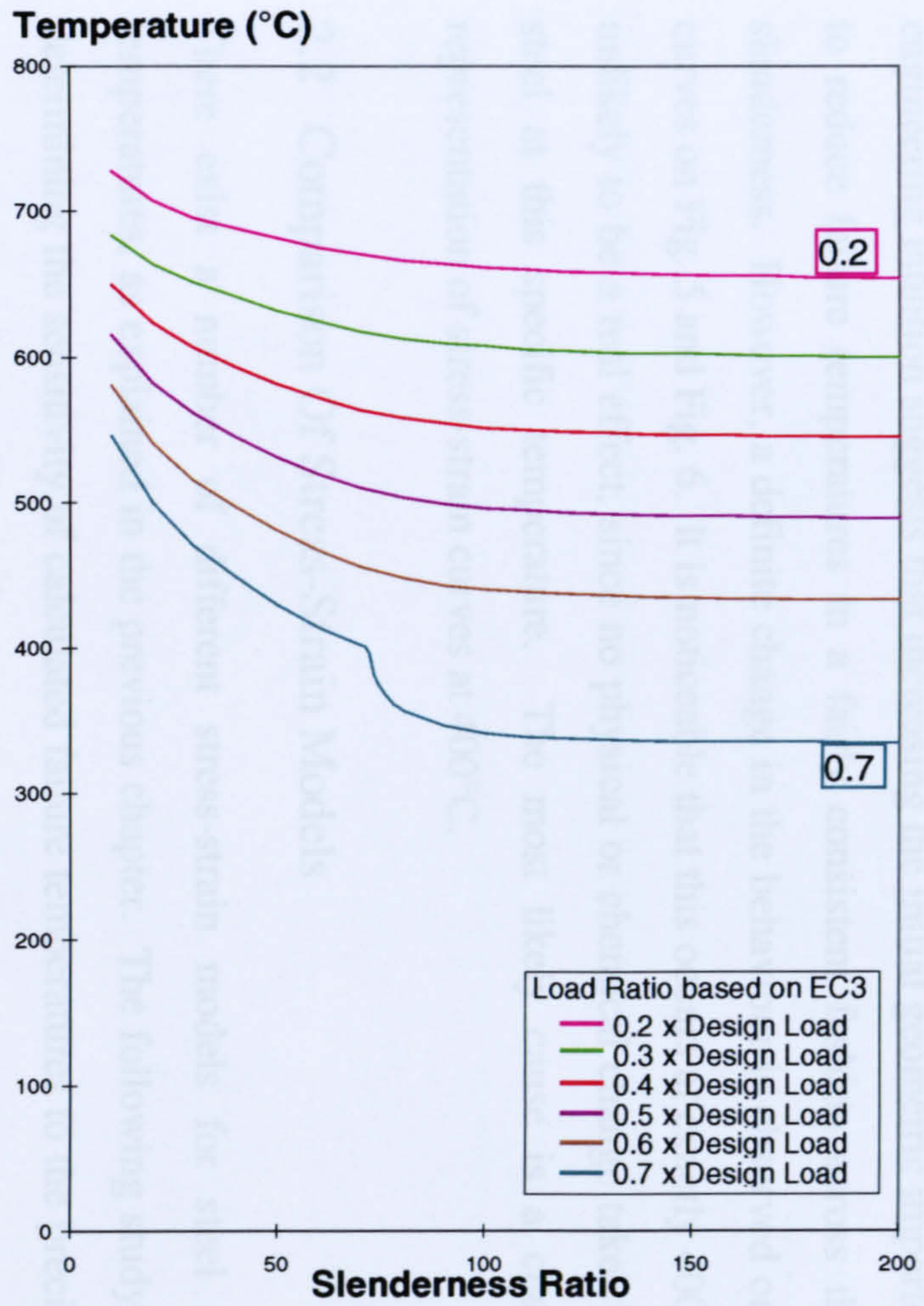

Fig. 6 Failure temperatures of loaded columns using Ramberg-Osgood stress-strain curves

There is a noticeable change in the behaviour of the columns at 400°C. Normal engineering intuition suggests that increasing the initial geometric imperfection tends to reduce failure temperatures in a fairly consistent fashion across the range of slenderness. However, a definite change in the behaviour is observed on the lowest curves on Fig. 5 and Fig. 6. It is noticeable that this occurs at exactly 400°C. This is unlikely to be a real effect, since no physical or chemical change takes place in the steel at this specific temperature. The most likely cause is a change in the representation of stress-strain curves at 400°C.

2.2 Comparison Of Stress-Strain Models

There exist a number of different stress-strain models for steel at elevated temperatures, as explained in the previous chapter. The following study is aimed at determining the sensitivity of calculated failure temperatures to the precise nature of the constitutive relationship used.

2.2.1 The Ramberg-Osgood Model

The Ramberg-Osgood model for steel at elevated temperatures modifies the strain at a given stress by the use of three temperature-dependent parameters, A_t, B_t and n_t. If ε_t represents strain and σ_t represents stress at temperature t, then

$$\varepsilon_t = \left(\frac{\sigma_t}{A_t}\right) + \frac{1}{100}\left(\frac{\sigma_t}{B_t}\right)^{n_t} \qquad (13)$$

The values of these parameters are plotted as coloured lines in Fig. 7. It can be seen that there is a sudden change in the rate of variation of the coefficients A_t and B_t at 400°C.

Polynomials were constructed to impose a gradual change of the coefficients between 350°C and 450°C, which are shown as thick lines in Fig. 7. The minimal polynomials required to match the value and gradient of each coefficient at both 350°C and 450°C are cubic.

$$A_t = 3\text{x}10^{-6}\, t^3 - 1.27025\ t^2 + 748.0725\, t + 38651.625$$

$$B_t = -6\text{x}10^{-8}\, t^3 - 0.003061\, t^2 + 2.16475\, t - 138.1175 \qquad (14)$$

The coefficients required between 650°C and 750°C are as follows.

$$A_t = -0.0113\,t^3 + 25.0470\,t^2 - 18638\,t + 4673770$$

$$B_t = 9.4 \times 10^{-8}\,t^3 + 0.001136\,t^2 - 2.2220\,t + 1024.09 \qquad \textbf{(15)}$$

This model will be referred to as the Smoothed Ramberg-Osgood (SR-O) model.

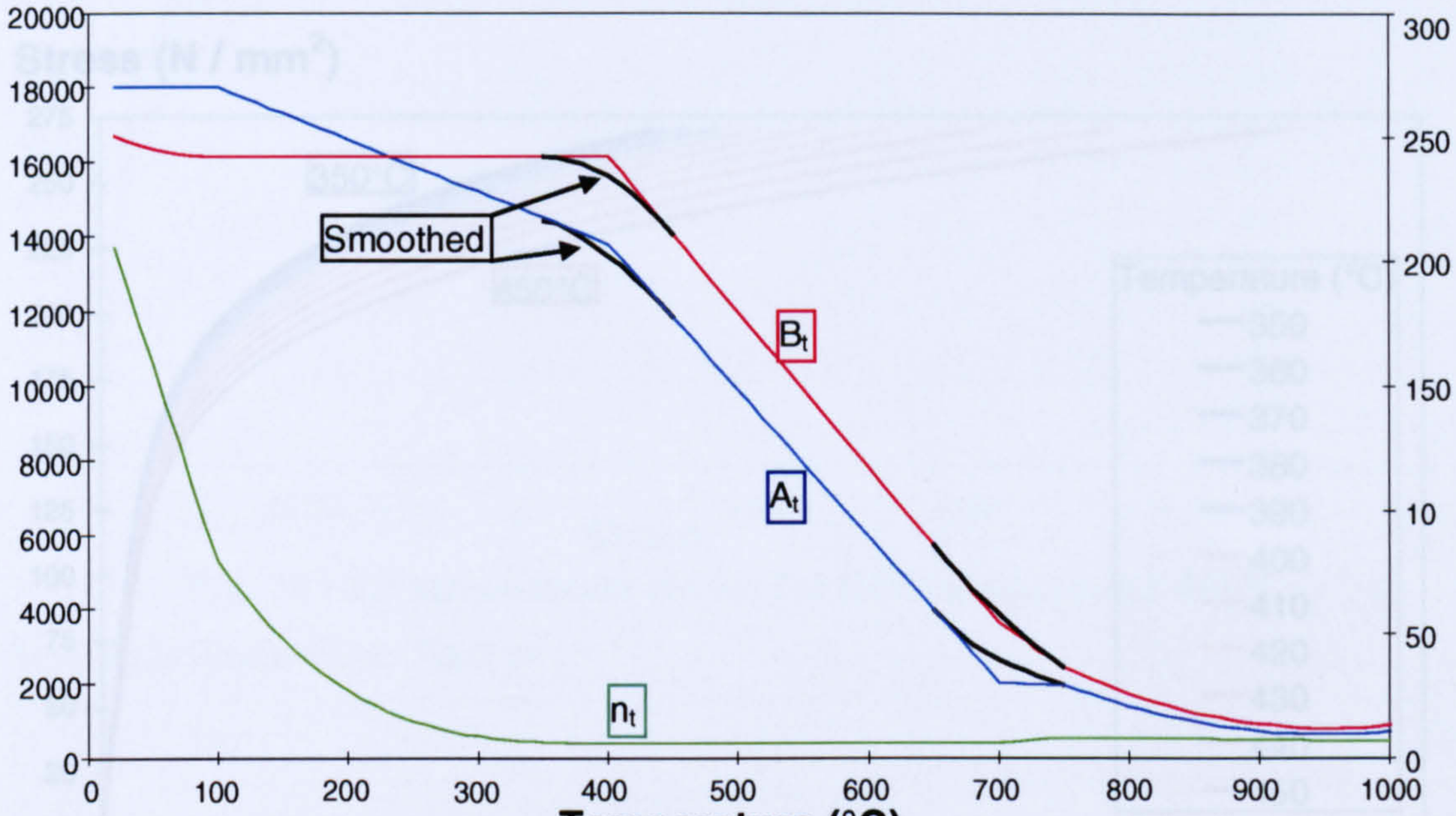

Fig. 7 Ramberg-Osgood parameters

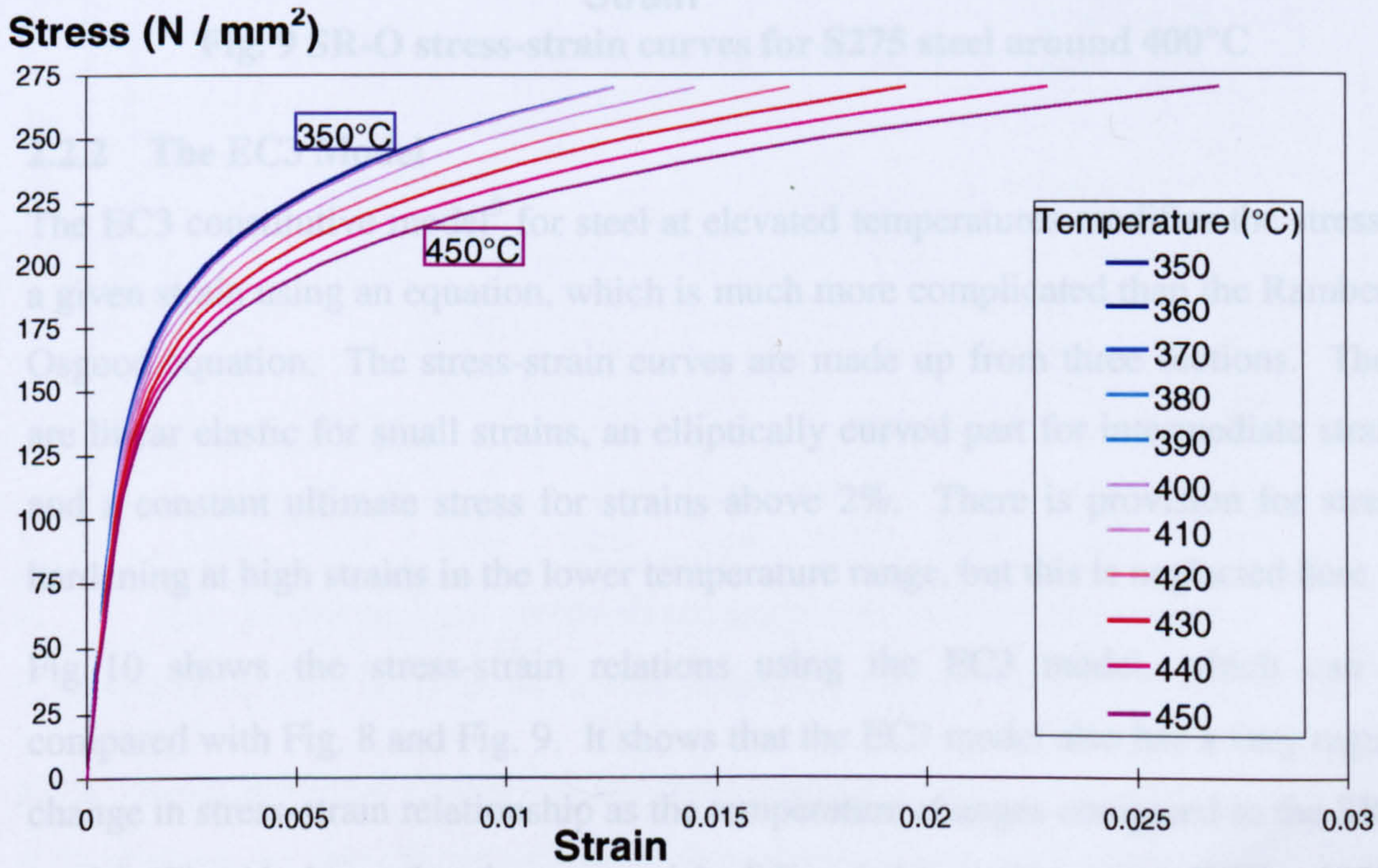

Fig. 8 R-O stress-strain curves for S275 steel around 400°C

From Fig. 8 it can be seen that the stress-strain relationships for the standard Ramberg-Osgood model just below 400°C have very similar curves, which lie nearly on top of each other. Just above 400°C the curves separate and become regularly spaced. Fig. 9 however, shows that the Smoothed model has a monotonic spread of curves and so no sudden changes in behaviour of the steel are seen. The effect of this change can be seen by a re-analysis of imperfect, slender columns using the SR-O model in Section 2.2.3.

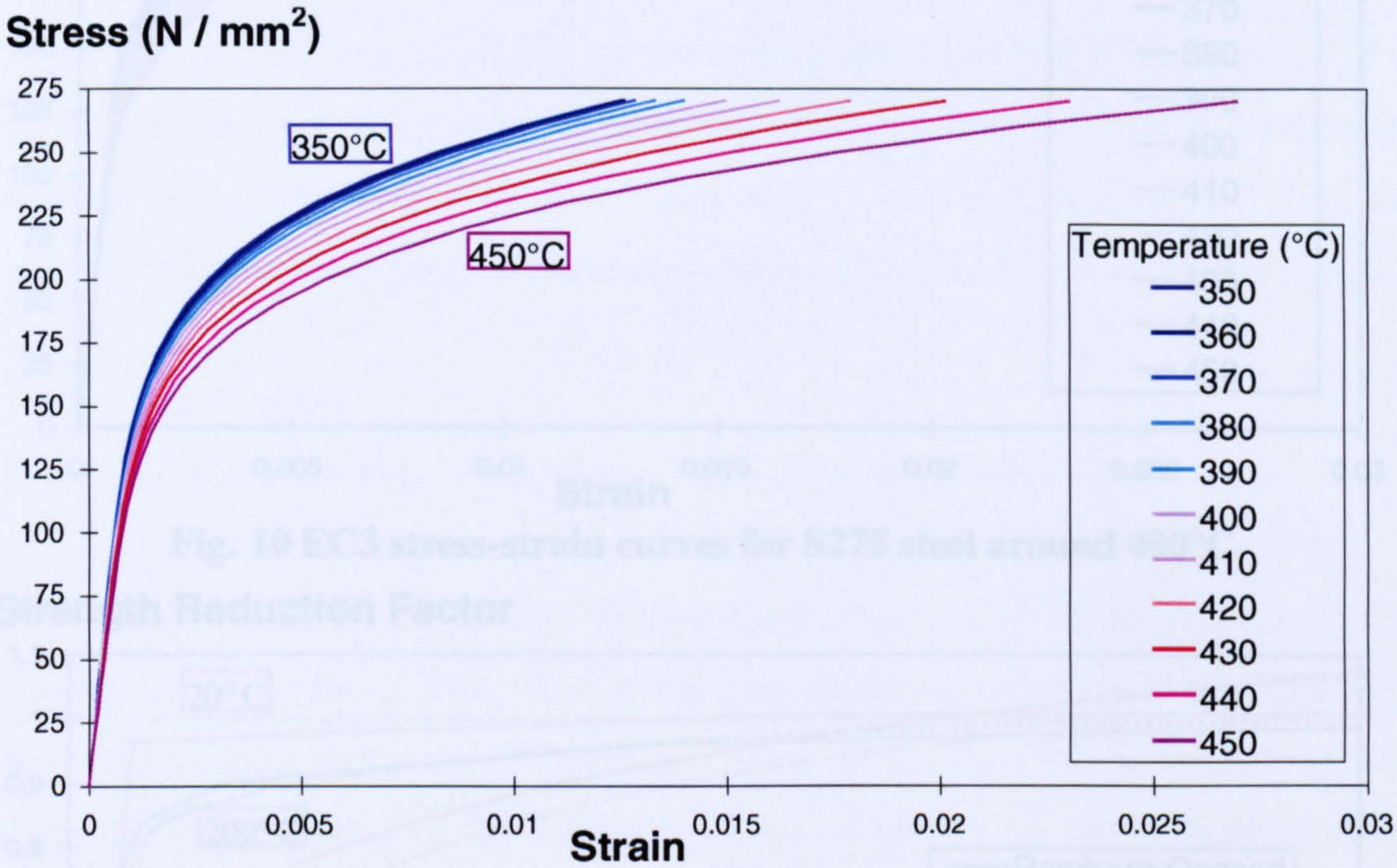

Fig. 9 SR-O stress-strain curves for S275 steel around 400°C

2.2.2 The EC3 Model

The EC3 constitutive model[5] for steel at elevated temperatures modifies the stress at a given strain using an equation, which is much more complicated than the Ramberg-Osgood equation. The stress-strain curves are made up from three sections. These are linear elastic for small strains, an elliptically curved part for intermediate strains and a constant ultimate stress for strains above 2%. There is provision for strain-hardening at high strains in the lower temperature range, but this is neglected here.

Fig. 10 shows the stress-strain relations using the EC3 model, which can be compared with Fig. 8 and Fig. 9. It shows that the EC3 model also has a very regular change in stress-strain relationship as the temperature changes compared to the SR-O model. Fig. 11 shows that the two models differ visibly in the range 400°C – 600°C.

At a given level of strain, the EC3 model gives a much lower level of stress than the Ramberg-Osgood model.

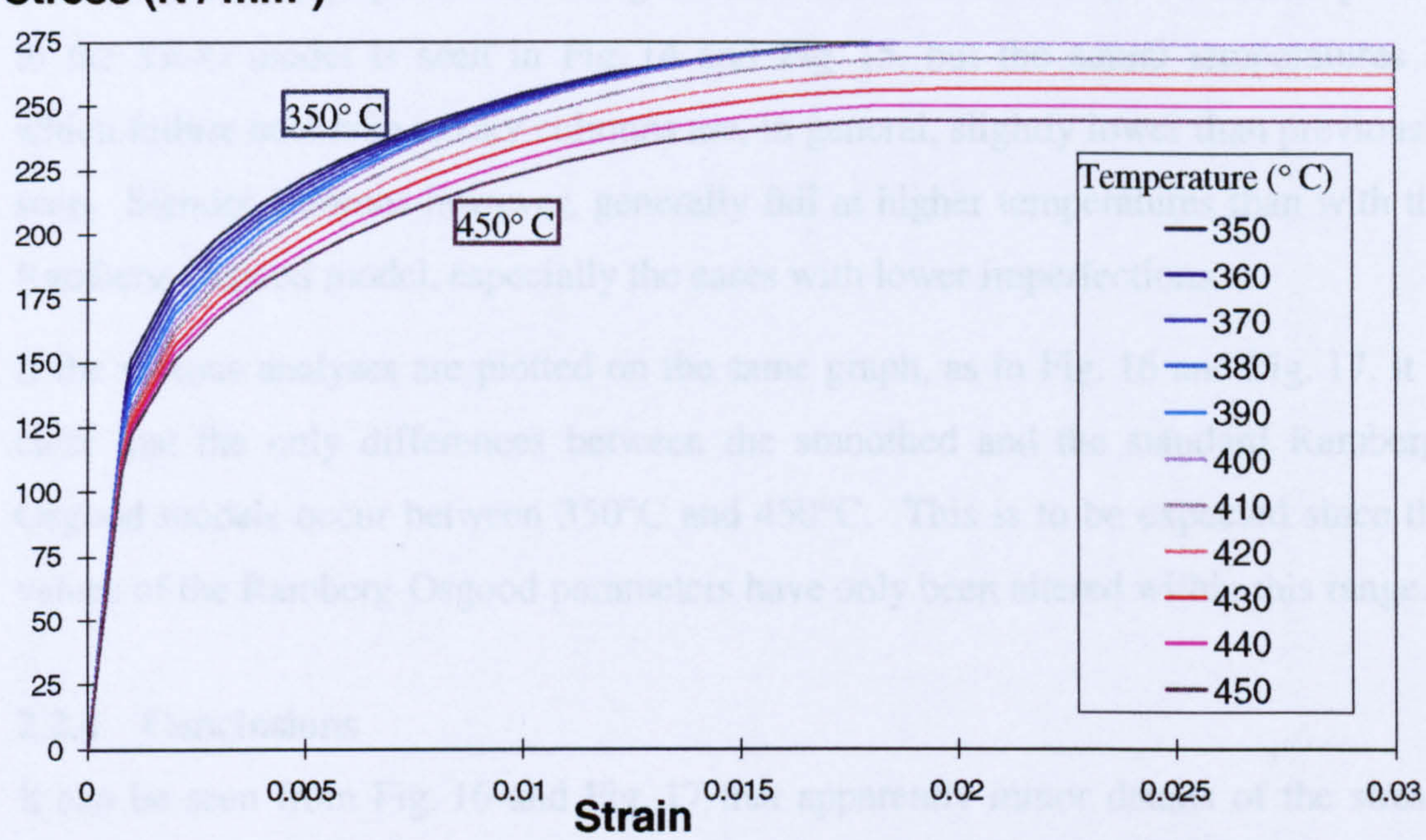

Fig. 10 EC3 stress-strain curves for S275 steel around 400°C

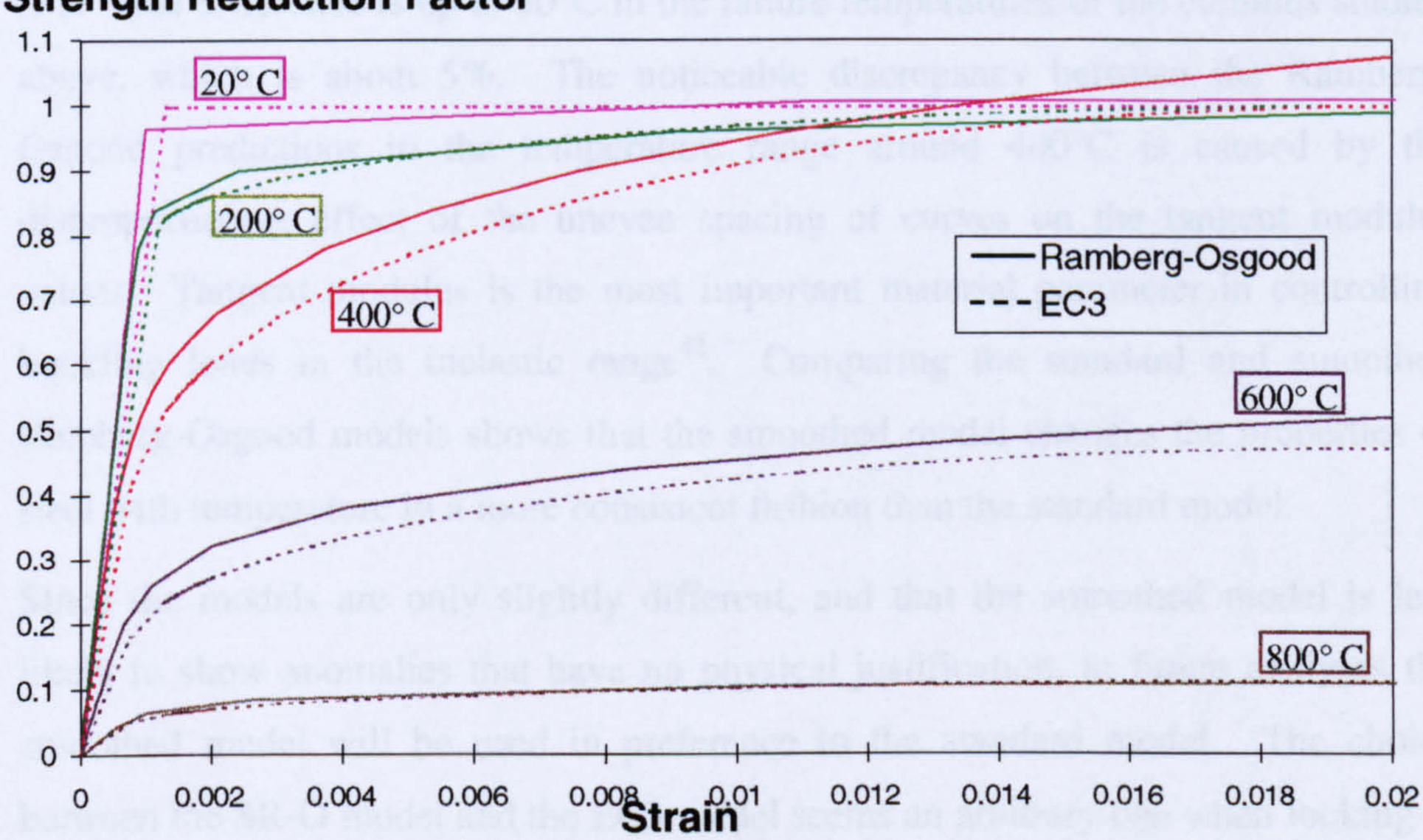

Fig. 11 Normalised stress-strain curves at various temperatures

Comparing EC3 (broken line) with Ramberg-Osgood (solid line) equations

2.2.3 Re-analysis Of Uniformly Heated Columns

A re-analysis of the effects of initial imperfection and load ratio on the failure temperatures of uniformly heated slender columns was conducted using the SR-O

model. The results can be seen on Fig. 12 and Fig. 13, and show that there is no sudden change in behaviour at 400°C using this model.

A third analysis was performed using the EC3 stress-strain curves. A similar pattern to the SR-O model is seen in Fig. 14 and Fig. 15, but the actual temperatures at which failure occurs in stocky columns are, in general, slightly lower than previously seen. Slender columns however, generally fail at higher temperatures than with the Ramberg-Osgood model, especially the cases with lower imperfections.

If the various analyses are plotted on the same graph, as in Fig. 16 and Fig. 17, it is clear that the only differences between the smoothed and the standard Ramberg-Osgood models occur between 350°C and 450°C. This is to be expected since the values of the Ramberg-Osgood parameters have only been altered within this range.

2.2.4 Conclusions

It can be seen from Fig. 16 and Fig. 17 that apparently minor details of the stress-strain model can make a noticeable difference to the behaviour of steel columns in fire. This difference is up to 30°C in the failure temperatures of the columns studied above, which is about 5%. The noticeable discrepancy between the Ramberg-Osgood predictions in the temperature range around 400°C is caused by the disproportionate effect of the uneven spacing of curves on the tangent modulus values. Tangent modulus is the most important material parameter in controlling buckling loads in the inelastic range[42]. Comparing the standard and smoothed Ramberg-Osgood models shows that the smoothed model changes the properties of steel with temperature in a more consistent fashion than the standard model.

Since the models are only slightly different, and that the smoothed model is less likely to show anomalies that have no physical justification, in future analyses the smoothed model will be used in preference to the standard model. The choice between the SR-O model and the EC3 model seems an arbitrary one when looking at column behaviour in the study above. However, there is one major difference in the way the two models are implemented in the VULCAN program. The solution method of the program calculates strains and then converts them into stresses using the chosen model. The EC3 stress-strain model equation expresses the stress in terms of strain and so makes the program's solution routine straightforward.

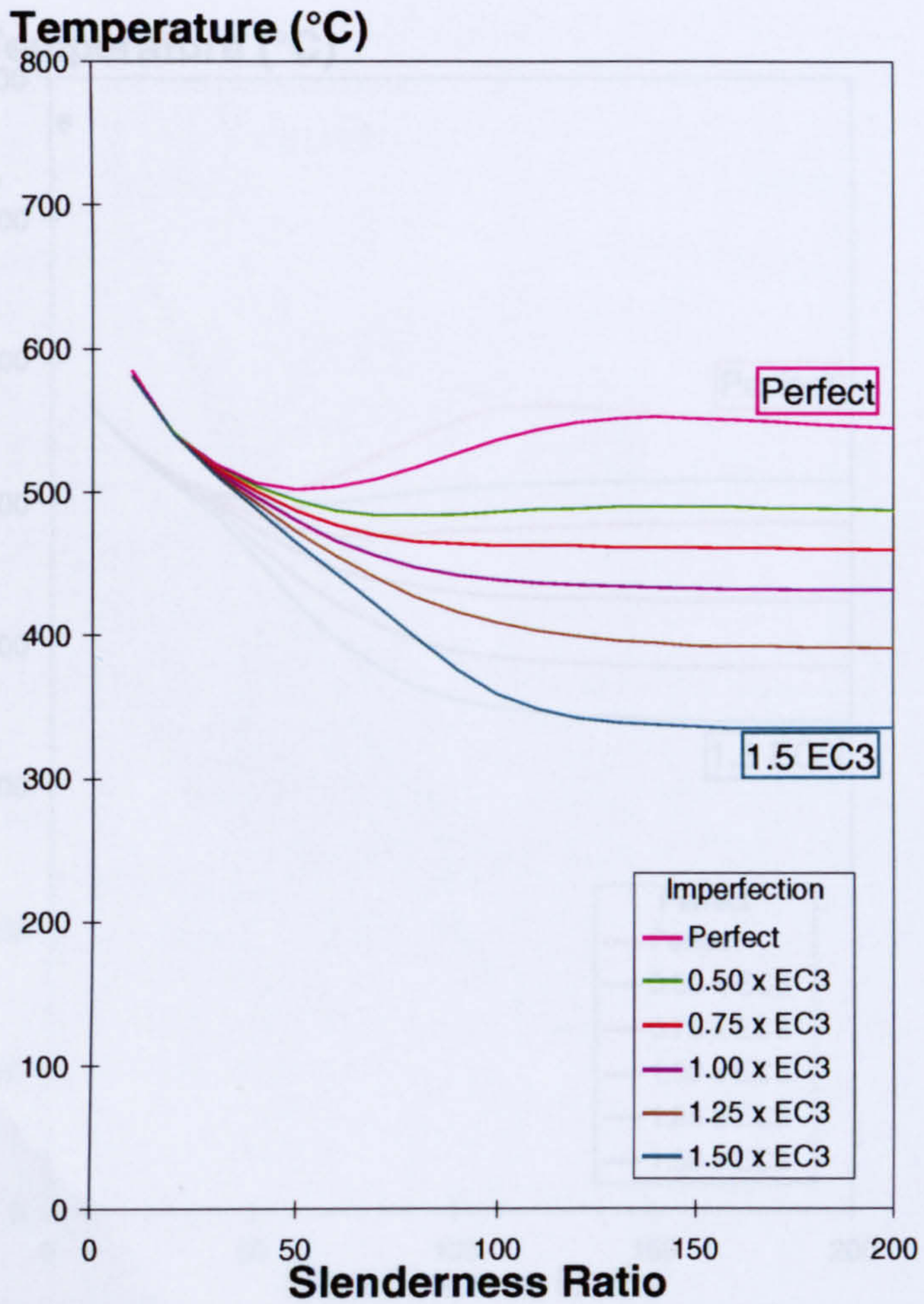

Fig. 12 Failure temperatures of imperfect columns using smoothed Ramberg-Osgood curves

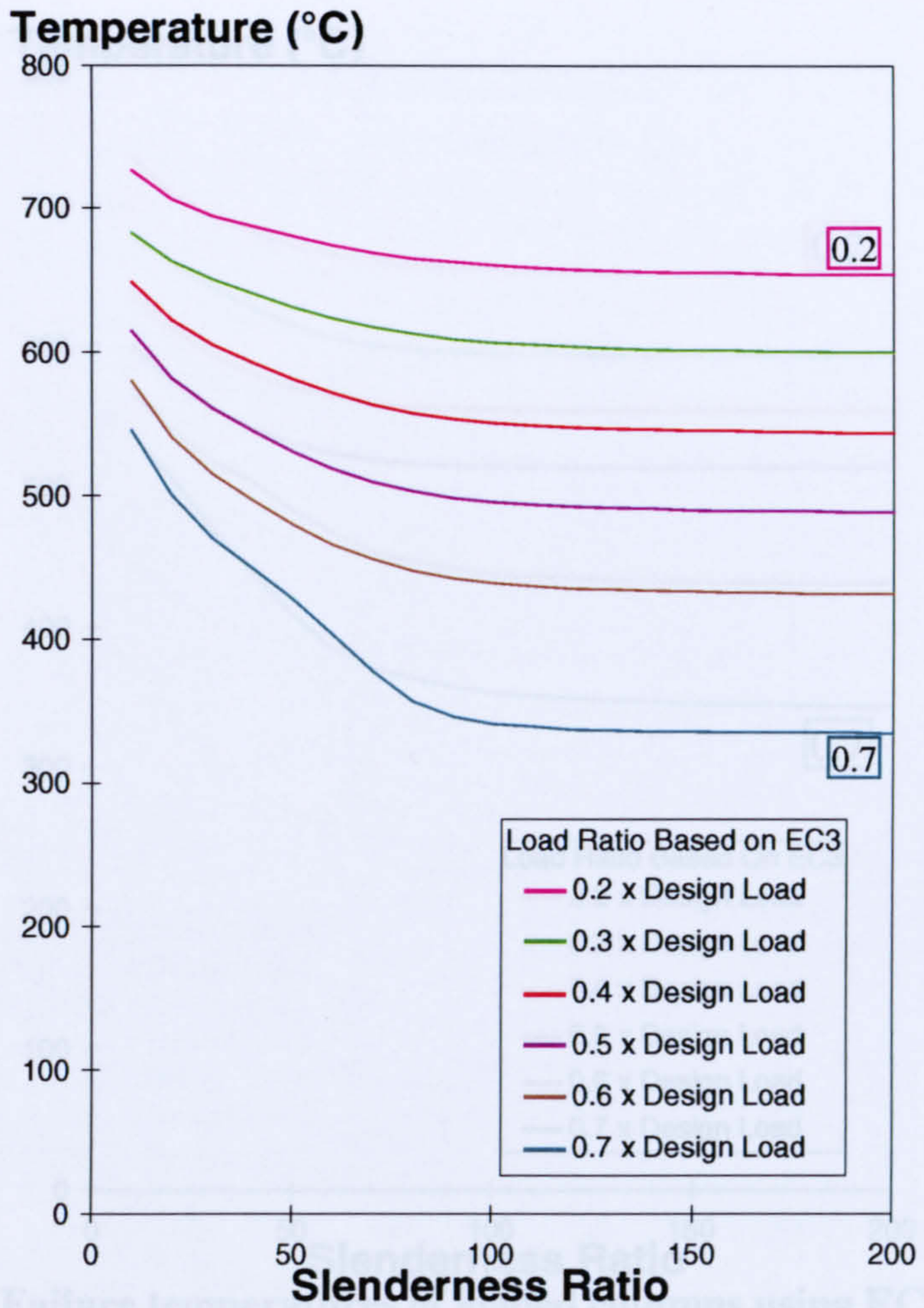

Fig. 13 Failure temperatures of loaded columns using smoothed Ramberg-Osgood curves

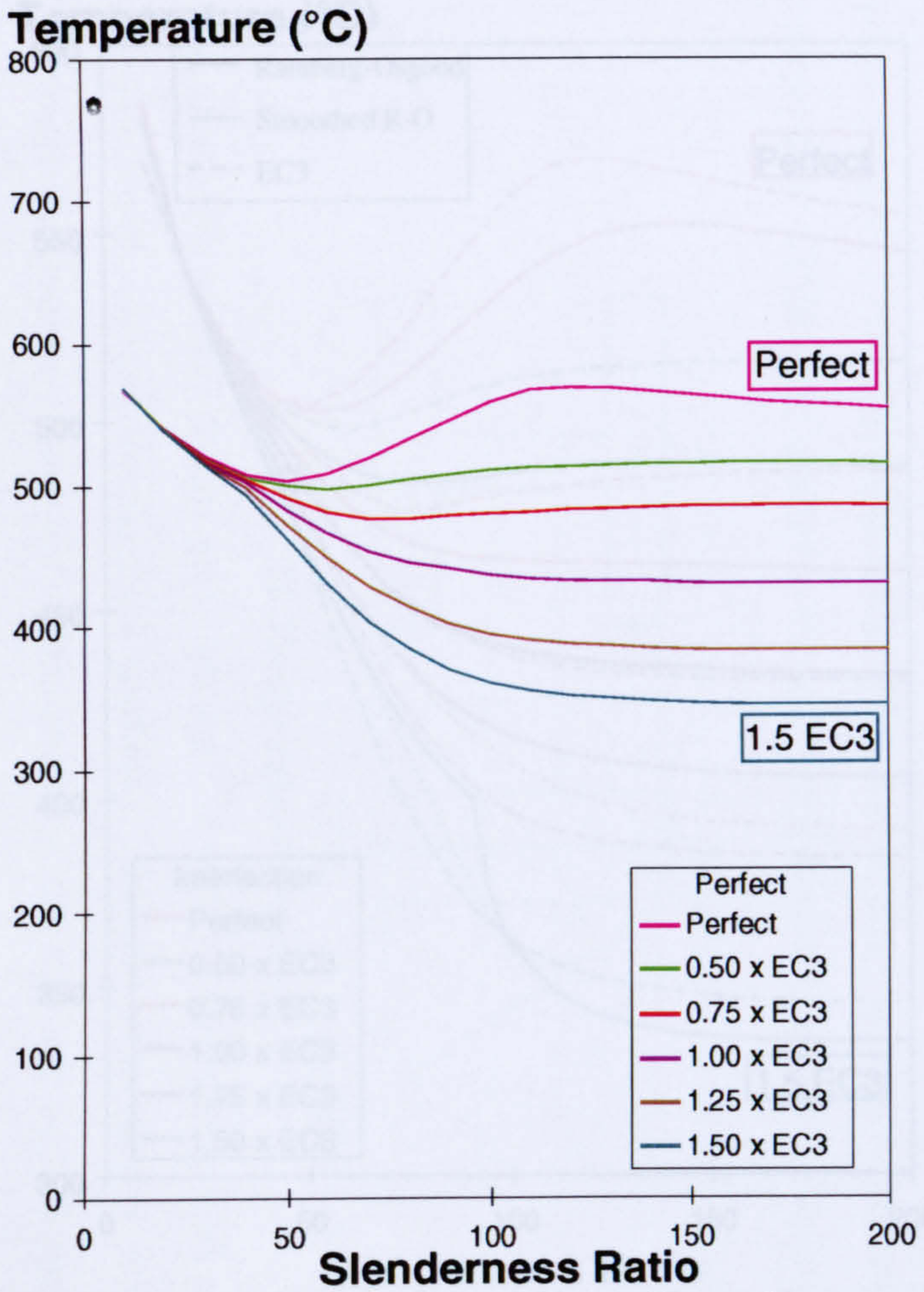

Fig. 14 Failure temperatures of imperfect columns using EC3 stress-strain curves

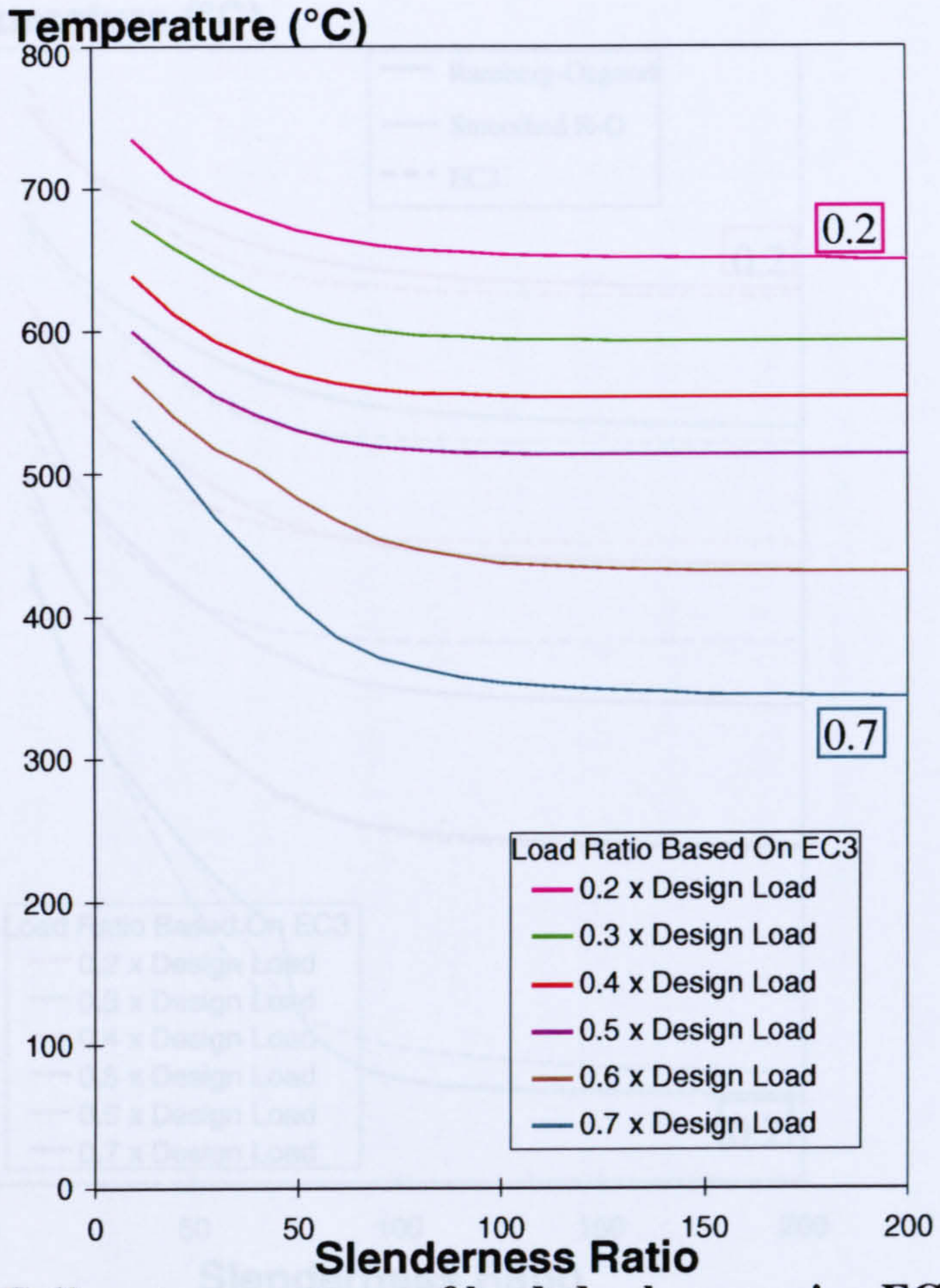

Fig. 15 Failure temperatures of loaded columns using EC3 stress-strain curves

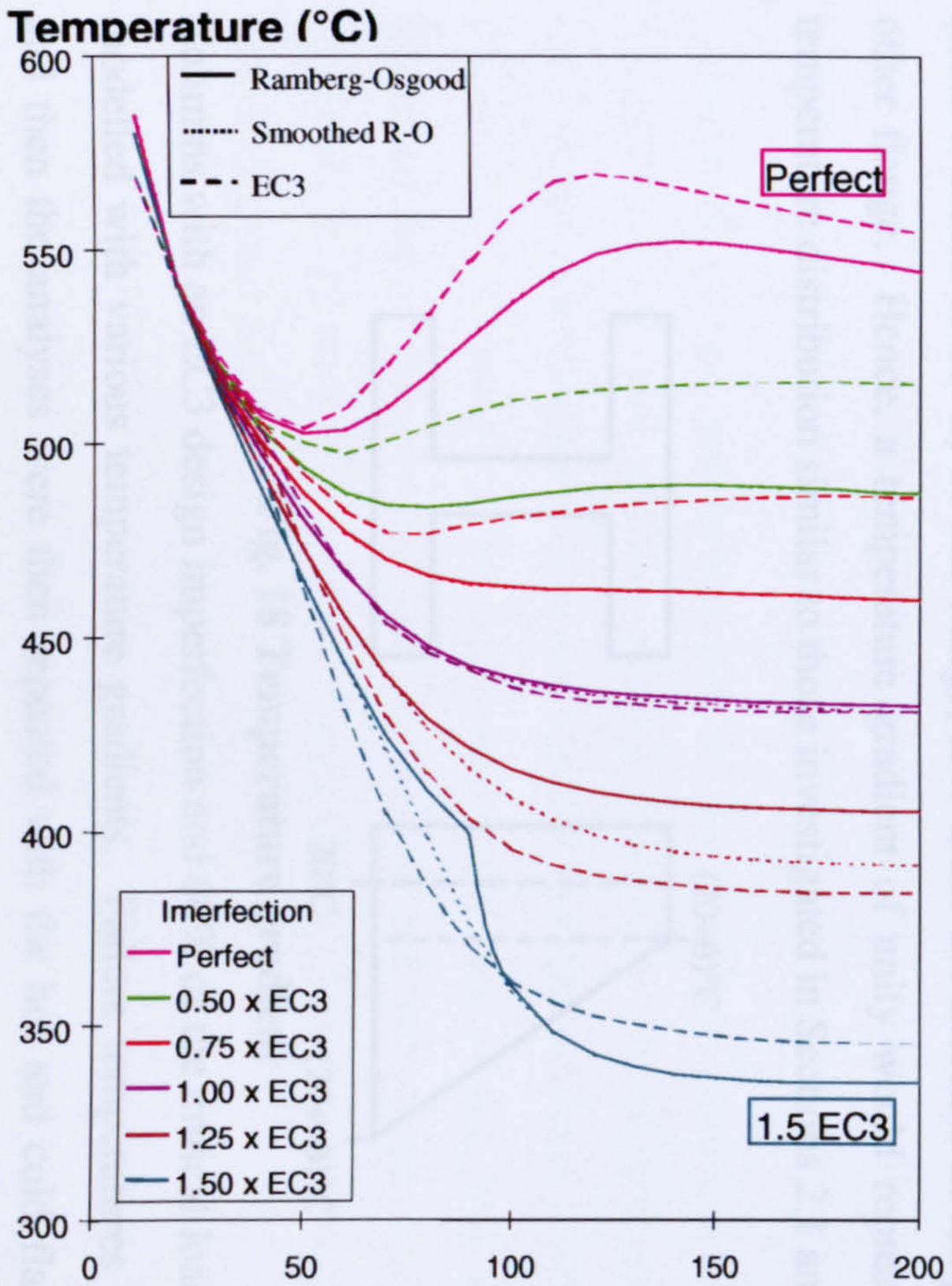

Fig. 16 Comparison of imperfect columns

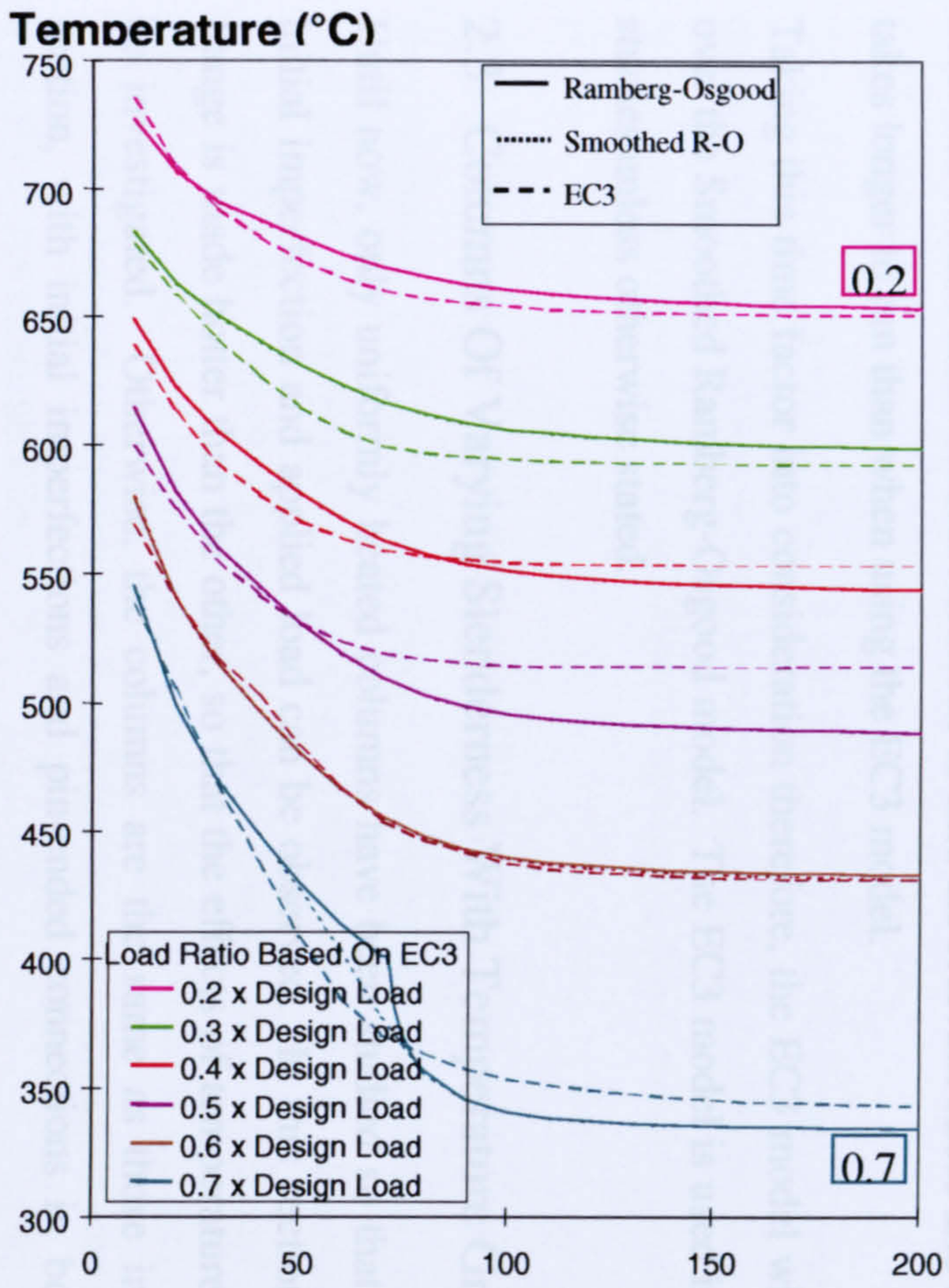

Fig. 17 Comparison of loaded columns

The Ramberg-Osgood model equation, however, expresses the strain in terms of stress, and so a bisection routine is required to find the stress at a given strain. This bisection routine takes several iterations to find the relevant stress and so the problem takes longer to run than when using the EC3 model.

Taking this time factor into consideration therefore, the EC3 model will be favoured over the Smoothed Ramberg-Osgood model. The EC3 model is used in all the future studies unless otherwise stated.

2.3 Columns Of Varying Slenderness With Temperature Gradients

Until now, only uniformly heated columns have been studied so that the effects of initial imperfection and applied load can be observed. In this section, one column flange is made hotter than the other, so that the effects of temperature gradients can be investigated. Otherwise, the columns are the same as those in the previous section, with initial imperfections and pin-ended connections in both major and minor axes.

2.3.1 Introduction

Temperature gradients were introduced into the column cross-sections as shown in Fig. 18. A temperature gradient factor of n implies that the increase in temperature (from a datum of 20°C) of one flange, is n times the increase in temperature of the other flange. Hence, a temperature gradient of unity would represent a uniform temperature distribution similar to those investigated in Sections 2.1 and 2.2.

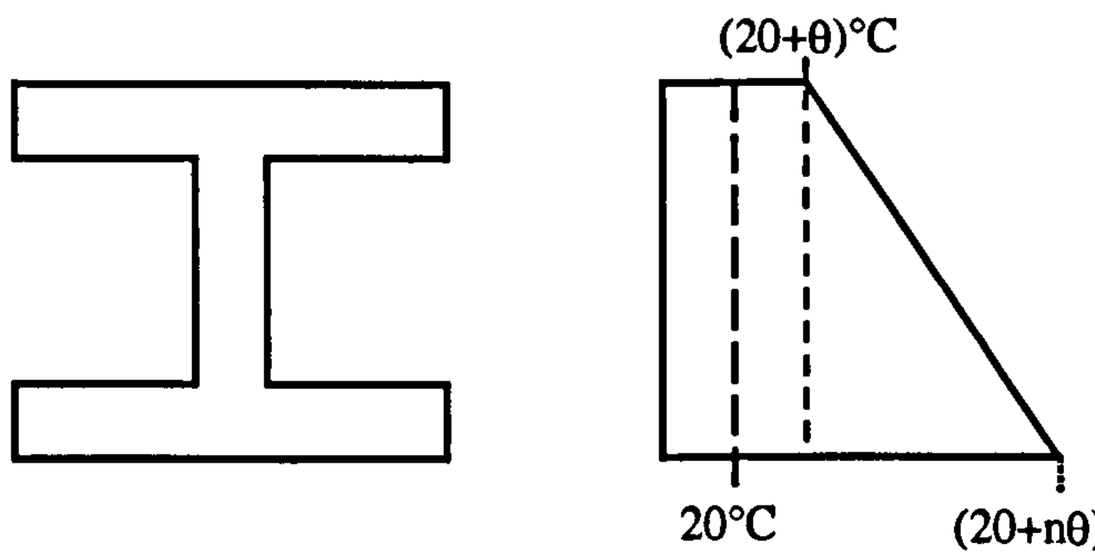

Fig. 18 Temperature gradient

Columns with an EC3 design imperfection and 60% of the critical load applied were modelled with various temperature gradients. Failure temperatures were recorded and then the analyses were then repeated with the hot and cold flanges reversed.

This is equivalent to having the initial imperfections *towards* and *away-from* the heat source.

2.3.2 Results

The results are shown on Fig. 19 and Fig. 20. There is clearly a peak in the failure temperatures for columns around slenderness 80. The curves cross over in the very slender range, and the case of imperfection away from the fire produces a sharper peak.

Plots of temperature against lateral deflection for the mid-points of the columns showed that the only significant difference in behaviour of columns either side of the peak was in their major-axis deflection. To help isolate the phenomenon, columns with negligibly thin webs were studied. These were subjected to major-axis imperfection only and the web was made to be 1 mm thick for analytical purposes. This is thin enough to remove any significant bending resistance while retaining the integrity of the cross-section.

These thin-webbed columns were analysed with EC3 Imperfections, half-EC3 imperfections and zero imperfection. To simplify this idealised case, the imperfection was in the major axis only. They showed the same behaviour as the standard columns. Strain data for the flanges of the idealised section showed that the strain was constant across each flange. This was to be expected since there is no initial imperfection in that direction. Hot- and cold-flange strains for the case with no initial imperfection are shown on Fig. 21.

Columns on the low-slenderness side of the peak have strains on the hot flange which slightly increase and then rapidly decrease as the temperature nears failure. Cold flange strains slightly decrease initially and then increase towards the failure temperature. Columns on the high-slenderness side of the peak however, have strains on the hot flange which increase slightly and then continue to increase at an accelerating rate near failure. Cold flange strains slightly decrease initially, with a further decrease near failure.

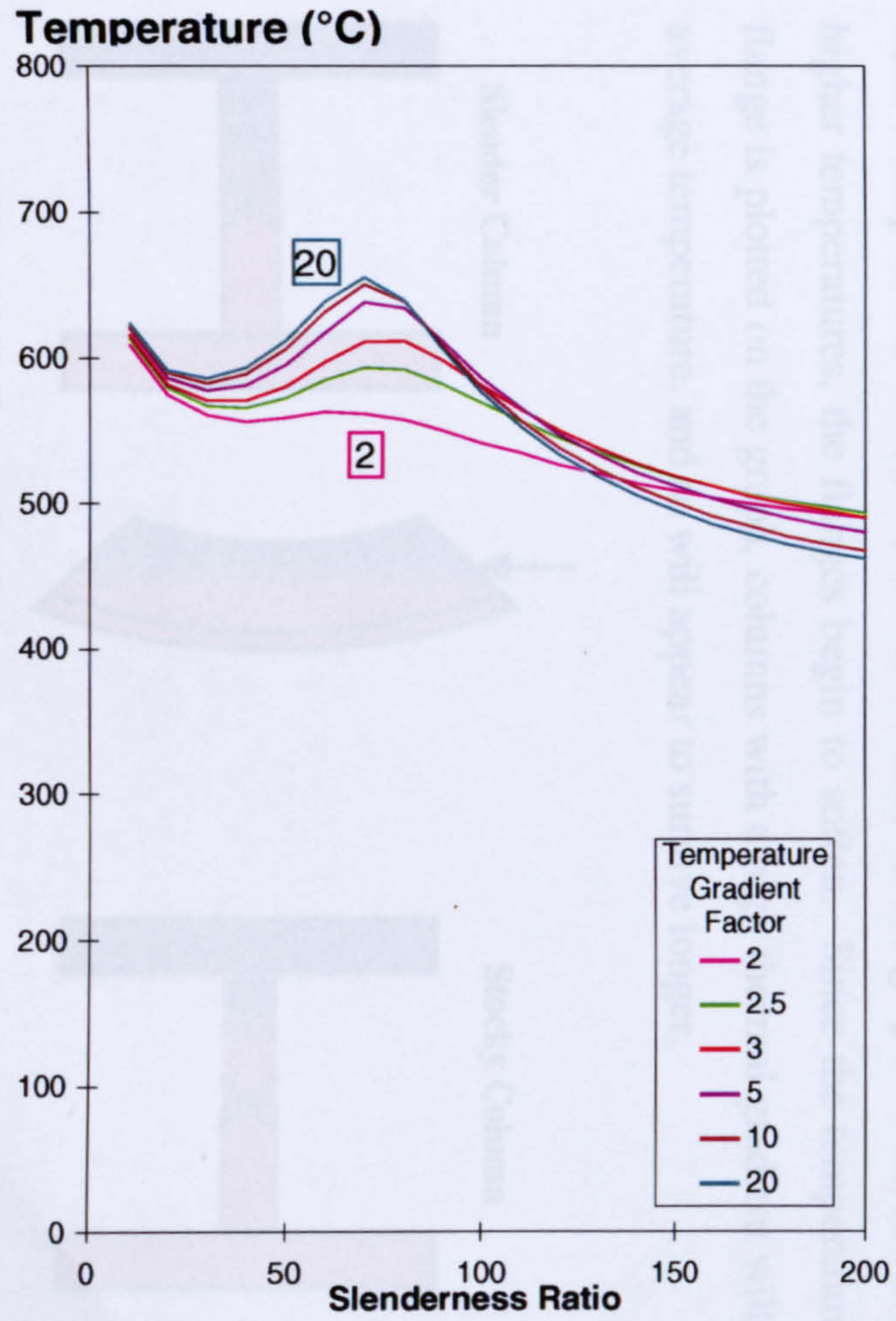

Fig. 19 Columns with initial imperfection away from fire

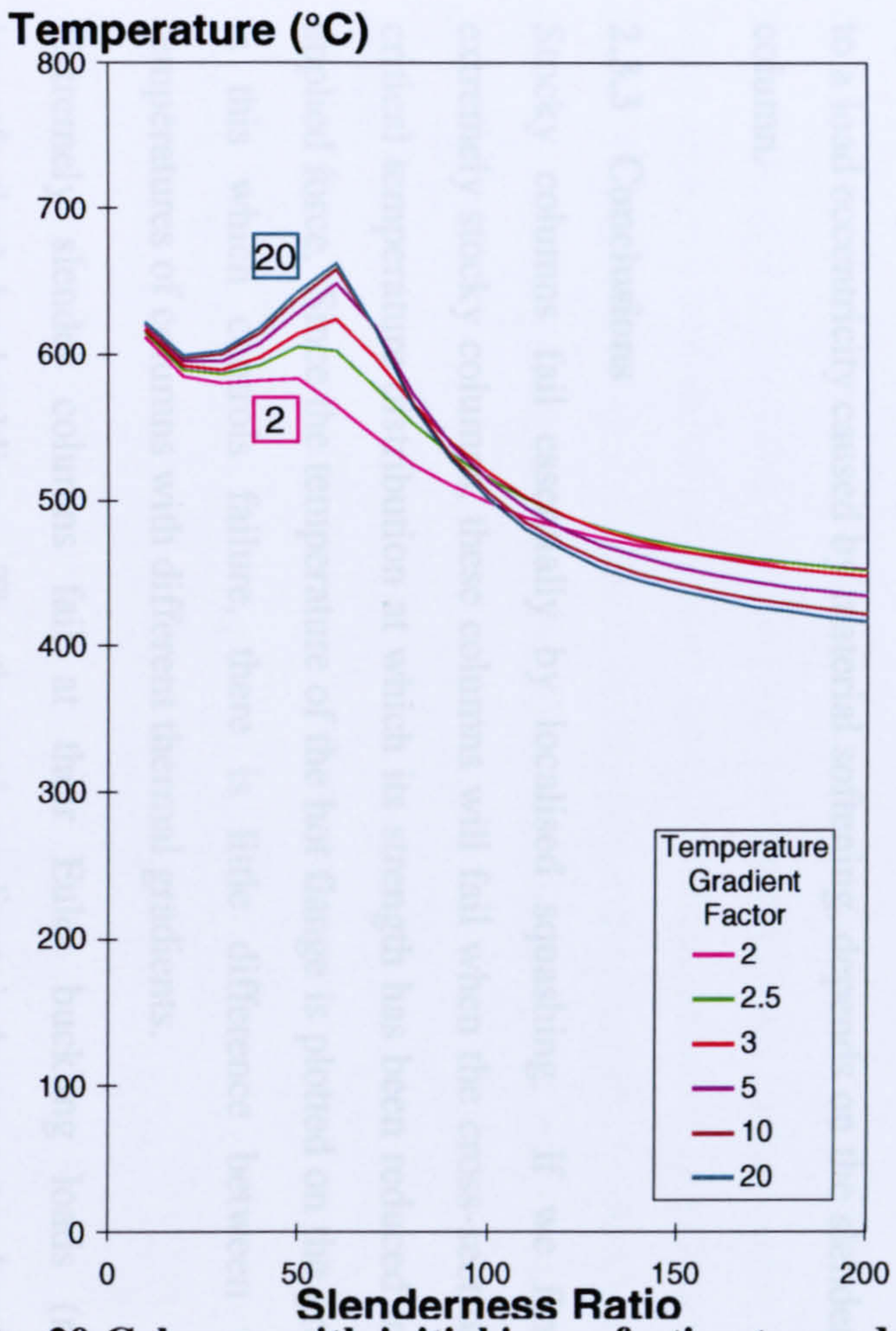

Fig. 20 Columns with initial imperfection towards fire

These curves show that the presence of thermal gradients can cause columns to fail by buckling about their major axes. Whether this occurs due to thermal bowing, or to a load eccentricity caused by material softening, depends on the slenderness of the column.

2.3.3 Conclusions

Stocky columns fail essentially by localised squashing. If we first consider extremely stocky columns, these columns will fail when the cross-section reaches a critical temperature distribution at which its strength has been reduced to below the applied force. Since the temperature of the hot flange is plotted on the graphs, and it is this which controls failure, there is little difference between the failure temperatures of columns with different thermal gradients.

Extremely slender columns fail at their Euler buckling loads (reduced by imperfection) by buckling. The thermal gradient induces extra bending in the column towards the hot flange, since this expands more than the cold flange and becomes the outer face of the curve. This can result in the column's major-axis resistance actually becoming weaker than its minor axis resistance. The higher the temperature gradient, the more thermal-bowing is induced and the sooner the column will fail.

As the column slenderness decreases, its Euler buckling load increases and so the failure temperature increases, as can be seen on the graphs. As the column reaches higher temperatures, the flanges begin to soften. Since the temperature of the hot flange is plotted on the graph, columns with a high thermal gradient will be at lower average temperature, and so will appear to survive longer.

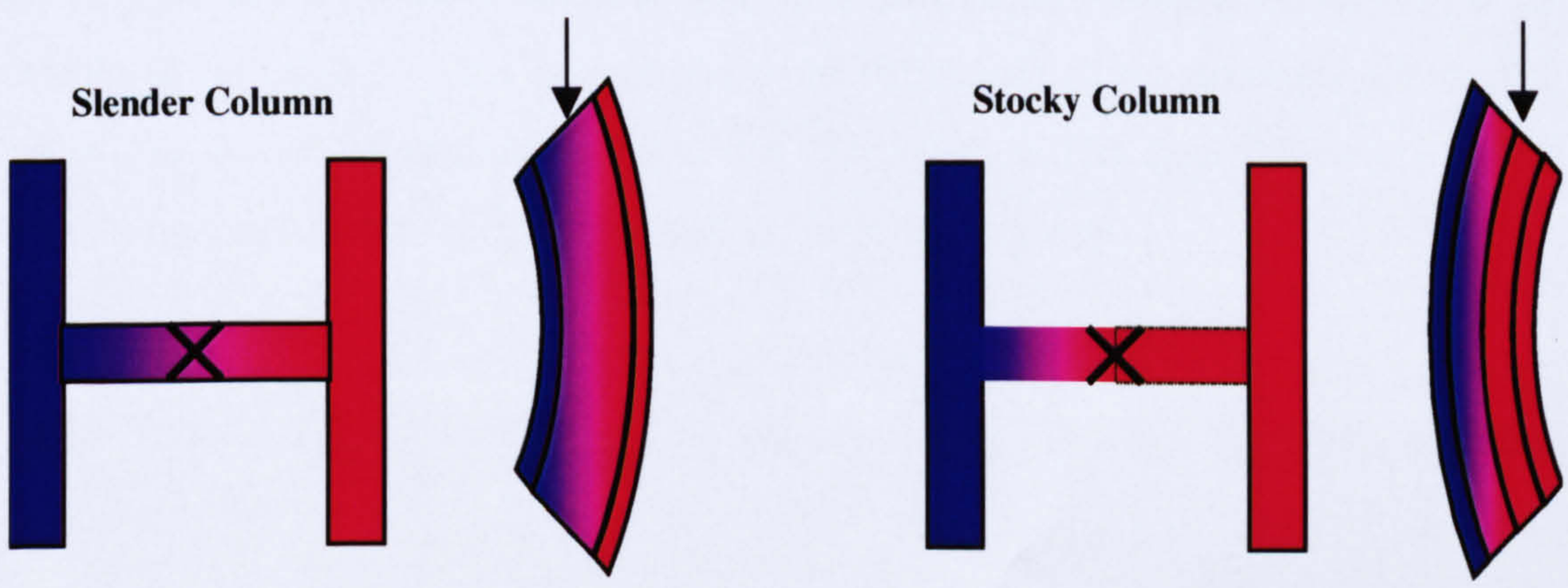

Fig. 21 Failure of columns on slender- and stocky-side of peak

Since VULCAN applies the load at the centre of the web, an eccentricity between the lines of action of the applied force and the internal resultant force is introduced when the hot flange becomes much softer than the cold flange. At very high temperatures, the hot flange is so soft that its effect can be neglected and so the load is effectively being applied a half-depth away from the cool flange, which is in effect, supporting the load. This causes the column to bend back and eventually to buckle away from the fire. This explains why the strains in the hot flange of these columns reverse direction.

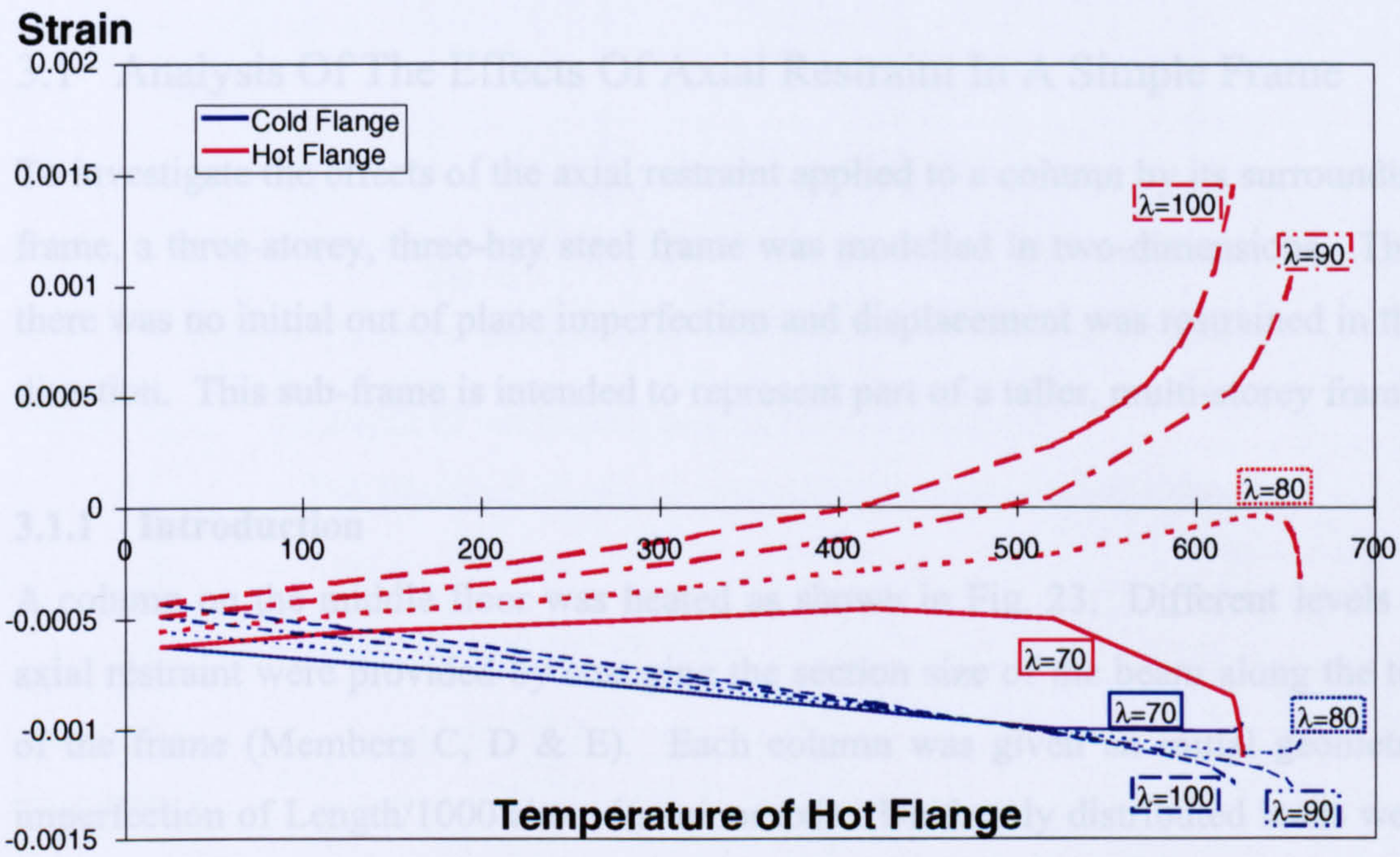

Fig. 22 Strain in thin-webbed columns with no initial imperfection and temperature gradient factor 10

3 Initial Investigation Into Frame Restraint

It has been shown[13,43] that a number of factors effect the behaviour of steel frames in fire. This chapter looks in particular at axial restraint and compares analyses of sub-frames with analyses of isolated members combined with restraining spring elements. In this way, an understanding of the way results from furnace tests on isolated members can be extrapolated to explain the behaviour of frames can be gained.

3.1 Analysis Of The Effects Of Axial Restraint In A Simple Frame

To investigate the effects of the axial restraint applied to a column by its surrounding frame, a three-storey, three-bay steel frame was modelled in two-dimensions. Thus there was no initial out of plane imperfection and displacement was restrained in this direction. This sub-frame is intended to represent part of a taller, multi-storey frame.

3.1.1 Introduction

A column on the middle floor was heated as shown in Fig. 23. Different levels of axial restraint were provided by changing the section size of the beam along the top of the frame (Members C, D & E). Each column was given an initial geometric imperfection of Length/1000 about its minor axis. Uniformly distributed loads were applied along every beam and additional loads superimposed at the top of each column to give a multiple of the design load according to BS5950[11].

The Relative Restraint Factor α defines the ratio of the axial restraint stiffness provided by the frame K_s to the axial stiffness of the heated column K_c. This is actually produced by the cumulative end-shear stiffnesses of beams A, B, C & D as calculated in Table 1. This ignores the axial stiffnesses of the columns above and below the heated column, since these are very much stiffer than the beams. The relative restraint factor can be expressed in the following way.

$$\alpha = \frac{K_S}{K_C} = \frac{12\,\mathrm{E}\sum_{\mathrm{A,B,C\&D}} I \Big/ L_S^3}{EA_C \Big/ L_C} = \frac{12L_C \sum_{\mathrm{A,B,C\&D}} I}{L_S^3 A_C} \qquad (16)$$

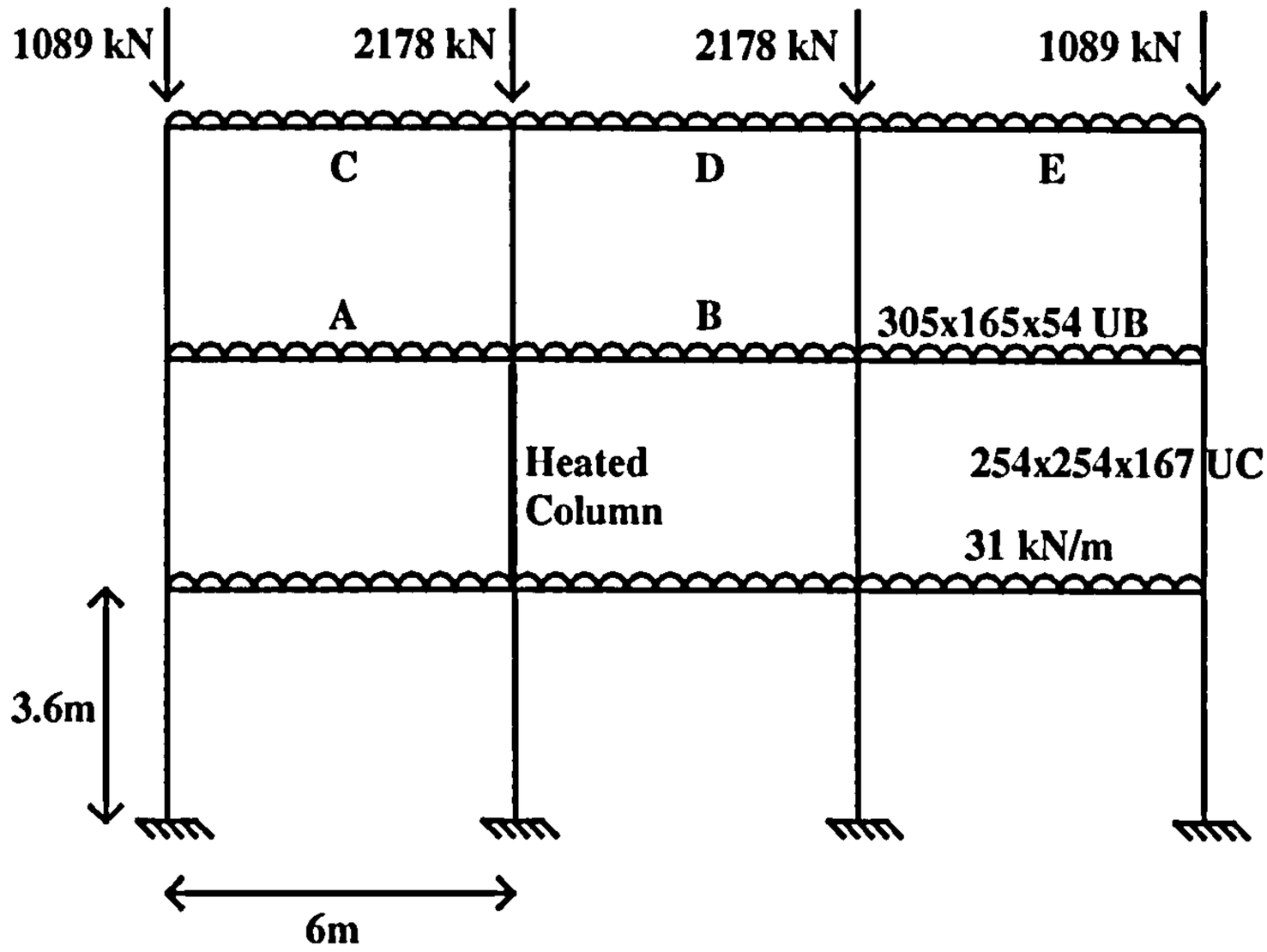

Fig. 23 Plane frame used for analysis of 0.6 x design load case

where $L_{s/c}$ = Length of restraining beams / heated column

$I_{s/c}$ = 2nd Moment of area of restraining beams / heated column

A_c = Area of column

E = Young's modulus of steel

$$\text{in which } K_s = \frac{12EI_s}{L_s^3} = \frac{12E\sum_{A,B,C\&D} I}{L_s^3} \text{ and } K_c = \frac{EA_c}{L_c} \tag{17}$$

3.1.2 Results

Two load cases were analysed for each of 13 relative restraint factors. In the first case, the column has a load ratio of 0.6 and in the second of 0.7. Table 1 shows the cases analysed and the corresponding results in terms of failure temperatures. The resulting failure temperatures are plotted against restraint factor on Fig. 24, showing that a larger amount of axial restraint leads to a higher failure temperature. In interpreting these failure temperatures, it should be noted that they represent the temperatures at which the analysis terminated. This is not equal to the physical failure of the column, although a qualitative indication can be deduced. The vertical displacement of the top of the heated column is shown on Fig. 25 and the ends of the curves indicate the temperatures at which the analyses terminated. The axial force in the heated column is plotted on Fig. 26.

Frame Set-up		*Failure Temperature (°C)*	
Restraint Factor	**Top Beam Section**	**0.6 Load**	**0.7 Load**
0.004	305 x 165 x 54	606.4	575.8
0.00735	406 x 178 x 74	611.2	579.3
0.0089	457 x 152 x 82	614.8	582.0
0.0165	533 x 210 x 122	630.9	597.1
0.031	610 x 305 x 179	654.5	619.9
0.0407	610 x 305 x 238	672.9	637.7
0.047	762 x 267 x 197	671.7	637.1
0.0548	838 x 292 x 194	677.0	642.0
0.0635	914 x 305 x 201	684.6	649.1
0.0731	914 x 305 x 224	697.5	661.1
0.0844	914 x 305 x 253	716.2	676.0
0.097	914 x 305 x 289	743.4	693.9
0.138	914 x 419 x 388	950^{+}	815.0

Table 1 Failure temperatures of frames with top beam details

As can be seen from these graphs, a case with low axial restraint expands as the temperature rises but little change of axial force is induced into the column. At around 500°C the column has softened sufficiently to be pushed back by the load and by 600°C it has returned to its original length. In fact, every restraint case returns to its original length at the same temperature, and the curves on Fig. 25 can be seen to cross through a single point. This is to be expected since, when at their original length, the columns do not exert a force on the restraining beams above, and no restraint force is being exerted on the column by the beams above. Thus the extra displacement caused by thermal expansion has been exactly compensated for by contraction due to the material softening due to heating and the superstructure loading. These two factors are independent of the restraint stiffness, and so since the restraint is not brought into play, the temperature at which this occurs is also independent of the restraint stiffness.

Once shorter than its original length, more and more load is being supported by the beams above the column as it shortens. Eventually, too much load is supported by the top beam, causing it to yield and the frame fails.

In effect, this crossover point signifies the boundary between the two types of action. At lower temperatures, the restraint can be seen as detrimental, since the column pushes against the restraining beams, inducing an extra axial force. At higher temperatures, the restraint can be seen as beneficial, since the restraining beams support the column by a bridging action.

Cases with more axial restraint allow the column to expand less as the temperature rises, inducing greater change of axial force in the heated column. Again, by 600°C the column has softened sufficiently to return to its original length, and once shorter than this, the load is supported largely by the top beam.

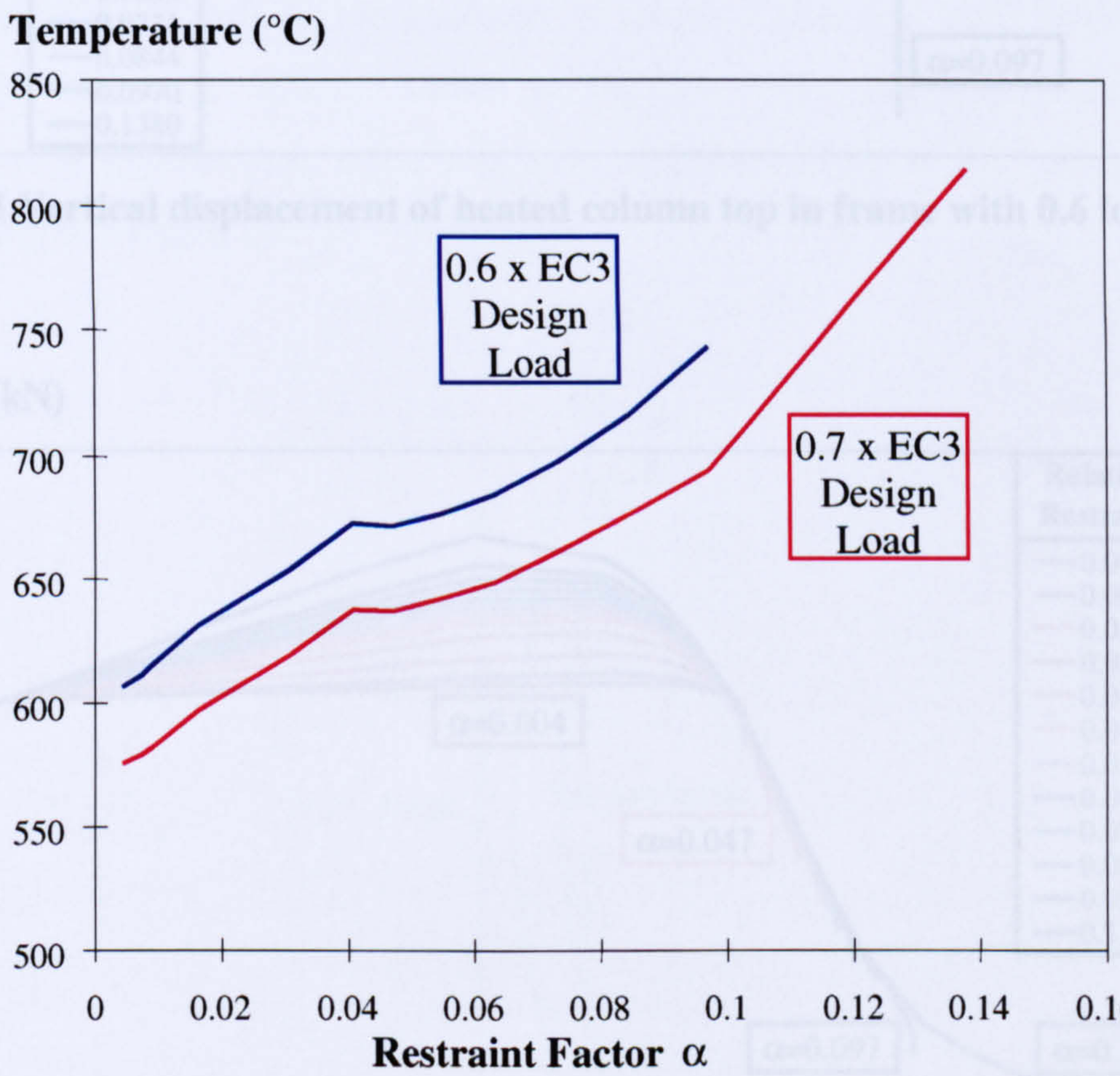

Fig. 24 Failure temperature of restrained columns

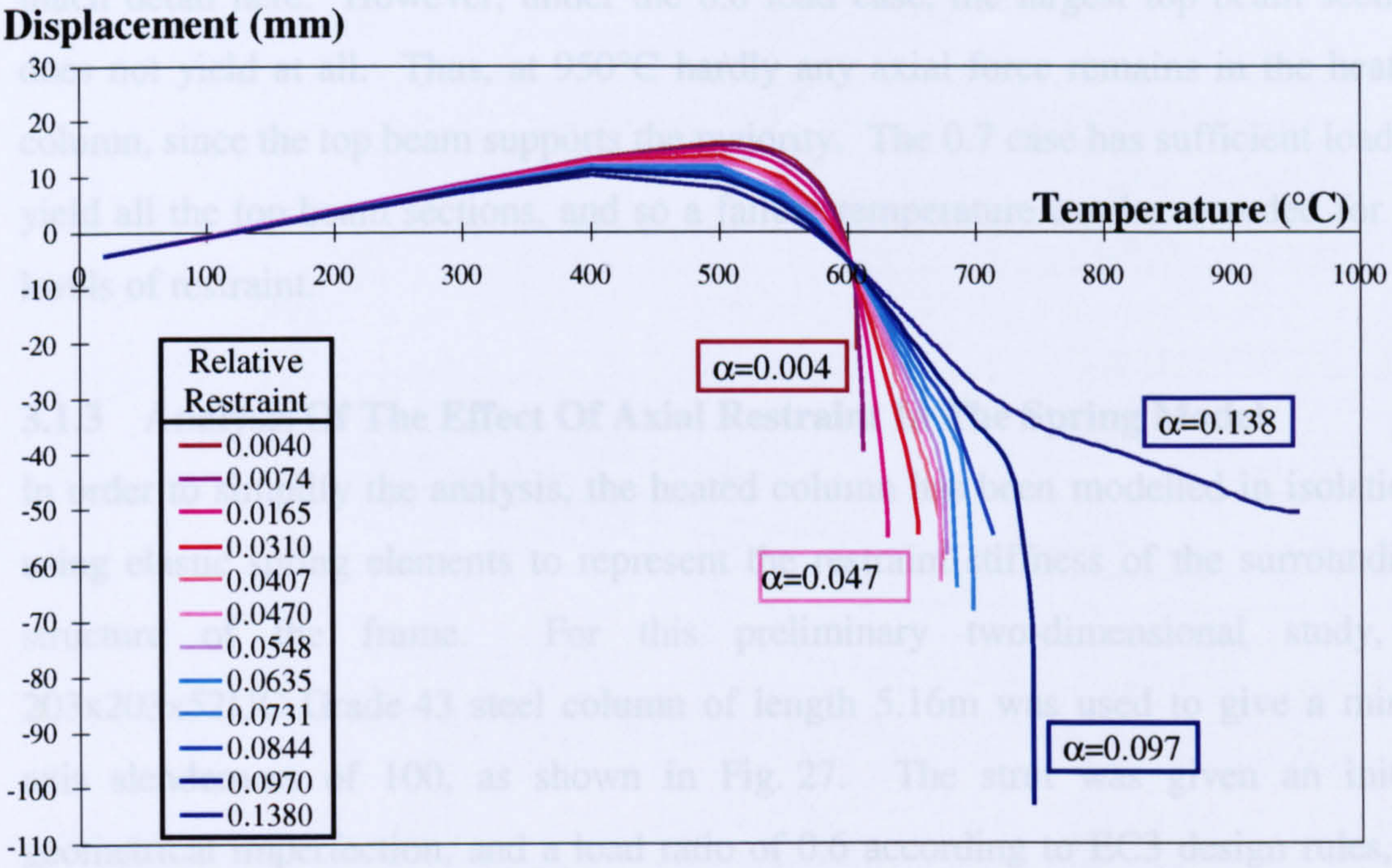

Fig. 25 Vertical displacement of heated column top in frame with 0.6 load ratio

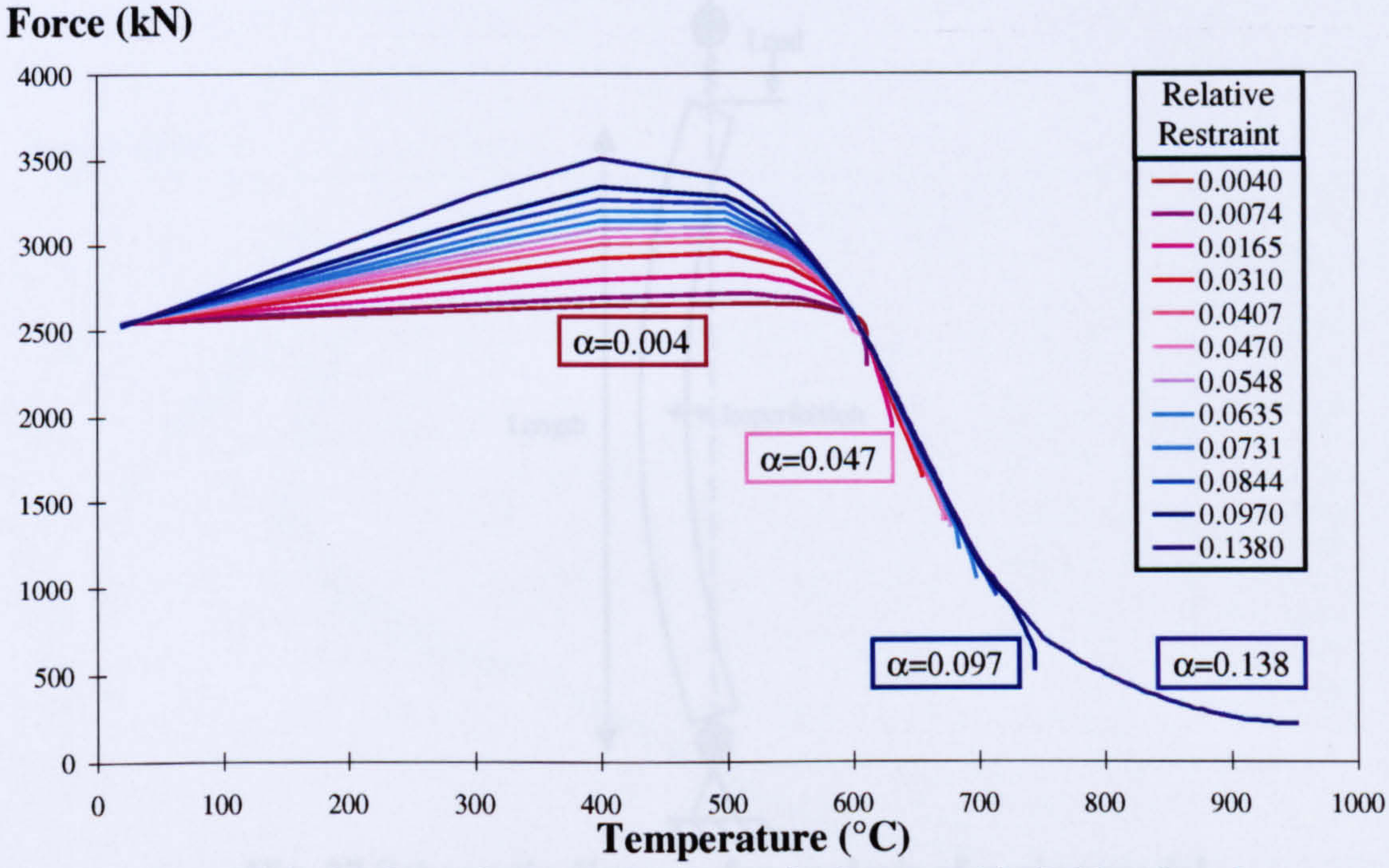

Fig. 26 Axial force in heated column in frame with 0.6 load ratio

To provide high values of axial restraint, large section sizes are used for the top beam. These large sections support a much higher column force before yielding, resulting in higher failure temperatures.

The two load cases behave very similarly, and so the 0.7 load case is not shown in as much detail here. However, under the 0.6 load case, the largest top beam section does not yield at all. Thus, at 950°C hardly any axial force remains in the heated column, since the top beam supports the majority. The 0.7 case has sufficient load to yield all the top beam sections, and so a failure temperature can be recorded for all levels of restraint.

3.1.3 Analysis Of The Effect Of Axial Restraint In The Spring Model

In order to simplify the analysis, the heated column has been modelled in isolation, using elastic spring elements to represent the restraint stiffness of the surrounding structure of the frame. For this preliminary two-dimensional study, a 203x203x52UC Grade 43 steel column of length 5.16m was used to give a minor axis slenderness of 100, as shown in Fig. 27. The strut was given an initial geometrical imperfection, and a load ratio of 0.6 according to EC3 design rules, as described in Section 1.3.

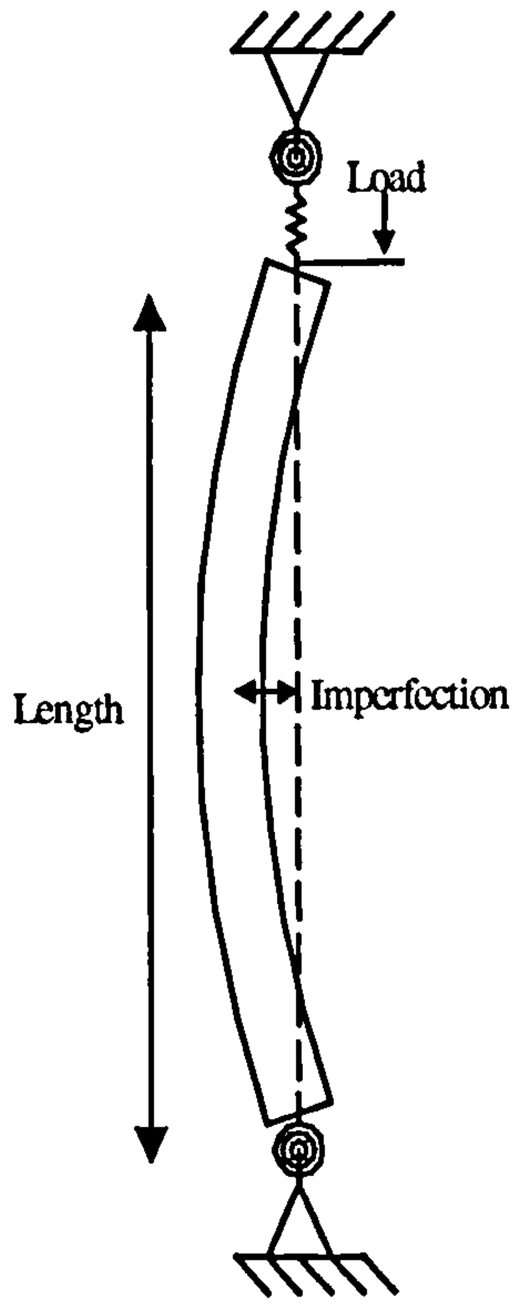

Fig. 27 Schematic diagram for analysis of spring model

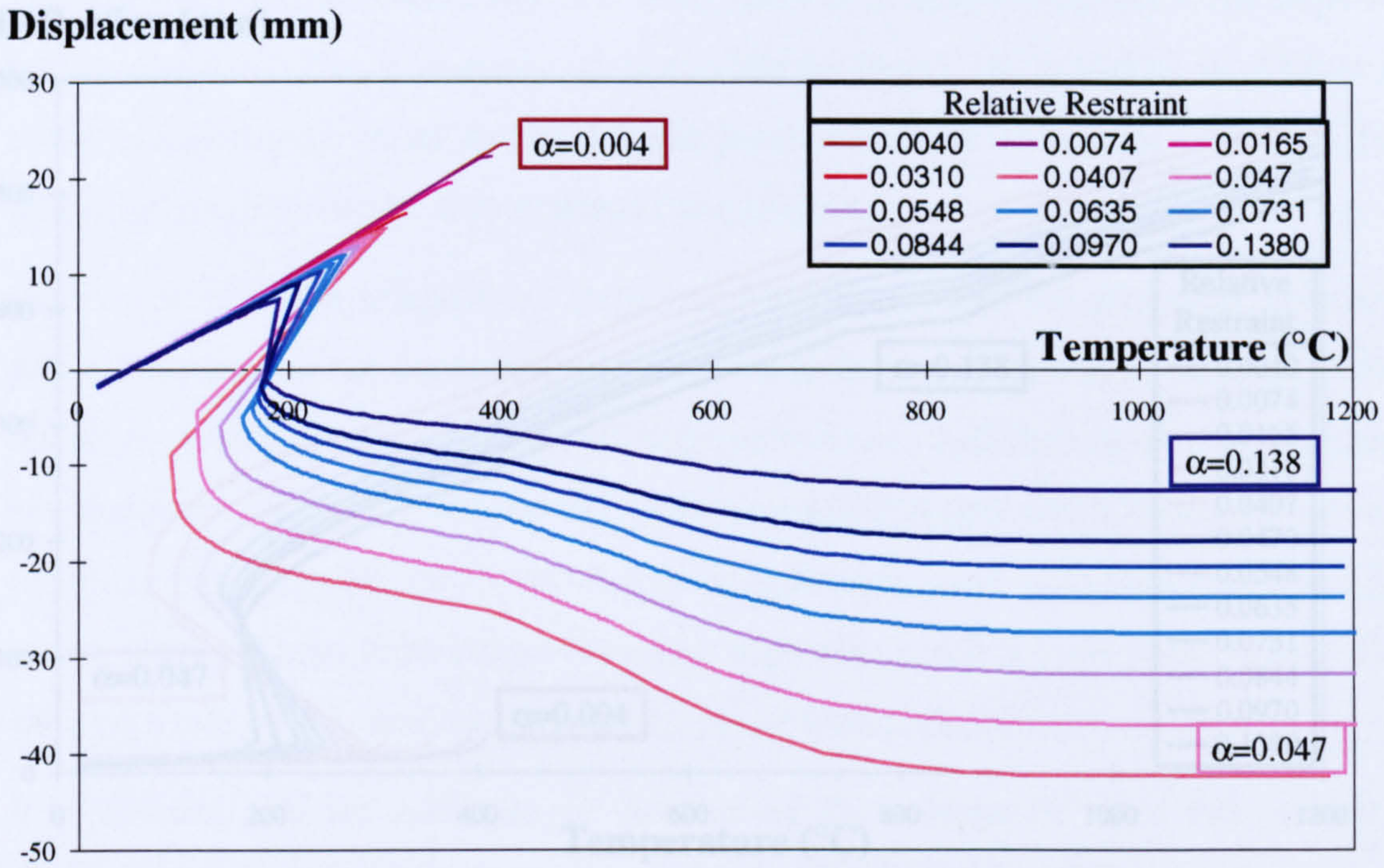

Fig. 28 Axial displacement of top of heated column of spring model

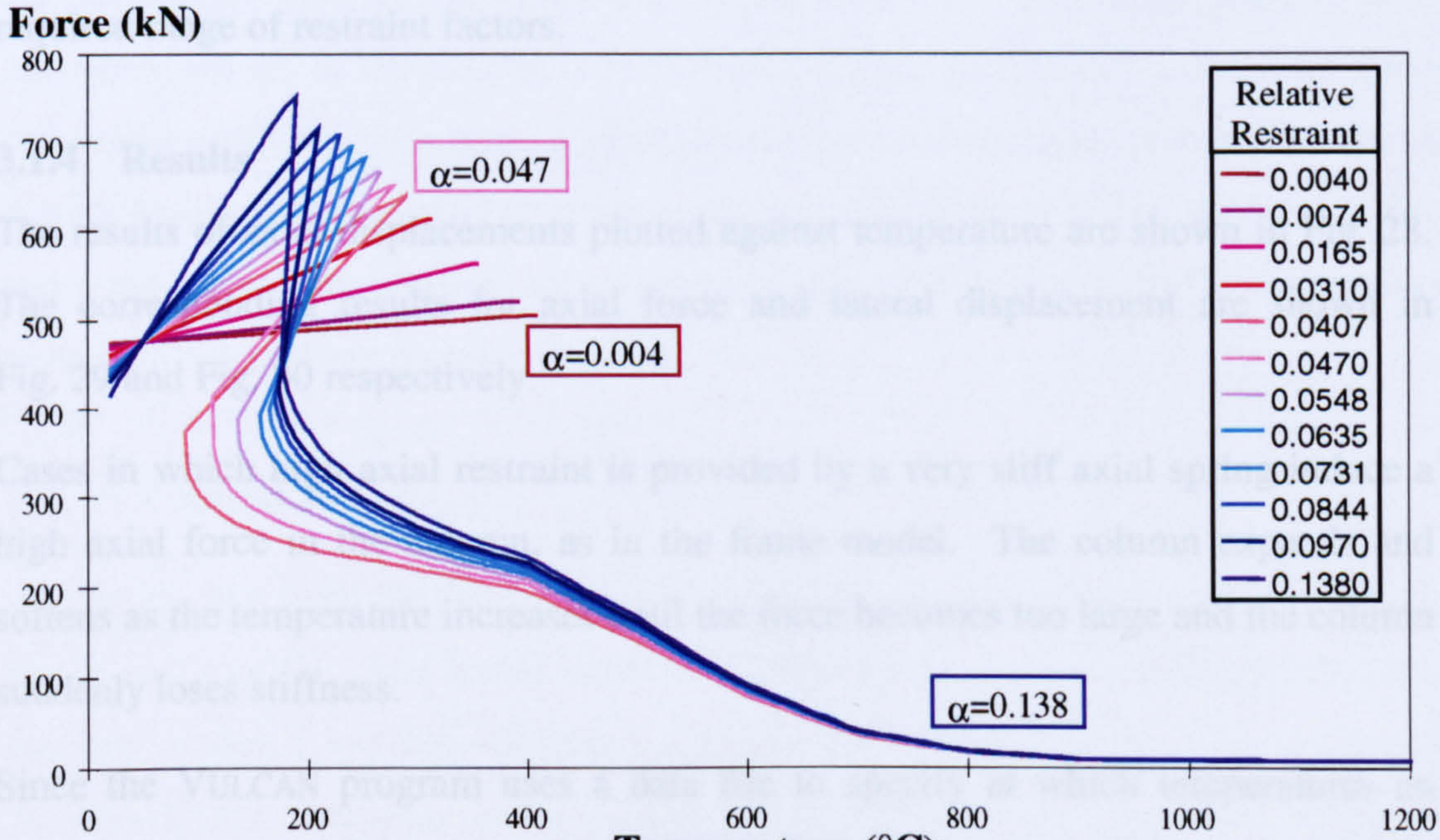

Fig. 29 Axial force in heated column of spring model

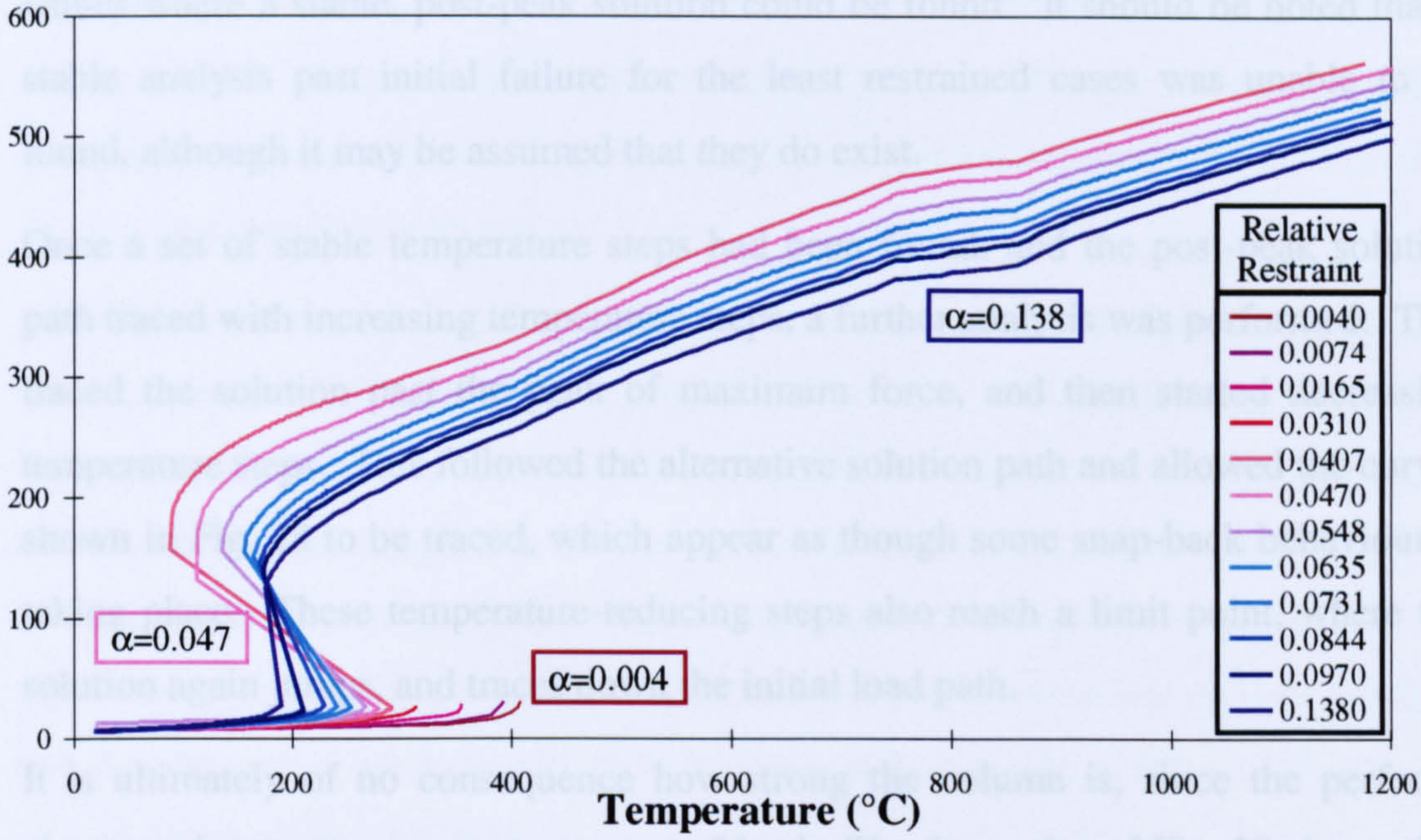

Fig. 30 Minor axis deflection of heated column of spring model

A rotational spring element was placed at each end to represent a pin-ended column. In addition, a purely elastic axial spring was placed at the same end of the column as the applied load. The elastic stiffness of this axial spring was varied to give the required range of restraint factors.

3.1.4 Results

The results of axial displacements plotted against temperature are shown in Fig. 28. The corresponding results for axial force and lateral displacement are shown in Fig. 29 and Fig. 30 respectively.

Cases in which high axial restraint is provided by a very stiff axial spring induce a high axial force in the column, as in the frame model. The column expands and softens as the temperature increases until the force becomes too large and the column suddenly loses stiffness.

Since the VULCAN program uses a data file to specify at which temperatures an analysis is to be performed, a preliminary analysis had to be performed to trace the increasing force in the column. This analysis would then pass the point of maximum force and often jump to a stable solution, with the load largely supported by the spring in tension. The analysis would then continue to trace the shedding of load

from the column to the spring. The analysis around the point of maximum force was very unstable and trial and error had to be used in setting the temperature steps to values where a stable, post-peak solution could be found. It should be noted that a stable analysis past initial failure for the least restrained cases was unable to be found, although it may be assumed that they do exist.

Once a set of stable temperature steps had been found, and the post-peak solution path traced with increasing temperature steps, a further analysis was performed. This traced the solution past the peak of maximum force, and then started decreasing temperature steps. This followed the alternative solution path and allowed the curves shown in Fig. 28 to be traced, which appear as though some snap-back behaviour is taking place. These temperature-reducing steps also reach a limit point, where the solution again jumps, and traces down the initial load path.

It is ultimately of no consequence how strong the column is, since the perfectly elastic spring can support any amount of load. The force plot of Fig. 29 shows that the force in the column suddenly snaps back to a very small value and tails off towards zero as the temperature increases above this failure region. This idea is supported by the axial displacement plot of Fig. 28 in which the displacement suddenly snaps through the failure region and back down to a stable region. After this point, the top of the column only displaces slightly further due to the axial spring extending under the extra force applied, creating the reduction in force in the column. Cases that provide less axial restraint by having axial springs of low stiffness deflect more than the stiffer springs, which provide large axial restraint, as the temperature rises above the failure region.

3.2 Conclusions

As can be seen from the figures, there is a marked difference between the behaviour of the two models. The actual values of failure temperature are unimportant, since the two models have very different section sizes, effective lengths and rotational restraint levels. However, the general trend of columns with large restraint factors having higher failure temperatures no longer applies.

3.2.1 Effect Of Restraint

As the spring model indicates, the loads in a framed structure are, in essence, supported by two components in series. The first component is the relatively stiff column, which efficiently transfers loads to the ground. The second component is comprised of the beams, which frame into the column and support loads by bridging from the surrounding columns.

Since the column is arranged to support loads axially, it is much stiffer in the vertical direction than the framing beams, which act laterally. Thus, for a given super-imposed load, causing the beam- column junction to displace, the column supports a significantly larger proportion of this load. However, this column may begin to buckle, in which case the beams begin to support an increasing proportion of the super-imposed load. These beams may or may not yield, depending on their strength and the amount of load they have to support, and it is this which determines the overall failure of the structure.

In the case of fire in buildings, it is the degradation of material properties combined with the thermal expansion which initiates column buckling. As the temperature increases, the strength and stiffness of the column decreases, and thus the imbalance of stiffness between the beams and column starts to diminish. However, this effect is independent of the level of axial restraint present. At the same time, thermal expansion of the column pushes against the restraint, causing the axial force to increase. The rate of increase of this force depends upon the stiffness of the restraint, and therefore can be a more dominant effect than material degradation.

3.2.2 Beam Yielding

It must be noted that neither the frame nor spring models accurately represent the behaviour of a column in an axial restraint test rig of the type shown in Fig. 31 as used for the University of Ulster test programme. The test rig can impose axial restraint to an expanding column, but does not support the column once it becomes shorter than its original length. Therefore we would expect the test rig to behave in a similar fashion only whilst the column is longer than its original length. Once the column is shorter than this, the applied force begins to lift off the column in the model, and the results are no longer comparable.

There are two points during a fire at which the restraining beams may yield. During initial column heating, the beams resist the thermal expansion of the column. This reverses the sign of the moments at their remote ends and increases those at the ends attached to the heated column and it is feasible that the beams may yield under this scenario. However, this is unlikely, since considerable deflection is needed before any strain reversal takes place.

The more likely beam yielding mechanism will occur when the heated column has buckled and the beams cannot support a sufficient amount of the super-imposed load. This is the case identified in the frame model above. However, with a suitably braced frame design, this could occur long after the column has buckled using the inherent strength of the surrounding frame for fire engineering benefit.

4 Ulster Tests

As part of a joint research project involving the Universities of Ulster and Sheffield, a series of steel columns were furnace-tested at Ulster[41,44]. The test series included columns that were free to expand, as well as some which were subject to various levels of axial spring restraint. A typical test was modelled in great detail to give an indication of the parameters which are important when modelling columns of this type. Parametric studies were conducted to investigate the sensitivity of the analyses to various parameters.

4.1 Introduction

This section describes the configuration of the test rig in detail. For each test, a complementary programme of numerical analyses has been performed at Sheffield using the VULCAN software. Thus, this section also describes the models used and the assumptions made.

4.1.1 Description Of Tests

The test specimens were all 1.8m long and were 152x152x23UC, 178x102x19UB or 127x76x13UB sections giving a minor axis slenderness of 48, 75 or 98 respectively. The columns were instrumented with one axial displacement transducer at the top, one at the bottom and two lateral displacement transducers measuring minor axis deflections at mid-height. A schematic diagram of the test rig can be seen in Fig. 31.

There were four groups of thermocouples, two groups equally spaced on the top half of the column and two groups equally spaced on the bottom half as shown in Fig. 32. Each group comprised between five and seven thermocouples symmetrically placed around the column cross-section. Heat was provided by two gas burners situated at the bottom of the furnace, and various load levels were applied via two hydraulic rams at the top of the column.

The major design feature of the rig is the fact that the top of the column is free to move vertically by sliding along the threaded rods. The axial restraint stiffness was provided by two rubber springs on the bars, which were fixed in place with nuts after the initial load had been applied. The column itself was seated on two half-round bearings to provide simulate pinned supports, allowing only minor-axis rotation.

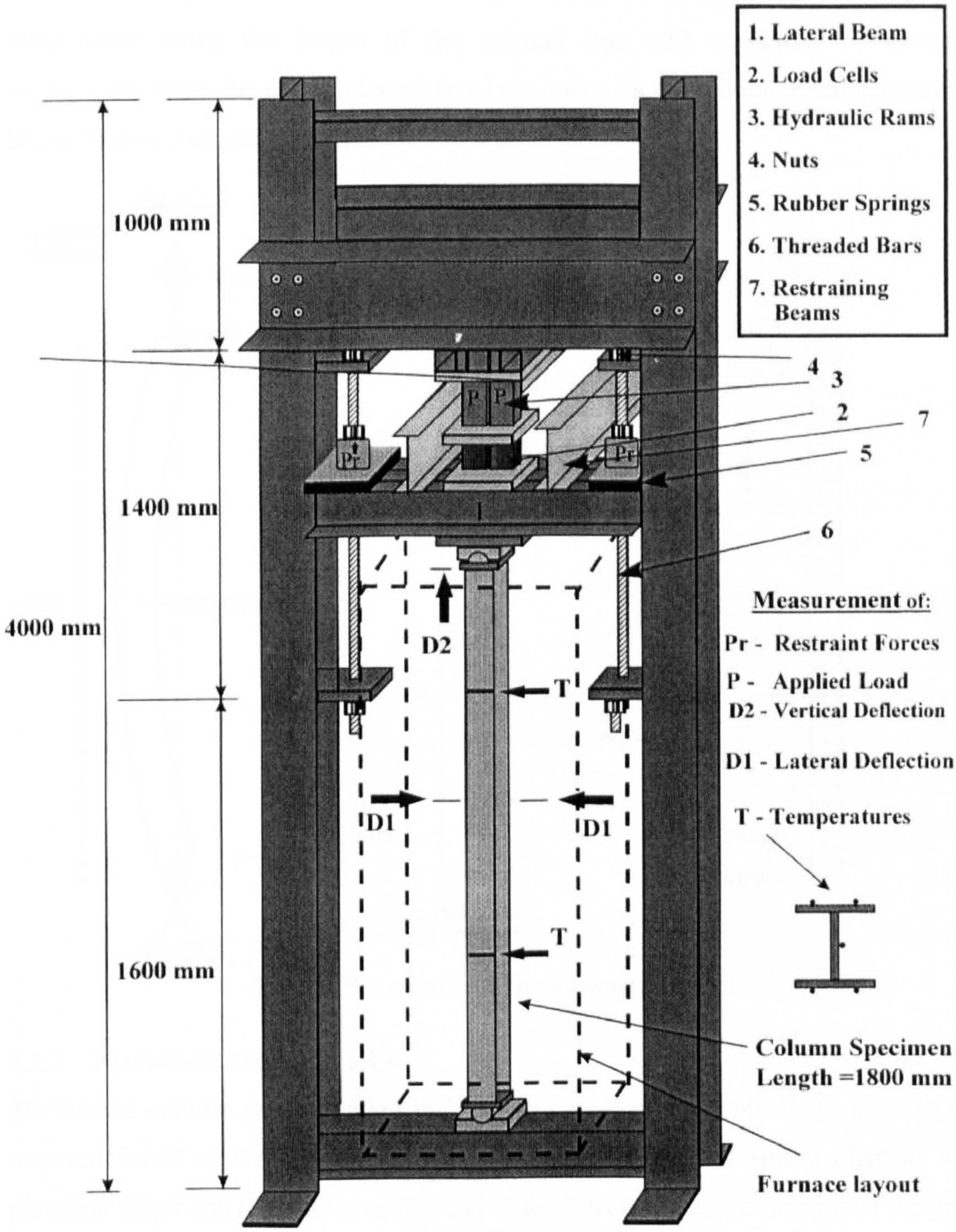

Fig. 31 Ulster test rig

The tests were conducted in two stages. Firstly, the columns were loaded in four steps, each applying one-quarter of the final load, with displacement readings being taken at each stage. When the entire load had been applied, the nuts were hand tightened on the threaded rods and the gas burners were ignited. Subsequent readings taken at 10- or 20-second intervals. For the purpose of this chapter, only the heating stage of the test will be considered.

The furnace exhaust flue was adjusted to minimise the temperature difference between the top and bottom of the furnace. However, since some variation in temperature along the length of the column was still expected, the average temperature along the column length has been taken as the reference temperature to be used when comparing results.

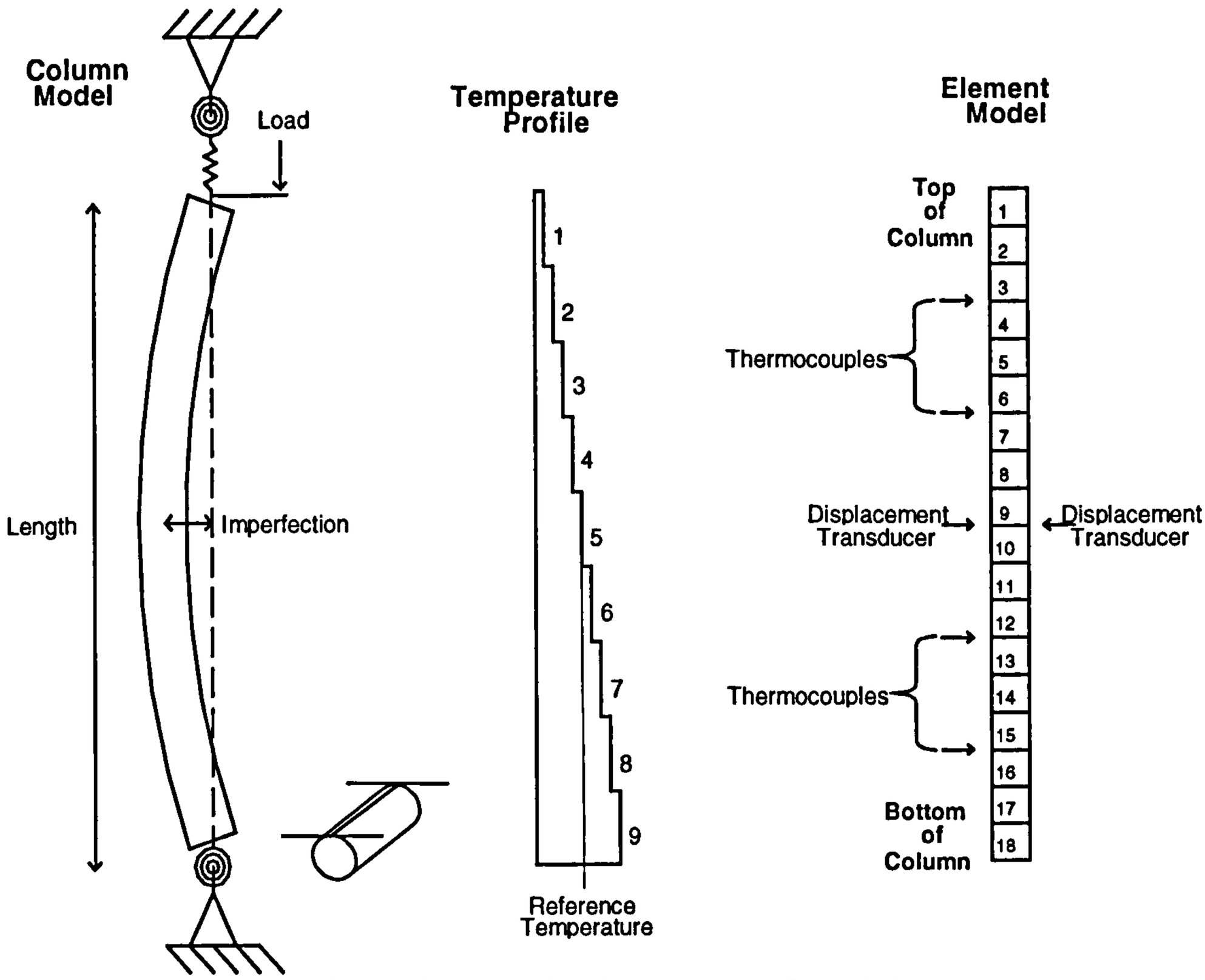

Fig. 32 Schematic of the assumed model

4.1.2 Numerical Model Details

The heated column was modelled in VULCAN using spring elements to provide the required levels of rotational and axial restraint. A rotational spring element was placed at either end to allow investigation of the effects of support friction at the ends of a pin-ended column. In addition, a purely elastic axial spring was placed at the same end of the column as the applied load. The elastic stiffness of this axial spring was varied, to simulate the various levels axial restraint provided by the test rig. This is shown in Fig. 32. The column was modelled using 18 equally sized elements. A temperature profile of nine steps was defined to represent the temperature gradient along the length of the column. Temperature steps 2 and 8 were matched with the temperatures given by the thermocouples in the test, with the other temperature steps

interpolated to give a constant temperature gradient along the column between thermocouple sites.

4.2 Initial Parametric Studies

This section investigates the sensitivity of the analyses to some basic physical variables. The effect of each parameter is assessed against a standard set of assumptions.

4.2.1 Basic Test Comparison

In order to model these tests, a number of assumptions have to be made about the material properties of the test columns. A parametric study of a typical unrestrained test has been conducted to determine the sensitivity of the model to a number of variables. Thus, a 0.2 x EC3 design load, applied to a 178x102x19UB section with no axial restraint was analysed. The temperature readings from the test are shown as solid lines in Fig. 33. For the purpose of analysis, the temperature across a cross-section was assumed constant and taken as the average of the thermocouple readings at this position. This ensures that no extreme temperature gradients are introduced, so the effects of the parameters can be studied without complications. Since VULCAN refines its temperature steps using bisection when near the region of failure, linear changes in temperature have to be assumed in this range. The temperature profiles assumed for the analysis are shown as the dotted lines on Fig. 33 and these assumptions mean that precise correlation with the results from the test is not expected. The measured test column displacements have been plotted against average temperature in Fig. 34.

Some of the other test columns have not been tested to determine their yield strength or Young's modulus, so nominal values have to be assumed, and the sensitivity assessed. Initial column imperfection was measured by placing the column in a frame and using a slide-vernier mounted on a track. In this case, the imperfection amplitude was found to be 0.21mm, but since there are inherent difficulties in measuring this, a nominal imperfection of Length/1000 has also been analysed. The physical dimensions of the section have also been measured and found to differ from those given in standard section tables so both have been analysed to determine whether this is significant.

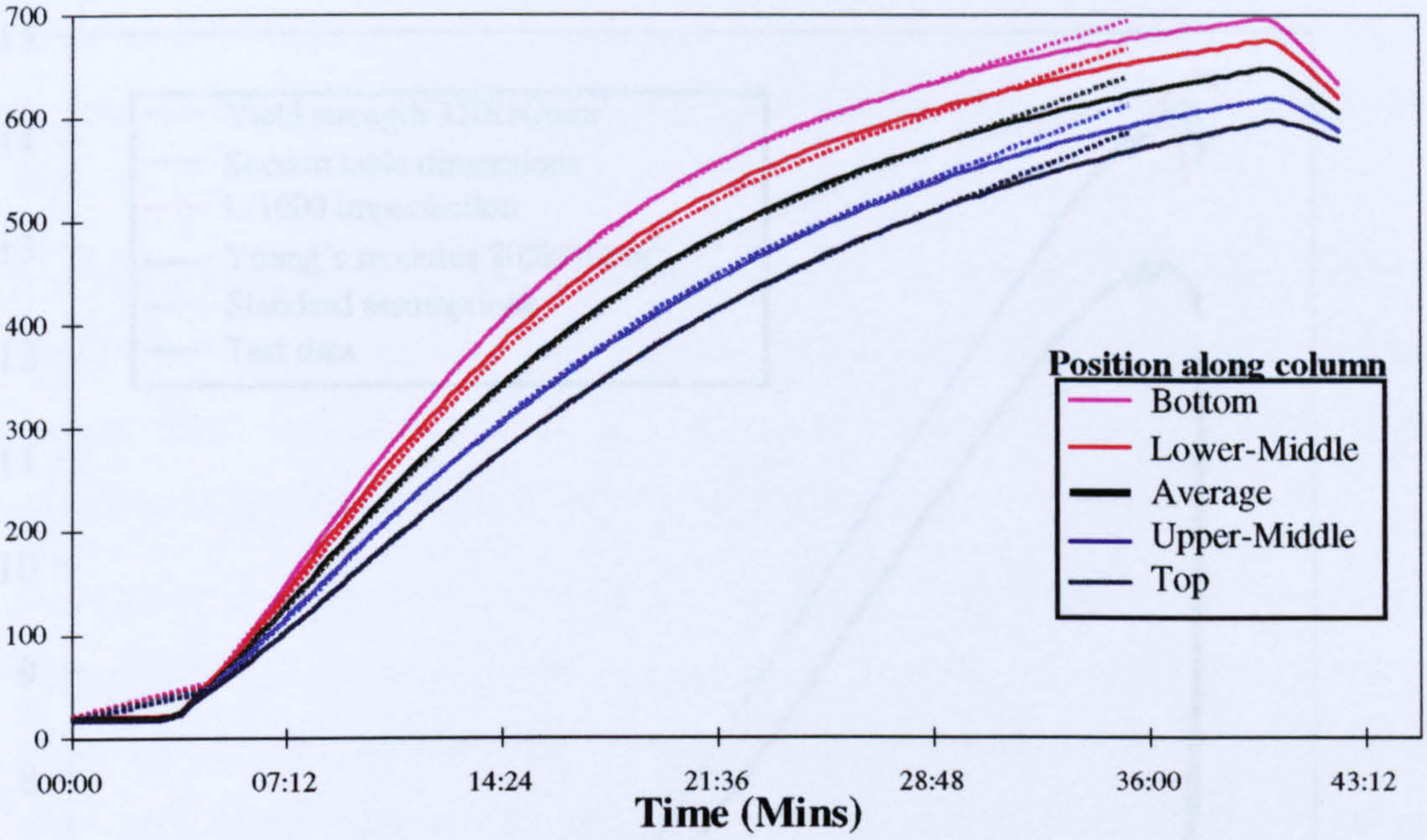

Fig. 33 Temperature along the length of the column

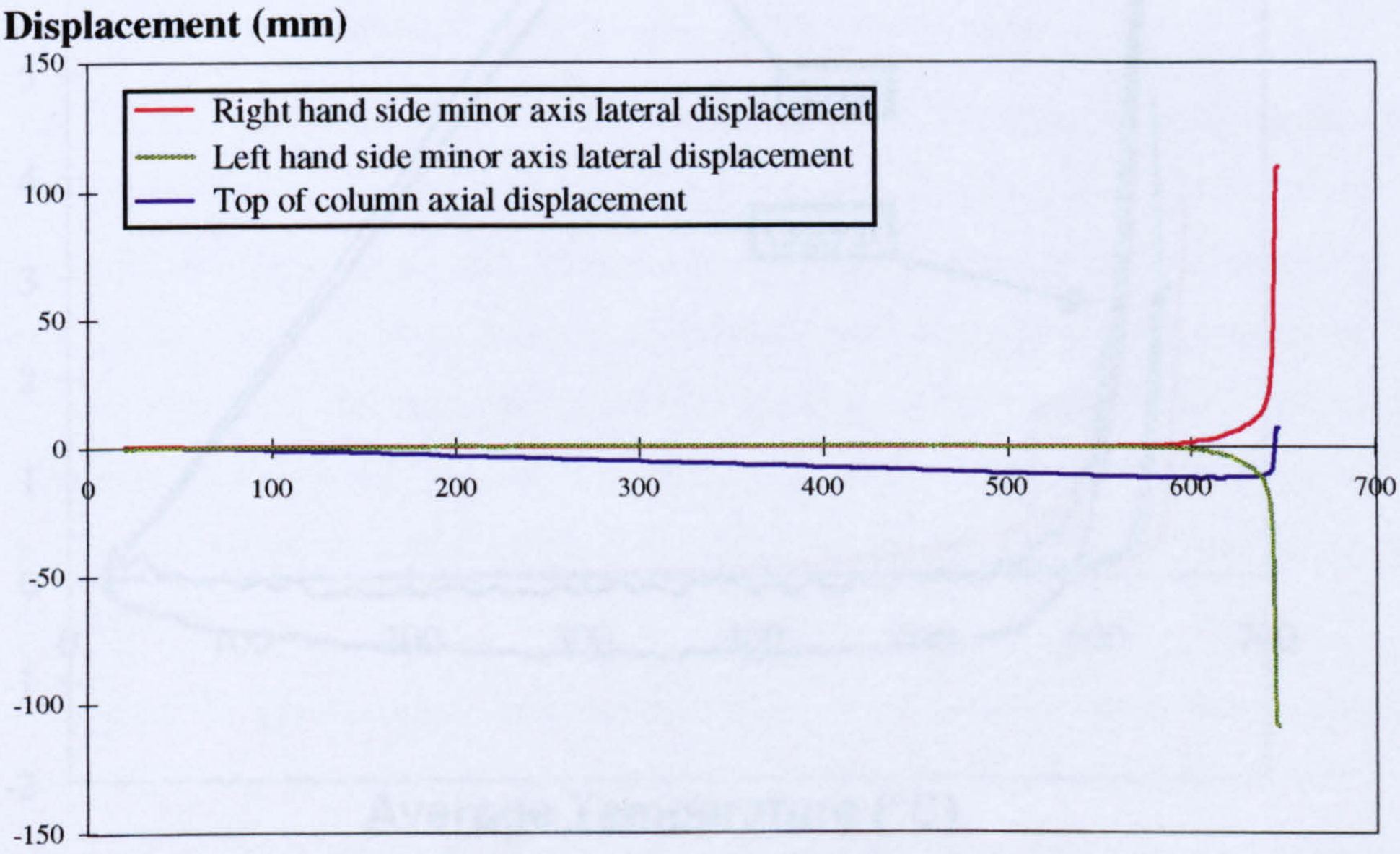

Fig. 34 Displacement of test column during heating

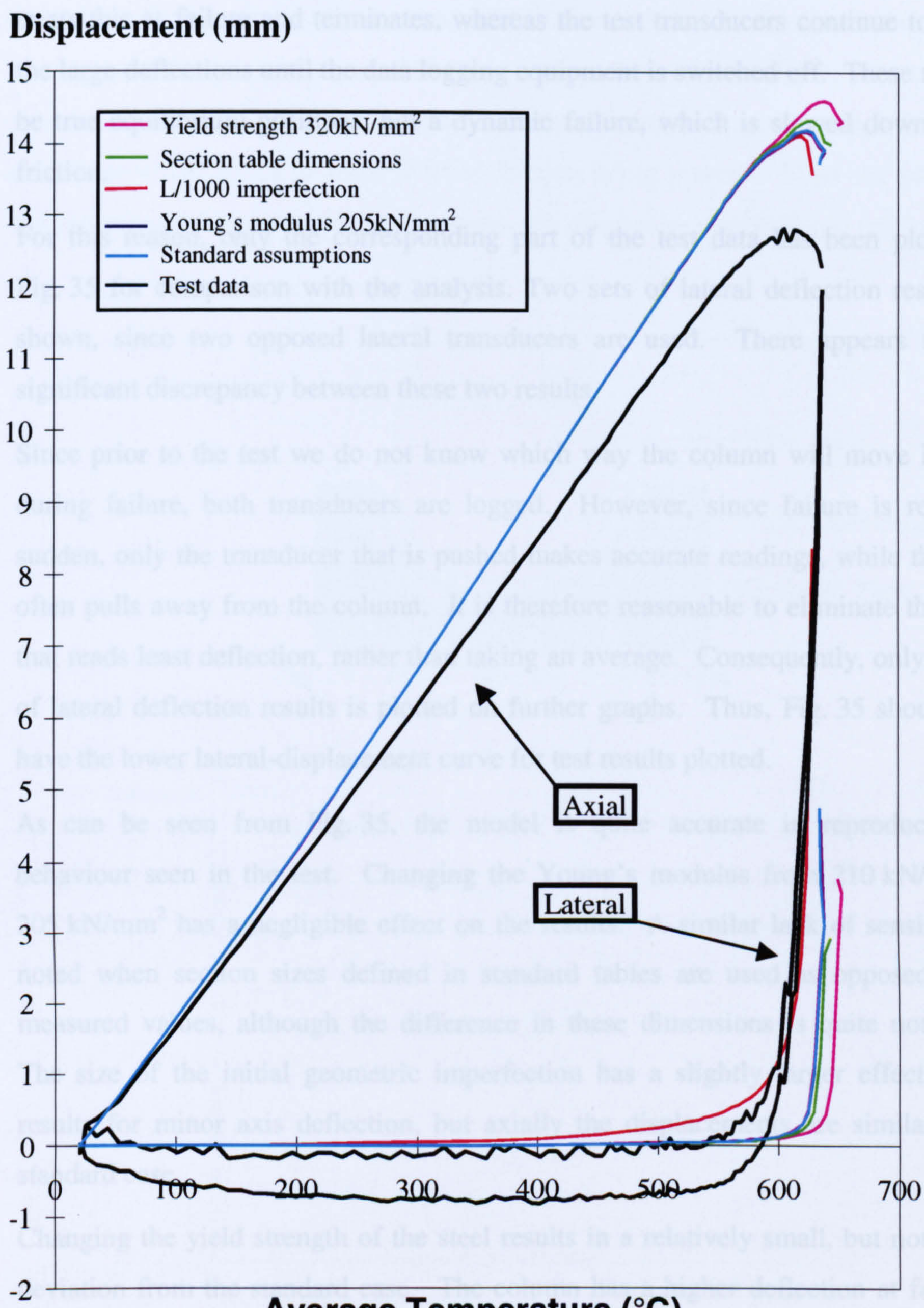

Fig. 35 Displacement of model columns with different material properties

The effects that these various material properties have on the analysis are shown on Fig. 35. Each case plotted is a variation on the standard analysis of a column with 0.21-mm imperfection using measured section sizes, yield strength of 275kN/mm^2 and Young's modulus of 210kN/mm^2. In no case does the analysis show deflections as large as those eventually shown by the test. This is because the column has lost nearly all of its stiffness at this stage and begins to deflect very rapidly. The program

treats this as failure and terminates, whereas the test transducers continue to record the large deflections until the data logging equipment is switched off. These may not be true equilibrium positions, but a dynamic failure, which is slowed down due to friction.

For this reason, only the corresponding part of the test data has been plotted on Fig. 35 for comparison with the analysis. Two sets of lateral deflection results are shown, since two opposed lateral transducers are used. There appears to be a significant discrepancy between these two results.

Since prior to the test we do not know which way the column will move laterally during failure, both transducers are logged. However, since failure is relatively sudden, only the transducer that is pushed makes accurate readings, while the other often pulls away from the column. It is therefore reasonable to eliminate the curve that reads least deflection, rather than taking an average. Consequently, only one set of lateral deflection results is plotted on further graphs. Thus, Fig. 35 should only have the lower lateral-displacement curve for test results plotted.

As can be seen from Fig. 35, the model is quite accurate in reproducing the behaviour seen in the test. Changing the Young's modulus from 210 kN/mm^2 to 205 kN/mm^2 has a negligible effect on the results. A similar lack of sensitivity is noted when section sizes defined in standard tables are used as opposed to the measured values, although the difference in these dimensions is quite noticeable. The size of the initial geometric imperfection has a slightly larger effect on the results for minor axis deflection, but axially the displacements are similar to the standard case.

Changing the yield strength of the steel results in a relatively small, but noticeable, deviation from the standard case. The column has a higher deflection at failure in this case, and this occurs at a higher temperature than previously seen. In cases when the yield strength of the steel used in the test is not known, a value of 275 kN/mm^2 will be assumed for analysis. All the other parameters referred to appear to have little effect on the failure temperature, so the standard set of parameters is used.

4.2.2 Effects Of Rotational Restraint

Because of the way in which the test rig supports the column, which is shown on Fig. 36, it seemed important to investigate the effects of some rotational restraint on

the column's behaviour. This restraint is introduced due to friction between the bearings and the graphite tape. Although the tape is unaffected by any heat which may be transferred to through the base-plate from the hot column, the high levels of axial force could result in some level of friction being present. Since the previous analysis assumed that no friction is present, this may be an inaccuracy in our model.

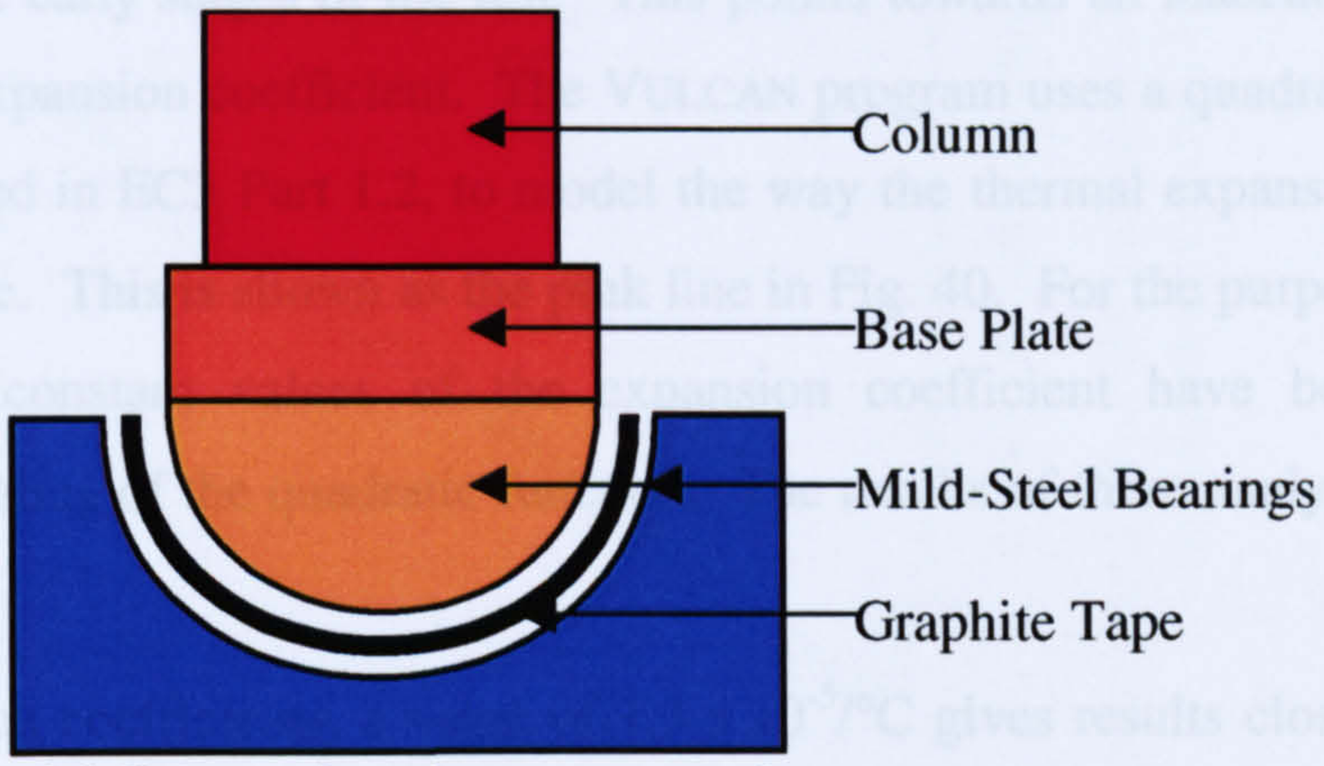

Fig. 36 Column bearing cross-section

Fig. 37 Moment-rotation models

The effect, of even fairly minor frictional moments at the ends, is to reduce a column's effective length near to its buckling load, and this could thus have a significant strengthening effect. As well as analysing the effects of a constant value of rotational restraint, a bilinear model was used. This more accurately represents frictional effects, since friction resists rotation until it is overcome, after which point the change in resistance is smaller and the force effectively constant. These models are described in Fig. 37. The effects produced by these levels of rotational restraint

are shown in Fig. 38, from which it is very clear that this does not have a major effect on the collapse behaviour in this case.

4.2.3 Effects Of Thermal Expansion

The major discrepancy between experimental results and analysis in Fig. 35 is in the axial displacement in the early stages of the test. This points towards an inaccurate assumption of thermal expansion coefficient. The VULCAN program uses a quadratic function, which is defined in EC3 Part 1.2, to model the way the thermal expansion changes with temperature. This is shown as the pink line in Fig. 40. For the purpose of this study, various constant values of the expansion coefficient have been analysed, as well as a scaling of the quadratic function. The results of these analyses are shown in Fig. 39.

Of the constant expansion coefficients, a value of 1.3×10^{-5}/°C gives results closest to those of the test. However, the results suggest the value of the expansion coefficient does in fact change with temperature. In the lower temperature range, the analysis using a constant expansion coefficient shows deflections larger than those recorded in the test. However, when the temperatures approach the failure region, the deflections are lower than those recorded in the test.

The case where the thermal strain represented by the quadratic function has been scaled by 92% gives the best overall match with the test data. It consistently shows deflections in line with those of the test and is close to the test deflections at failure. This consistent correlation indicates that the test column expands in a similar way to that assumed in EC3 Part 1.2, although to a slightly lesser degree.

British Steel has performed a series of experiments to determine the expansion coefficient for Grade 43 steel at elevated temperatures[6] and these values are shown in Table 2. Linear interpolation is suggested to determine intermediate values. These results have been plotted on Fig. 40 for comparison with the EC3 values.

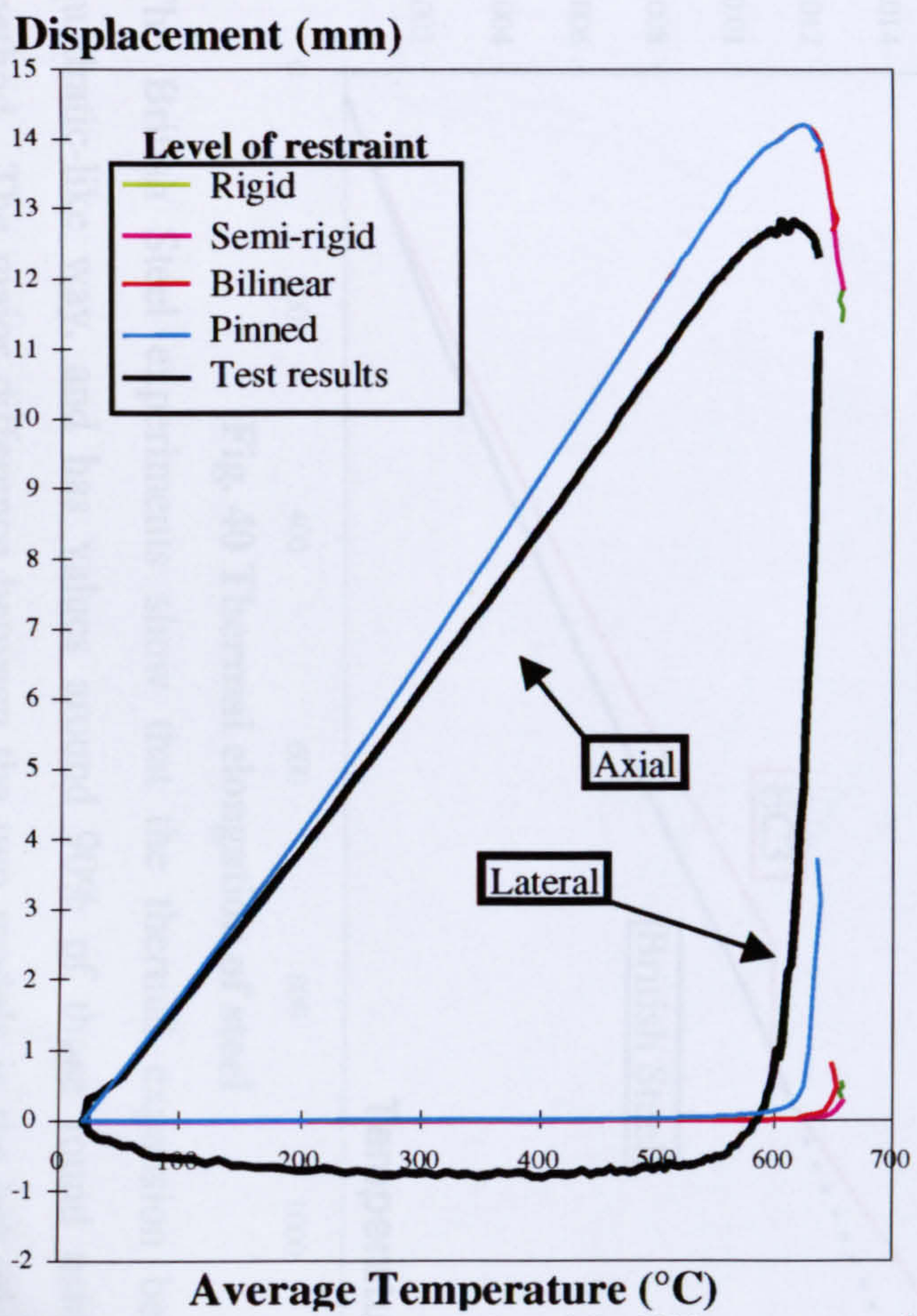

Fig. 38 Displacement of models with different rotational end-restraint

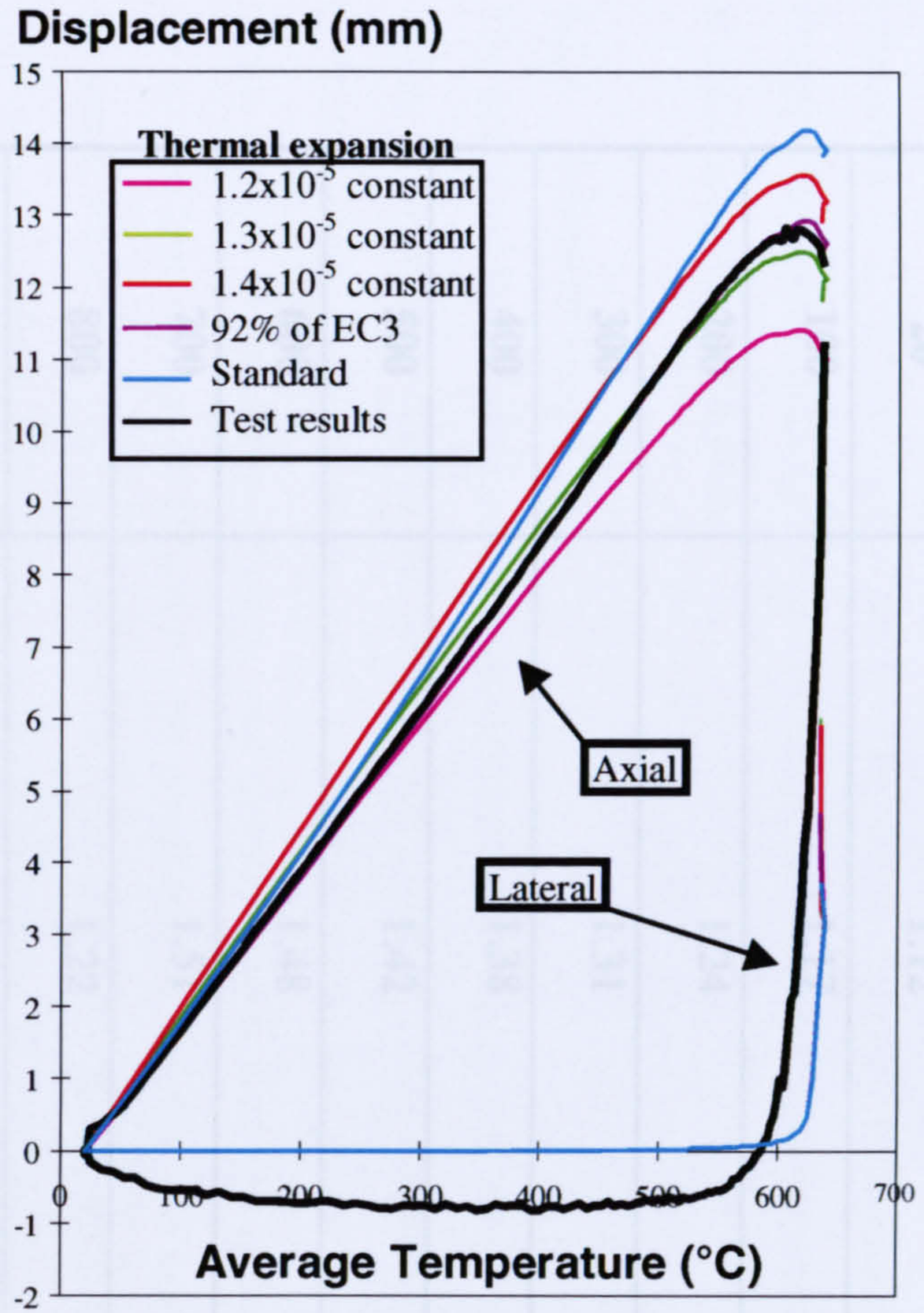

Fig. 39 Displacement of model columns with different thermal expansion characteristics

Temperature (°C)	*Thermal Expansion Coefficient ($x10^{-5}$/°C)*
20	1.12
100	1.17
200	1.24
300	1.31
400	1.38
500	1.42
600	1.48
700	1.51
800	1.22
900	1.35

Table 2 British Steel thermal expansion coefficient results

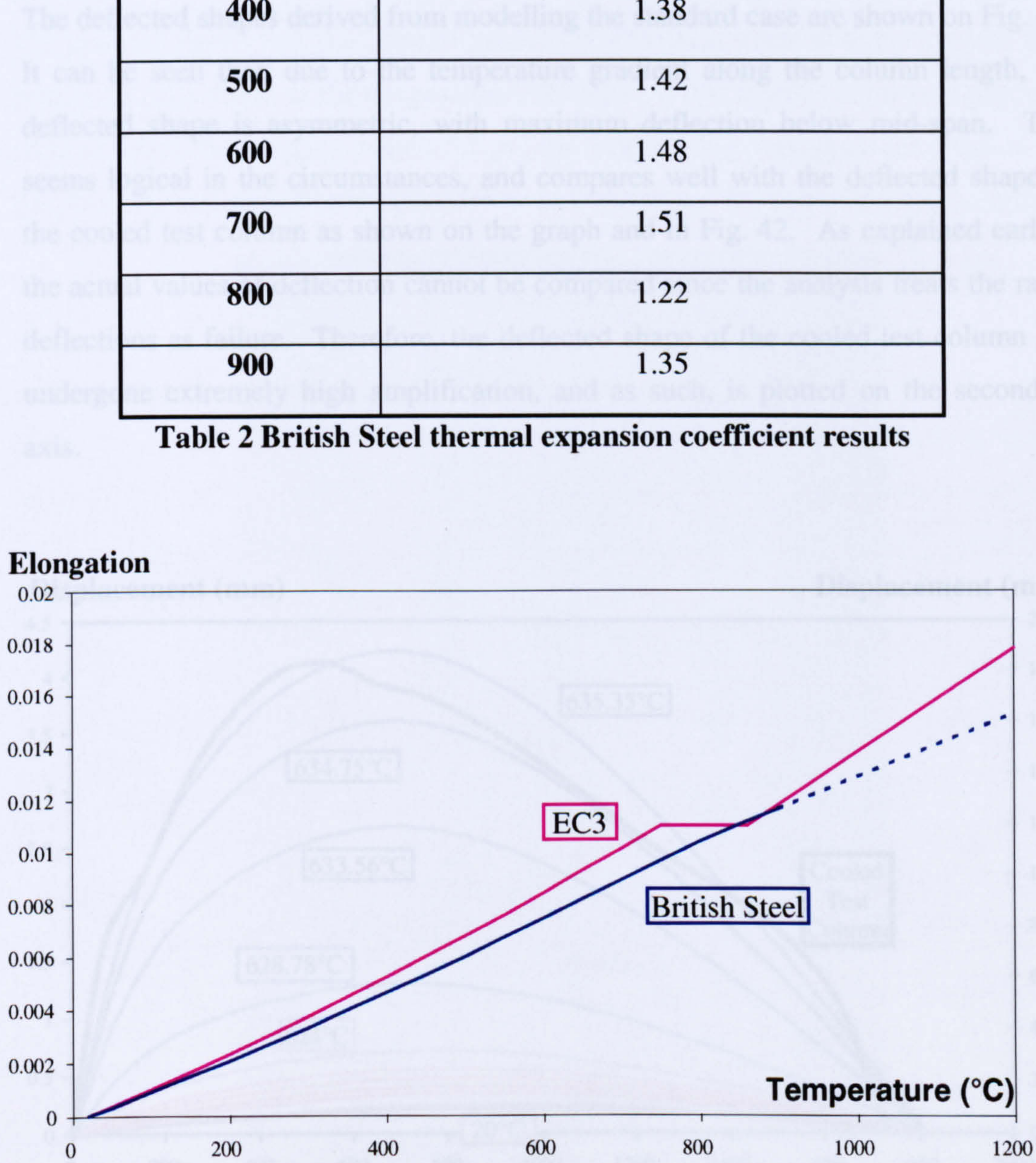

Fig. 40 Thermal elongation of steel

The British Steel experiments show that the thermal expansion behaves in a quadratic-like way, and has values around 90% of those found using the EC3 method. The major difference between the two models is the behaviour between 750°C and 860°C. The EC3 model assumes that no increase in thermal expansion

coefficient occurs, since the steel is going through a phase change. The results from British Steel indicate that this is not the case, and although there is slightly less expansion it is by no means zero. The Ulster column fails around 600°C and therefore no conclusions can be drawn about the actual behaviour within the range of phase change from this data.

4.2.4 Deflected Shape

The deflected shapes derived from modelling the standard case are shown on Fig. 41. It can be seen that, due to the temperature gradient along the column length, the deflected shape is asymmetric, with maximum deflection below mid-span. This seems logical in the circumstances, and compares well with the deflected shape of the cooled test column as shown on the graph and in Fig. 42. As explained earlier, the actual values of deflection cannot be compared since the analysis treats the rapid deflections as failure. Therefore, the deflected shape of the cooled test column has undergone extremely high amplification, and as such, is plotted on the secondary axis.

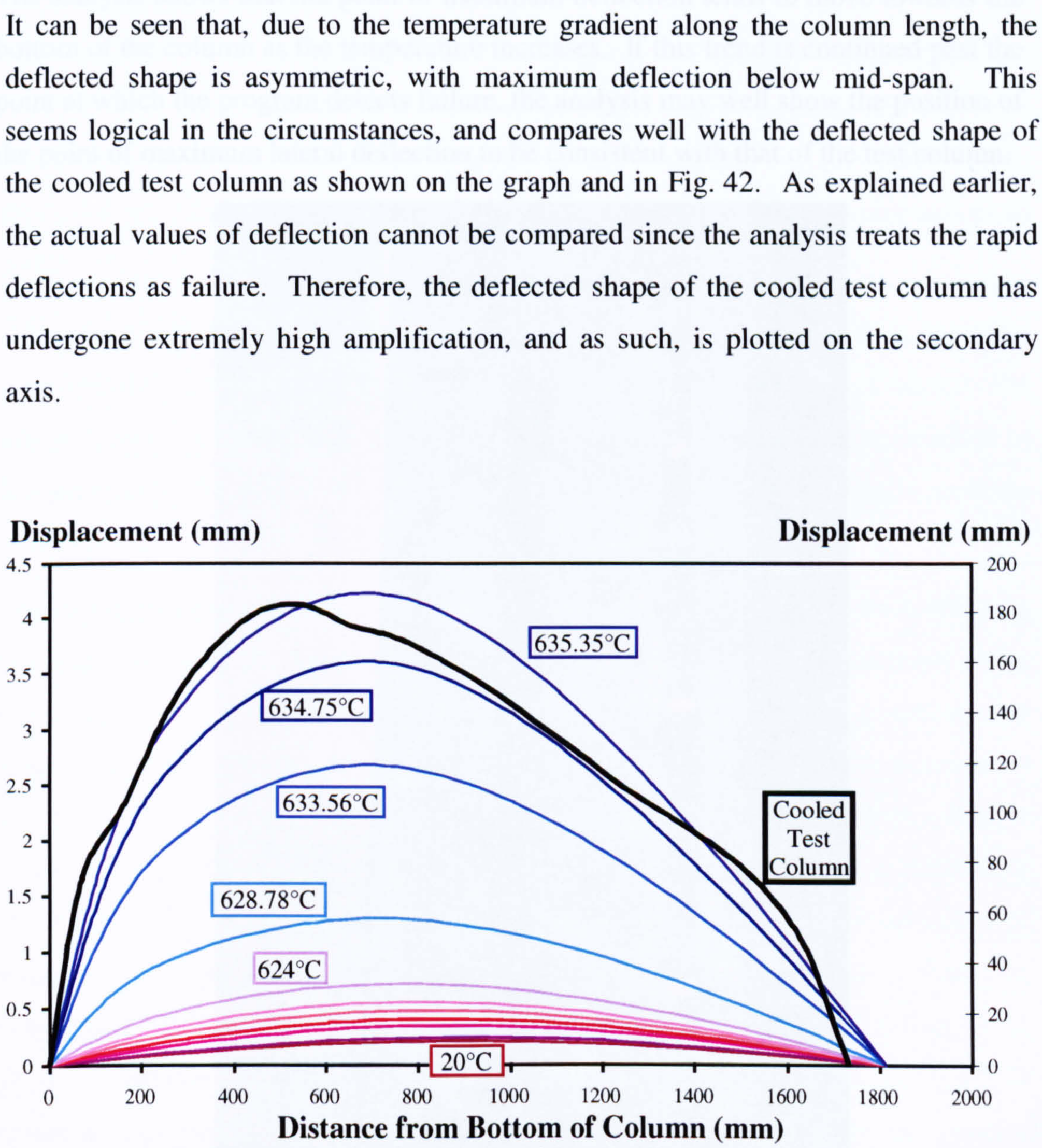

Fig. 41 Deflected shape of column with specified average temperature

The lateral transducers are placed 900 mm from the base of the column and show deflections rising to over 100 mm, after which the data logging equipment is switched off, as shown Fig. 34. The deflected shape of the cooled column shows

lateral deflections at that point of around 160 mm. This indicates that the column deflected substantially after the equipment was switched off, especially since this deflection will reduce as the column cools. The cooling effect, along with the bending of the column, explains why the cold test column seems shorter than the shape found in analysis.

The position of the point of maximum lateral deflection of the cooled column is about 200 mm nearer to the bottom of the column than that shown in the analysis. The analysis shows that the point of maximum deflection tends to move towards the bottom of the column as the temperature increases. If this trend is continued past the point at which the program detects failure, the analysis may well show the position of the point of maximum lateral deflection to be consistent with that of the test column.

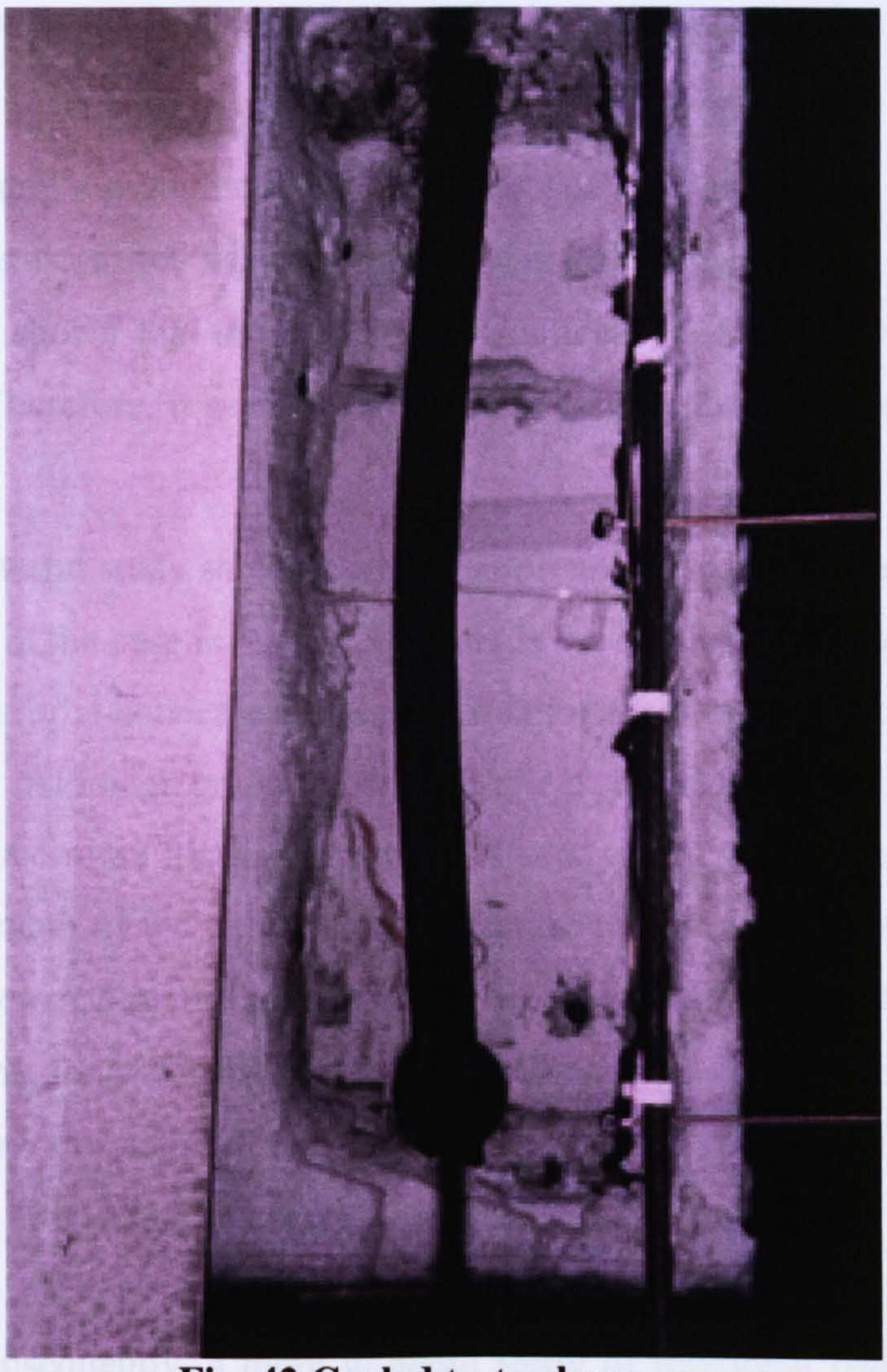

Fig. 42 Cooled test column

4.3 Conclusions

It can be concluded from the initial study of section 4.2.1 that the general set-up of the experiment is stable. Measured discrepancies in system variables such as geometric imperfection and Young's modulus will not affect the results to the extent that accurate modelling becomes impossible. However a number of issues have been raised by this initial study.

4.3.1 General Conclusions

The parameter with the largest effect and possibly the greatest variability is the material yield stress. It was therefore accepted by the Ulster team that this was to be measured and reported for each batch of steel used. The study into the Ulster tests in the following chapter uses measured values for imperfection, section size and yield stress.

Although the Young's modulus of the steel has not been measured, it is generally accepted that this does not vary significantly in differing batches of steel. The analysis here has shown that the model is not noticeably affected by a variation in this parameter. Therefore, it seems reasonable to assume that the Young's modulus is 210kN/mm^2.

The rotational restraint study shows, perhaps surprisingly, that the effect of rotational restraint is minor in the case investigated. This is the area of most uncertainty as far as experimental error is concerned, since the rotational restraint is not measured and is assumed small. Although graphite bearings are used, the high axial forces present are sure to introduce some frictional restraint effects, which would result in a change in the effective length of the column. Any friction present seems not to noticeably affect the displacements in the case studied here and no alternative assumptions of rotational restraint are available since no measurements were made. Thus, for subsequent studies the support conditions are assumed pinned. However, it is expected that the effects may increase with slenderness ratio and the 127x76x13UB columns may be affected to a greater extent than the 178x102x19UB columns studied here. Consequently, a more in-depth study of rotational restraint has been performed in Chapter 6.

The investigation into the effect of thermal expansion shows a discrepancy between the behaviour assumed by VULCAN and that shown in the test. The experimental data provided by British Steel seems to have a much better correlation with the test. However, the two models are very different at temperatures above 750°C. This initial study cannot shed any light on the suitability of the two models at these temperatures. It would therefore be unwise to make any change in assumptions based on this single test comparison. The EC3 model will therefore continue to be used in further studies until further validation of the British Steel results is available.

4.3.2 "Best Guess" Analysis

Taking all the information derived from this study into account, a final analysis is possible, which should give the best possible match to the test data. This uses the standard set of assumptions from the previous section, since they provide quite an accurate analysis and do not have a huge effect on the results. However, the yield stress has been shown to be important, and the yield strength of the batch of steel has consequently been tested. A more realistic value of 302kN/mm^2 can therefore be used for this column.

Although it has not been validated sufficiently for use in future studies, there are indications that the British Steel values for thermal expansion represent a more accurate model for the column analysed here. Thus, these values will be used in this analysis.

The axial and lateral displacement results from this best-guess are shown on Fig. 43. An extremely good correlation with the test results is seen. The maximum axial displacement of the model column is almost exactly the same as that achieved by the test column. In addition, this peak axial displacement occurs within 10°C of the same point in the test. The lateral deflection of the model is much more stable than the lateral deflection of the test column, which is subject to experimental inaccuracies. However, the points at which these lateral deflections begin to increase rapidly towards failure occur at very similar temperatures. The most impressive correlation is that the axial displacement of the test column at temperatures below the failure region is matched extremely well by the model. The behaviour in this region is dominated by thermal expansion effects and thus the British Steel thermal expansion model does indeed look promising.

The generally accurate correlation seen here validates the use of VULCAN in this way for further analyses of the Ulster test columns.

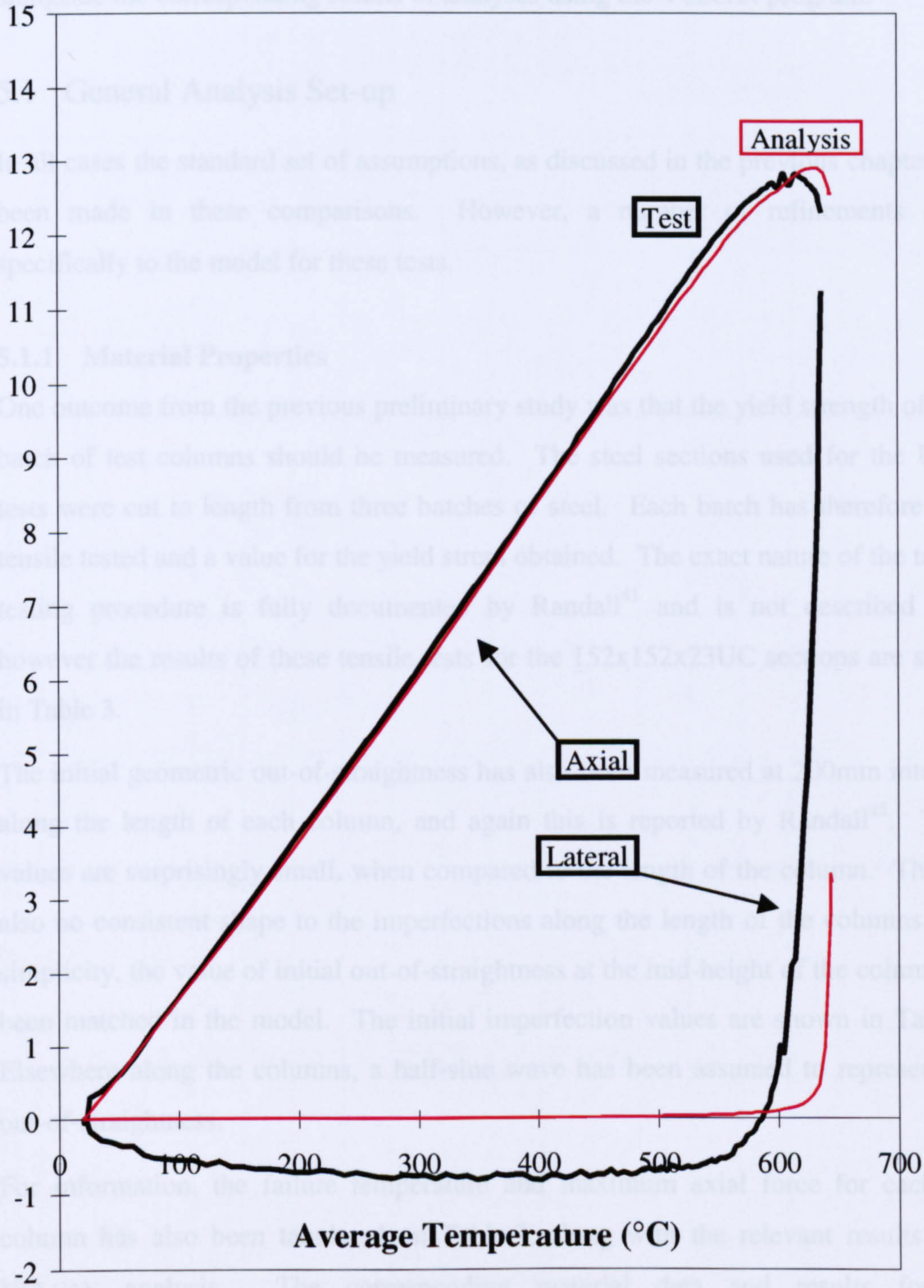

Fig. 43 Best guess analysis displacements

5 Analysis Of Ulster Tests

This chapter reports the results from the tests carried out at the University of Ulster, alongside the corresponding results of analyses using the VULCAN program.

5.1 General Analysis Set-up

In all cases the standard set of assumptions, as discussed in the previous chapter, has been made in these comparisons. However, a number of refinements apply specifically to the model for these tests.

5.1.1 Material Properties

One outcome from the previous preliminary study was that the yield strength of each batch of test columns should be measured. The steel sections used for the Ulster tests were cut to length from three batches of steel. Each batch has therefore been tensile tested and a value for the yield stress obtained. The exact nature of the tensile testing procedure is fully documented by Randall[41] and is not described here, however the results of these tensile tests for the 152x152x23UC sections are shown in Table 3.

The initial geometric out-of-straightness has also been measured at 200mm intervals along the length of each column, and again this is reported by Randall[45]. These values are surprisingly small, when compared to the length of the column. There is also no consistent shape to the imperfections along the length of the columns. For simplicity, the value of initial out-of-straightness at the mid-height of the column has been matched in the model. The initial imperfection values are shown in Table 3. Elsewhere along the columns, a half-sine wave has been assumed to represent the out-of-straightness.

For information, the failure temperature and maximum axial force for each test column has also been tabulated on Table 3, along with the relevant results from VULCAN analysis. The corresponding material data and results for the 178x102x19UB and 127x76x13UB tests are shown on Table 4 and Table 5 respectively.

152x152x23UC		*x EC3 Design Load*	*Measured Yield Stress*	*Imperfection*	*Test*		*Analysis*	
Section	**α**	**(x 660 kN)**	**(kN / mm^2)**	**(mm)**	**Fail Temp**	**Force**	**Fail Temp**	**Force**
1	0.0	0.2	302	---	701	132	---	---
2	0.0	0.4	302	0.09	626	264	575	264
3	0.0	0.6	302	0.29	557	396	485	396
4	0.1	0.0	321	0.97	---	355	534	340
5	0.1	0.2	321	0.28	640	458	494	437
6	0.1	0.4	321	0.45	598	549	459	544
7	0.1	0.6	321	0.59	547	585	414	633
8	0.2	0.0	316	0.17	---	465	448	488
9	0.2	0.2	316	0.58	583	584	414	538
10	0.2	0.4	316	0.29	517	641	384	629
11	0.2	0.6	316	0.25	485	632	393	721
5Repeat	0.1	0.2	316	0.77	560	427		
6Repeat	0.1	0.4	316	0.13	530	457		
7Repeat	0.1	0.6	316	0.66	553	573		
9Repeat	0.2	0.2	316	0.59	704	514		
10Repeat	0.2	0.4	316	2.00	506	569		
11Repeat	0.2	0.6	316	0.15	377	695		

Table 3 Material properties for 152x152x23UC columns assumed in VULCAN model, with corresponding test results

178x102x19UB		*x EC3 Design Load*	*Measured Yield Stress*	*Imperfection*	*Test*		*Analysis*	
Section	**α**	**(x 465 kN)**	**(kN / mm^2)**	**(mm)**	**Fail Temp**	**Force**	**Fail Temp**	**Force**
1	0.0	0.2	302	0.02	644	93	653	93
2	0.0	0.4	302	0.06	629	183	599	183
3	0.0	0.6	302	0.30	539	276	527	276
4	0.1	0.0	316	0.50	552	325	542	286
5	0.1	0.2	316	0.09	555	392	452	341
6	0.1	0.4	316	0.11	466	435	467	387
7	0.1	0.6	316	0.71	364	429	379	409
8	0.2	0.0	316	0.85	507	381	510	410
9	0.2	0.2	302	1.18	455	426	414	447
10	0.2	0.4	316	0.00	432	440	402	481
11	0.2	0.6	316	0.19	408	477	391	501

Table 4 Material properties for 178x102x19UB columns assumed in VULCAN model, with corresponding test results

127x76x13UB		*x EC3 Design Load*	*Measured Yield Stress*	*Imperfection*	*Test*		*Analysis*	
Section	**α**	**(x 245 kN)**	**(kN / mm^2)**	**(mm)**	**Fail Temp**	**Force**	**Fail Temp**	**Force**
1	0.0	0.2	316	0.24	717	49	740	49
2	0.0	0.4	316	0.27	658	97	640	97
3	0.0	0.6	316	0.31	567	146	581	146
4	0.1	0.0	316	0.53	445	209	526	192
5	0.1	0.2	316	0.29	536	250	498	224
6	0.1	0.4	316	0.08	333	252	456	250
7	0.1	0.6	316	0.11	386	258	431	283
8	0.2	0.0	316	0.20	530	268	423	269
9	0.2	0.2	316	0.26	441	277	397	285
10	0.2	0.4	316	0.10	410	306	392	299
11	0.2	0.6	316	0.01	336	304	311	305
12	0.3	0.0	316	0.09	417	317	389	317
13	0.3	0.2	316	0.05	401	329	347	324
14	0.3	0.4	316	0.33	384	350	315	335
15	0.3	0.6	316	0.04	306	339	273	341

Table 5 Material properties for 127x76x13UB columns assumed in VULCAN model, with corresponding test results

5.1.2 Temperature Distribution

The analyses in the previous chapter neglected the presence of thermal gradients across the section, allowing the effects of other parameters to be investigated independently. The steel temperatures have been recorded[45], usually at the five points across the column labelled θ_a-θ_e in Fig. 44, and at four sections along the column length. The VULCAN program defines the temperature at thirteen points across the cross-section of the member, numbered 1-13 in Fig. 44. Therefore, some degree of interpolation is required to fit a temperature distribution to the analysis model that accurately reflects the temperature gradients of the test.

The cross-sectional thermal gradients were defined by assuming a linear gradient across each flange. Thus, for example, the temperatures of elements 1-5 are defined by θ_a and θ_b by the equations shown in Fig. 44. The temperature of element 3 is the average of θ_a and θ_b. The temperature of element 6 is then defined as the average of element 3 and θ_c. This process is repeated for elements 8-13 on the other side of the cross-section.

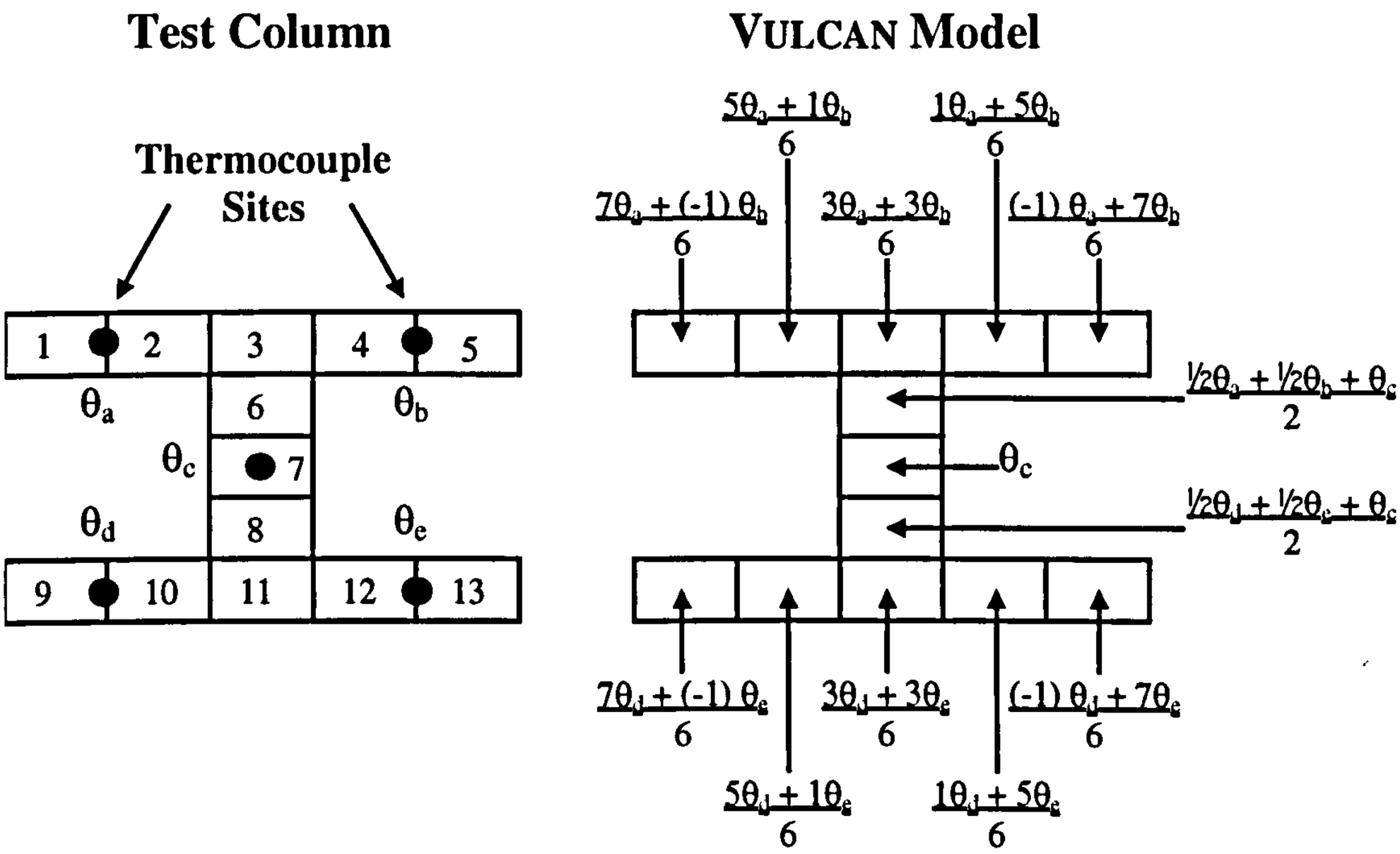

Fig. 44 Thermocouple positions and analysis interpolation over cross-section

Four column cross-sections were instrumented, but the VULCAN analyses were performed using nine elements along the length of each column to provide the required accuracy. Therefore, some degree of interpolation was also required along the length of the column, as shown in Fig. 45.

This shows that element 2 is at exactly the same position as the bottom set of thermocouples. Therefore, the cross-sectional temperatures of element 2 are exactly as calculated above using the results from the bottom thermocouples. Each cross-sectional temperature of element 5 can similarly be found by averaging the respective cross-sectional values from the middle two sets of thermocouple results. Fig. 45 shows how the temperatures are calculated for the other elements along the length of the column, and in each case the temperature at the same cross-sectional position is used for calculation.

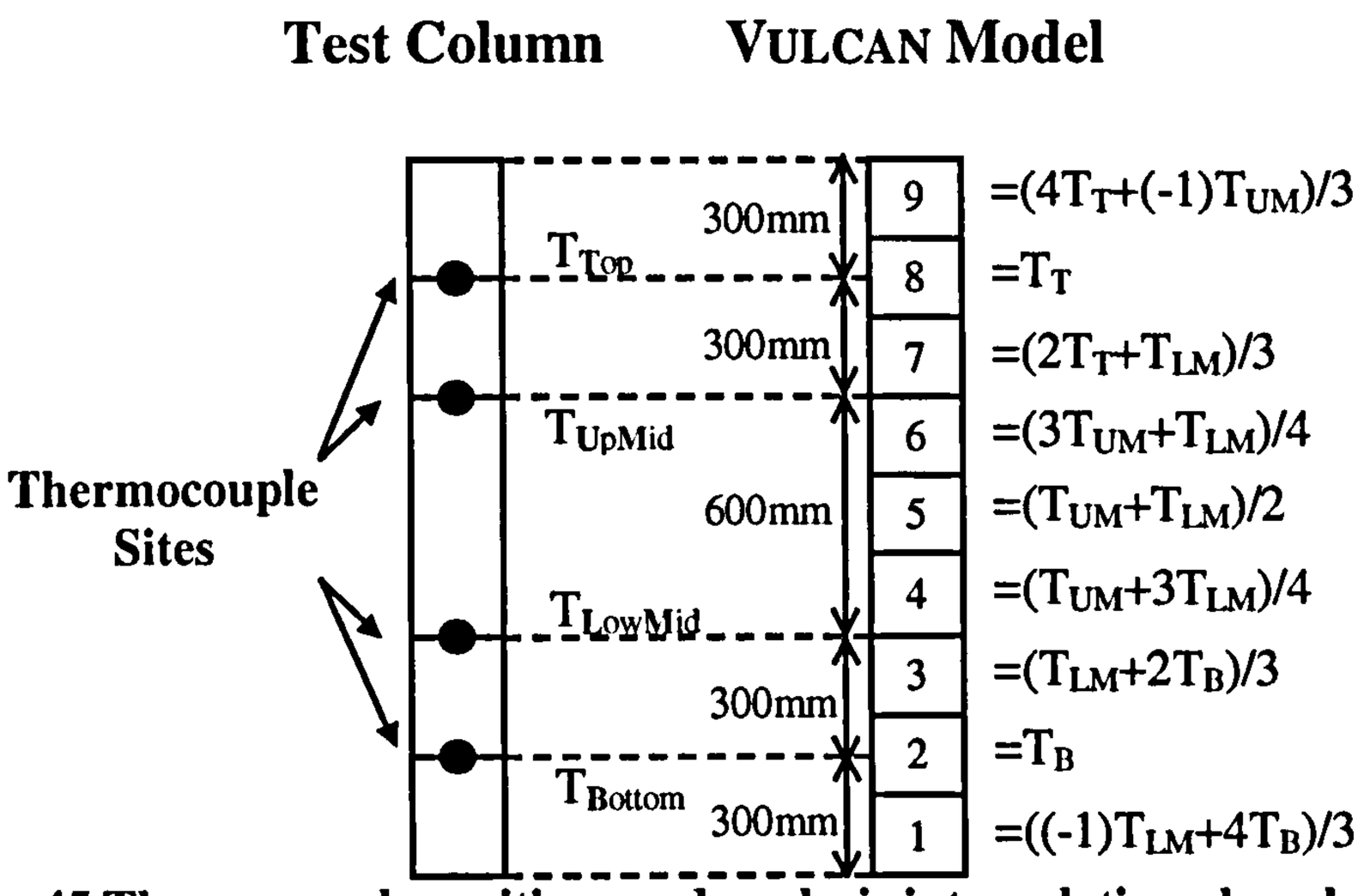

Fig. 45 Thermocouple positions and analysis interpolation along length

5.2 Failure Temperatures

A general overview of the tests can be obtained by choosing a single parameter and comparing it across a broad range of tests. The indicator chosen for this section is the failure temperature of the column, thus allowing a single figure to represent each test, rather than a set of curves such as a displacement or force measurement with time. Although this is simplistic and does not show the full details of the behaviour, it allows a comparison between many tests in a broad sense. For the purpose of this chapter, the failure temperature is defined as the temperature at which the column supports its highest axial force. During the tests this was easily identifiable, especially for the more slender columns, which often failed extremely suddenly accompanied by a large amount of noise.

5.2.1 Results

The total axial forces in all the 152x152x23UC test columns have been plotted against their failure temperatures on Fig. 46, and are indicated by solid markers. Most of the columns failed within the 400°C – 700°C temperature range. Within this range, the yield strength and Young's modulus of the steel changes in approximately linear fashion with temperature, as described in Chapter 2. Thus, the failure temperatures are also expected to change linearly with temperature.

A linear regression has therefore been performed on these results to give an overview of the general behaviour of these columns, and is shown as the solid line on Fig. 46. This line forms a failure boundary, where columns closer to the origin are unbuckled, and columns further from the origin have buckled. Hence, the line is defined by data from columns that have just buckled.

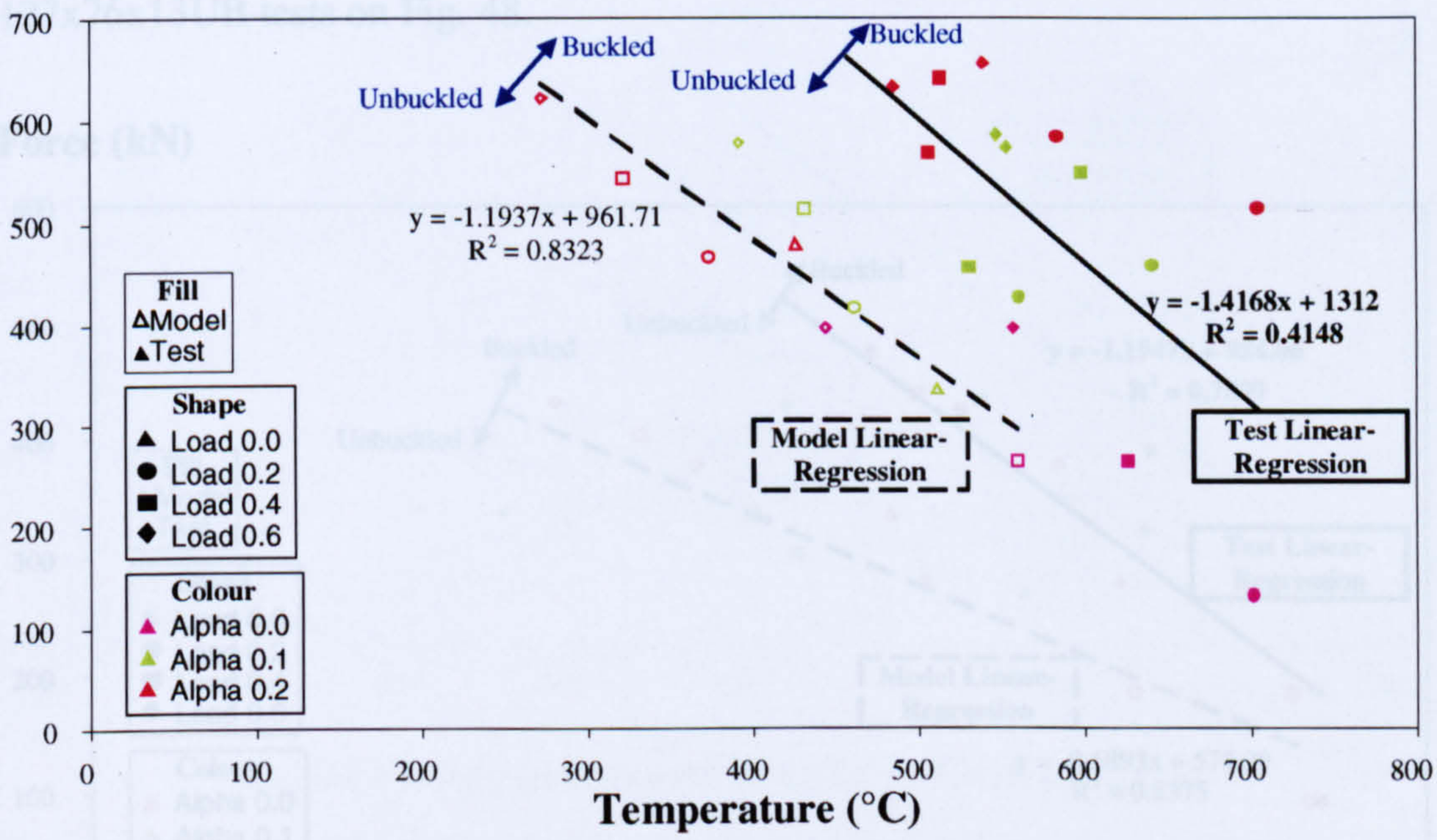

Fig. 46 Failure boundaries of 152x152x23UC columns

The R^2 value for the regression is a measure of how accurately the results fit the linear model. The closer this value is to unity, the closer the data fits the linear trend-line. Thus, it can be clearly seen that there is a large amount of scatter in the test result data. This is to be expected, as there are unavoidable differences in the way any two supposedly similar tests are performed on different days, and with different specimens. As further confirmation of the suitability of the linear model, a quadratic

regression model was applied to the data, which resulted in a change in R^2 value of only 0.1%.

Experimental errors such as introducing eccentricities when bolting the column to the frame and inexact load and restraint values all introduce scatter in the data, as do the well-documented[46,47] effects of inherent geometrical and material imperfections. Also, the temperature profiles vary quite considerably between tests, and this introduces further scatter into the data.

Fig. 46 also shows the results for the VULCAN analyses as outlined markers with the corresponding linear regression, or failure boundary, shown as a dashed line. These results show much less scatter, since experimental error is not a factor in the model set-up. The varying temperature profiles, which come from test data, still cause similar tests to behave differently and introduce some scatter. The results for the 178x102x19UB tests are shown in a similar fashion on Fig. 47 and for the 127x76x13UB tests on Fig. 48.

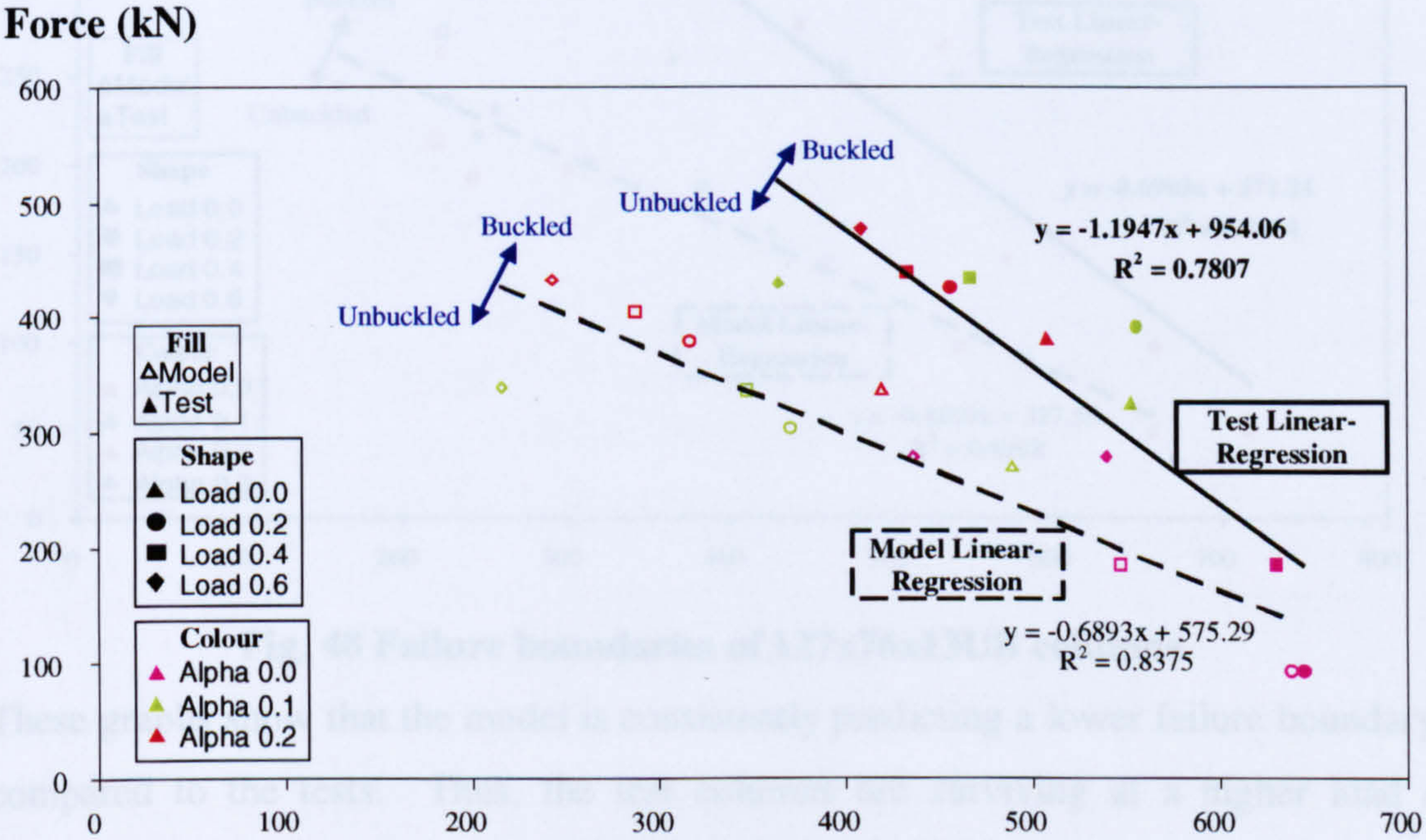

Fig. 47 Failure boundaries of 178x102x19UB columns

5.2.2 Conclusions

The gradients of the trend-lines for the tests and the modelling are very similar, showing that the way the stress-strain model is assumed to change with temperature is close to that seen in experiments.

The intercepts of the trend-lines with the temperature axis might be said to indicate the melting point of the steel, since they would indicate temperatures at which columns fail under zero axial force. However, this is not really the case, since the linear change in steel properties with temperature only holds between 400°C and 700°C. Above this range, steel undergoes a crystal structure change and a corresponding non-linear change in yield-stress is seen. The intercepts of the trend-lines with the force axis could similarly be said to indicate the ambient temperature failure load of the 152x152x23UC column, which in this case should be 660kN. However, again this is not the case, since below 400°C there is a completely different form of variation of steel properties with temperature. The elastic modulus continues to change while the strength is almost constant near the ambient temperature value.

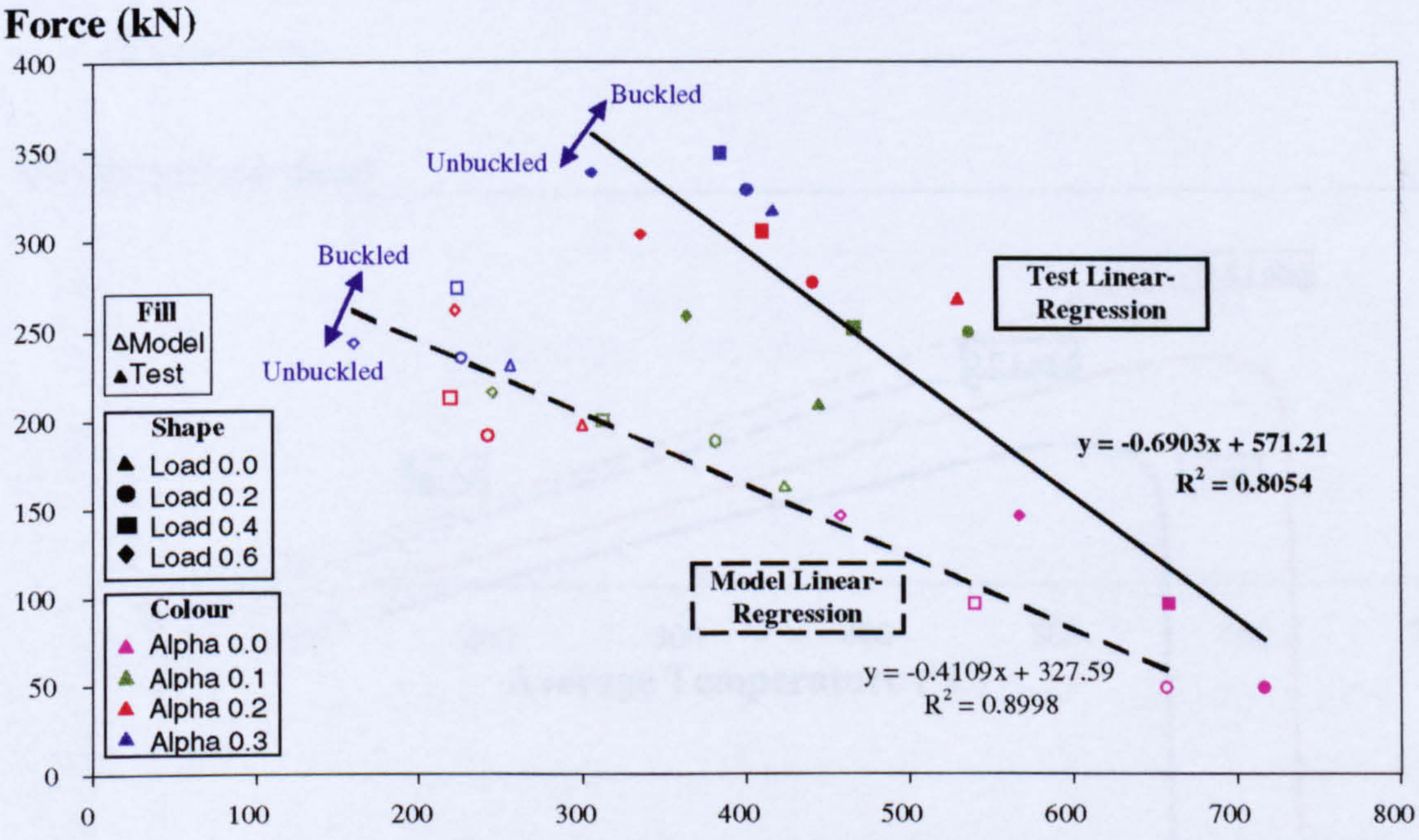

Fig. 48 Failure boundaries of 127x76x13UB columns

These graphs show that the model is consistently predicting a lower failure boundary compared to the tests. Thus, the test columns are surviving at a higher load / temperature level than the corresponding model column. It is suggested that one cause of this discrepancy may be the effect of friction in the bearings of the test column, which is not present in the model. This has been shown in Chapter 2 to be an insignificant effect in the case examined, but further investigation will be conducted in the following chapter.

In each group of tests, the modelling results behave in a more linear fashion and thus have an R^2 value closer to unity when compared with the R^2 value for the tests.

However, there is much less scatter for the UB test results than for the 152x152x23UC columns. The R^2 value seems to indicate that the linear model is indeed a suitable approximation for the results, although the 152x152x23UC tests are particularly prone to some experimentally-induced error.

5.3 152x152x23UC Results

This section concentrates on the results for the 152x152x23UC sections and compares test results with VULCAN analyses.

5.3.1 Axial Displacements

Fig. 49 shows the axial displacement for the two tests on 152x152x23UC sections with no axial restraint. The dashed lines are the results from the corresponding VULCAN analyses.

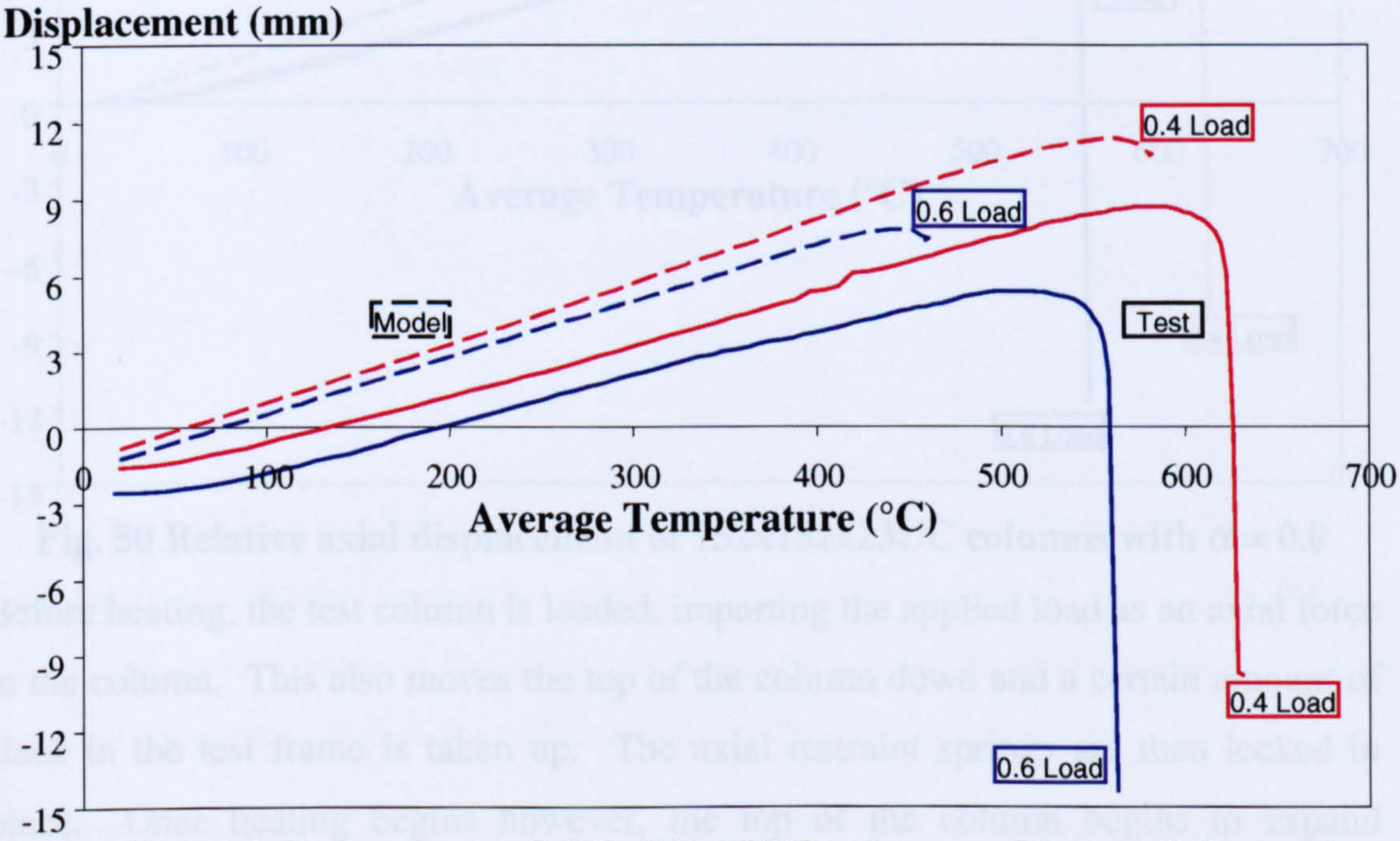

Fig. 49 Axial displacement of 152x152x23UC columns with no axial restraint

A problem can immediately be seen in that the initial axial displacement of the test columns is different from that of the model columns. This displacement is due to the loading of the columns, since the displacement transducers are zeroed before loading. This is also the case for the model column, but this initial displacement is much lower since it is solely due to the column shortening under loading. In the case of the test column however, there is also a certain amount of bedding-in occurring, which increases the initial displacement, but should remain essentially constant during the

heating phase at constant load. To remove this effect, the displacements plotted in subsequent graphs will be shifted so that the initial value is zero, as in Fig. 50.

It can now be seen that the test columns initially displace at a slower rate than the model. The curves in the later stages of the test have similar gradients, with the gradient of the test results being only slightly lower. This implies that the expansion coefficients for the steel in the test is slightly lower than that assumed for analysis, as indicated by the initial study in the previous chapter. Thus, the initial lack of expansion in the tests must be due to some other effect.

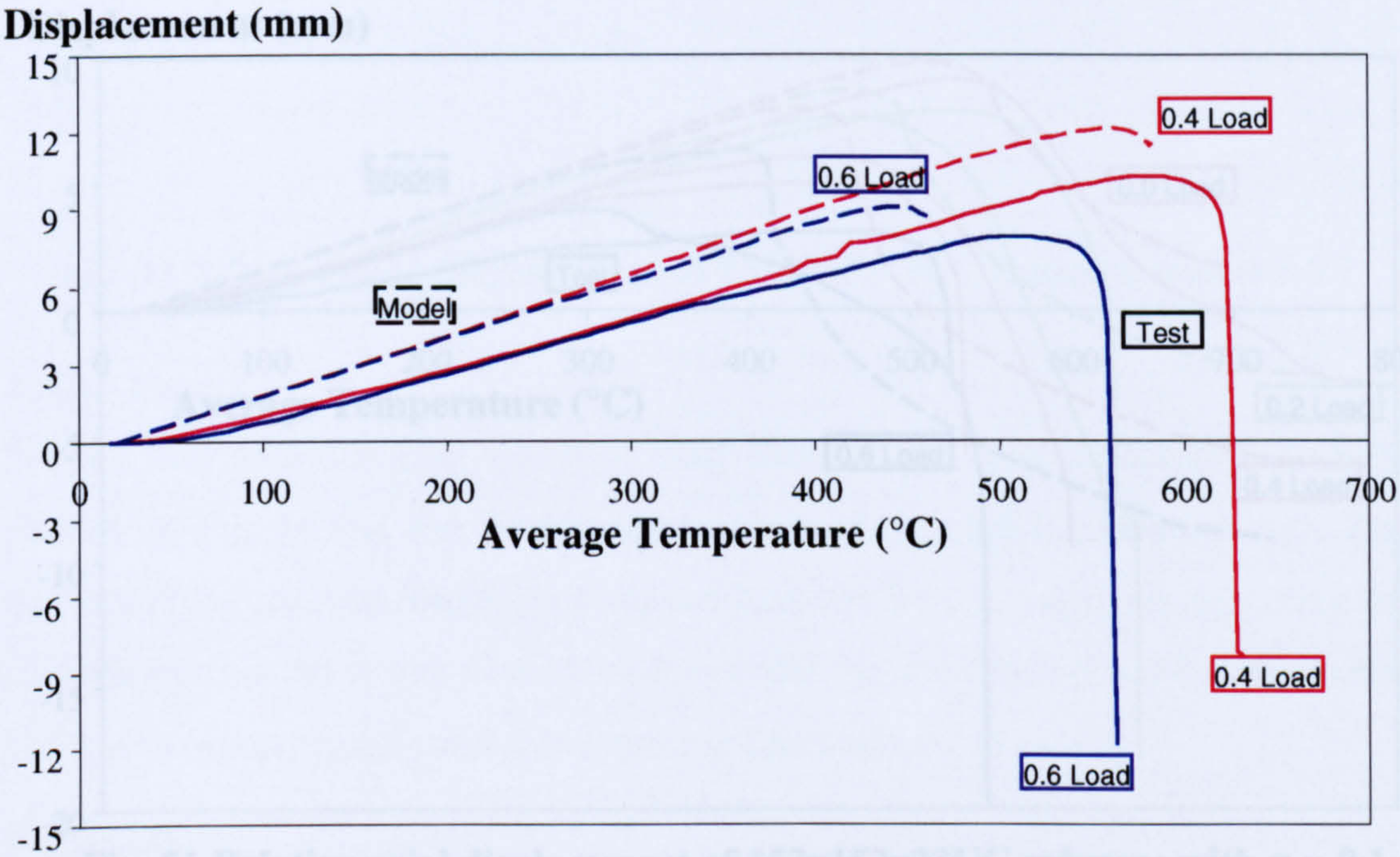

Fig. 50 Relative axial displacement of 152x152x23UC columns with $\alpha = 0.0$

Before heating, the test column is loaded, imparting the applied load as an axial force in the column. This also moves the top of the column down and a certain amount of slack in the test frame is taken up. The axial restraint springs are then locked in place. Once heating begins however, the top of the column begins to expand upwards, and pushes against the restraint springs. This process will close any gaps and lack of fit in the restraint system, without inducing a corresponding rise in restraint force. It is this bedding-in effect which is attributed to the initial non-linearity of the test column axial displacement.

One solution to this might be to artificially translate the analysis curve to the right, equivalently imposing some similar level of bedding-in on the model. However, if it were really at this higher temperature, the model would have a lower Young's

modulus and yield strength. Thus, the curves should also be translated downwards slightly to compensate. In-fact, the gradient of the translation would be similar to that found by regression as in the previous section. The only difference being the regression should be performed on failure temperature plotted against displacement rather than force.

The corresponding results for columns with an alpha factor of 0.1 are shown in Fig. 51 and for an alpha factor of 0.2 in Fig. 52. The stiffness of the test rig itself is insufficient to apply restraint levels above 0.2.

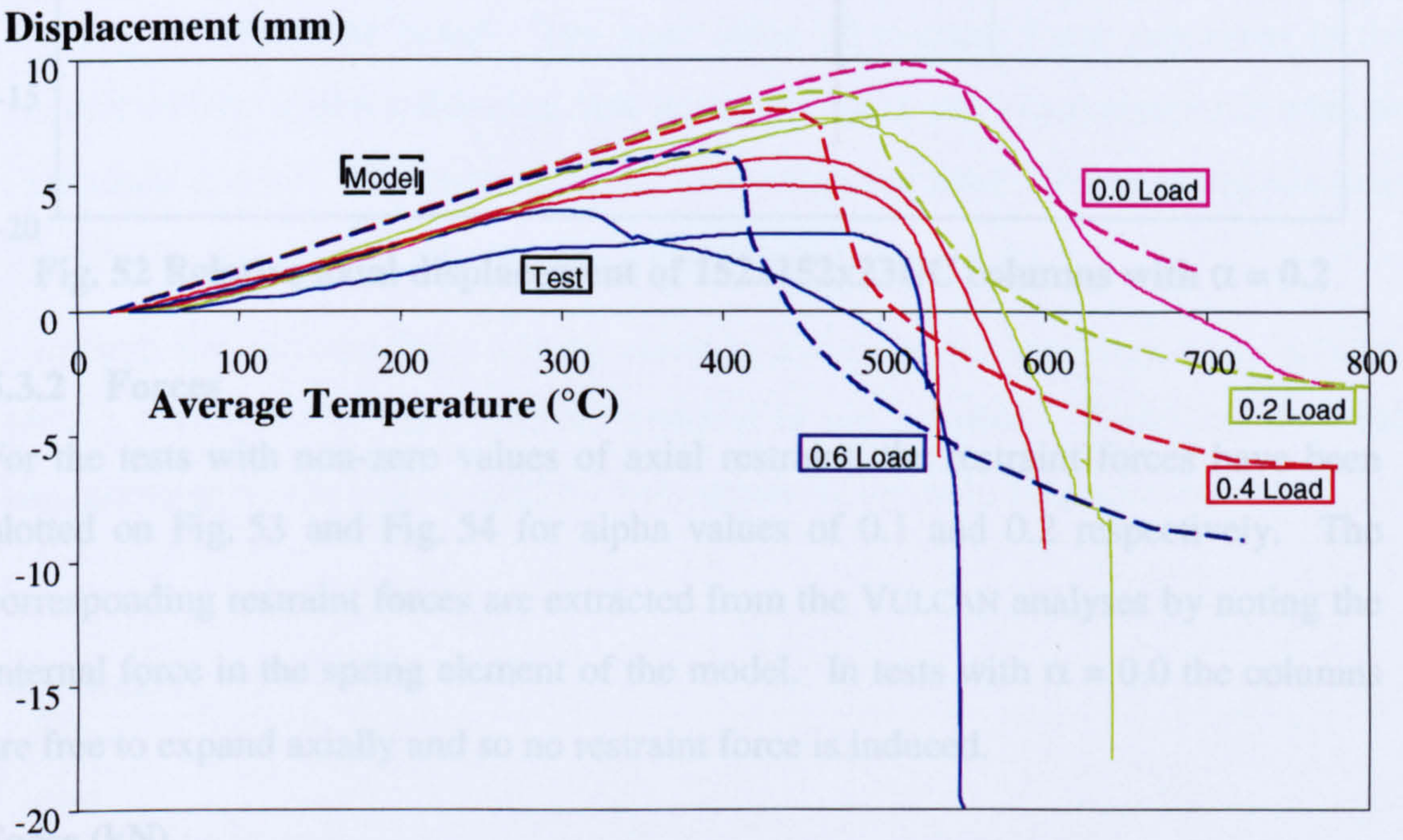

Fig. 51 Relative axial displacement of 152x152x23UC columns with $\alpha = 0.1$

Again, some bedding-in can be seen in the initial stages of the test. The effect is expected to be greater in the tests that have some level of axial restraint, since the restraint springs will need to bed-in as well as the bearings.

In most cases for 152x152x23UC sections, more than one test was conducted for each set of parameters. The difference in set-up between these tests is explained in detail in the next chapter, but a fair amount of agreement is still expected. The variation in results between these pairs of tests shows the inherent unpredictability of the tests and is mainly due to differences in temperature distribution. This indicates a large tolerance on the results and thus the model has quite an acceptable agreement with the test. Where a test was repeated, the temperature data of the later test was used for the analysis.

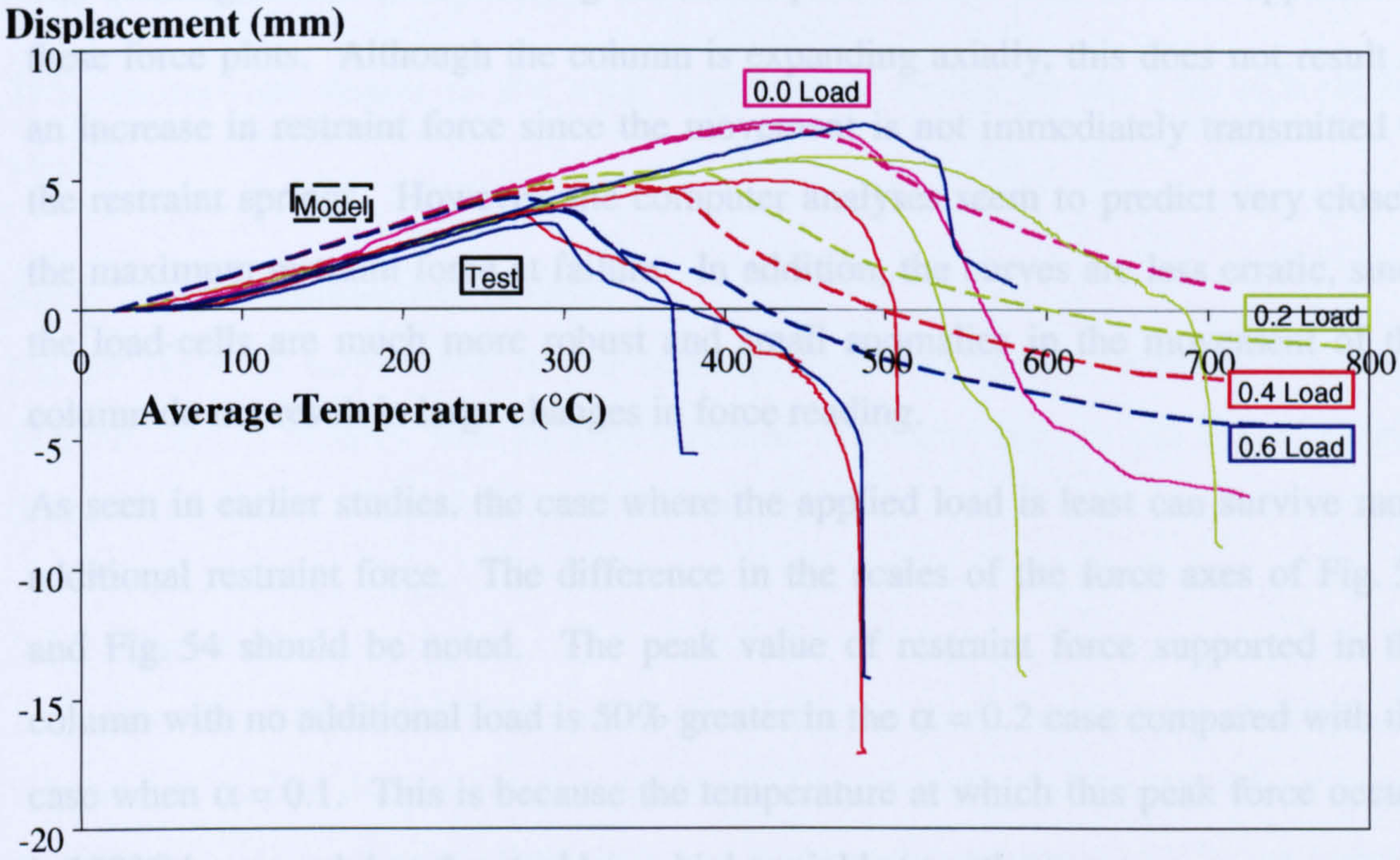

Fig. 52 Relative axial displacement of 152x152x23UC columns with $\alpha = 0.2$

5.3.2 Forces

For the tests with non-zero values of axial restraint, the restraint forces have been plotted on Fig. 53 and Fig. 54 for alpha values of 0.1 and 0.2 respectively. The corresponding restraint forces are extracted from the VULCAN analyses by noting the internal force in the spring element of the model. In tests with $\alpha = 0.0$ the columns are free to expand axially and so no restraint force is induced.

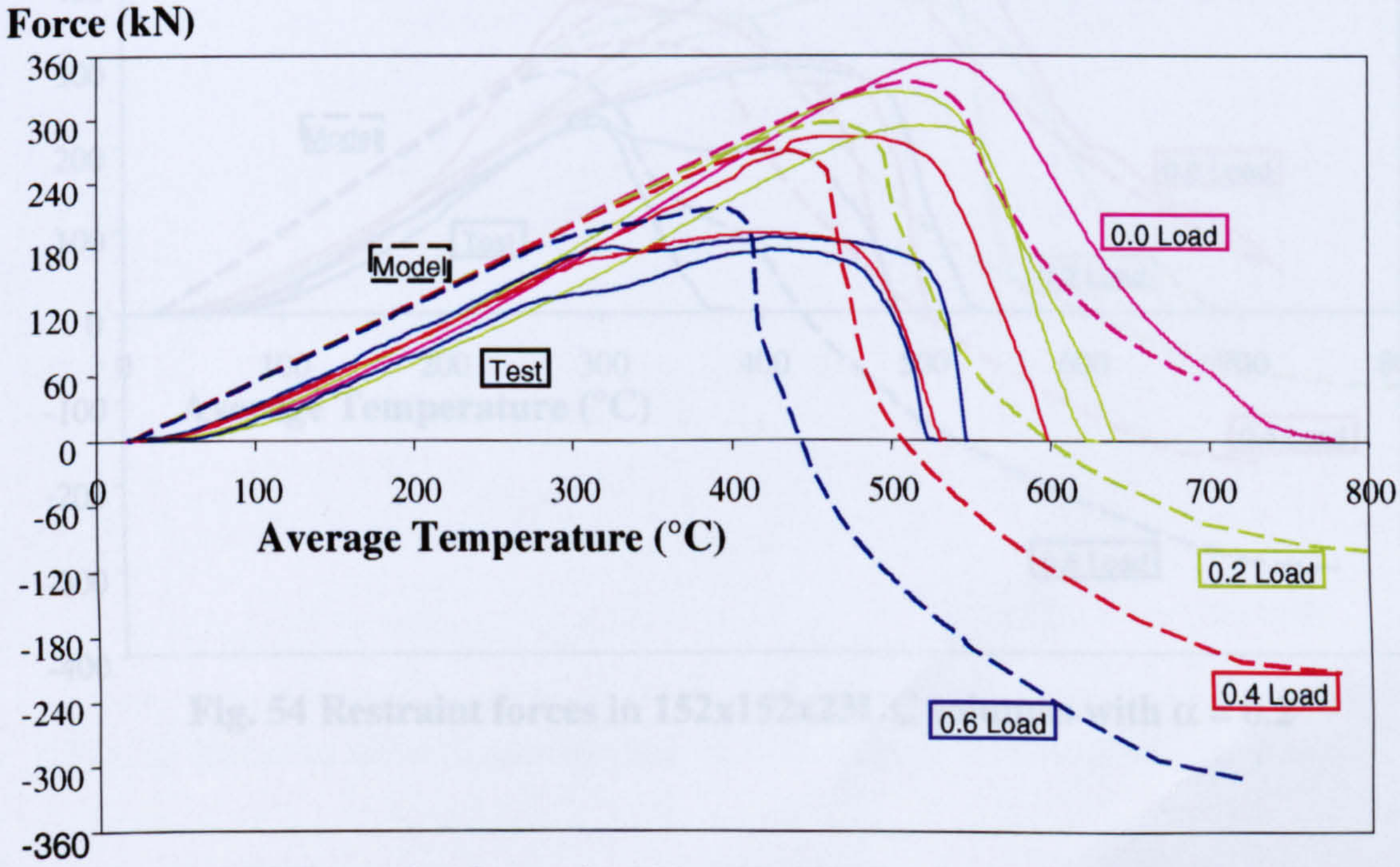

Fig. 53 Restraint forces in 152x152x23UC columns with $\alpha = 0.1$

The bedding-in that occurs during the initial phase of the tests is more apparent in these force plots. Although the column is expanding axially, this does not result in an increase in restraint force since the movement is not immediately transmitted to the restraint springs. However, the computer analyses seem to predict very closely the maximum restraint force at failure. In addition, the curves are less erratic, since the load-cells are much more robust and small anomalies in the movement of the column do not result in large changes in force reading.

As seen in earlier studies, the case where the applied load is least can survive most additional restraint force. The difference in the scales of the force axes of Fig. 53 and Fig. 54 should be noted. The peak value of restraint force supported in the column with no additional load is 50% greater in the $\alpha = 0.2$ case compared with the case when $\alpha = 0.1$. This is because the temperature at which this peak force occurs is 100°C lower and thus the steel has a higher yield strength.

Although the restraint-force results seem to allow for better comparison between tests, a correlation of tests with no restraint is not possible. Therefore, the axial displacement results will be used for comparison in the following sections.

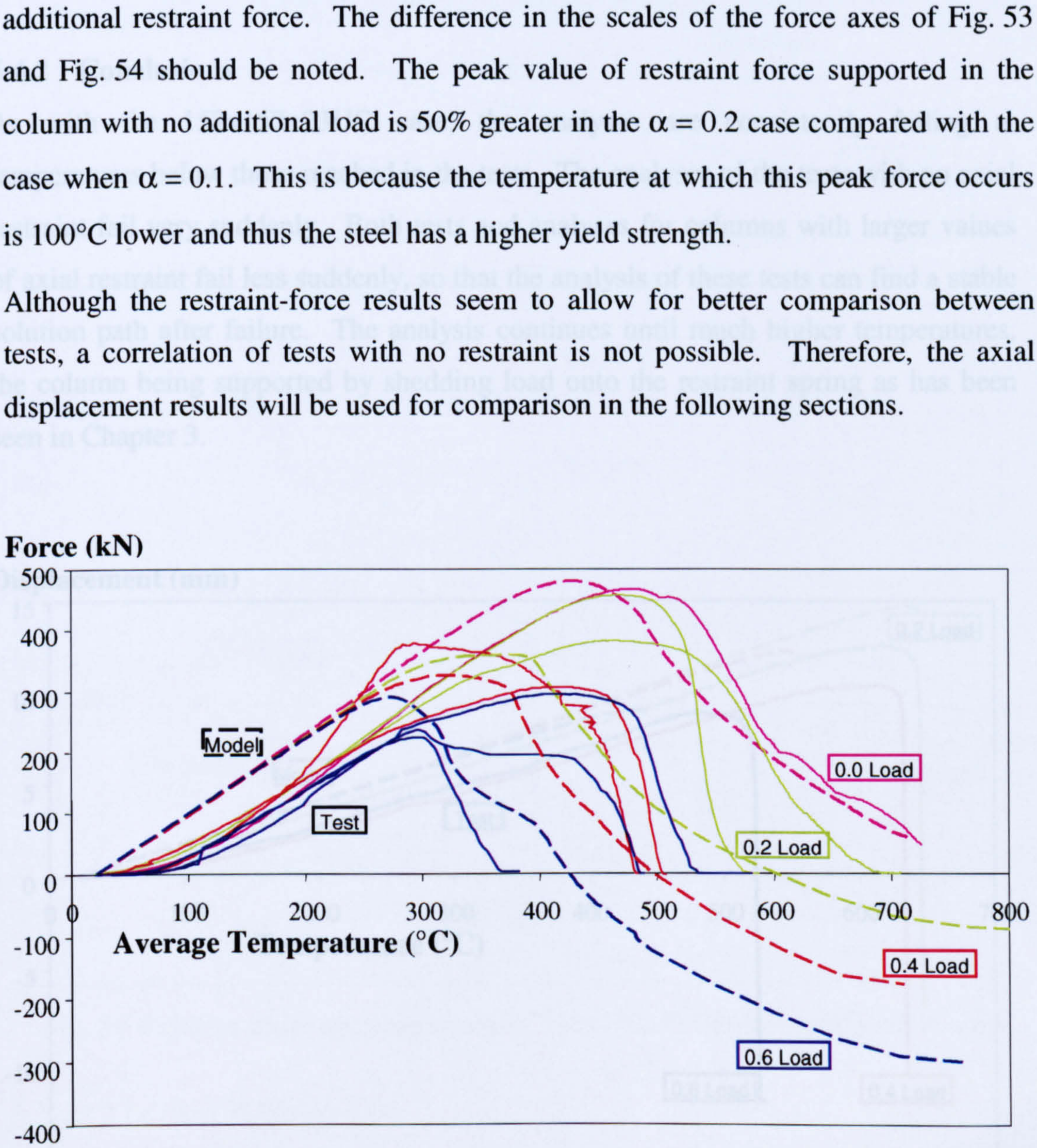

Fig. 54 Restraint forces in 152x152x23UC columns with $\alpha = 0.2$

5.4 178x102x19UB Results

This section concentrates on the axial displacement results for the 178x102x19UB sections.

5.4.1 Axial Displacement Results

Fig. 55 shows a comparison of the axial displacement results from the tests on 178x102x19UB sections with no axial restraint. Similarly, Fig. 56 and Fig. 57 show the results for cases with $\alpha = 0.1$ and 0.2 respectively.

5.4.2 Conclusions

As with the 152x152x23UC case, the analyses are consistently failing at temperatures below those reached in the tests. The analyses of the tests with no axial restraint fail very suddenly. Both tests and analyses for columns with larger values of axial restraint fail less suddenly, so that the analysis of these tests can find a stable solution path after failure. The analysis continues until much higher temperatures, the column being supported by shedding load onto the restraint spring as has been seen in Chapter 3.

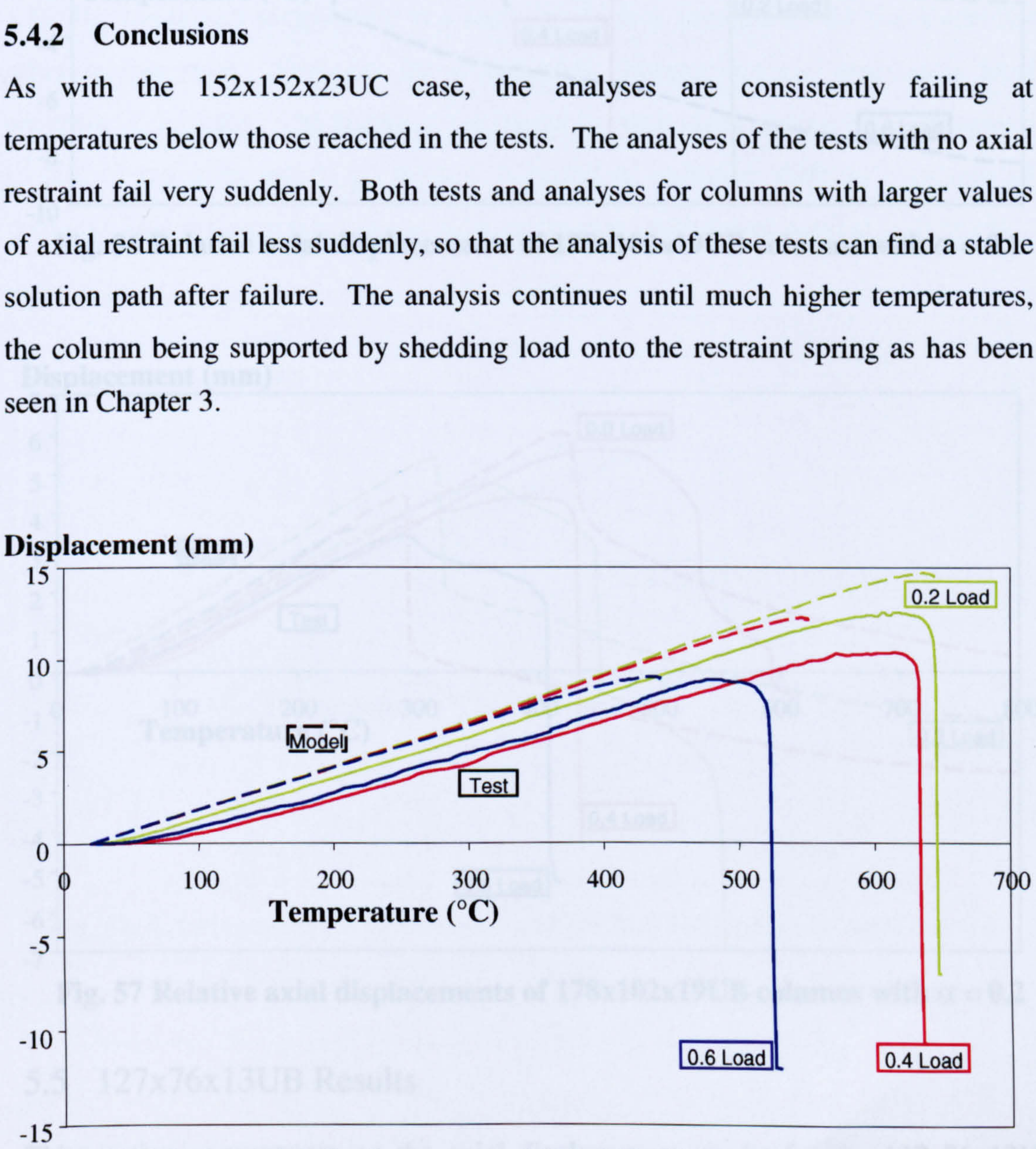

Fig. 55 Relative axial displacements of 178x102x19UB columns with $\alpha = 0.0$

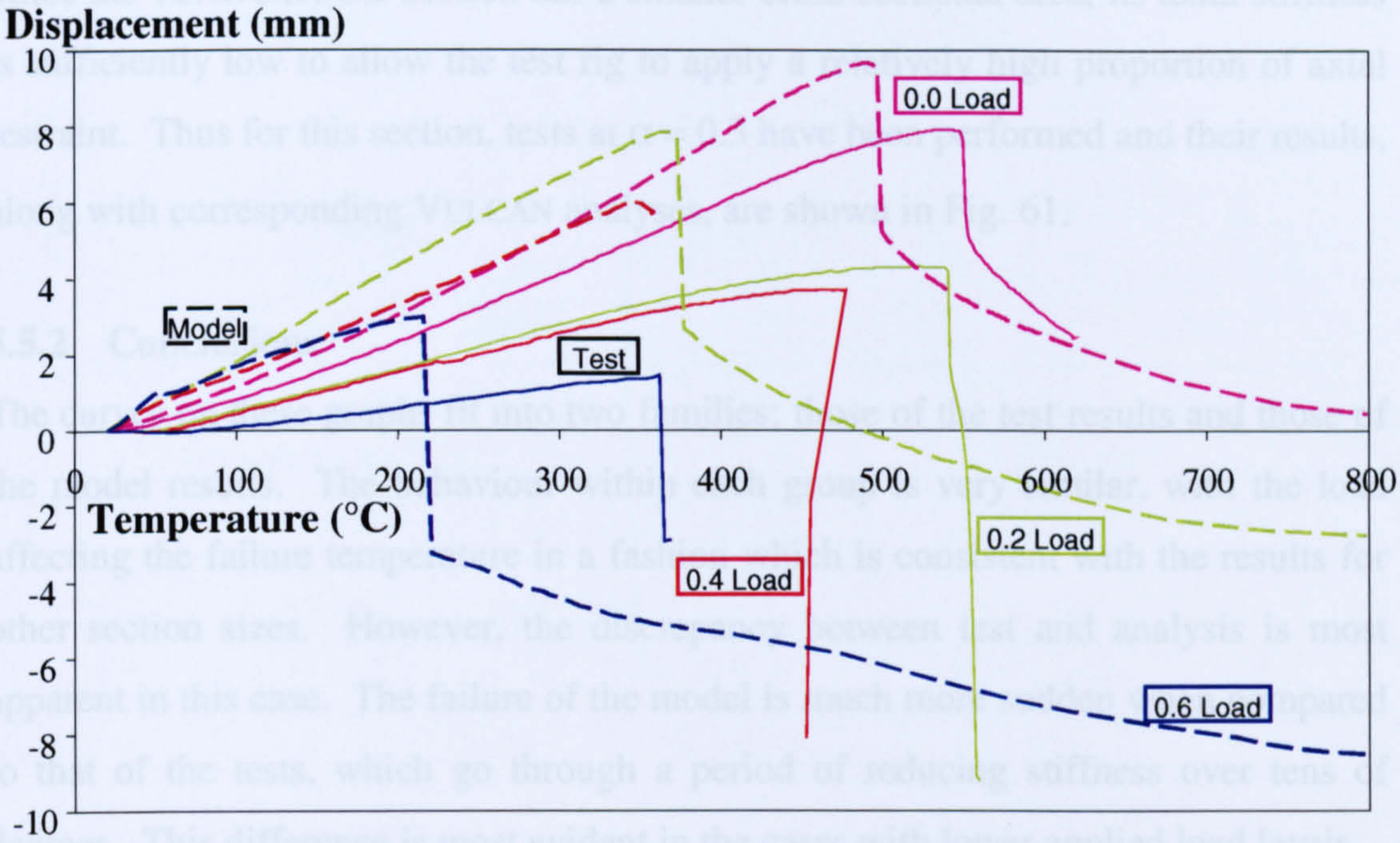

Fig. 56 Relative axial displacements of 178x102x19UB columns with $\alpha = 0.1$

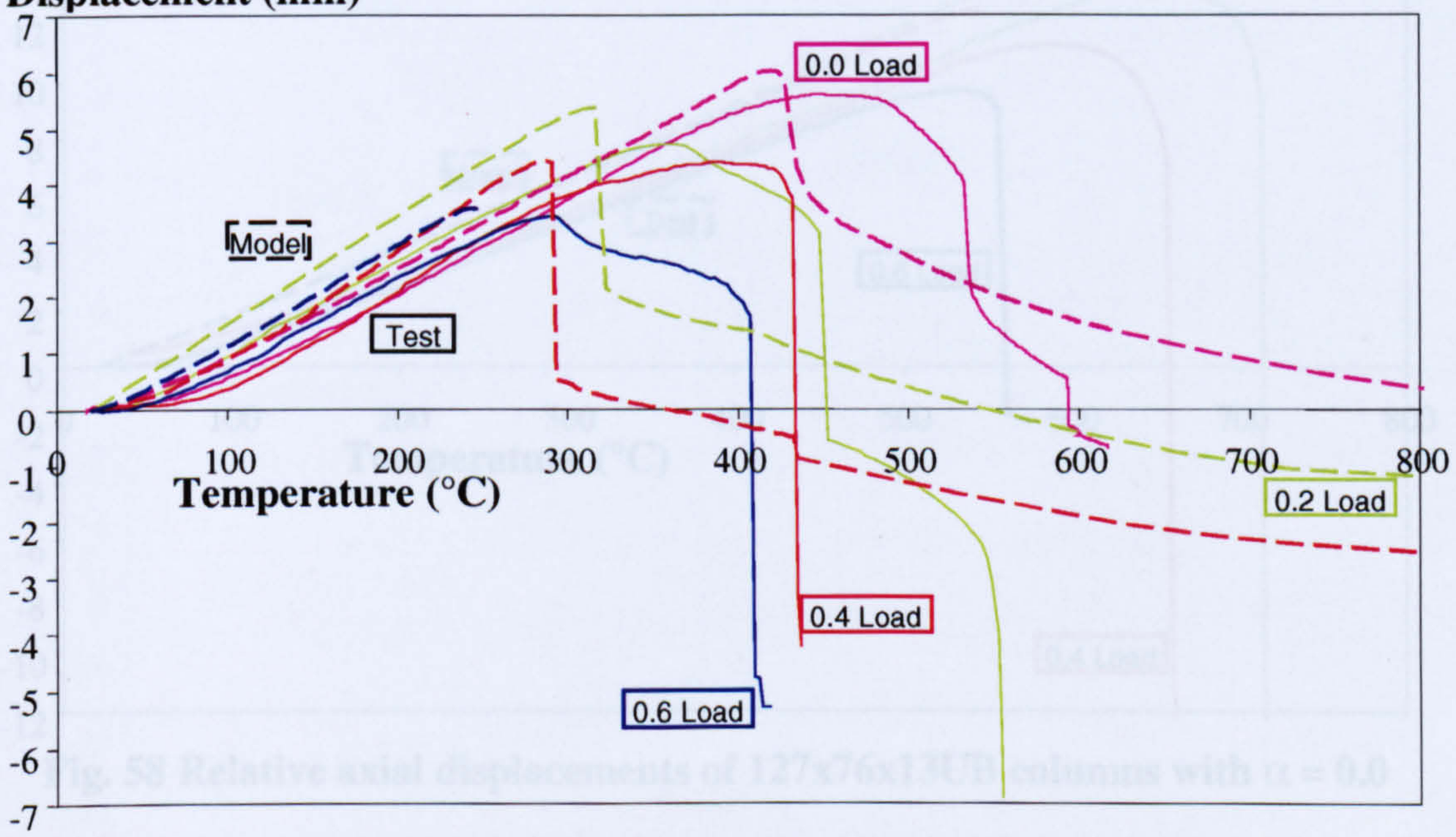

Fig. 57 Relative axial displacements of 178x102x19UB columns with $\alpha = 0.2$

5.5 127x76x13UB Results

This section concentrates on the axial displacement results for the 127x76x13UB sections.

5.5.1 Axial Displacement Results

Since the 127x76x13UB section has a smaller cross-sectional area, its axial stiffness is sufficiently low to allow the test rig to apply a relatively high proportion of axial restraint. Thus for this section, tests at $\alpha = 0.3$ have been performed and their results, along with corresponding VULCAN analyses, are shown in Fig. 61.

5.5.2 Conclusions

The curves on these graphs fit into two families; those of the test results and those of the model results. The behaviour within each group is very similar, with the load affecting the failure temperature in a fashion which is consistent with the results for other section sizes. However, the discrepancy between test and analysis is most apparent in this case. The failure of the model is much more sudden when compared to that of the tests, which go through a period of reducing stiffness over tens of degrees. This difference is most evident in the cases with lower applied load levels.

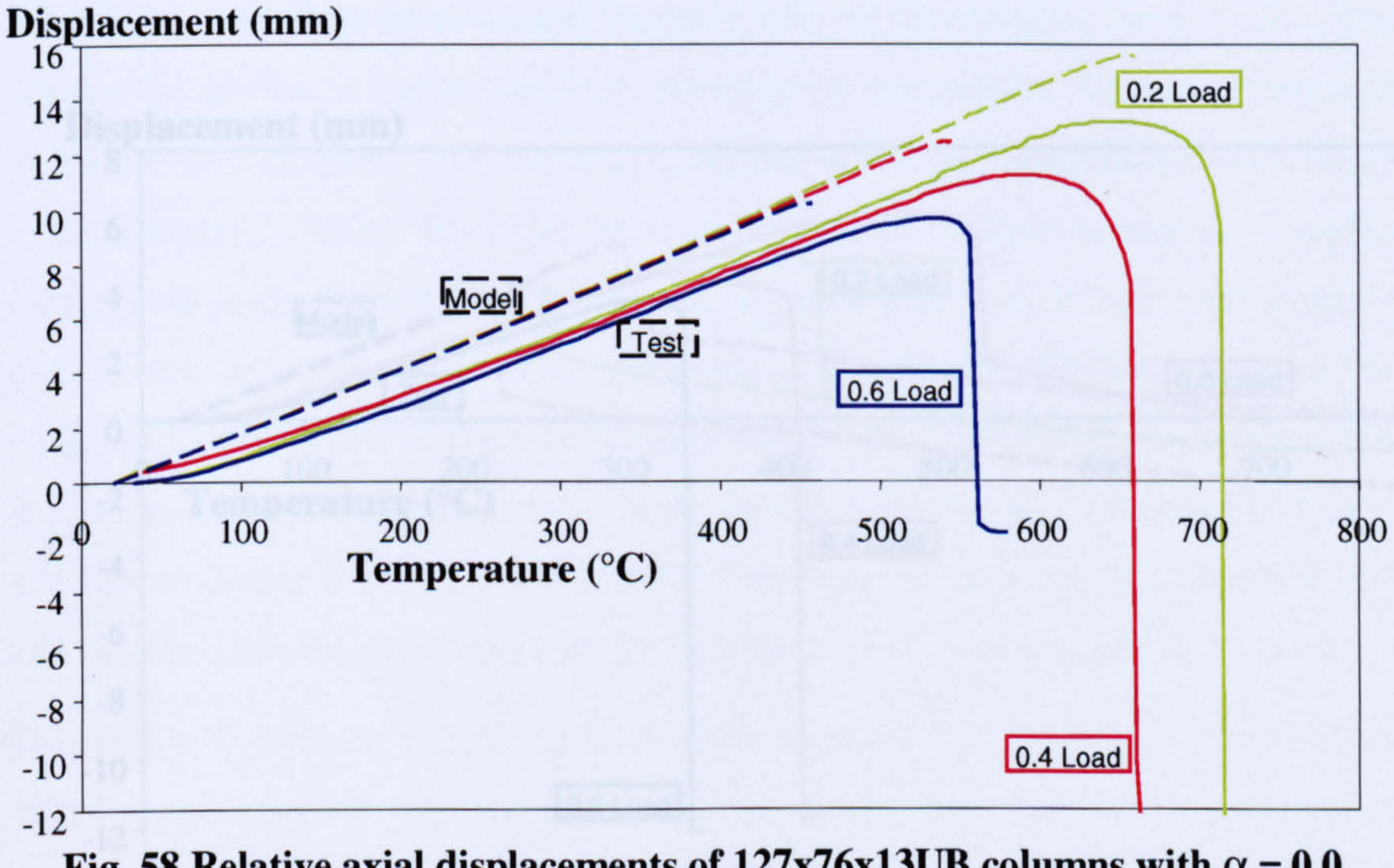

Fig. 58 Relative axial displacements of 127x76x13UB columns with $\alpha = 0.0$

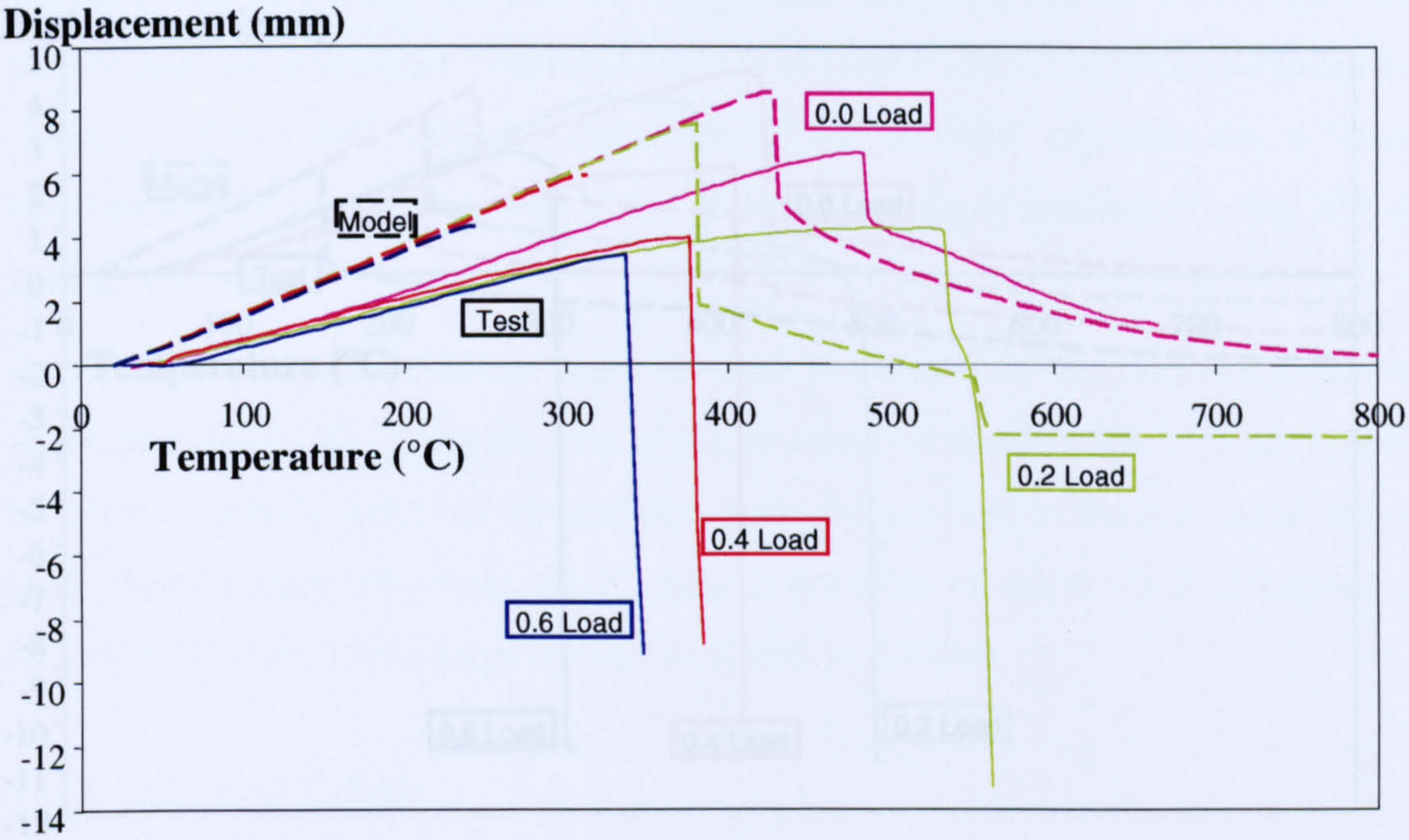

Fig. 59 Relative axial displacements of 127x76x13UB columns with $\alpha = 0.1$

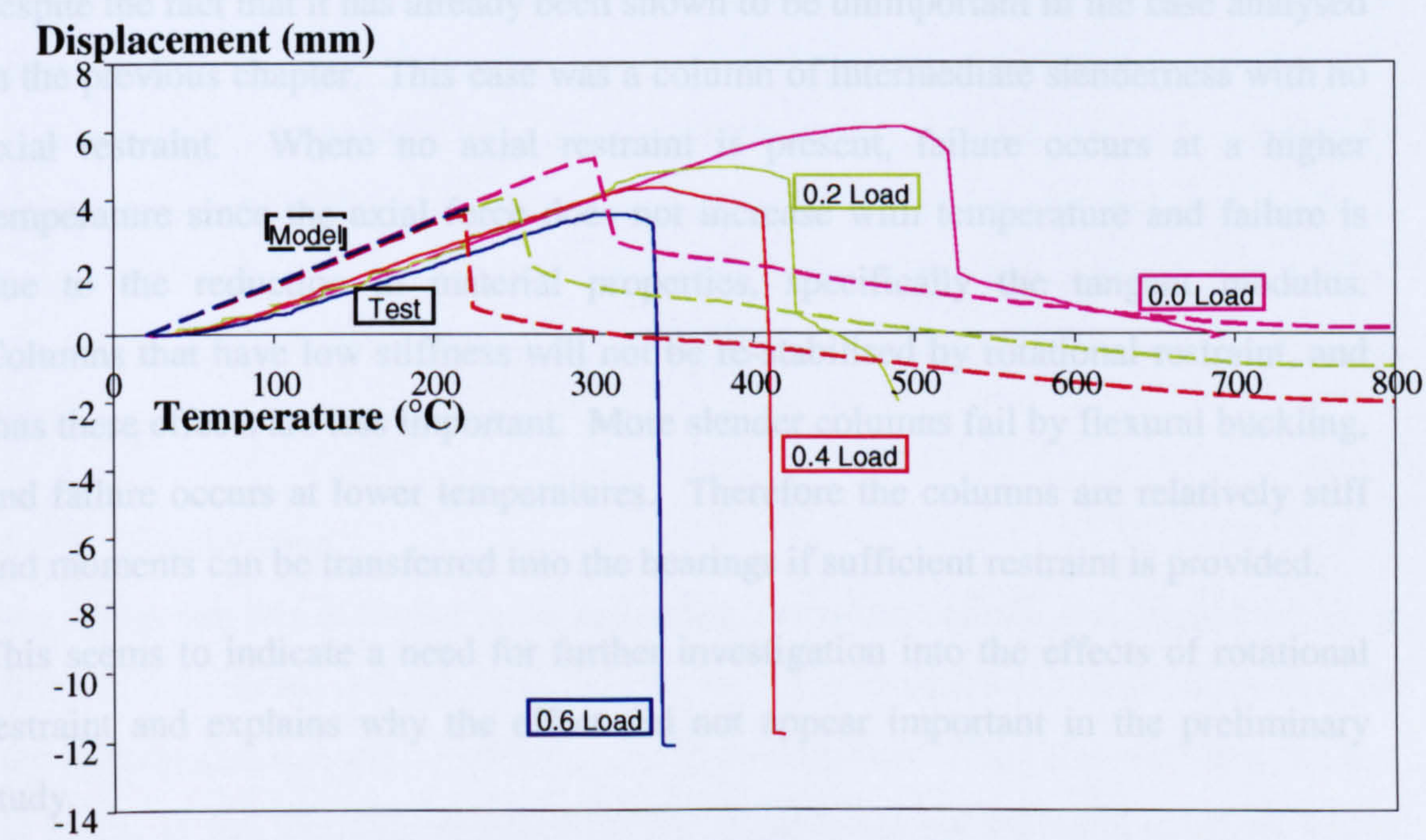

Fig. 60 Relative axial displacements of 127x76x13UB columns with $\alpha = 0.2$

Since this difference is most apparent in the case of the most slender section size, it is sensible to assume that the buckling behaviour is different in test and model. This is because buckling becomes the most dominant factor in the failure of slender columns, as shown in Chapter 2. Buckling is controlled by the effective length of the strut, which is dependent upon rotational restraint.

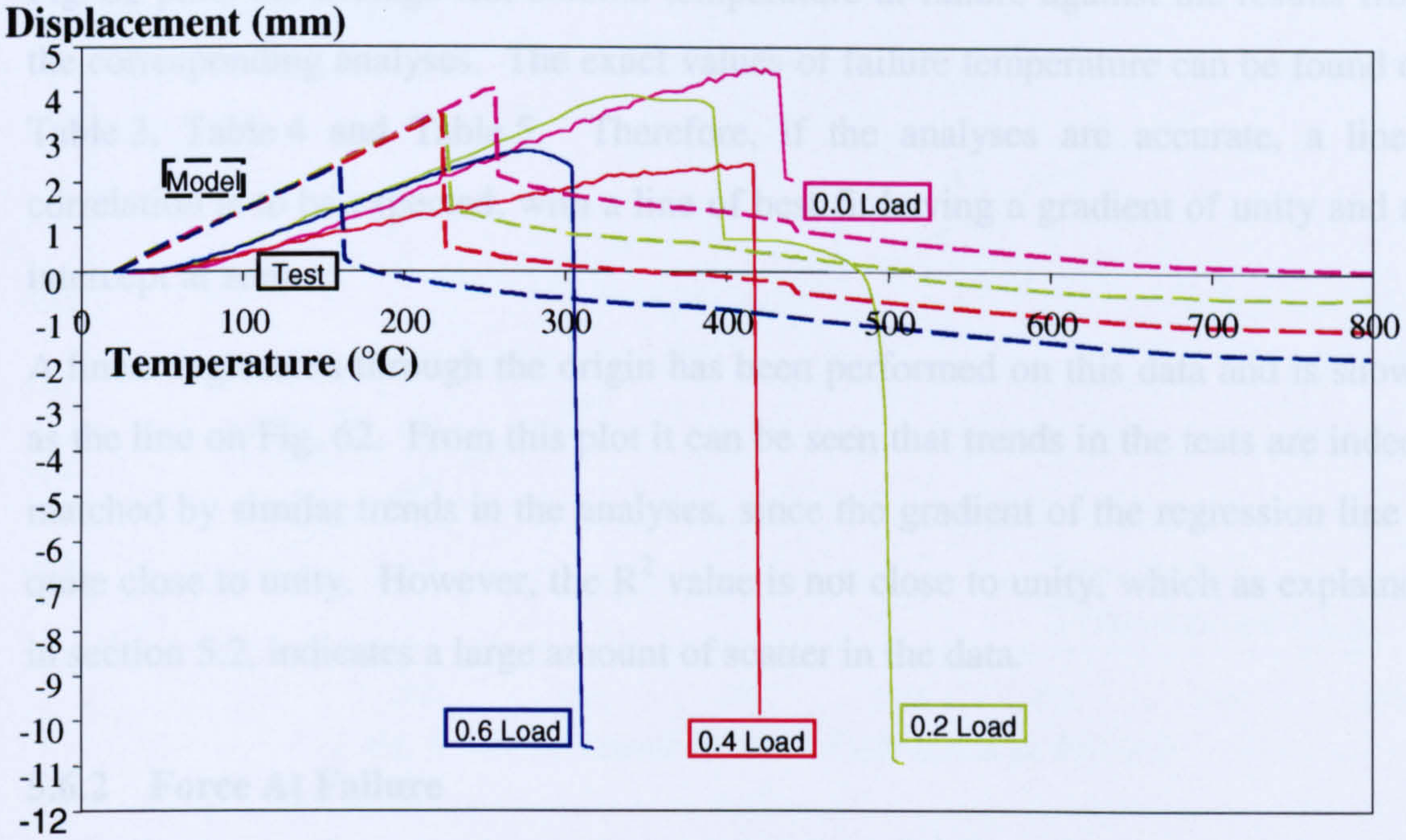

Fig. 61 Relative axial displacements of 127x76x13UB columns with $\alpha = 0.3$

Therefore, the effects of rotational restraint will be investigated more thoroughly, despite the fact that it has already been shown to be unimportant in the case analysed in the previous chapter. This case was a column of intermediate slenderness with no axial restraint. Where no axial restraint is present, failure occurs at a higher temperature since the axial force does not increase with temperature and failure is due to the reduction in material properties, specifically the tangent modulus. Columns that have low stiffness will not be re-stabilised by rotational restraint, and thus these effects are less important. More slender columns fail by flexural buckling, and failure occurs at lower temperatures. Therefore the columns are relatively stiff and moments can be transferred into the bearings if sufficient restraint is provided.

This seems to indicate a need for further investigation into the effects of rotational restraint and explains why the effect did not appear important in the preliminary study.

5.6 Overall Comparisons

This section gives an overall comparison of the way the results of the analyses differ from those found in the tests.

5.6.1 Temperature At Failure

Fig. 62 plots the average test-column temperature at failure against the results from the corresponding analyses. The exact values of failure temperature can be found on Table 3, Table 4 and Table 5. Therefore, if the analyses are accurate, a linear correlation is to be expected, with a line of best fit having a gradient of unity and an intercept at zero.

A linear regression through the origin has been performed on this data and is shown as the line on Fig. 62. From this plot it can be seen that trends in the tests are indeed matched by similar trends in the analyses, since the gradient of the regression line is quite close to unity. However, the R^2 value is not close to unity, which as explained in section 5.2, indicates a large amount of scatter in the data.

5.6.2 Force At Failure

A similar comparison can be made between the axial force in the test columns at failure, and the corresponding axial force in the model columns. The resulting graph is shown as Fig. 63 along with a linear regression through the origin. Again, the exact values of force at failure can be found on Table 3, Table 4 and Table 5. However, the axial force at failure in the columns with no axial restraint is obviously equal to the applied load in both test and analysis. Therefore, this test data has been omitted from Fig. 63, since it does not give an indication of the correlation of results. An excellent agreement between test and analysis can be seen, with both the gradient and R^2 value of the regression very close to unity.

5.6.3 Explanation

A column fire test is similar to an ambient temperature column test, in that the axial force in the column increases towards the buckling or squashing load (depending on the column slenderness), at which point the column fails. The difference in a fire test is that it is the thermal expansion of the column against the axial restraint which increases the load. In addition, the material properties of the steel change with temperature, so that the buckling load is reduced as the axial force is increased.

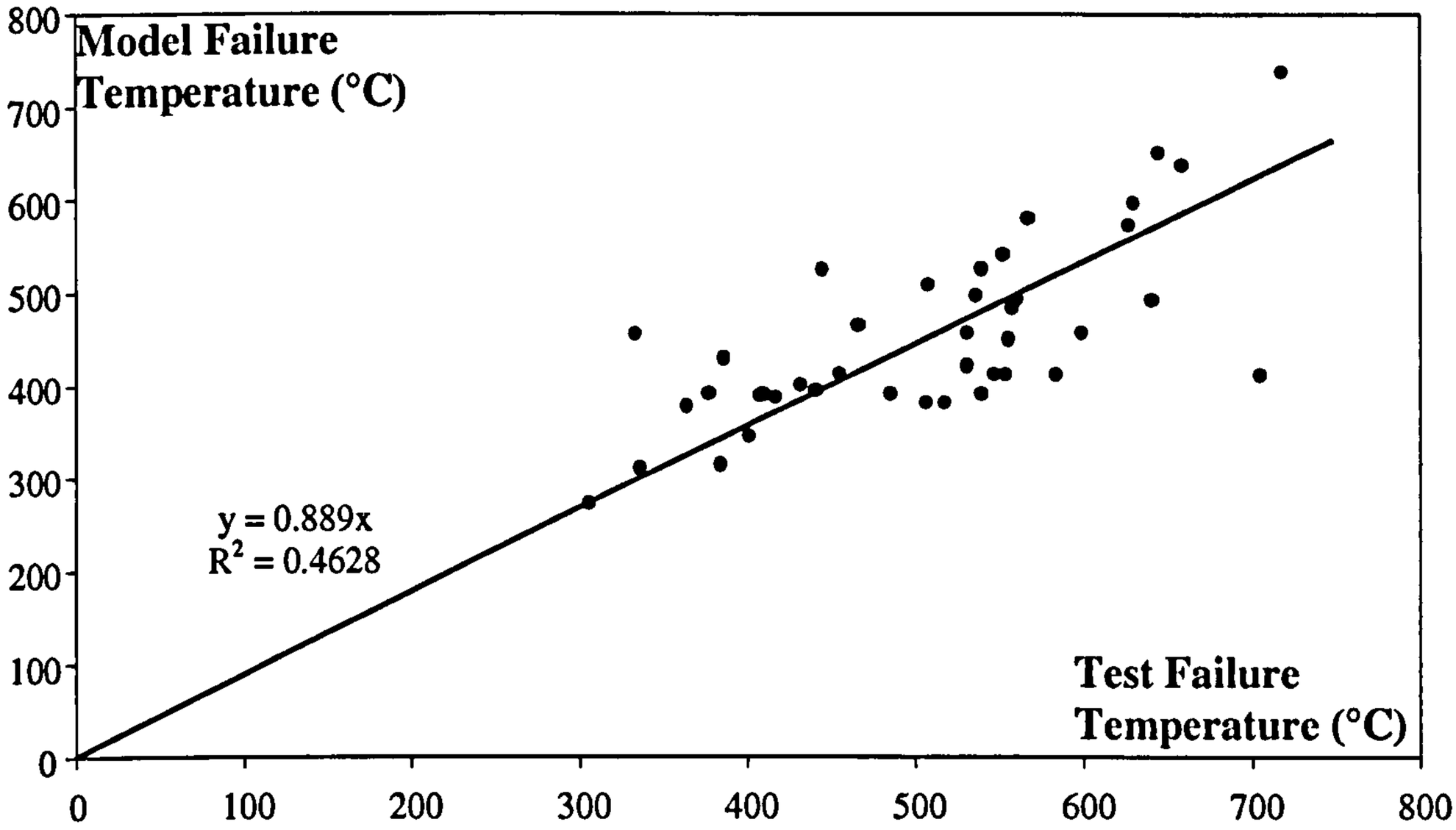

Fig. 62 Average temperature of columns at failure

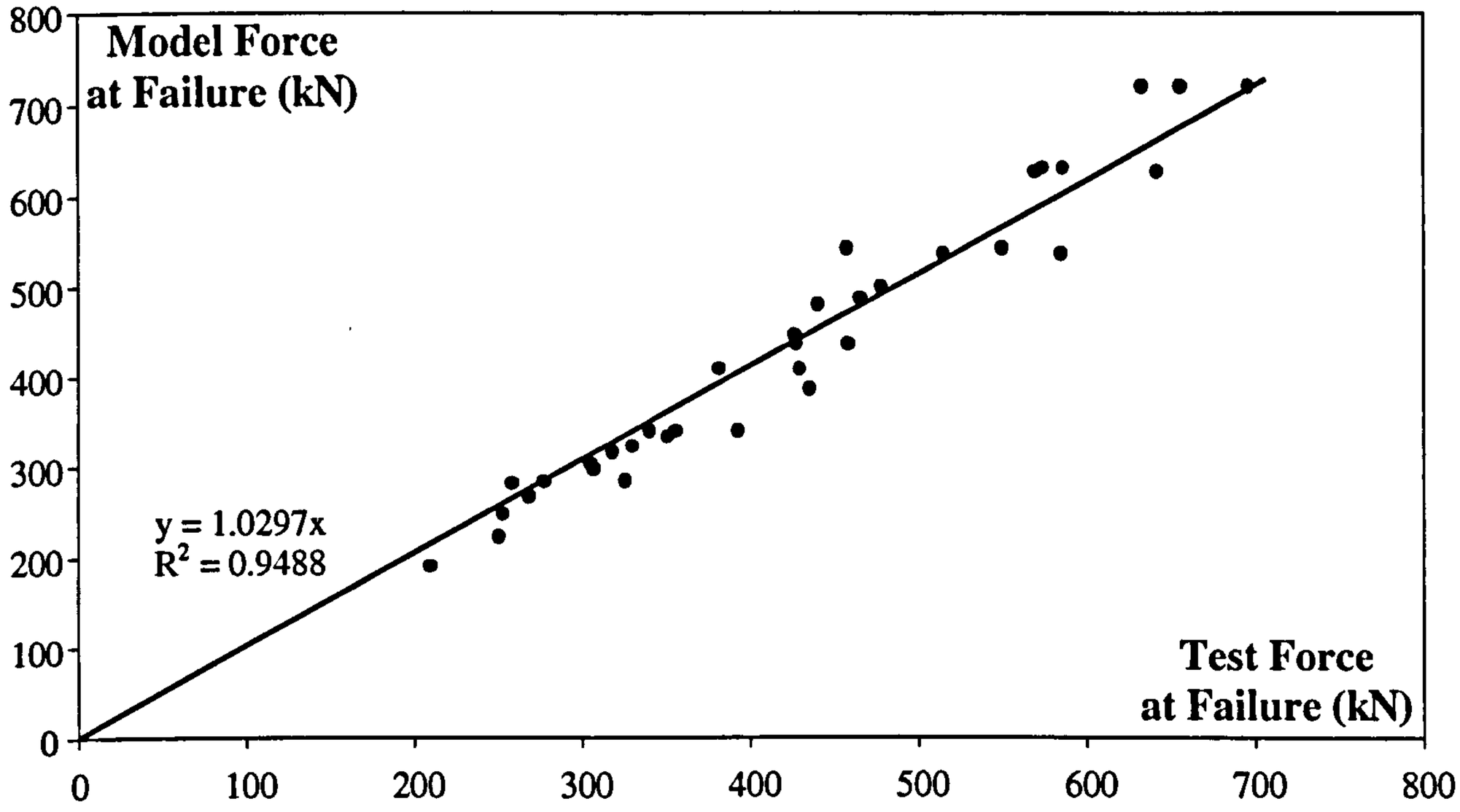

Fig. 63 Axial force in columns at failure

The fact that the above regression of axial force at failure shows such a good correlation indicates that the VULCAN model is accurate in assessing the buckling load for columns. However, this occurs at a different temperature to the corresponding failure in the test column. Therefore, the test and analysis columns will have different tangent modulus and yield strength at failure. Therefore, this close correlation is perhaps slightly misleading.

The design of the test rig allows the axial force in the test column to be measured directly by two pairs of load cells. One measures the applied load, the other measures the extra force, induced by thermal expansion against the axial restraint. It is not surprising therefore, that the measured values of axial force closely correlate with the theoretical values obtained from analysis.

Similarly, the thermocouples are attached to the column in such a way as to give the most accurate reading of steel temperature at a particular point and these temperature values are input directly into the analysis. Since the column is heated symmetrically from the bottom of the furnace, and exhaust gasses removed from the top, it is logical to assume a linear variation in temperature between thermocouple sites. Therefore, a similar level of correlation between results would be expected.

However, as discussed in section 5.3.1 and later, bedding-in has a significant effect on the behaviour of all test columns. The test columns are able to expand by a certain amount before the axial force begins to rise due to the closing of gaps in the restraining system. Since bedding-in is neglected in the analyses, the model columns have, in effect, a head start of around 50°C.

If we assume an initial thermal expansion coefficient of 1.3×10^{-5}, then the thermal strain induced by a 50°C rise in temperature would be $1.3 \times 10^{-5} \times 50 = 6.5 \times 10^{-4}$. Over a column length of 1.8m, this would result in a movement of only $6.5 \times 10^{-4} \times 1800 = 1.17$mm. It is quite feasible that the test rig has this level of lack-of-fit. Thus, the first 50°C of the column test are concerned with removing this lack of fit, without inducing any axial restraint force.

This then explains why a lack of correlation is seen in the temperatures at column failure, but not in the axial force at failure. The VULCAN model very accurately predicts the failure force of the column. The temperature at which this force is induced, however, is higher in the case of the test columns, since they take-up slack in the restraint system as they expand, without introducing a corresponding restraint force. This also explains the discrepancies in failure boundaries shown in Fig. 46 and Fig. 47.

6 Extensions To The Ulster Tests

For many practical reasons, the types of columns the Ulster rig is capable of testing are limited. Columns must be of a certain size and there are limits to the level of applied load and restraint. Computer analyses are not bound by such constraints, which makes them a valuable tool for performing parametric studies once they have been validated against test results. This chapter extends the Ulster test program in this way, and attempts to give an insight into the behaviour of steel columns in fire.

6.1 Effect Of Axial Restraint Stiffness

The Ulster rig can apply a maximum relative restraint factor of 0.3, and this is only possible by using 127x76x13UB sections and removing the rubber springs to utilise the rig itself as restraint. VULCAN can be used to analyse the behaviour of columns with any amount of restraint applied by specifying a particular stiffness for the restraint spring. This small study shows how changing the restraint factor over a wide range of values affects the behaviour of the column.

6.1.1 Results

To isolate the effect of restraint, the columns are heated uniformly, so temperature gradients are not a factor. Both 152x152x23UC and 127x76x13UB column sections have been analysed to show how the behaviour changes between stocky and slender columns. The section size and level of imperfection is based on the test with 0.6 Load Ratio and 0.0 Restraint Factor for each slenderness.

The axial displacement for 152x152x23UC columns is shown on Fig. 64 and for 127x76x13UB columns on Fig. 65. The test results are shown as broken lines for comparison only, and it should be remembered that the tests had longitudinal temperature profiles very different from the uniform profile assumed in the model.

It must also be remembered that the test set-up is such that the restraint springs are unable to carry any tension force. Therefore, when the axial displacement of the column top is negative, the column is shortening relative to its original length, and the test becomes totally unrestrained. The column's displacement will then go into run-away rather than allowing the restraint to stabilise the behaviour. This is a very important distinction between the tests and the analyses on all graphs.

The relatively squat 152x152x23UC sections fail by squashing and their failure temperature is thus dominated by the material properties and heating regime. It is unsurprising therefore, that these column tests behave fairly consistently and are accurately modelled by VULCAN. Indeed the analyses accurately predict the maximum level of axial displacement attained, although there is some disagreement as to the temperature at which this occurs. From the two dashed green curves on Fig. 64, which show the results from the two tests performed with a relative restraint factor of 0.1, a similar level of discrepancy between two supposedly similar column tests can be seen. This is almost certainly attributable to the differing heating regimes imposed on these two columns, although there is also a difference in the measurement of the axial displacement, which is discussed later.

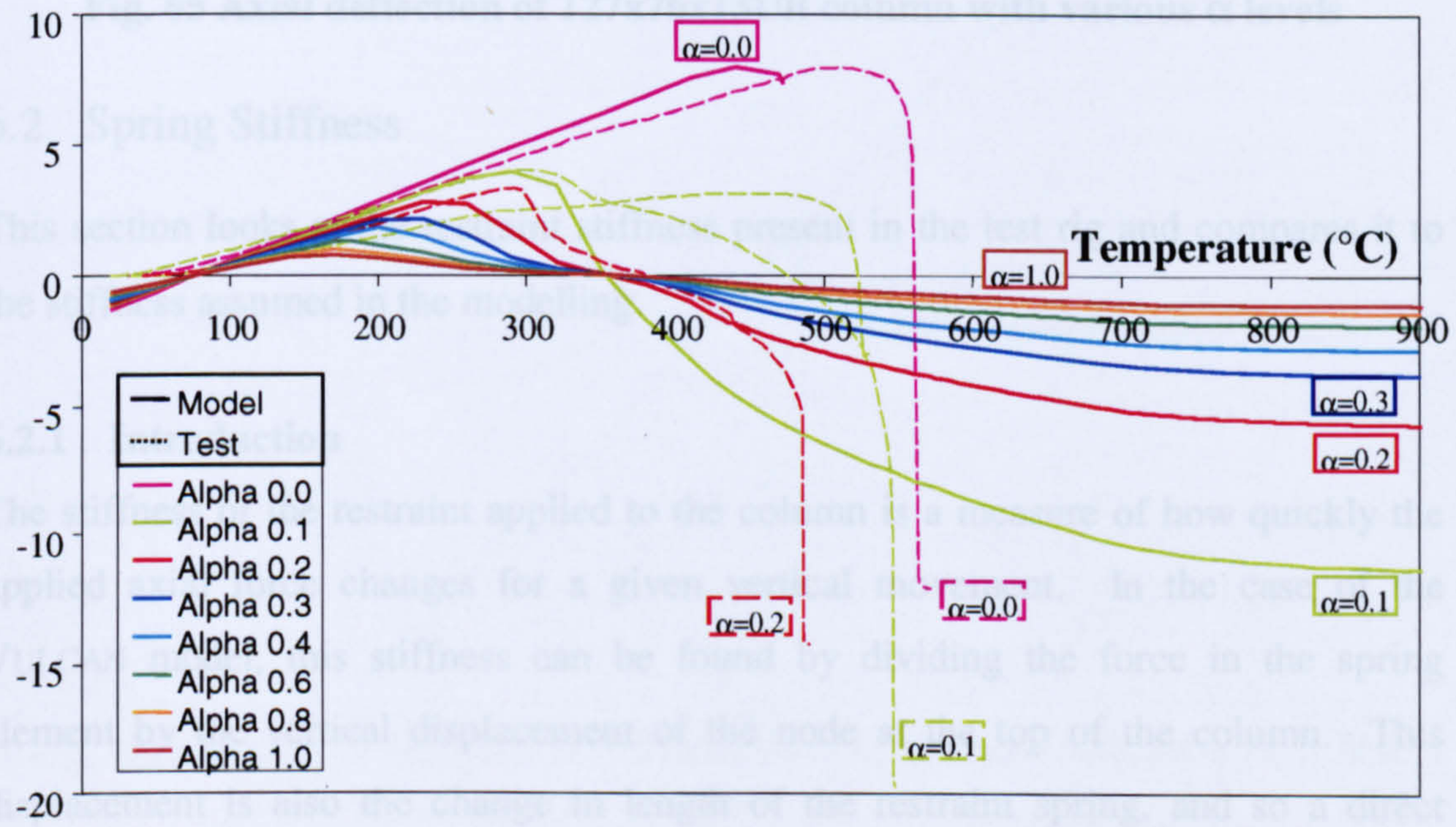

Fig. 64 Axial deflection of 152x152x23UC column with various α levels

The analyses of the slender 127x76x13UB columns also behave consistently, showing a steady decrease in maximum axial displacement as the restraint is increased. The familiar crossing of the curves can also be seen when the column returns to its original length. However, the test results do not show this trend as clearly, and the cases that have some degree of axial restraint fail with similar levels of axial expansion. This could be attributed to differences in temperature profiles. However, the slender columns fail by buckling, which is much more sensitive to geometric and material imperfections. These effects can also contribute to the inconsistency of the results and are not incorporated into the VULCAN analyses.

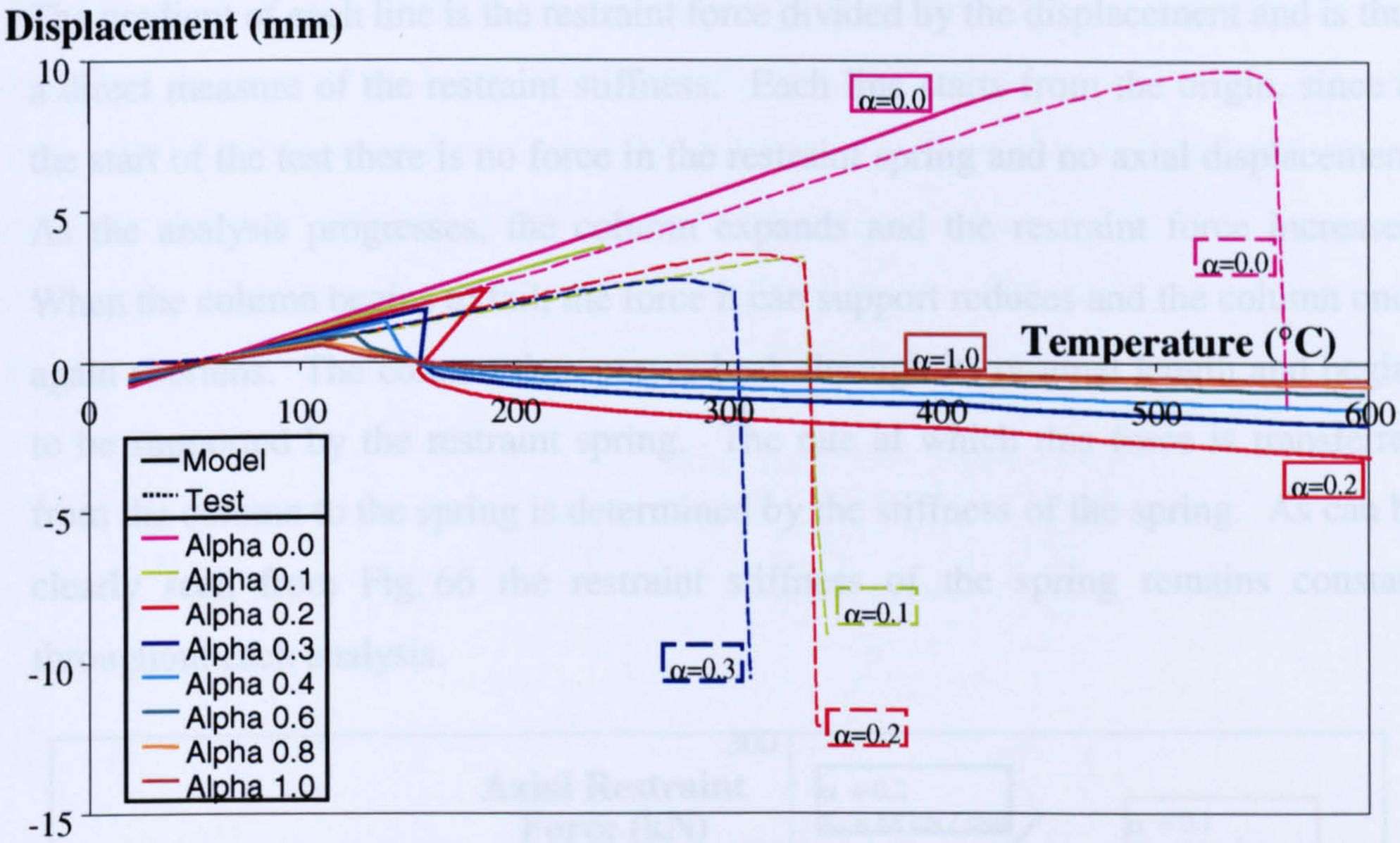

Fig. 65 Axial deflection of 127x76x13UB column with various α levels

6.2 Spring Stiffness

This section looks at the restraint stiffness present in the test rig and compares it to the stiffness assumed in the modelling.

6.2.1 Introduction

The stiffness of the restraint applied to the column is a measure of how quickly the applied axial force changes for a given vertical movement. In the case of the VULCAN model, this stiffness can be found by dividing the force in the spring element by the vertical displacement of the node at the top of the column. This displacement is also the change in length of the restraint spring, and so a direct measurement of the restraint stiffness is possible. Similarly, a measure of the restraint stiffness present in the test rig can be found by dividing the measured force in the restraint springs by the vertical displacement of the top of the column.

6.2.2 Restraint In VULCAN Model

Fig. 66 shows the restraint force and axial displacement that should ideally be present in the 152x152x23UC model column tests with 0.6 x the EC3 design load. The curve for the test with zero axial restraint lies along the displacement axis since negligible restraint force is induced during the analysis.

The gradient of each line is the restraint force divided by the displacement and is thus a direct measure of the restraint stiffness. Each line starts from the origin, since at the start of the test there is no force in the restraint spring and no axial displacement. As the analysis progresses, the column expands and the restraint force increases. When the column begins to fail, the force it can support reduces and the column once again shortens. The column then passes back through its original length and begins to be supported by the restraint spring. The rate at which this force is transferred from the column to the spring is determined by the stiffness of the spring. As can be clearly seen from Fig. 66 the restraint stiffness of the spring remains constant throughout each analysis.

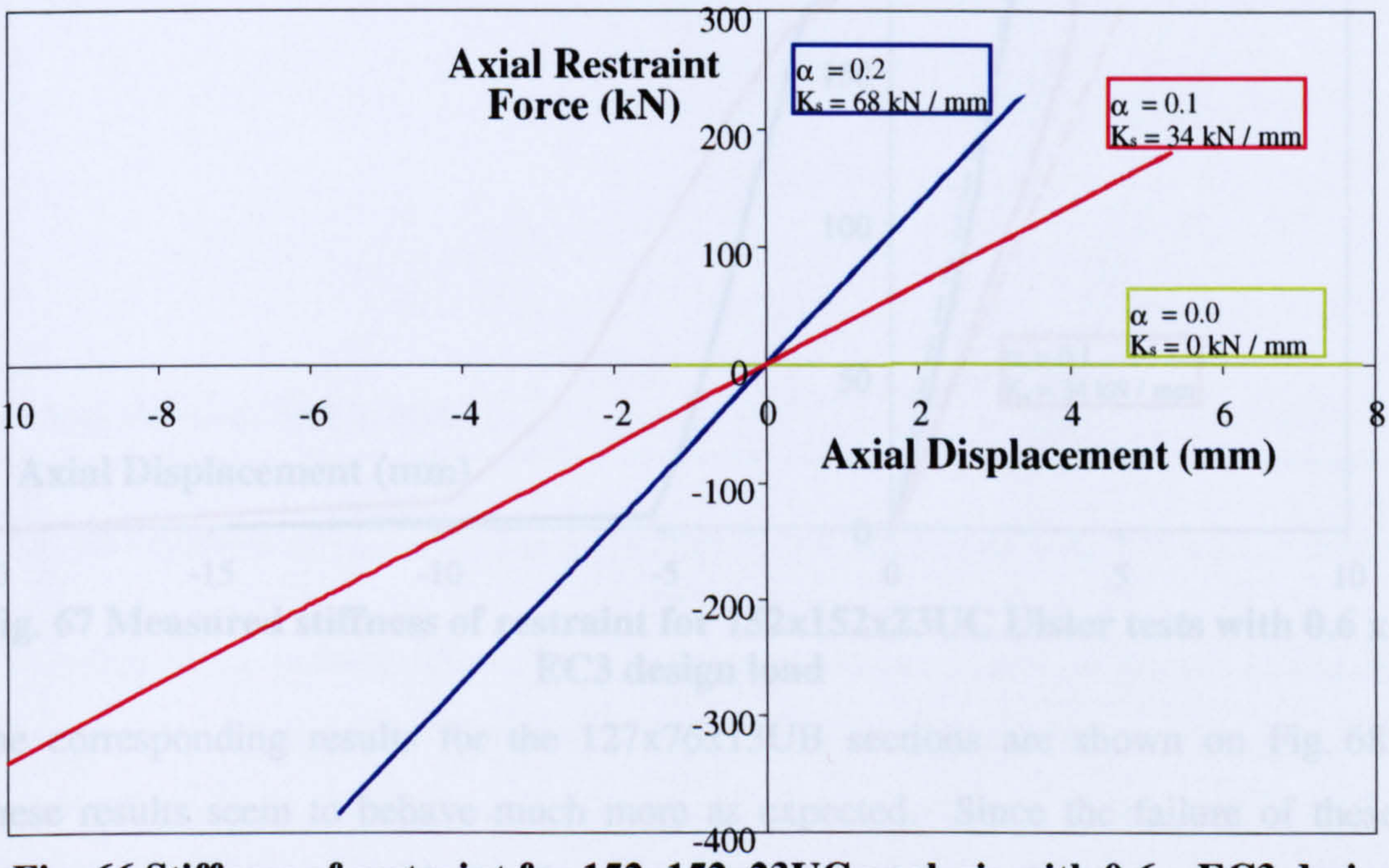

Fig. 66 Stiffness of restraint for 152x152x23UC analysis with 0.6 x EC3 design load

6.2.3 Restraint In Ulster Tests

In a similar fashion, the restraint stiffness present in the Ulster test rig can be derived from the gradient in the axial force – displacement graph of Fig. 67. There are no results for the test with zero axial restraint since the load-cells were not present in this test.

Dashed lines of constant gradient equal to the restraint stiffness expected in each test are shown for comparison with the measurements. It can be seen that in the initial part of the test, as the columns expand the restraint force increases. The stiffness is indeed close to that expected, since the test curves have a similar initial gradient to

the dashed lines. However, as the column load reaches a maximum and then begins to reduce as the columns begin to shorten, the force does not drop off at the expected rate. This introduces a hysteresis into the curves. Once the columns are much shorter than their original length, the stiffness again seems to be close to that expected. However, it would seem from these results that during the "failure" process, the stiffness of the supporting system changes dramatically.

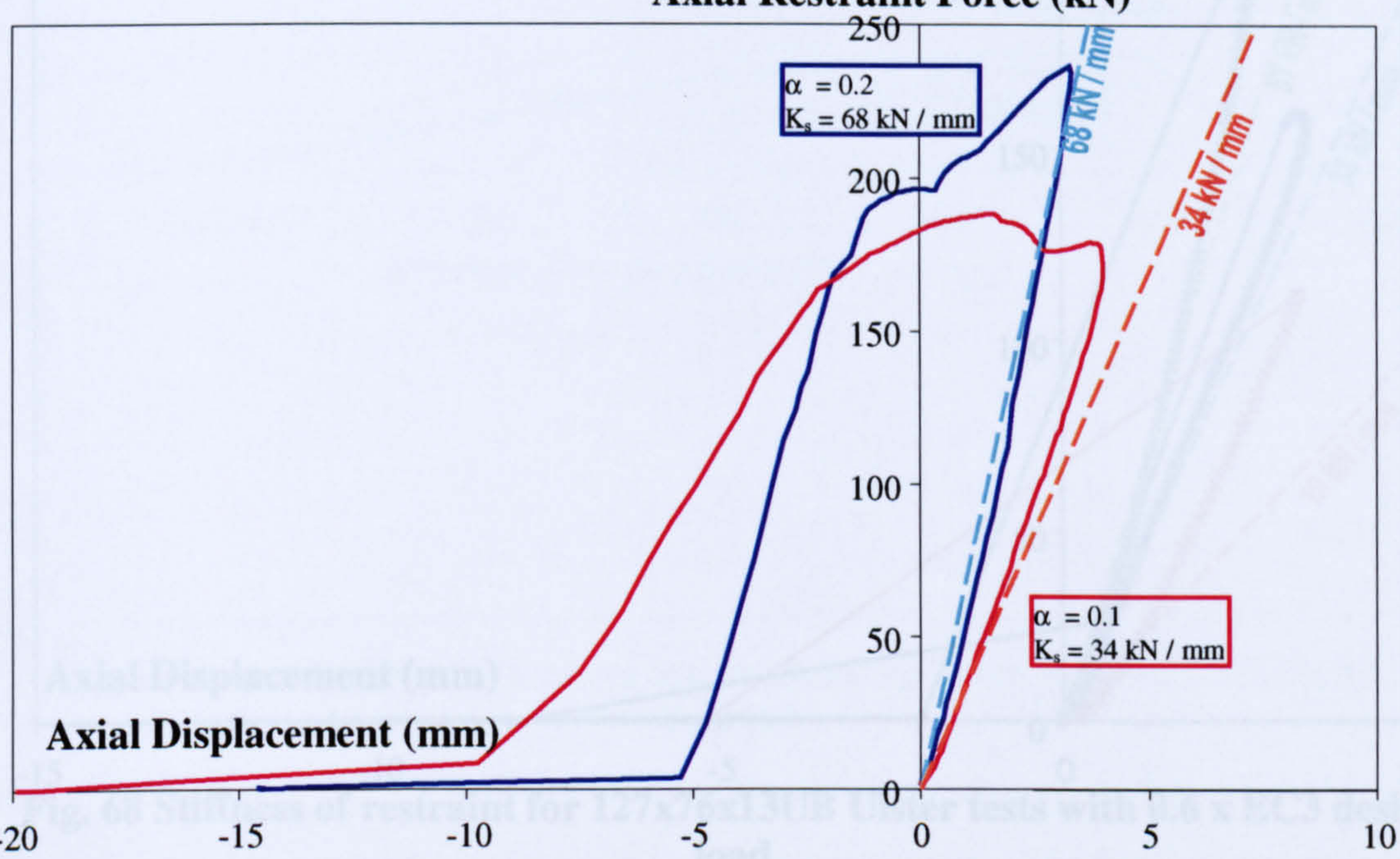

Fig. 67 Measured stiffness of restraint for 152x152x23UC Ulster tests with 0.6 x EC3 design load

The corresponding results for the 127x76x13UB sections are shown on Fig. 68. These results seem to behave much more as expected. Since the failure of these columns happens very suddenly, there are few data points on the descending part of the curve. However, in the region of "failure", the curves reverse direction along a path that has much the same stiffness as that at which loads increased. Although behaving more linearly, the 127x76x13UB test with lowest restraint stiffness seems to have a much higher level of restraint than expected.

These worrying discrepancies in the assumed and actual stiffnesses of the restraint for the test columns were thoroughly investigated. The effect was generally most pronounced in the 152x152x23UC tests where failure occurred over a long period.

It was deduced that the restraining beam at the top of the rig was not moving freely on its guide rods, causing a rotation. This rotation was not measured since, at the top of the column, the axial displacement was only measured at the middle of the top

restraining-beam of the test rig. A repeat test was performed (Test B) in which the axial displacement was additionally measured at either end of the beam. No applied load was present, so that only the effects of restraint were observed. Thermocouples were introduced on the top restraining-beam to ascertain whether heat escaping from the furnace was also introducing thermal bowing in the top beam.

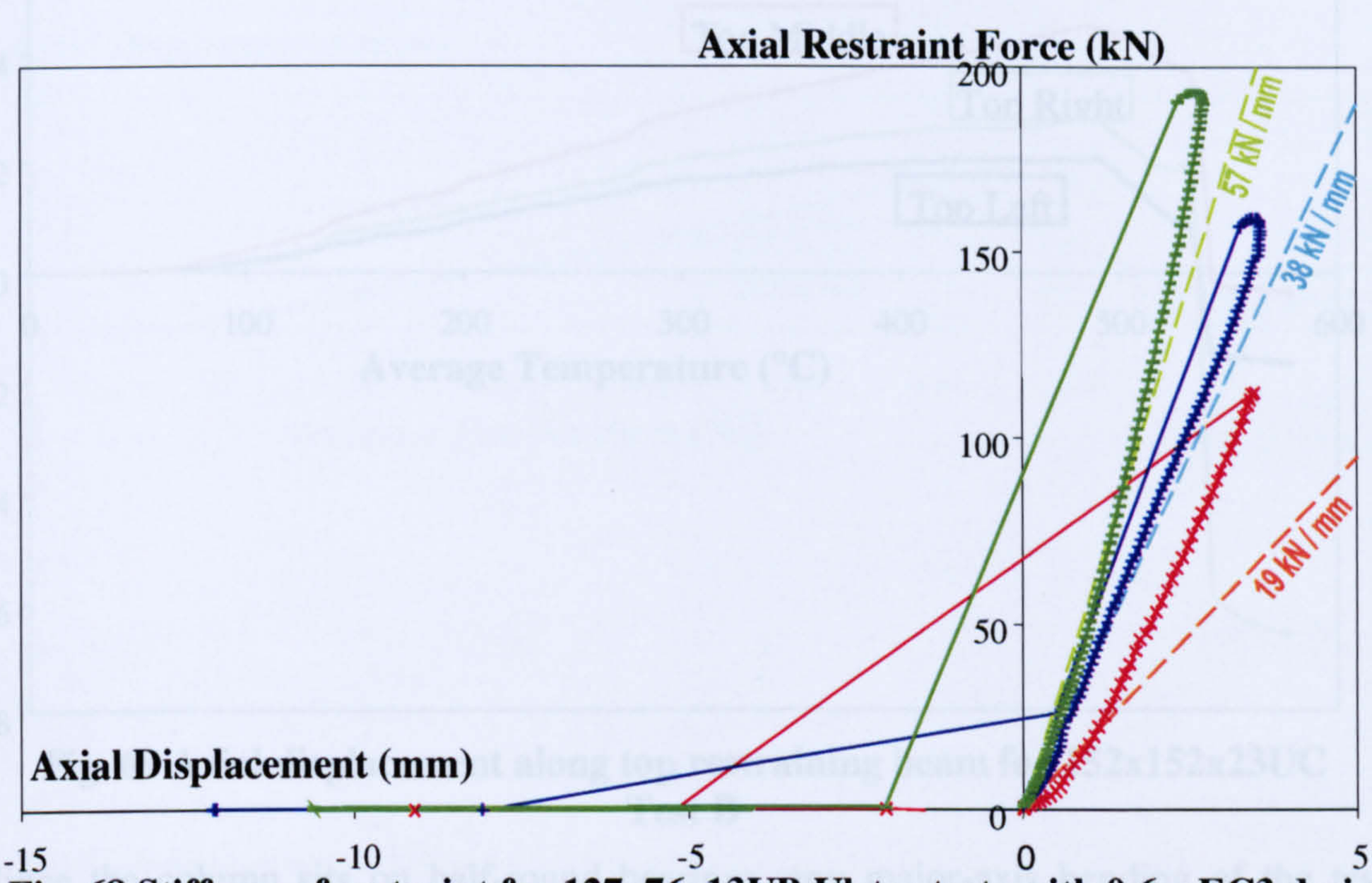

Fig. 68 Stiffness of restraint for 127x76x13UB Ulster tests with 0.6 x EC3 design load

Little difference between these three displacements was found, as shown in Fig. 69. The greatest displacement was found in the middle of the beam. This was to be expected since the beam is pushed upwards by the column at the middle and is restrained by the springs at the ends of the beam. However, there is only about 1mm of difference between the displacement of the left and right hand sides of the beam, indicating that the beam remains almost horizontal during the test. The thermocouples also showed that thermal expansion of the restraining beam was not a factor, since its temperature never rose above 50°C.

The restraining forces are measured at either end of the restraining beam, and these are added together to give the total restraint force. Therefore, it is sensible to use the average axial displacement of the ends of the restraining beam to calculate the restraint stiffness. However, as Fig. 69 shows, there is so little difference in the movement of either end of the beam that refining these measurements does not solve the problem of an apparent change in restraint stiffness. It was suggested that this

discrepancy was due to the top restraining beam rotating about its own axis. This is likely to happen if thermal gradients or initial geometric imperfections are present with respect to the major axis of the test column.

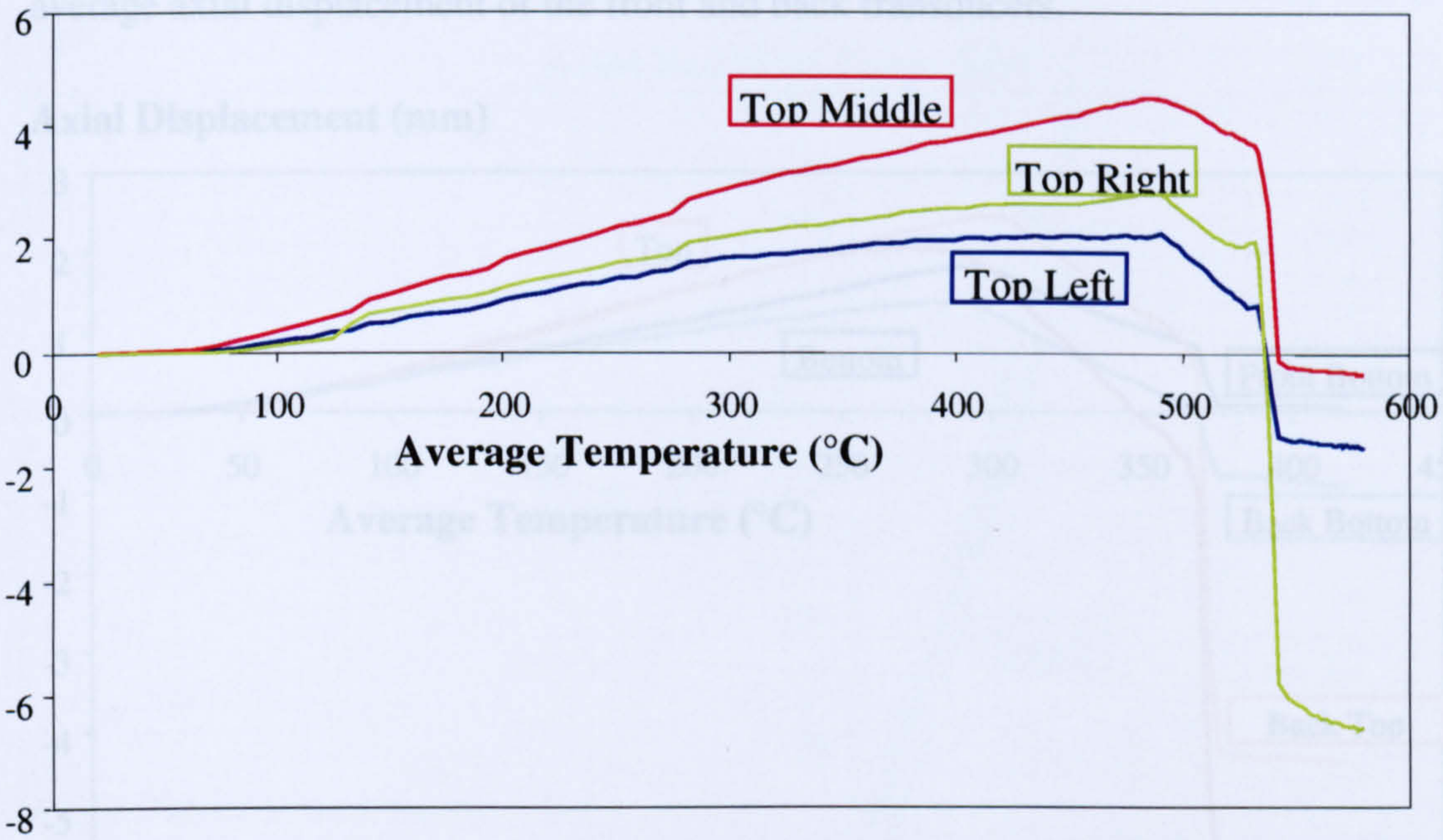

Fig. 69 Axial displacement along top restraining beam for 152x152x23UC Test B

Since the column sits on half-round bearings, any major-axis bending of the test column would be converted into a rotation in the top beam. The back of the restraint beam is able to move downwards, releasing the reaction force, whilst the front of the beam remains stationary. By only measuring the displacement at the front of the beam, it appears that no axial movement occurs, even though the mean force decreases. A second repeat test (Test C) was performed with axial displacement transducers placed at the back of the restraining beam, as well as at the standard position at the front of the beam. These displacements are plotted on Fig. 70.

An out-of-plane beam section was added to the test rig in this case, to minimise top-beam rotation. With this rig modification, it can be seen from Fig. 70 that the beam does not now rotate about its own axis. The difference in axial displacement is only a matter of a couple of millimetres, and over the width of the restraining beam (248mm) results in a rotation of less than 0.5°. This means that near failure, the force in the restraint springs cannot now reduce without a corresponding axial shortening being measured.

By taking an average of the displacement at the front and back of the beam, the axial movement transferred to the restraint springs can be calculated, and thus a more accurate idea of the restraint stiffness is found. A new Force – Displacement graph has been plotted in Fig. 71. Here, the axial displacement used for the X-axis is the average axial displacement of the front and back transducers.

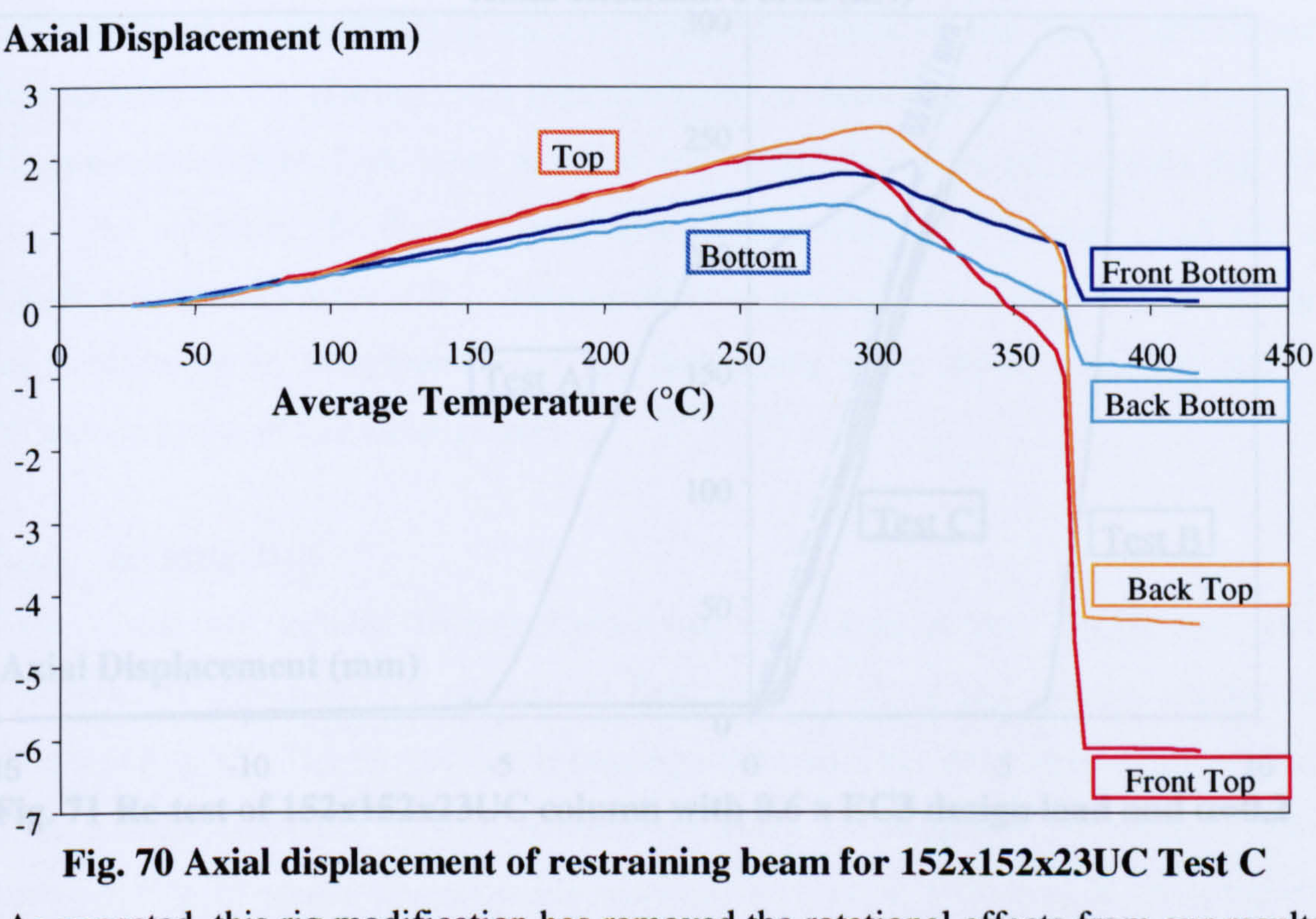

Fig. 70 Axial displacement of restraining beam for 152x152x23UC Test C

As expected, this rig modification has removed the rotational effects from our results and the restraint applied to the column now appears reasonably linear. A further repeat test of the $\alpha = 0.1$ case was conducted and the results are shown on Fig. 72. This evidence resulted in the re-testing of all 152x152x23UC column-sections, using the modified rig, which minimised out of plane rotation.

The presence of the lateral beam can certainly be seen to improve the linearity of the response of the restraint to the increasing load and displacement, especially within the region of failure. However, the gradient of the black curve on Fig. 72 is not constant as the test progresses. This could be due to a non-linear behaviour of the rubber springs. However, these have been tested in isolation and have been shown to be linear in the rage of stresses present during the tests. Therefore, it must be assumed that the restraint stiffness is indeed linear, and it is inaccuracies in measuring the axial displacements which leads to this effect. For example, the presence of the lateral beam reduces, but does not totally eliminate rotation of the top

beam about its own axis. Thus, the level of major axis bending in the test column will be seen to change the restraint stiffness of the rig, whereas in fact it is simply the measurement of the axial displacement which is inaccurate.

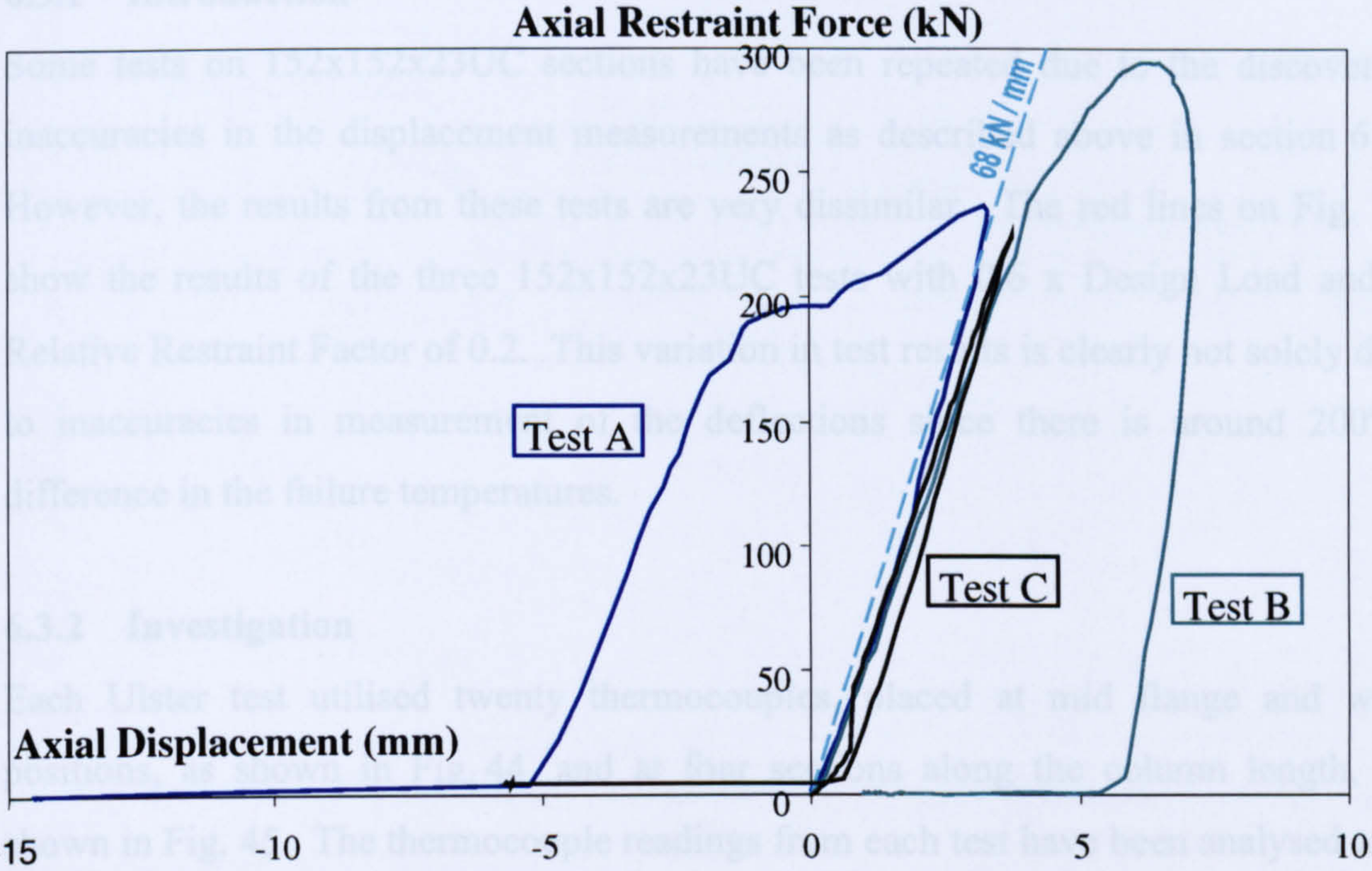

Fig. 71 Re-test of 152x152x23UC column with 0.6 x EC3 design load and α=0.2

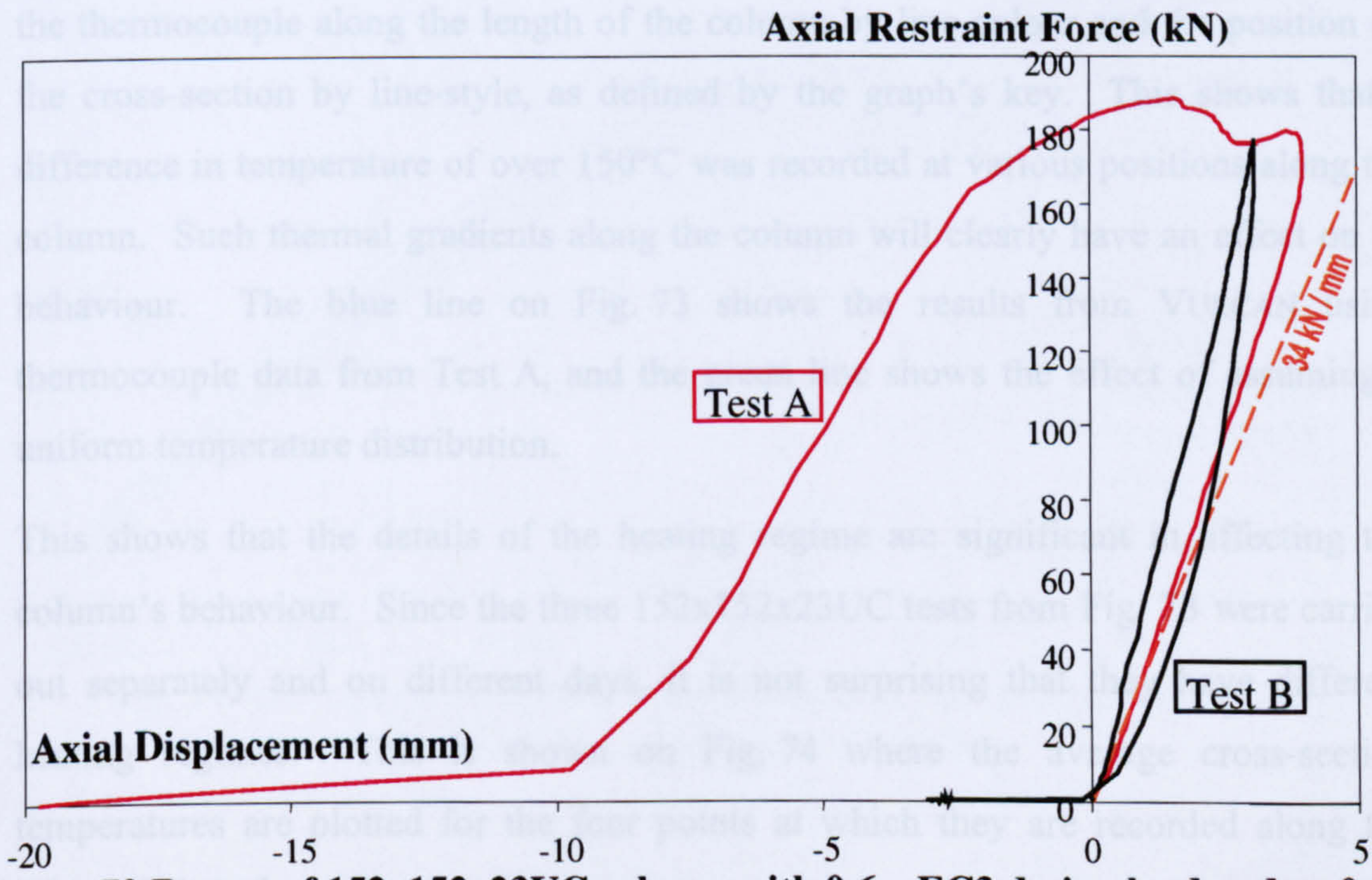

Fig. 72 Re-test of 152x152x23UC column with 0.6 x EC3 design load and α=0.1

6.3 Effect Of Temperature Distribution

This section investigates the effect of temperature distribution on the behaviour of the column.

6.3.1 Introduction

Some tests on 152x152x23UC sections have been repeated due to the discovered inaccuracies in the displacement measurements as described above in section 6.2. However, the results from these tests are very dissimilar. The red lines on Fig. 73 show the results of the three 152x152x23UC tests with 0.6 x Design Load and a Relative Restraint Factor of 0.2. This variation in test results is clearly not solely due to inaccuracies in measurement of the deflections since there is around 200°C difference in the failure temperatures.

6.3.2 Investigation

Each Ulster test utilised twenty thermocouples, placed at mid flange and web positions, as shown in Fig. 44, and at four sections along the column length, as shown in Fig. 45. The thermocouple readings from each test have been analysed and show a large difference in steel temperature along the length of the section. For example, Fig. 75 shows thermocouple readings for Test A, indicating the position of the thermocouple along the length of the column by line-colour and the position on the cross-section by line-style, as defined by the graph's key. This shows that a difference in temperature of over 150°C was recorded at various positions along the column. Such thermal gradients along the column will clearly have an effect on its behaviour. The blue line on Fig. 73 shows the results from VULCAN using thermocouple data from Test A, and the green line shows the effect of assuming a uniform temperature distribution.

This shows that the details of the heating regime are significant in affecting the column's behaviour. Since the three 152x152x23UC tests from Fig. 73 were carried out separately and on different days, it is not surprising that they have different heating regimes. This is shown on Fig. 74 where the average cross-section temperatures are plotted for the four points at which they are recorded along the column's length.

Much more critical in affecting the column behaviour is a thermal gradient between different points within cross-sections. Fig. 75 shows that there is typically around 50°C difference between the temperatures of column flanges for Test A.

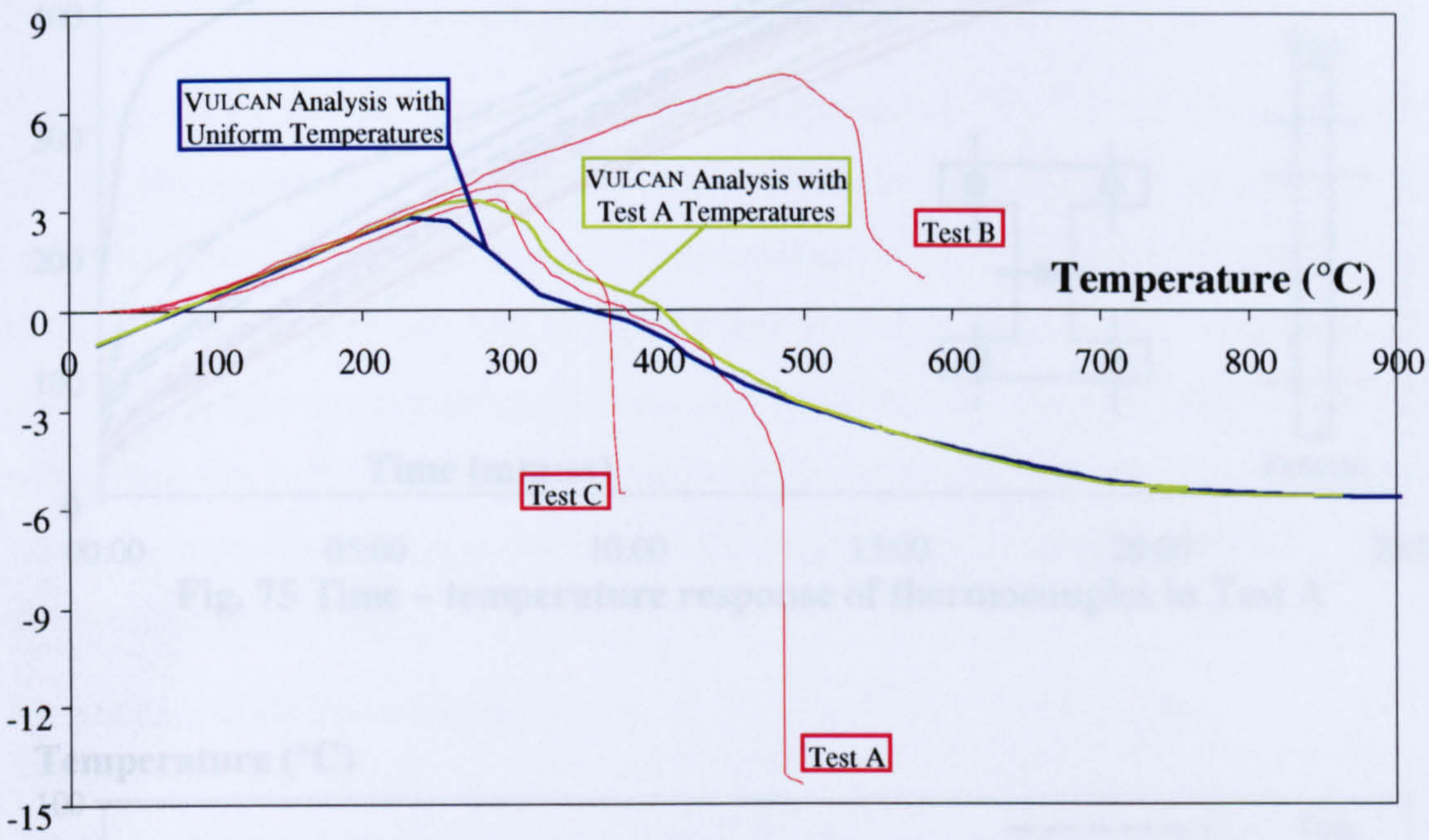

Fig. 73 Effect of temperature profile on 152x152x23UC column (α = 0.2)

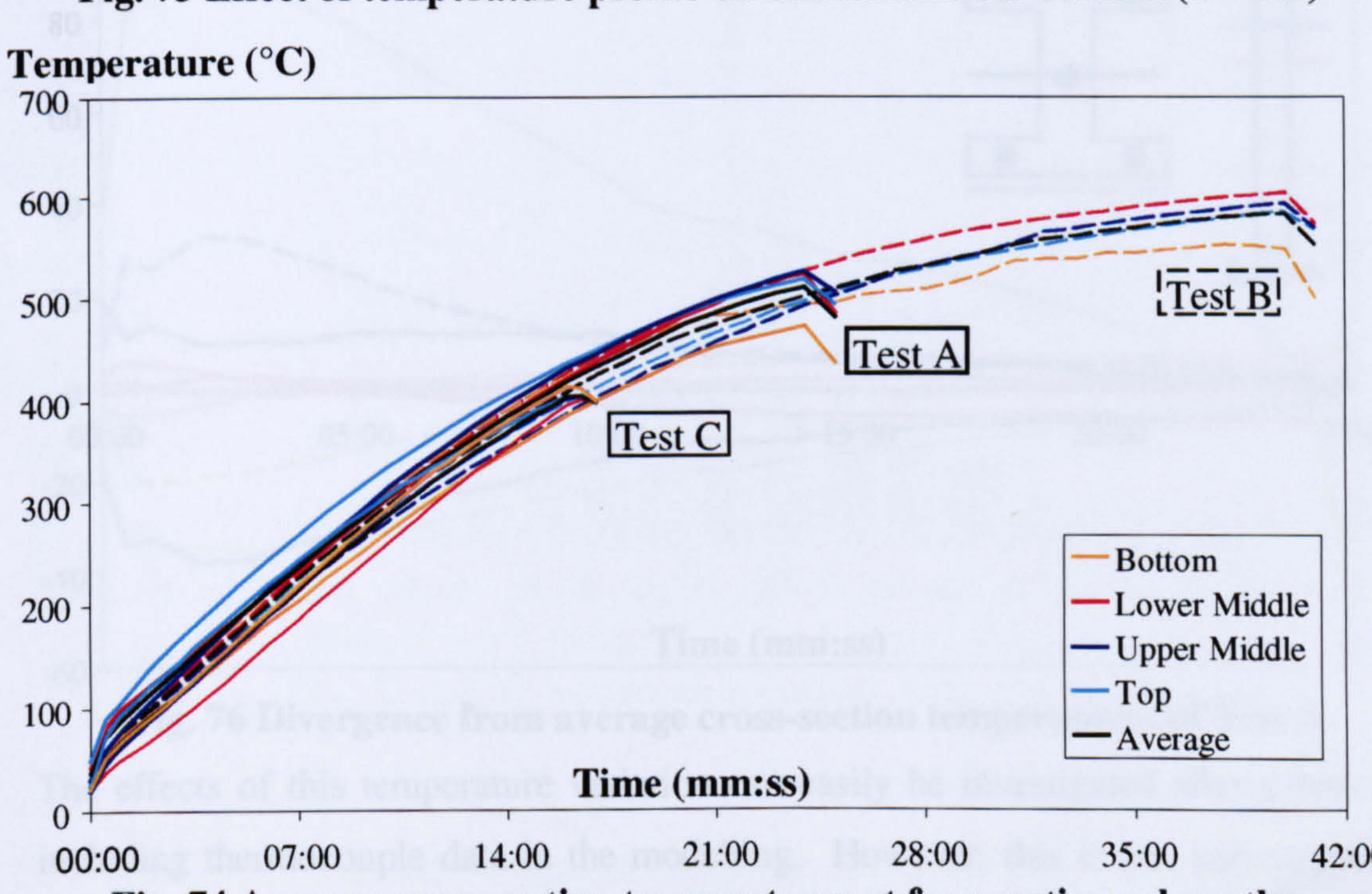

Fig. 74 Average cross-section temperatures at four sections along the 152x152x23UC column length

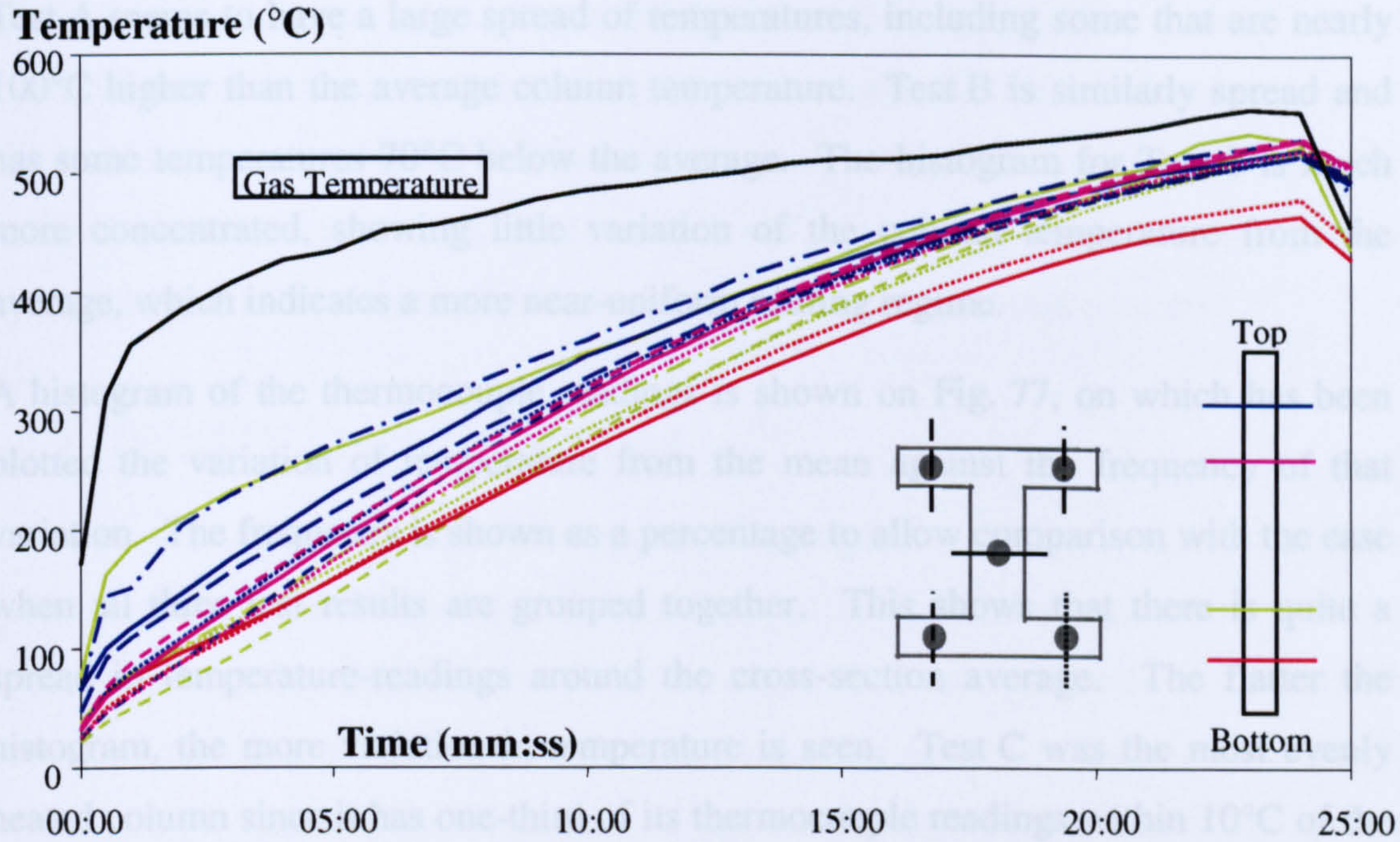

Fig. 75 Time – temperature response of thermocouples in Test A

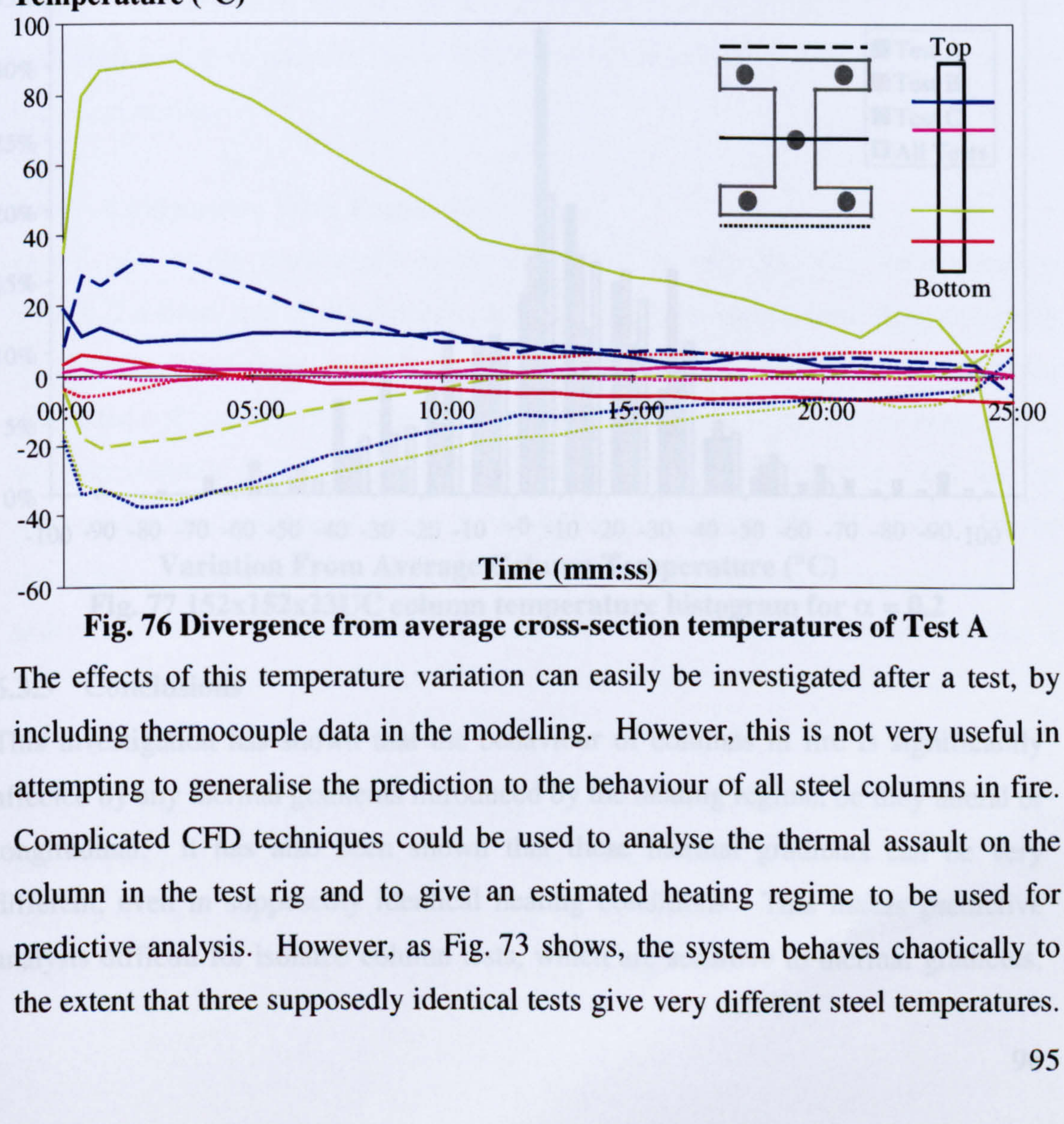

Fig. 76 Divergence from average cross-section temperatures of Test A

The effects of this temperature variation can easily be investigated after a test, by including thermocouple data in the modelling. However, this is not very useful in attempting to generalise the prediction to the behaviour of all steel columns in fire. Complicated CFD techniques could be used to analyse the thermal assault on the column in the test rig and to give an estimated heating regime to be used for predictive analysis. However, as Fig. 73 shows, the system behaves chaotically to the extent that three supposedly identical tests give very different steel temperatures.

Test A seems to have a large spread of temperatures, including some that are nearly 100°C higher than the average column temperature. Test B is similarly spread and has some temperatures 70°C below the average. The histogram for Test C is much more concentrated, showing little variation of the column temperature from the average, which indicates a more near-uniform heating regime.

A histogram of the thermocouple readings is shown on Fig. 77, on which has been plotted the variation of temperature from the mean against the frequency of that variation. The frequency is shown as a percentage to allow comparison with the case when all three test results are grouped together. This shows that there is quite a spread in temperature-readings around the cross-section average. The flatter the histogram, the more variation in temperature is seen. Test C was the most evenly heated column since it has one-third of its thermocouple readings within 10°C of the cross-sectional average.

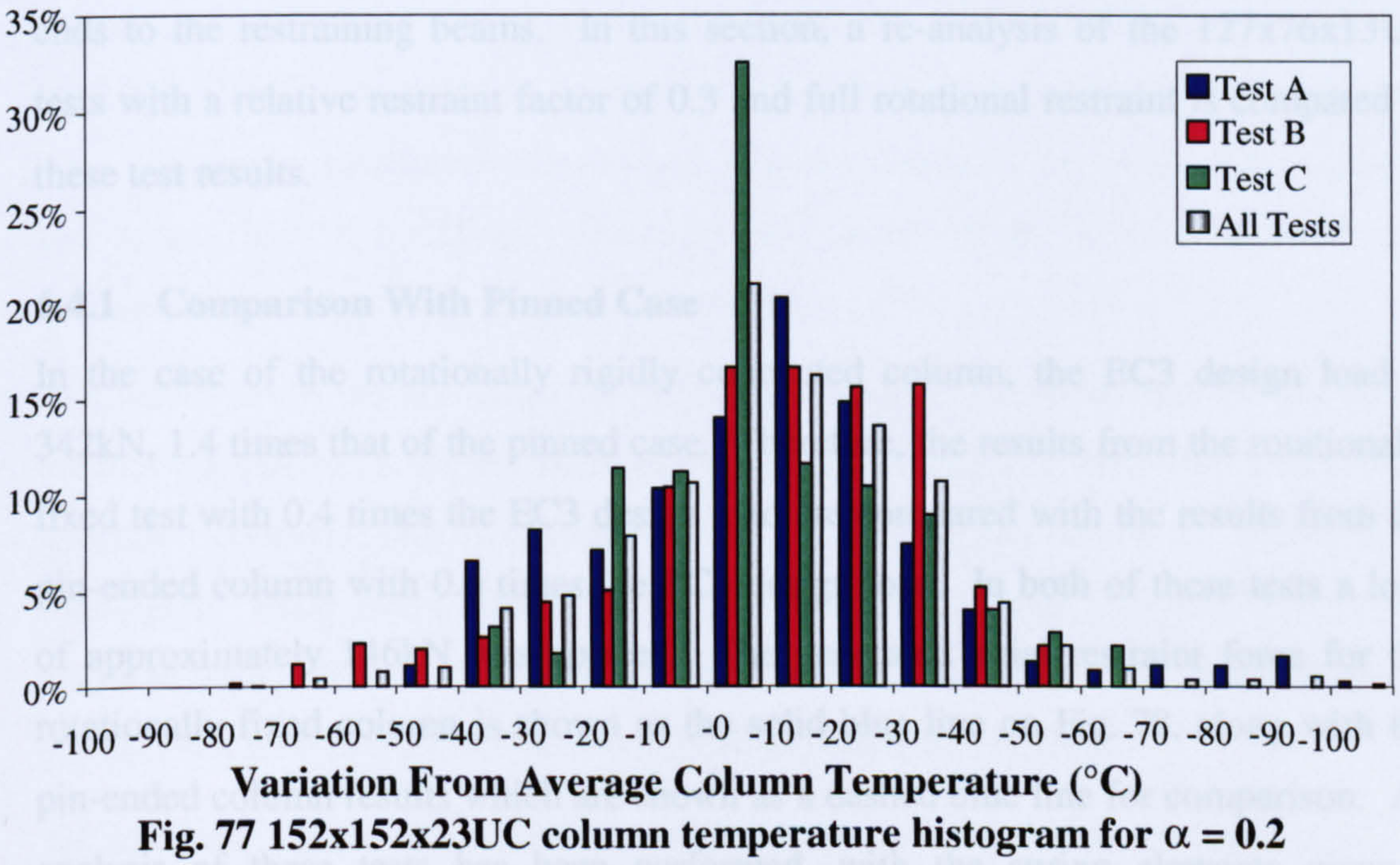

Fig. 77 152x152x23UC column temperature histogram for $\alpha = 0.2$

6.3.3 Conclusions

This investigation has shown that the behaviour of columns in fire is significantly affected by any thermal gradients introduced by the heating regime, be they lateral or longitudinal. It has also been shown that these thermal gradients can be very different, even in supposedly identical heating conditions. This makes predictive analysis difficult for isolated column tests, which are sensitive to thermal gradients,

unless a method of generating a more uniform heating effect can be found. Alternatively, this statistical data could be used to calculate the mean and variance of probable heating regimes. A Monte-Carlo simulation could then be performed, in which random thermal data is generated and analysed. The results from these simulations can be used to provide a statistically likely structural response.

6.4 Effect Of Rotational Restraint

Due to the importance of rotational restraint implied by other research[13] and the analyses of the previous chapter, a restricted series of columns was tested with full rotational restraint. The column sections chosen for these tests were 127x76x13UB sections with $\alpha = 0.3$. These were chosen since the axial restraint was provided in this case by utilising the stiffness of the whole rig, without the need for the restraining beam to move on the guiding rods. Therefore, the column could be restrained rotationally by removing the half-round bearings and rigidly attaching its ends to the restraining beams. In this section, a re-analysis of the 127x76x13UB tests with a relative restraint factor of 0.3 and full rotational restraint is compared to these test results.

6.4.1 Comparison With Pinned Case

In the case of the rotationally rigidly connected column, the EC3 design load is 342kN, 1.4 times that of the pinned case. Therefore, the results from the rotationally fixed test with 0.4 times the EC3 design load are compared with the results from the pin-ended column with 0.6 times the EC3 design load. In both of these tests a load of approximately 146kN was applied. The generated axial restraint force for the rotationally fixed column is shown as the solid blue line on Fig. 78, along with the pin-ended column results which are shown as a dashed blue line for comparison. An analysis of these tests has been performed, with the spring elements given a maximum rotational stiffness to simulate full rotational restraint. The results of the corresponding analyses are shown for comparison in red.

It can be seen that the level of rotational restraint does not significantly effect the results during the initial heating phase. This is due to the fact that during this stage, the column does not undergo a great deal of buckling deflection and therefore the ends of the column will not attempt to rotate significantly.

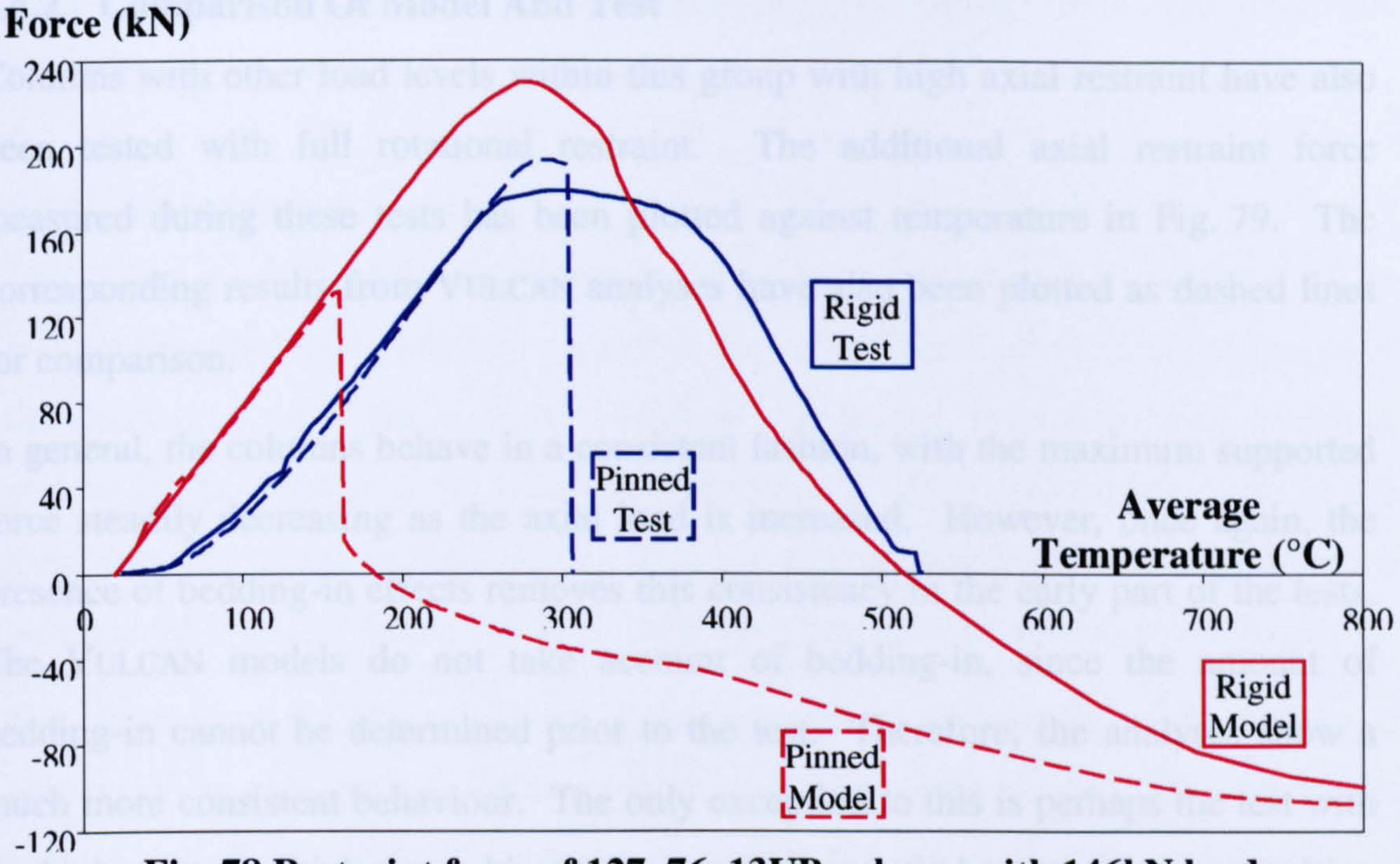

Fig. 78 Restraint force of 127x76x13UB column with 146kN load

Near to failure, the pin-ended column will buckle, resulting in a greater out-of-straightness, which in turn increases the instability of the system causing further buckling. This is responsible for the sudden failure seen in the pin-ended column tests. However, rotational restraint will reduce rotation of the ends of the column, and reduce overall buckling. Therefore, the failure of the column is much less sudden and buckling takes place progressively.

The results from the test data, shown in blue on Fig. 78, show that the pin-ended column supported a higher load before failure compared with the rotationally restrained column. This is unlikely to be a real effect, and indeed the shape of the rotationally fixed curve seems artificially flattened in the region of maximum restraint force. This anomaly is attributed to experimental error, since a similar effect is not seen in the other tests within this group (see Fig. 79).

As previously discussed, a bedding-in effect can be seen during the early stages of the test, which is not present in the VULCAN analysis. There is also a difference between the behaviour of the test and model. Specifically, the model column can support more load before failure occurs. However, this lack of agreement is less pronounced than for the standard, pinned column tests since the failure mode is more stable.

6.4.2 Comparison Of Model And Test

Columns with other load levels within this group with high axial restraint have also been tested with full rotational restraint. The additional axial restraint force measured during these tests has been plotted against temperature in Fig. 79. The corresponding results from VULCAN analyses have also been plotted as dashed lines for comparison.

In general, the columns behave in a consistent fashion, with the maximum supported force steadily decreasing as the axial load is increased. However, once again, the presence of bedding-in effects removes this consistency in the early part of the tests. The VULCAN models do not take account of bedding-in, since the amount of bedding-in cannot be determined prior to the test. Therefore, the analyses show a much more consistent behaviour. The only exception to this is perhaps the test with the highest load, which was subject to an unusually erratic heating scheme, resulting in large thermal gradients in the analysis temperature data.

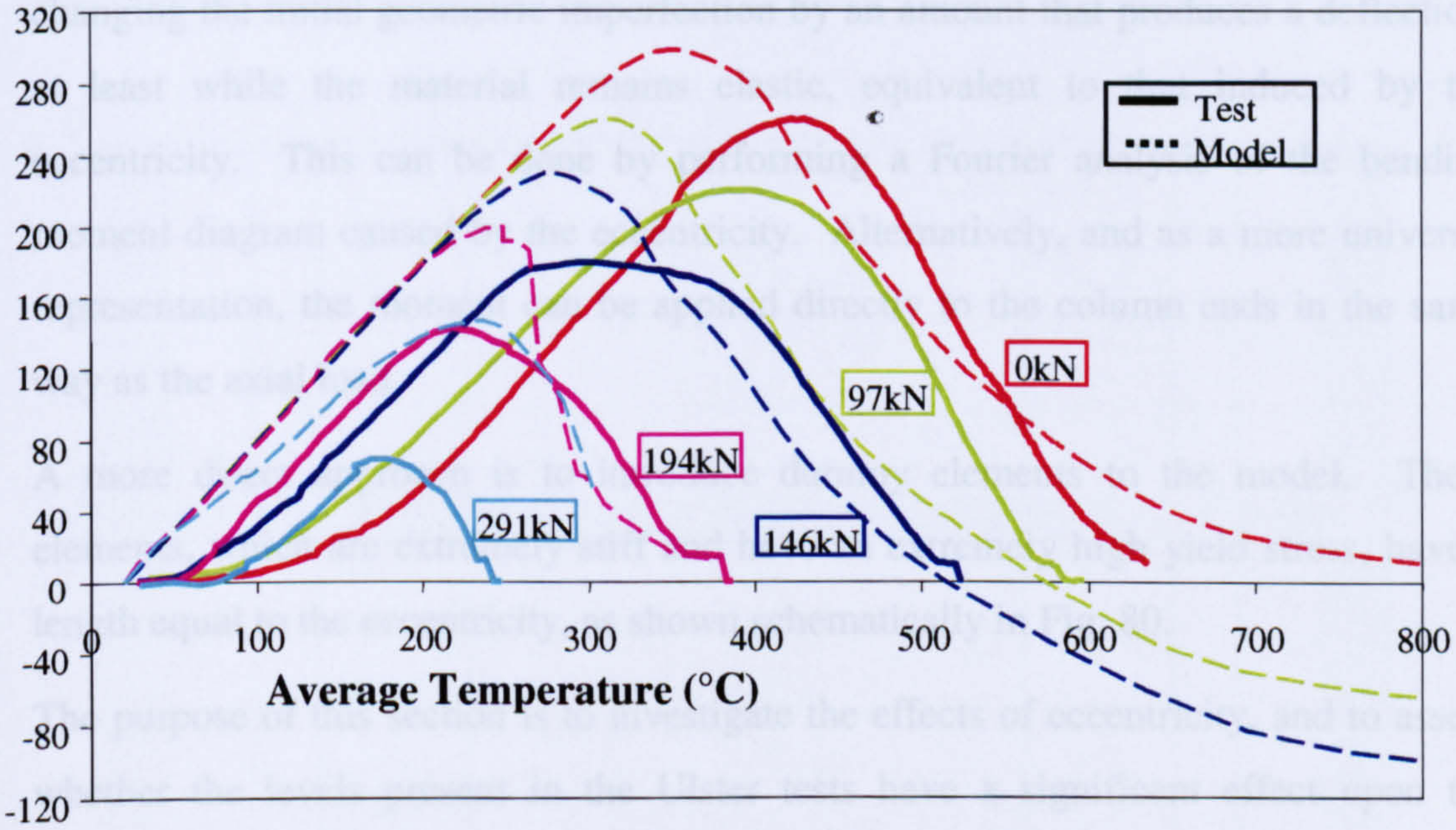

Fig. 79 Comparison of rotationally restrained columns

6.5 Effect of Eccentricity

Until now, the effects of the eccentricity of the supposedly axial loading at the column end-plates has been neglected in the VULCAN analyses. This has been justified by the extremely small values of measured imperfection. However, there

must be a certain level of experimental error in taking these measurements. Therefore, this section looks at the sensitivity of the analyses to loading eccentricity.

6.5.1 Introduction

The model used to analyse columns in VULCAN is described in Chapter 2. It is assumed that the load, which is applied at the top of the column, is concentrated at the exact centroid of the section. Similarly, the pinned support bearing, which is present at the bottom of the column, is assumed to apply its reaction force at the exact centroid of the section. In this way, a perfectly straight column would have a purely axial load and would fail at its Euler buckling load, as described in Chapter 1.

The distance of the line of action of the load from the centroid of the section is known as its eccentricity. The eccentricity induces a moment at the end of the column, which increases its tendency to bend. This results in an amplification of buckling deflection in a way analogous to deflection induced by an initial geometric imperfection. Thus, the effects of eccentric loading can be simulated in the model by changing the initial geometric imperfection by an amount that produces a deflection, at least while the material remains elastic, equivalent to that induced by the eccentricity. This can be done by performing a Fourier analysis of the bending moment diagram caused by the eccentricity. Alternatively, and as a more universal representation, the moment can be applied directly to the column ends in the same way as the axial load.

A more direct approach is to introduce dummy elements to the model. These elements, which are extremely stiff and have an extremely high yield stress, have a length equal to the eccentricity, as shown schematically in Fig. 80.

The purpose of this section is to investigate the effects of eccentricity, and to assess whether the levels present in the Ulster tests have a significant effect upon the results.

6.5.2 Ulster Measurements

Fig. 81 shows the measurements that were made of the column end-plates. Using these results, the eccentricity of the centre of the column from the centre of the end-plate can be calculated as follows.

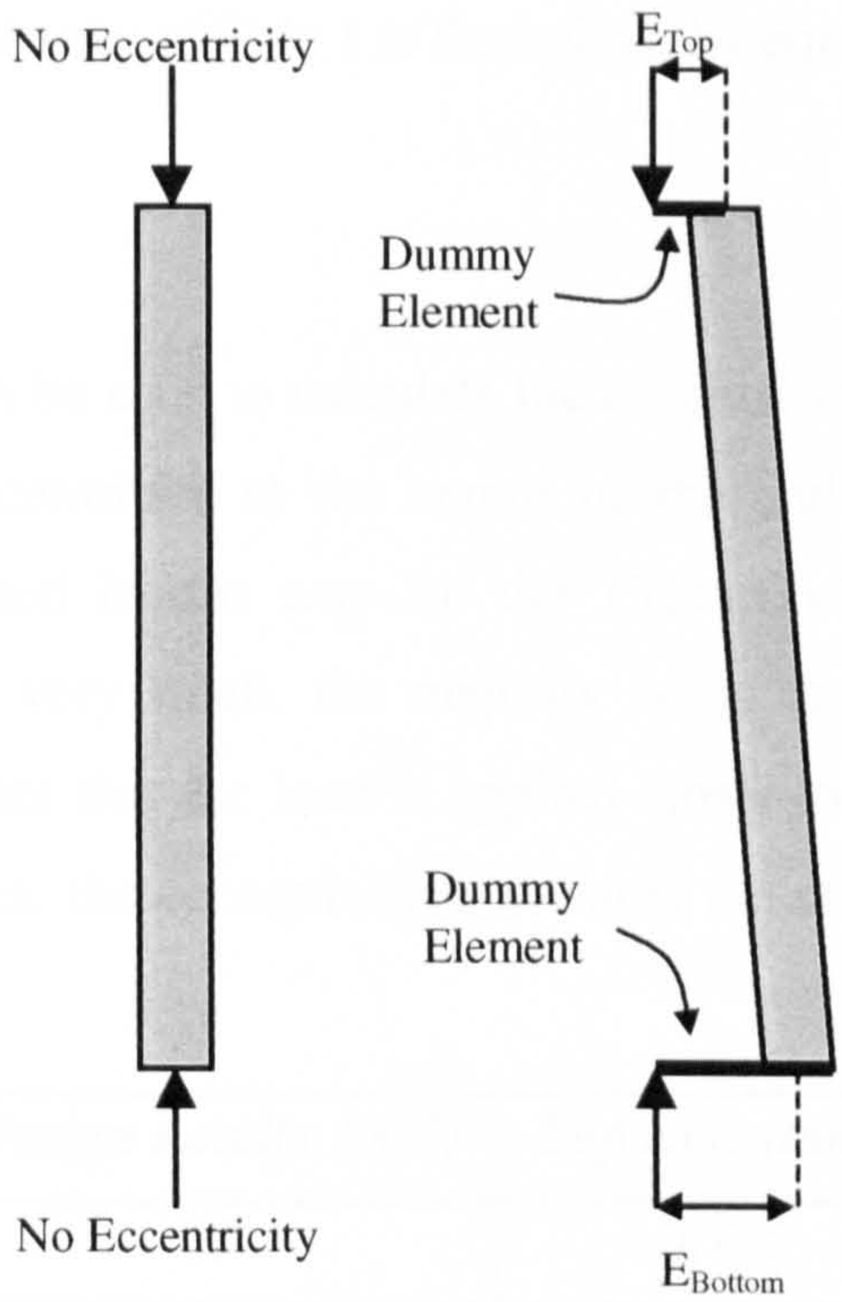

Fig. 80 Exaggerated diagram of VULCAN model with eccentricity

Firstly, the thickness of the web (W1) is calculated at the point between the holes on Side 1 of the section:

$$W1 = H1 - A1 - B1 \tag{18}$$

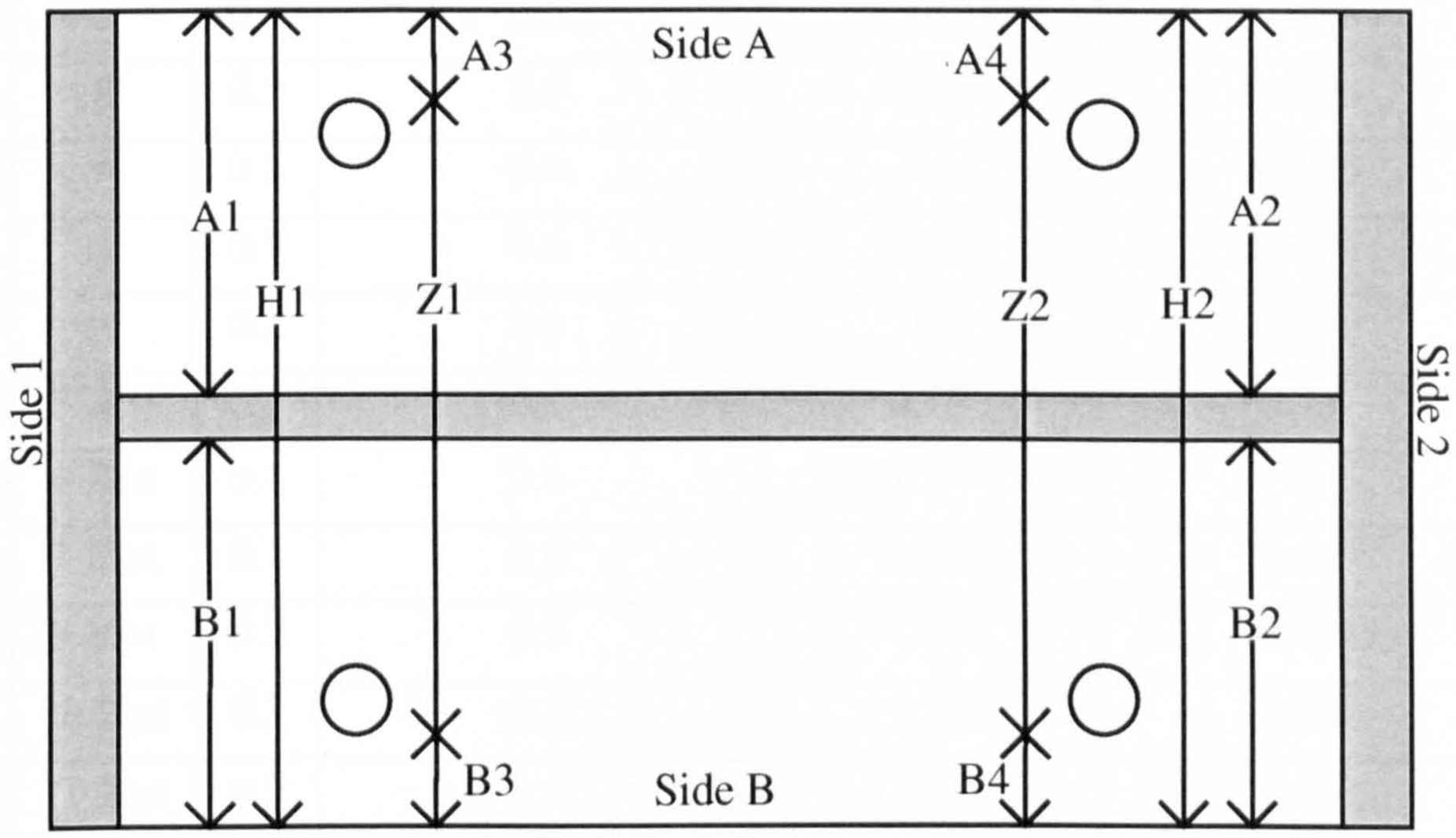

Fig. 81 End-plate measurement points

Then the top of the hole on Side 1 towards Side A is used as a reference datum. The distance of this point from the centre line of the web (Y1) can be calculated using eqn. (19).

$$Y1 = A1 - A3 + \frac{W1}{2} \tag{19}$$

The minor-axis eccentricity of Side 1 is then given by eqn. (20).

$$Ecc1 = \frac{Z1}{2} - Y1 \tag{20}$$

The same process can be used to calculate the eccentricity at Side 2, and an average taken to find the eccentricity at the centre of the end-plate. Table 6 shows the eccentricities calculated in this way for the 152x152x23UC Ulster test columns. These values are all very small, the majority being less than one millimetre. A positive value indicates that the load is applied closer to Side B than to Side A. In most, but not all cases, the eccentricity is towards the same side at the top as at the bottom.

23UC	*α*	*Design Load(x EC3)*	*Top Ecc. (mm)*	*Bottom Ecc. (mm)*
2	0.0	0.4	-0.125	-0.05
3	0.0	0.6	-0.125	-0.05
4	0.1	0.0	0.6375	0.5125
5	0.1	0.2	0.3	0.8125
6	0.1	0.4	0.475	-0.1875
7	0.1	0.6	-0.0125	0.6125
8	0.2	0.0	-0.05	1.4125
9	0.2	0.2	0.1	0.2775
10	0.2	0.4	0.575	0.0875
11	0.2	0.6	0.2	0.6375
5 Rpt	0.1	0.2	0.15	0.75
6 Rpt	0.1	0.4	-0.04	0
7 Rpt	0.1	0.6	0.575	0.25
9 Rpt	0.2	0.2	-1.425	-0.425
10 Rpt	0.2	0.4	1.35	1.15
11 Rpt	0.2	0.6	0.625	0.05

Table 6 Measured eccentricities of 152x152x23UC test columns

6.5.3 Description Of VULCAN Model

A 152x152x23UC column subject to 0.6 of the EC3 design load and a relative restraint factor of 0.1 has been chosen for the basic comparison. To simulate the eccentricity of the applied load and boundary restraints, dummy struts were

introduced on either end of the column, as shown in Fig. 82. These struts were given an artificially high yield stress of 2000N/mm^2 and a Young's modulus of 1000N/mm^2 so that they would behave elastically and their bending action would not influence the results. The only difference between this and the previous analysis is that the load is now acting eccentrically and an equivalent moment is induced in the test column. The columns are heated uniformly to remove the effects of temperature variation and the spring elements represent pinned connections so no rotational restraint effects can influence the results.

The lengths of the dummy struts can be altered independently to represent any values of eccentricity at the top or bottom of the column independently. However, for the purpose of this sensitivity study, only the case where the top and bottom eccentricities are equal in magnitude and in the same direction as the inherent geometric imperfection is investigated.

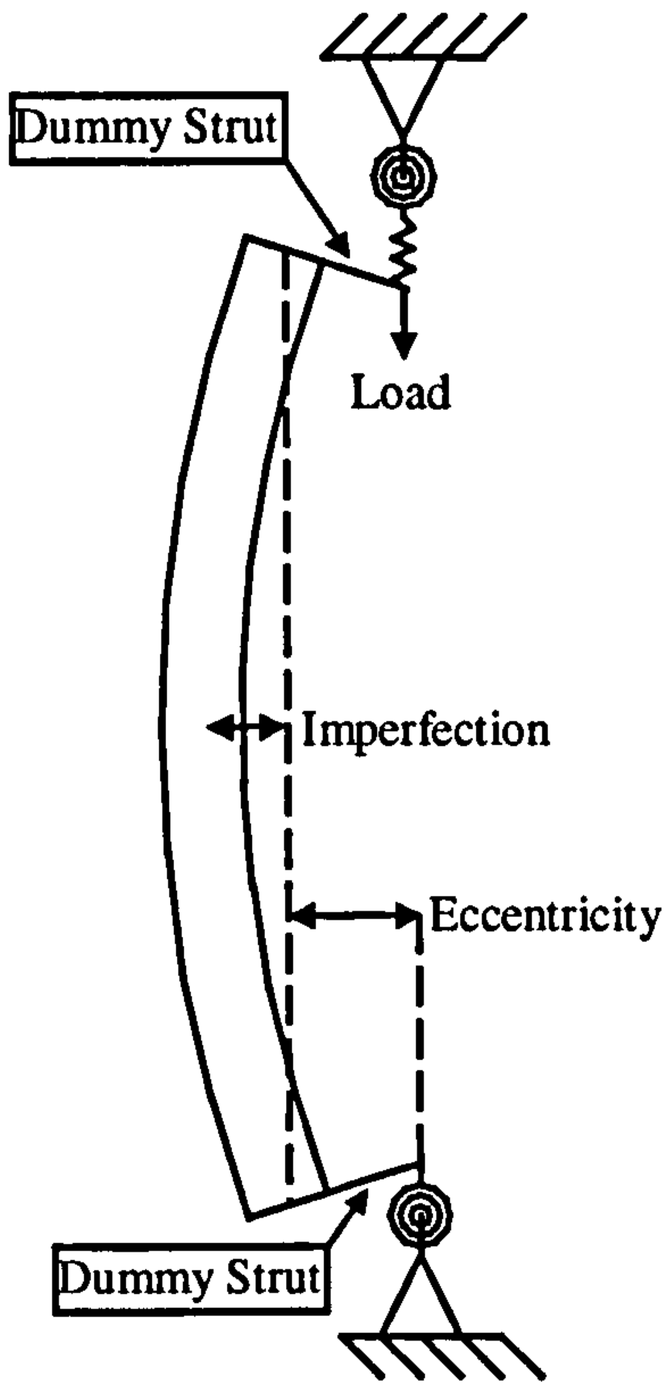

Fig. 82 Model of eccentrically loaded column

6.5.4 Results Of VULCAN Analyses

To form a basis for comparison, the relevant Ulster test column was analysed without eccentric dummy elements, and with a uniform temperature distribution. The axial restraint force applied to the column is shown as the blue line in Fig. 83. To check on the validity of the model with dummy struts, a model which includes strut-

elements of zero length was also analysed and found to give exactly the same results as when no struts were present. This is as expected, and the axial restraint force for this case is plotted in pink under the blue line on Fig. 83, although it cannot be distinguished from the previous case. Fig. 83 also shows the restraint force for models with levels of eccentricity similar to those measured in the Ulster tests and increasing up to more extreme cases to show the general change in behaviour with eccentricity.

It should be noted that the equivalent graph of displacement against temperature has the same shape, since the axial restraint spring is linear and no other members frame in to share in supporting the load.

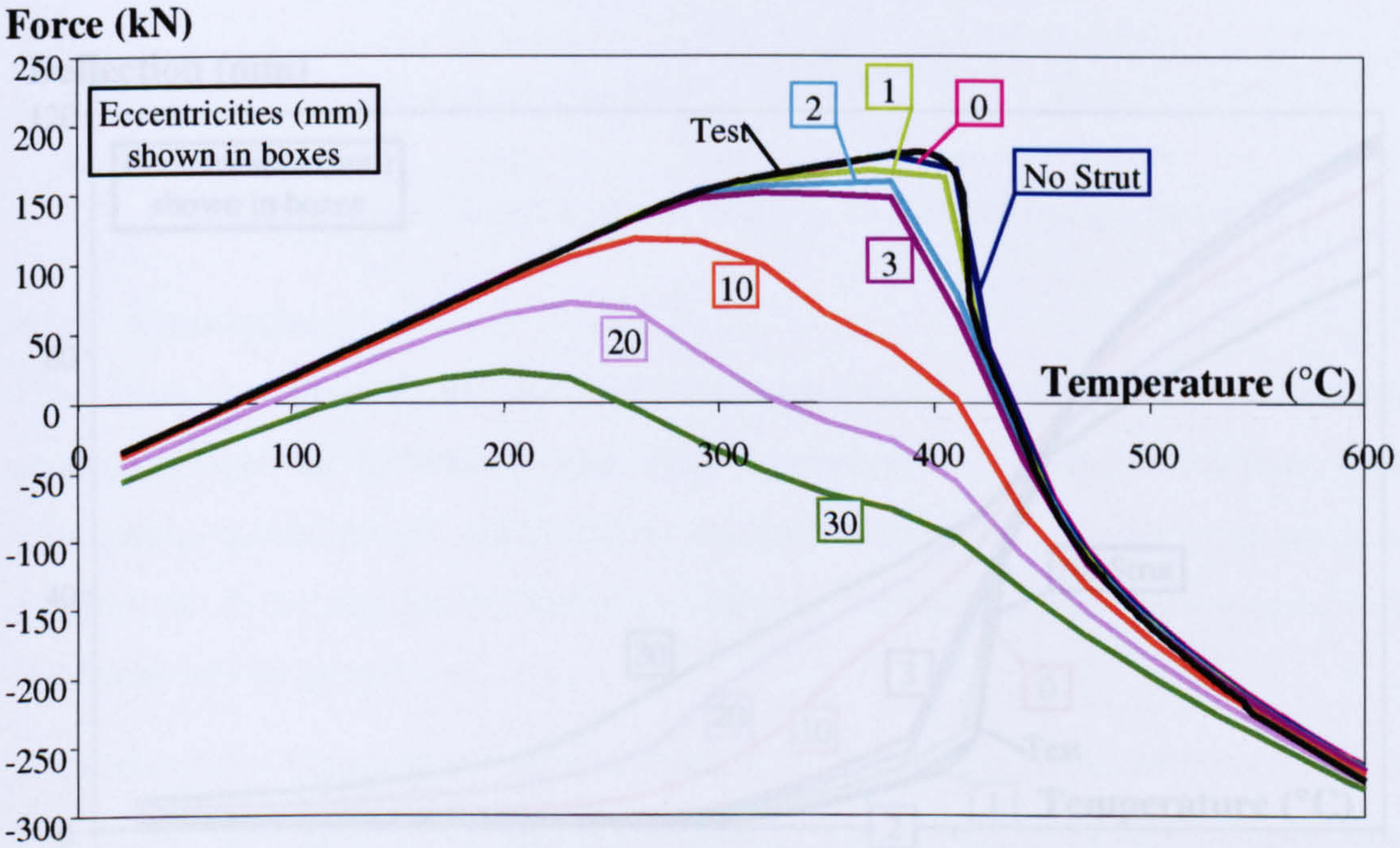

Fig. 83 Axial restraint force applied to eccentric columns

The effect of increasing eccentricity is to reduce the maximum axial force supported by the column, and decrease the temperature at which this occurs. As has been described above, the presence of eccentricity is equivalent to increasing the level of initial geometric imperfection or applying a moment at the supports. Therefore, the behaviour of the model is as expected.

Furthermore, the test results from the corresponding Ulster test have been plotted as the black line on Fig. 83. Although a uniform heating regime has been assumed in this parametric study, there is still evidence to show that the test column does indeed have an extremely low value of eccentricity, as measured by the Ulster team.

The results can be further explained by plotting the lateral displacement at the mid-height of the column in a similar way, as shown on Fig. 84. A positive value of lateral displacement indicates movement in the direction of the initial imperfection. It can clearly be seen that the greater the level of eccentricity, the earlier the column begins to buckle due to the increased axial force of the column's thermal expansion against restraint. At higher temperatures, Fig. 84 seems counter intuitive in that it shows that the lower the level of initial eccentricity, the more lateral deflection is seen after failure. It must be noted however that this deflection is measured relative to the initial geometry of the column. It is perhaps more logical to plot this deflection relative to the initial geometry of a non-eccentric column. This is shown on Fig. 85 for which the slight change in scale should be noted.

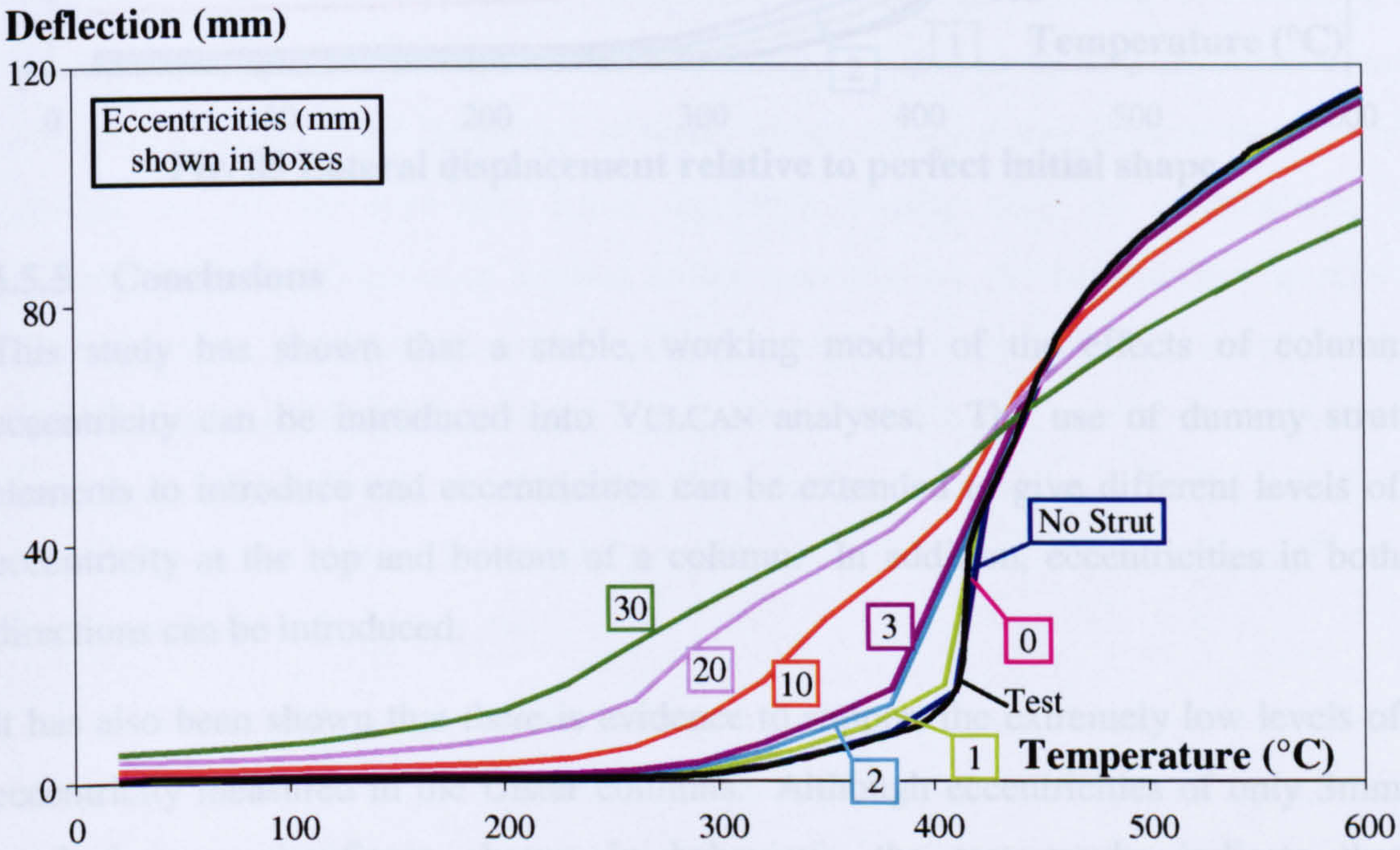

Fig. 84 Lateral displacement at the mid-height of eccentric columns

As has been discussed in previous chapters, in the post-buckling region of the analysis the column begins to shed load onto the restraint spring, and supports progressively less load itself. This explains why the axial restraint curves in Fig. 83 converge at high temperatures. As the load carried by the column decreases, so the sensitivity to eccentricities also decreases.

This axial force results in a certain level of curvature. Since the level of eccentricity is much less than the final values of lateral deflection, the eccentricity becomes less and less significant in forming a column of a certain curvature. Thus, the lateral deflection curves in Fig. 85 also tend to converge as the temperature increases.

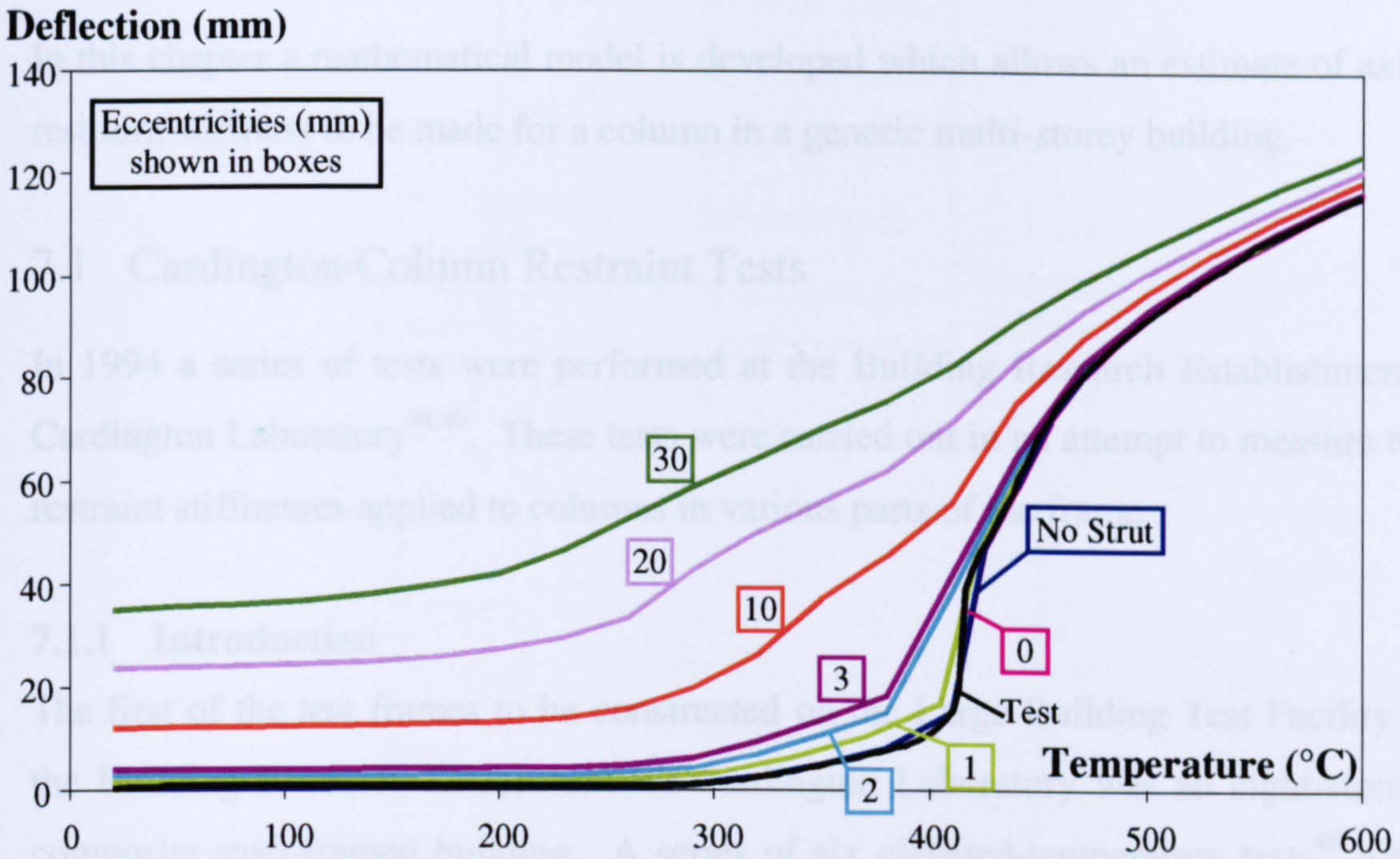

Fig. 85 Lateral displacement relative to perfect initial shape

6.5.5 Conclusions

This study has shown that a stable, working model of the effects of column eccentricity can be introduced into VULCAN analyses. The use of dummy strut elements to introduce end eccentricities can be extended to give different levels of eccentricity at the top and bottom of a column. In addition, eccentricities in both directions can be introduced.

It has also been shown that there is evidence to support the extremely low levels of eccentricity measured in the Ulster columns. Although eccentricities of only 3mm resulted in a significant change in behaviour, the test results indicate that eccentricities in the region of 1mm are present in the Ulster columns. At this level, the difference in behaviour from a non-eccentric column was small. It is therefore justifiable to neglect the effects of eccentricities in the modelling of the Ulster columns.

7 Mathematical Restraint Model

In this chapter a mathematical model is developed which allows an estimate of axial restraint stiffness to be made for a column in a generic multi-storey building.

7.1 Cardington Column Restraint Tests

In 1994 a series of tests were performed at the Building Research Establishment's Cardington Laboratory[48,49]. These tests were carried out in an attempt to measure the restraint stiffnesses applied to columns in various parts of the frame.

7.1.1 Introduction

The first of the test frames to be constructed on the Large Building Test Facility at the Building Research Establishment's Cardington Laboratory was an eight-storey, composite steel-framed building. A series of six elevated-temperature tests[48] were carried out on the bare-steel frame in 1994, shortly after its construction, to determine the axial restraint applied to the columns by the surrounding structure. Columns at two different positions within a storey were studied; an internal column with four beams framing into it and a corner column with only two beams attached at each floor. The columns were tested at Ground Floor, Third Floor and Seventh Floor levels, shown as thick, unbroken lines on Fig. 86. The six tests were repeated[49] after the concrete slabs had been cast.

To derive the axial restraint applied to a specific column, the column was heated over the majority of its length using a barrel furnace. This induced a thermal expansion in the column, pushing upwards on the structure above. The axial displacement of the top of the heated part of the column was measured using displacement transducers, which were anchored to the floor above. Strain gauges above the heated part of the column measured the additional force induced in the column by the restraint of the structure above.

7.1.2 Results Of The Tests

Due to problems with the data logging equipment used during these tests, axial restraint values could be found for only two of the six experiments performed.

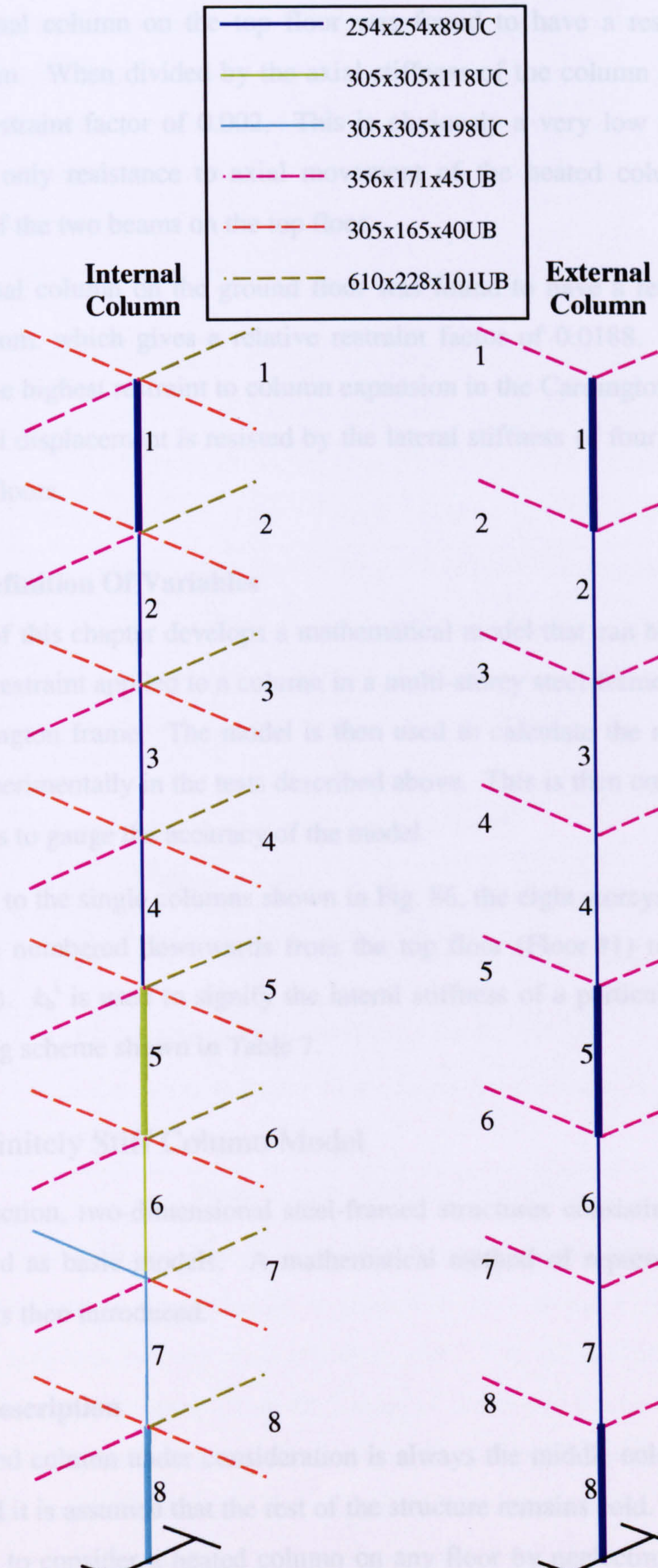

Fig. 86 Cardington frame layout for column restraint tests

The external column on the top floor was found to have a restraint stiffness of 1150 N/mm. When divided by the axial stiffness of the column itself, this gives a relative restraint factor of 0.002. This is obviously a very low value of restraint, since the only resistance to axial movement of the heated column is the lateral stiffness of the two beams on the top floor.

The internal column on the ground floor was found to have a restraint stiffness of 23160 N/mm, which gives a relative restraint factor of 0.0188. This much larger value is the highest restraint to column expansion in the Cardington bare-steel frame, since axial displacement is resisted by the lateral stiffness of four beams on each of the eight floors.

7.1.3 Definition Of Variables

The rest of this chapter develops a mathematical model that can be used to calculate the axial restraint applied to a column in a multi-storey steel-framed building such as the Cardington frame. The model is then used to calculate the restraint stiffnesses found experimentally in the tests described above. This is then compared against the test results to gauge the accuracy of the model.

Referring to the single columns shown in Fig. 86, the eight storeys in the Cardington frame are numbered downwards from the top floor (Floor #1) to the bottom floor (Floor #8). k_b^i is used to signify the lateral stiffness of a particular beam using the numbering scheme shown in Table 7.

7.2 Infinitely Stiff Column Model

In this section, two-dimensional steel-framed structures consisting of two bays are considered as basic models. A mathematical method of representing the restraint stiffness is then introduced.

7.2.1 Description

The heated column under consideration is always the middle column on the ground floor, and it is assumed that the rest of the structure remains cold. This model can be extended to consider a heated column on any floor by neglecting the floors below. These floors resist forces by transferring loads down the column directly to the foundation. Since the ground below the structure provides high restraint to

movement, we can assume that any deflections will appear in the structure above the heated column. The model can also be extended to three-dimensional structures by simply adding in the restraint applied by beams framing in from the out-of-plane directions. Beams of this kind act no differently from those that are in-plane, but have not been shown here for simplicity.

Variable	*Description*
$k_b^{1\&2}$	Lateral stiffness of the two 9m long 305x165x40UB sections
k_b^3	Lateral stiffness of the 6m long 356x171x45UB section
k_b^4	Lateral stiffness of the 9m long 610x228x101UB section
k_b^5	Lateral stiffness of the 2nd floor, 9m long 305x305x198UC section
k_b^6	Lateral stiffness of the 9m long 356x171x45UB perimeter beam
k_s^n	Total lateral stiffness of all the beams on the nth floor
k_r^n	Total lateral stiffness of the structure above and including the nth floor
k_c^n	Axial stiffness of the column on the nth floor
$I_{b/c}$	Second moment of area of beam / column
$L_{b/c}$	Length of beam / column
$A_{b/c}$	Cross-sectional area of beam / column
α^n	Relative restraint factor of column on the nth floor
α_i	Relative restraint factor of a ground floor column in a structure with i-storeys

Table 7 Description of variables

Since the axial stiffness of a typical column is much greater than the lateral stiffness of a typical beam, a simplification in modelling axial restraint would be to treat the unheated columns themselves as infinitely stiff. The only contribution to the axial restraint would then come from the beams of the floors above the heated column. This is a simplification of the true restraint, but it may be sufficiently accurate for practical purposes. The aim of this chapter is to evaluate the levels of axial restraint provided by different parts of the structure under different assumptions, and to give an indication of when they are important.

7.2.2 Lateral Stiffness Of Rigidly Connected Beams

The lateral stiffness of a beam restrained from rotation at both ends can be found using the slope-deflection equation shown below.

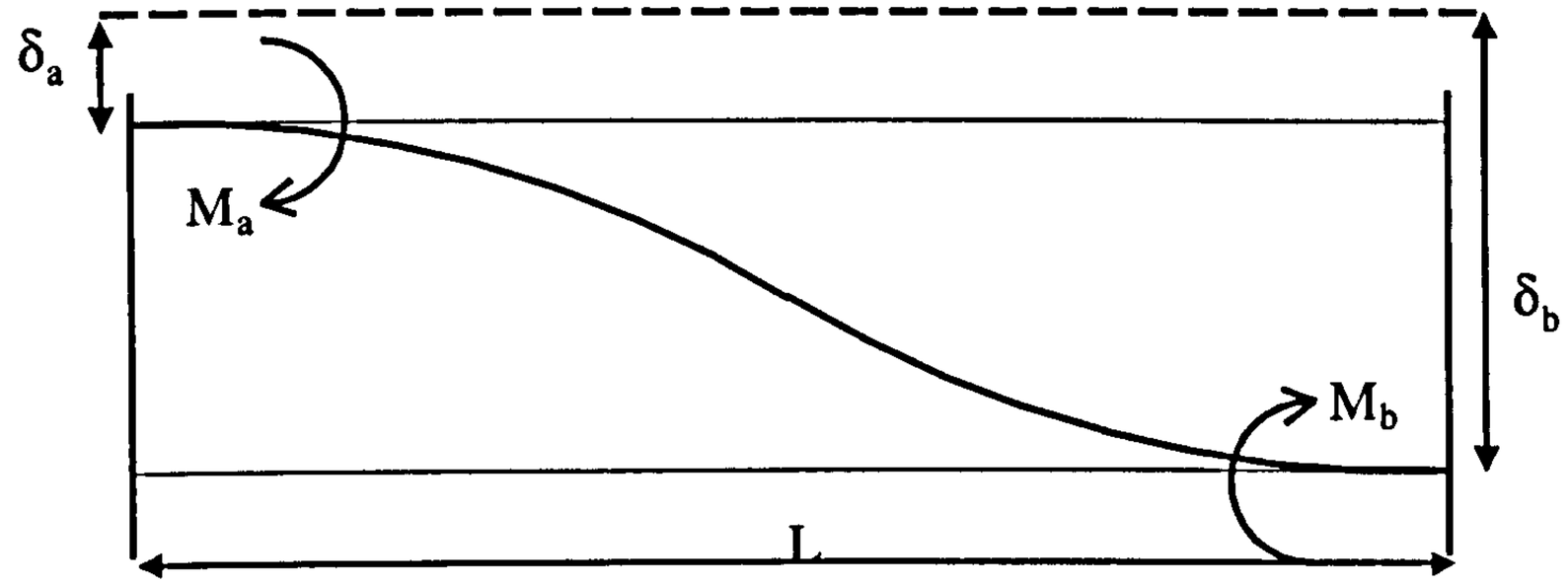

Fig. 87 A deflected beam-column arrangement

Firstly, the moment due to the deflection at end *a* of the beam is evaluated.

$$M_a = \frac{2EI}{L}\left[2\theta_a + \theta_b + \frac{3(\delta_a - \delta_b)}{L}\right] = \frac{2EI}{L}\left[0 + 0 + \frac{3(0-\delta)}{L}\right] = -\frac{6EI}{L^2} \qquad (21)$$

Symmetry or re-evaluating from side b finds the following equation:

$$M_b = \frac{2EI}{L}\left[2\theta_b + \theta_a + \frac{3(\delta_b - \delta_a)}{L}\right] = \frac{2EI}{L}\left[0 + 0 + \frac{3(0-\delta)}{L}\right] = -\frac{6EI}{L^2} \qquad (22)$$

Taking moments about one end and equating to zero for equilibrium gives:

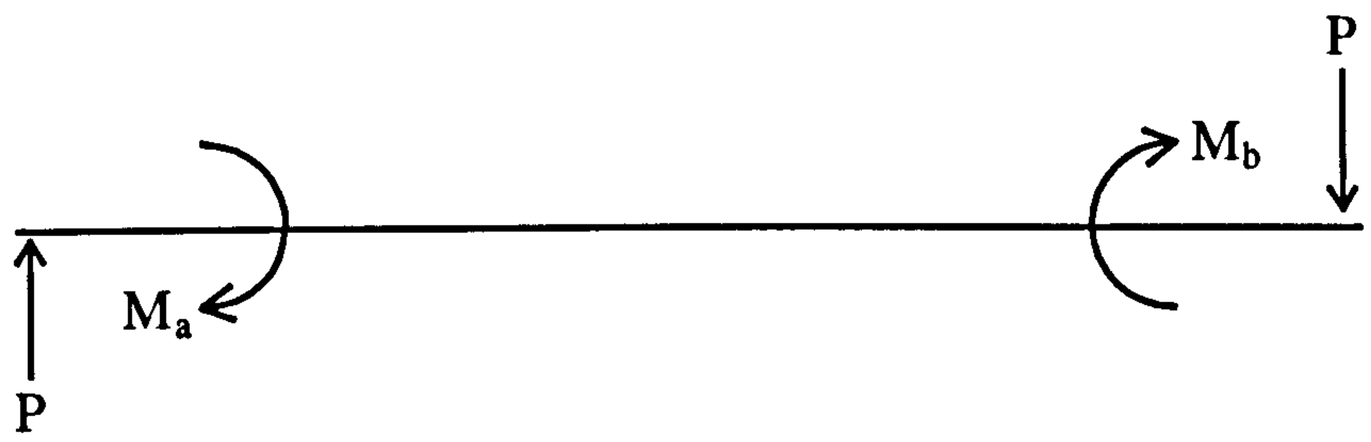

Fig. 88 Equate moments to zero

$$PL + M_a + M_b = 0 \qquad \text{so} \qquad PL = -M_a - M_b \qquad (23)$$

Therefore:

$$P = \frac{12EI\delta}{L^3} \qquad (24)$$

Stiffness

$$k_b = \frac{P}{\delta} = \frac{12EI\delta/L^3}{\delta} = \frac{12E_bI_b}{L_b^3} \qquad (25)$$

7.2.3 One Floor

Consider a single-storey structure as shown in Fig. 89. The axial restraint applied to the heated column is provided by the two beams that make up the roof. Obviously, the restraint that is provided by the structure as a whole, k_r, is just the restraint provided by a single storey k_s.

$$k_r = k_s \quad \Rightarrow \quad \alpha = \frac{k_s}{k_c} = \alpha_1 \tag{26}$$

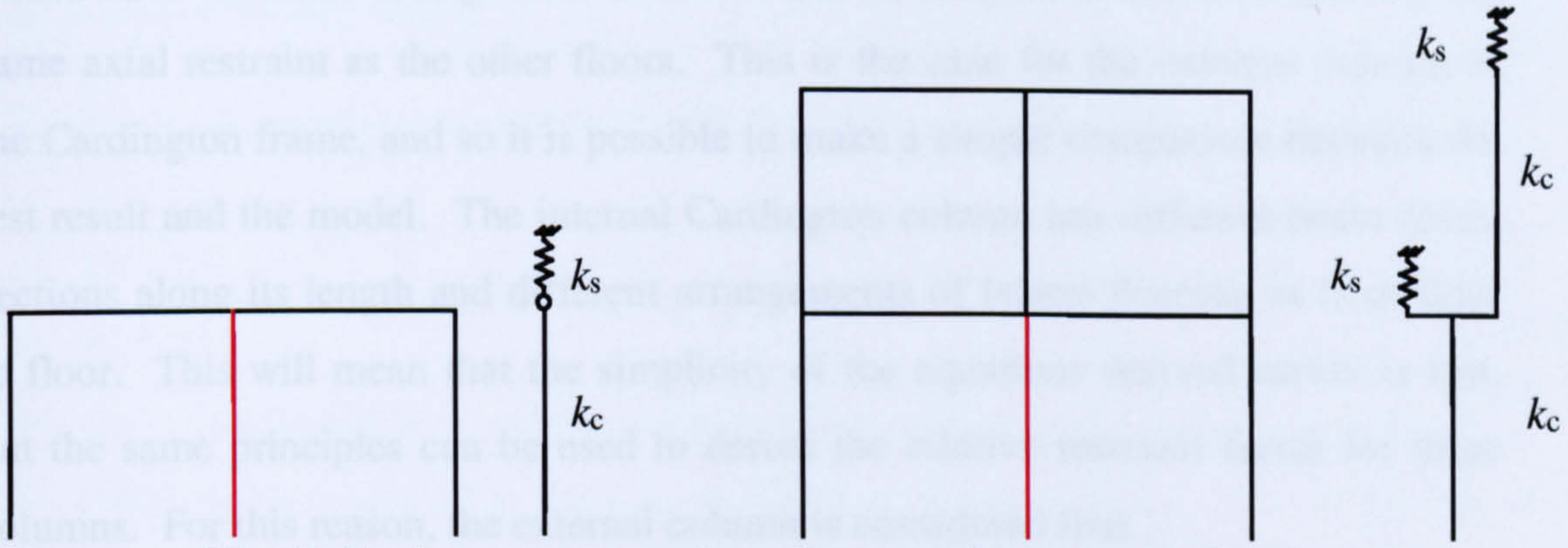

Fig. 89 Spring representation of one- and two-storey frames

7.2.4 Two Floors

If a two-storey structure is now considered, as shown in Fig. 89, it can be seen that there are two storeys that provide restraint to the heated column. Since it is assumed that the column on the first floor is considered to be infinitely stiff, the restraint provided by the beams at roof level is simply added to the restraint provided by the beams at floor level.

$$k_r = k_s + k_s = 2k_s \quad \Rightarrow \quad \alpha = \frac{2k_s}{k_c} = 2\alpha_1 = \alpha_2 \tag{27}$$

7.2.5 Generalisation

This simple investigation shows that adding a floor onto a structure adds the restraint provided by that floor's beams onto the total restraint provided by the rest of the floors above the heated column. If we assume that the beams of all the floors are identical, then we have the following equation, which is illustrated in Fig. 90.

$$\alpha = \alpha_n = n\alpha_1 \tag{28}$$

Where α = The total axial restraint factor provided by the frame to the heated column

α_n = The axial restraint provided by n floors to the heated column

n = The number of floors in the frame

7.2.6 Comparison Of External Column With Cardington Test

In developing the simple model of axial restraint, it was assumed that each floor would have the same arrangement of beams and columns, and therefore provide the same axial restraint as the other floors. This is the case for the external column of the Cardington frame, and so it is possible to make a simple comparison between the test result and the model. The internal Cardington column has different beam cross-sections along its length and different arrangements of beams framing in from floor to floor. This will mean that the simplicity of the equations derived earlier is lost, but the same principles can be used to derive the relative restraint factor for these columns. For this reason, the external column is considered first.

The corner column on the top floor is a 254x254x89UC section and has only two beams framing in. Both are 356x171x45UB sections, one 6m long (k_b^3) and the other 9m long (k_b^6). As shown earlier, these beams bend laterally and provide axial restraint to the column as calculated below.

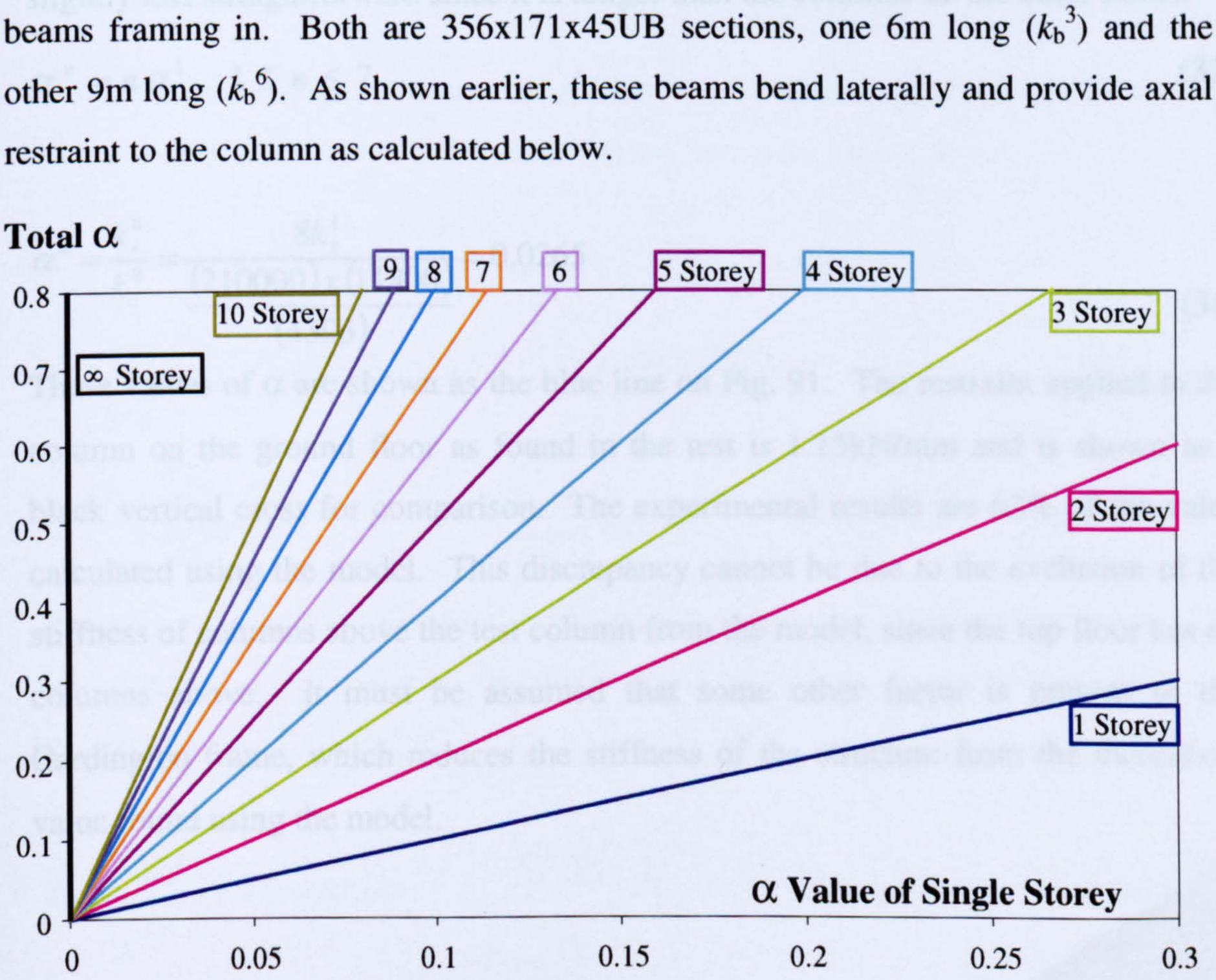

Fig. 90 Total value of restraint factor for multi-storey frames

$$k_b^3 = \frac{12EI_b}{L_b^3} = 1408\,\text{N/mm} \qquad k_b^6 = \frac{12EI_b}{L_b^3} = 417\,\text{N/mm} \tag{29a \& b}$$

This gives the total restraint from the beams on the top floor k_s^1 as

$$k_s^1 = k_b^3 + k_b^6 = 1825\,\text{N/mm} \tag{30}$$

The axial stiffness of the heated column itself is k_c^1.

$$k_c^1 = \frac{EA_c}{L_c} = 567025\,\text{N/mm} \tag{31}$$

Therefore, the relative restraint factor for the column on the top floor α^1 is given by

$$\alpha^1 = \frac{k_r^1}{k_c^1} = \frac{k_s^1}{k_c^1} = 0.00322 \tag{32}$$

Similarly, it is possible to calculate the restraint applied to the corner test column on the lower floors easily since these have identical beams framing in at all the floors above, with identical lateral stiffnesses. However, the ground floor column is slightly less straightforward since it is longer than the columns on the other floors.

$$\alpha^n = n\alpha^1 \quad 1 \le n \le 7 \tag{33}$$

$$\alpha^8 = \frac{k_r^8}{k_c^8} = \frac{8k_s^1}{\frac{(210000)x(11300)}{(4305)}} = 0.0265 \tag{34}$$

These values of α are shown as the blue line on Fig. 91. The restraint applied to the column on the ground floor as found in the test is 1.15kN/mm and is shown as a black vertical cross for comparison. The experimental results are 63% of the value calculated using the model. This discrepancy cannot be due to the exclusion of the stiffness of columns above the test column from the model, since the top floor has no columns above. It must be assumed that some other factor is present in the Cardington frame, which reduces the stiffness of the structure from the theoretical value found using the model.

7.2.7 Comparison Of Internal Column With Cardington Test

The model is now applied to the internal test column, noting that the internal structural member layout is less regular than it is for the external column. The column on the top floor is a 254x254x89UC section and has four beams framing in. Two of these are 9m long 305x165x40UB sections, one is a 6m long 356x171x45UB section and one is a 9m long 610x228x101UB section. The axial restraint provided by these beams is:

$$k_b^{1\&2} = \frac{12EI_b}{L_b^3} = 294\,\text{N/mm} \quad k_b^3 = \frac{12EI_b}{L_b^3} = 1408\,\text{N/mm} \qquad \textbf{(35a, b \& c)}$$

$$k_b^4 = \frac{12EI_b}{L_b^3} = 2620\,\text{N/mm}$$

$$\text{so} \quad k_s^1 = k_b^1 + k_b^2 + k_b^3 + k_b^4 = 4616\,\text{N/mm} \qquad \textbf{(36)}$$

And therefore:

$$\alpha^1 = \frac{k_s^1}{k_c^1} = 0.00814 \qquad \textbf{(37)}$$

Although the next four floors have similar beam arrangements, the columns on the fifth and sixth floors are of a different section size to the floors above:

$$\alpha^n = n\alpha^1 \quad 1 \le n \le 4 \qquad \textbf{(38)}$$

$$k_r^5 = 5k_s^1 = 23080\,\text{N/mm} \qquad k_c^5 = \frac{EA_c}{L_c} = 752688\,\text{N/mm} \qquad \textbf{(39a \& b)}$$

$$\alpha^5 = \frac{k_r^5}{k_c^5} = 0.0307 \qquad \alpha^6 = \frac{k_r^6}{k_c^6} = \frac{6k_s^1}{k_c^5} = 0.0368 \qquad \textbf{(40)}$$

The columns on Floor #7 and the ground floor are yet another section size. The beam lengths and sections on the floors above are similar except for one beam on Floor #7, which is 305x305x198UC:

$$k_b^5 = \frac{12EI_b}{L_b^3} = 1760\,\text{N/mm} \qquad \textbf{(41)}$$

So

$$k_s^7 = k_b^1 + k_b^3 + k_b^4 + k_b^5 = 6082 \text{ N/mm} \quad \textbf{(42)}$$

and

$$k_r^7 = 6k_s^1 + k_s^7 = 33778 \text{ N/mm} \quad \textbf{(43)}$$

$$k_c^7 = \frac{EA_c}{L_c} = 1229268 \text{ N/mm} \quad \Rightarrow \quad \alpha^7 = \frac{k_r^7}{k_c^7} = 0.0275 \quad \textbf{(44)}$$

$$k_r^8 = 7k_s^1 + k_s^7 = 38394 \text{ N/mm} \quad \Rightarrow \quad \alpha^8 = \frac{k_r^8}{k_c^7} = 0.0312 \quad \textbf{(45)}$$

This last value is smaller than that calculated for the column on Floor #6, which is due to the much larger section size of the ground floor column. The value found in the test is 23.16kN/mm, which is about 60% of the value found using the model. Aside from experimental errors, the axial flexibility of the columns above will play a significant role in making the model overestimate the correct stiffness. These values of α_n are plotted alongside the test result as the pink line on Fig. 91.

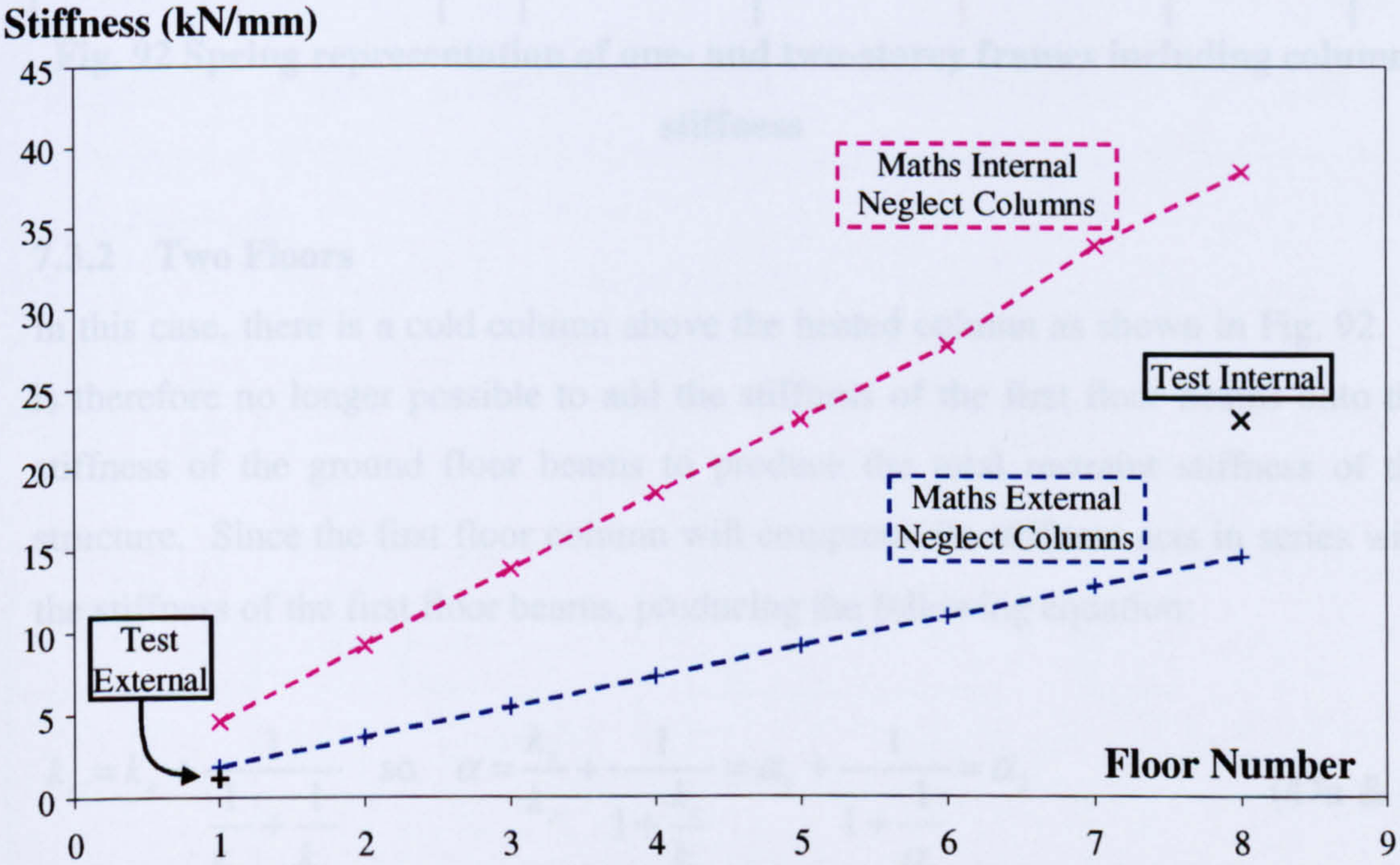

Fig. 91 Comparison of mathematical model and Cardington test

7.3 Inclusion Of Column Stiffness

The model will now be extended to take into account the axial flexibility of the columns above the heated column.

7.3.1 One Floor

This case is identical to the case where the stiffness of the column is neglected, since there are no columns above the heated column to consider:

$$k_r = k_s \quad \text{so} \quad \alpha = \frac{k_s}{k_c} = \alpha_1 \tag{46}$$

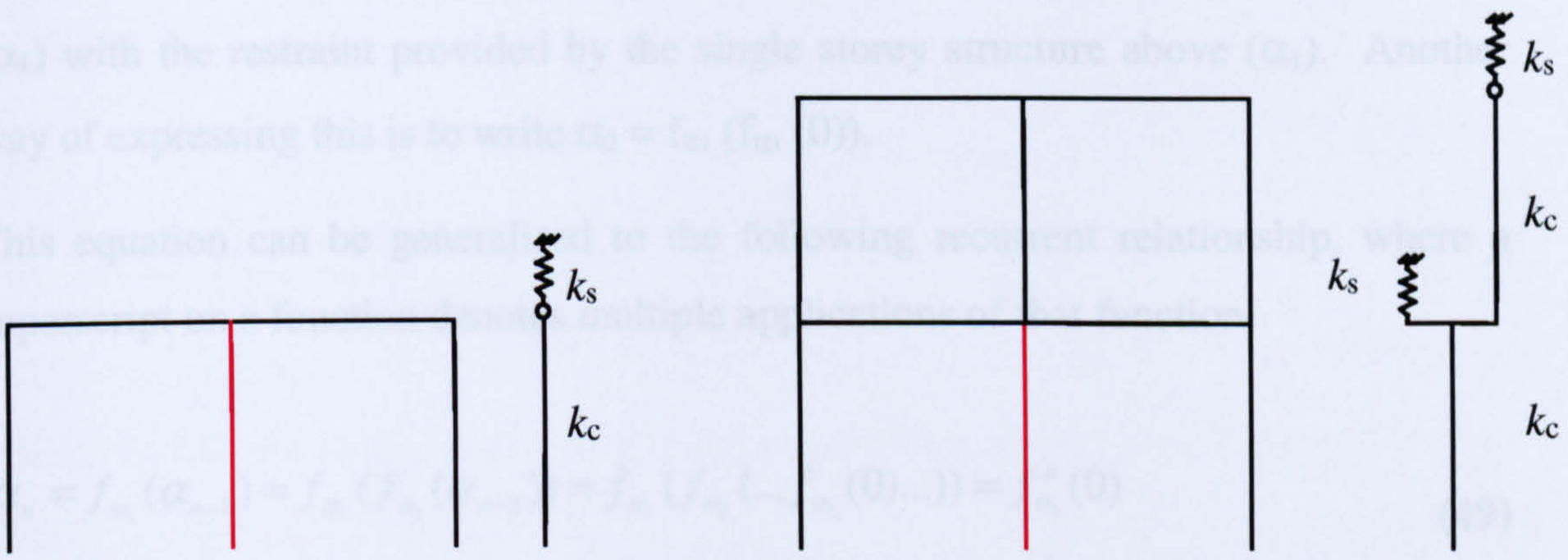

Fig. 92 Spring representation of one- and two-storey frames including column stiffness

7.3.2 Two Floors

In this case, there is a cold column above the heated column as shown in Fig. 92. It is therefore no longer possible to add the stiffness of the first floor beams onto the stiffness of the ground floor beams to produce the total restraint stiffness of the structure. Since the first floor column will compress, its stiffness acts in series with the stiffness of the first floor beams, producing the following equation:

$$k_r = k_s + \frac{1}{\frac{1}{k_c} + \frac{1}{k_s}} \quad \text{so} \quad \alpha = \frac{k_s}{k_c} + \frac{1}{1 + \frac{k_c}{k_s}} = \alpha_1 + \frac{1}{1 + \frac{1}{\alpha_1}} = \alpha_2 \tag{47a \& b}$$

7.3.3 Generalisation

When the axial shortening of the upper columns is taken into account, a more complicated relationship ensues. However, this equation makes sense if it is expressed in the form of a recursive function defined as follows:

$$f_a(b) = a + \frac{1}{1 + \frac{1}{b}} \qquad \textbf{(48)}$$

It can be seen that $\alpha_1 = f_{\alpha 1}(0)$ since this combines the restraint provided by the ground floor (α_1) with the restraint provided by the zero-floor structure above (0).

Similarly $\alpha_2 = f_{\alpha 1}(\alpha_1)$ since this combines the restraint provided by the ground floor (α_1) with the restraint provided by the single storey structure above (α_1). Another way of expressing this is to write $\alpha_2 = f_{\alpha 1}(f_{\alpha 1}(0))$.

This equation can be generalised to the following recurrent relationship, where a superscript on a function denotes multiple applications of that function.

$$\alpha_n = f_{\alpha_1}(\alpha_{n-1}) = f_{\alpha_1}(f_{\alpha_1}(\alpha_{n-2})) = f_{\alpha_1}(f_{\alpha_1}(\ldots f_{\alpha_1}(0)\ldots)) = f_{\alpha_1}^{n}(0) \qquad \textbf{(49)}$$

This equation is shown pictorially on Fig. 93. Considering a structure with an infinite number of floors, it is possible to find an equation for the upper bound to this restraint stiffness.

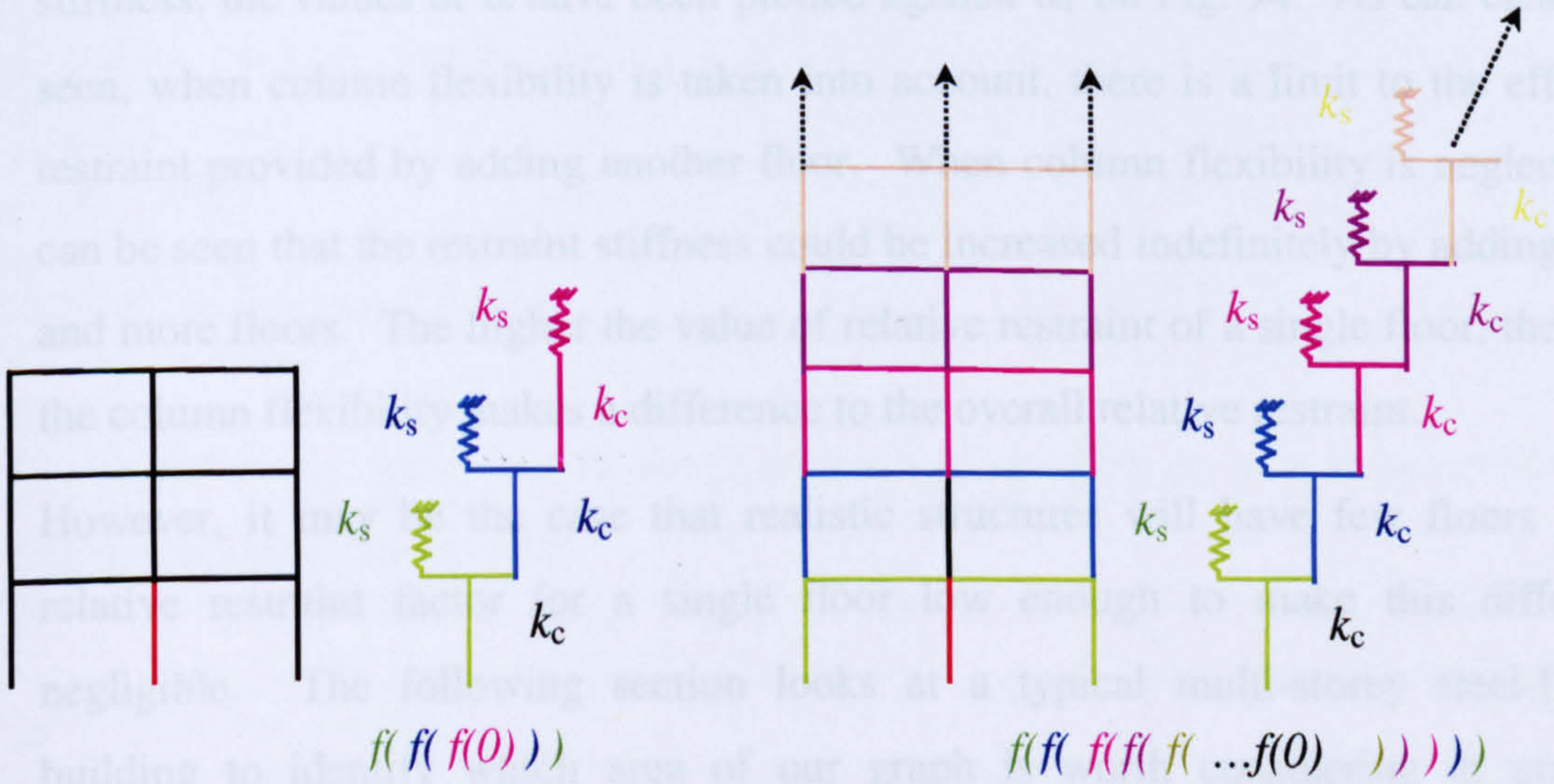

Fig. 93 Spring representation of three- and infinite-storey frames including column stiffness

$$\alpha_\infty = \alpha_1 + \cfrac{1}{1+\cfrac{1}{\alpha_1 + \cfrac{1}{1+\ddots}}} = \alpha_1 + \cfrac{1}{1+\cfrac{1}{\alpha_\infty}}$$

$$= \alpha_1 + \frac{\alpha_\infty}{\alpha_\infty + 1} = \frac{\alpha_1(\alpha_\infty + 1) + \alpha_\infty}{\alpha_\infty + 1} \tag{50}$$

$$\alpha_\infty(\alpha_\infty + 1) = \alpha_1(\alpha_\infty + 1) + \alpha_\infty \tag{51}$$

Solving this as a quadratic equation

$$\alpha_\infty{}^2 - \alpha_1\alpha_\infty - \alpha_1 = 0 \tag{52}$$

gives

$$\alpha_\infty = \frac{\alpha_1 \pm \sqrt{\alpha_1{}^2 + 4\alpha_1}}{2} \tag{53}$$

Since $\alpha_1 \geq 0$, the only solution which makes physical sense (i.e. $\alpha_\infty \geq 0$) is

$$\alpha_\infty = \frac{\alpha_1 + \sqrt{\alpha_1{}^2 + 4\alpha_1}}{2} \tag{54}$$

In order to see how much contribution the column makes to the overall structural stiffness, the values of α have been plotted against α_1 on Fig. 94. As can clearly be seen, when column flexibility is taken into account, there is a limit to the effect of restraint provided by adding another floor. When column flexibility is neglected, it can be seen that the restraint stiffness could be increased indefinitely by adding more and more floors. The higher the value of relative restraint of a single floor, the more the column flexibility makes a difference to the overall relative restraint.

However, it may be the case that realistic structures will have few floors and a relative restraint factor for a single floor low enough to make this difference negligible. The following section looks at a typical multi-storey steel-framed building to identify which area of our graph is worth considering in practical buildings.

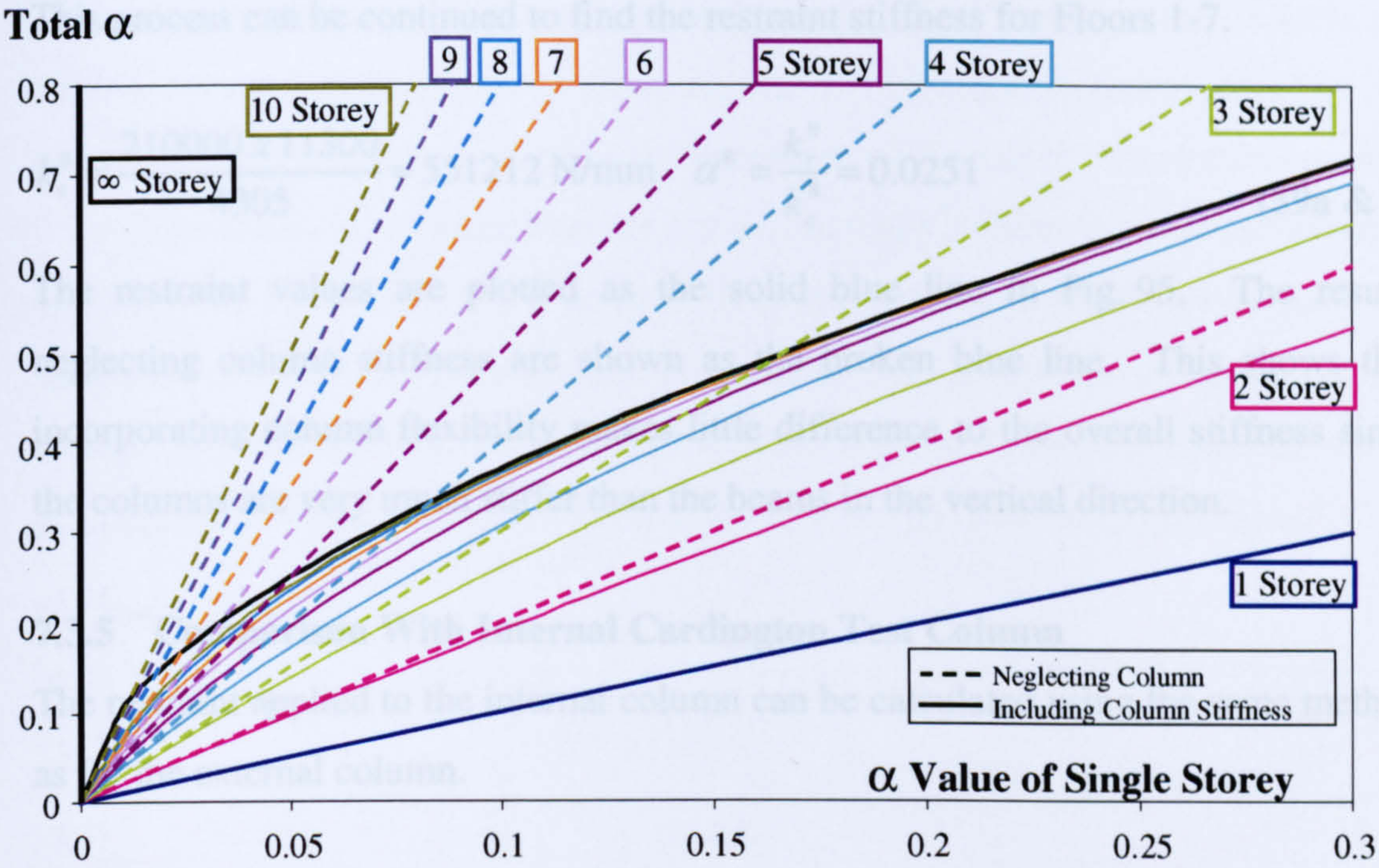

Fig. 94 Total value of α for multi-storey frames

7.3.4 Comparison With External Cardington Test Column

The column on the top floor has no columns above and so the restraint found using the extended model is the same as found previously.

$$\alpha^1 = \frac{k_r^1}{k_c^1} = \frac{k_s^1}{k_c^1} = 0.00322 \tag{55}$$

The test result is 63% of this value, and including column stiffness in the model has no effect. The second floor column however has its restraint slightly modified as follows.

$$\alpha^2 = \alpha^1 + \frac{1}{1 + \frac{1}{\alpha^1}} = 0.00643 \tag{56}$$

The restraint can easily be calculated for each lower floor by using the recurrence relationship given in eqn. (48).

$$\alpha^3 = \alpha^1 + \frac{1}{1 + \frac{1}{\alpha^2}} = 0.0096 \tag{57}$$

$$\alpha^4 = \alpha^1 + \frac{1}{1 + \frac{1}{\alpha^3}} = 0.0127 \tag{58}$$

This process can be continued to find the restraint stiffness for Floors 1-7.

$$k_c^8 = \frac{210000\,x\,11300}{4305} = 551212\ \text{N/mm} \quad \alpha^8 = \frac{k_r^8}{k_c^8} = 0.0251 \qquad \textbf{(59a \& b)}$$

The restraint values are plotted as the solid blue line in Fig. 95. The results neglecting column stiffness are shown as the broken blue line. This shows that incorporating column flexibility makes little difference to the overall stiffness since the columns are very much stiffer than the beams in the vertical direction.

7.3.5 Comparison With Internal Cardington Test Column

The restraint applied to the internal column can be calculated using the same method as for the external column.

Column	k_s *(N/mm)*	k_r *(N/mm)*	k_c *(N/mm)*	α
1	4616	4616	567025	0.00814
2	4616	9195	567025	0.0162
3	4616	13664	567025	0.0241
4	4616	17958	567025	0.0317
5	4616	22023	752688	0.0293
6	4616	26013	752688	0.0346
7	6082	31226	1264516	0.0247
8	4616	35089	1229268	0.0285

Table 8 Stiffness of restraint to internal columns

As can be seen from Table 8 the restraint applied to the column increases as the storey level decreases. However, since the column section changes at intervals, the relative restraint factor does not increase monotonically.

The restraint values are plotted against floor number and are shown as the solid pink line on Fig. 95. The restraint level is lower than when column stiffness was neglected, but is still one-and-a-half times the value found in the test. One obvious explanation for these discrepancies is experimental error, but this seems unlikely to be the only factor that lowers the test stiffness.

There are two important points to note at this stage of the investigation. Firstly, the relative restraint factors derived from the real steel-framed structure are all in the range 0.002 to 0.04 and so beam / column layouts with relative restraint factors over 0.1 will be exceptional rather than the norm. Secondly, within this realistic range of values of α, the effect of the column flexibility from the floors above makes a noticeable difference to the restraint. For instance, the ground floor internal column reduces its α value from 0.0312 to 0.0285 when column stiffness is included, which is a reduction of nearly 10% in a fairly low-rise structure with stocky columns.

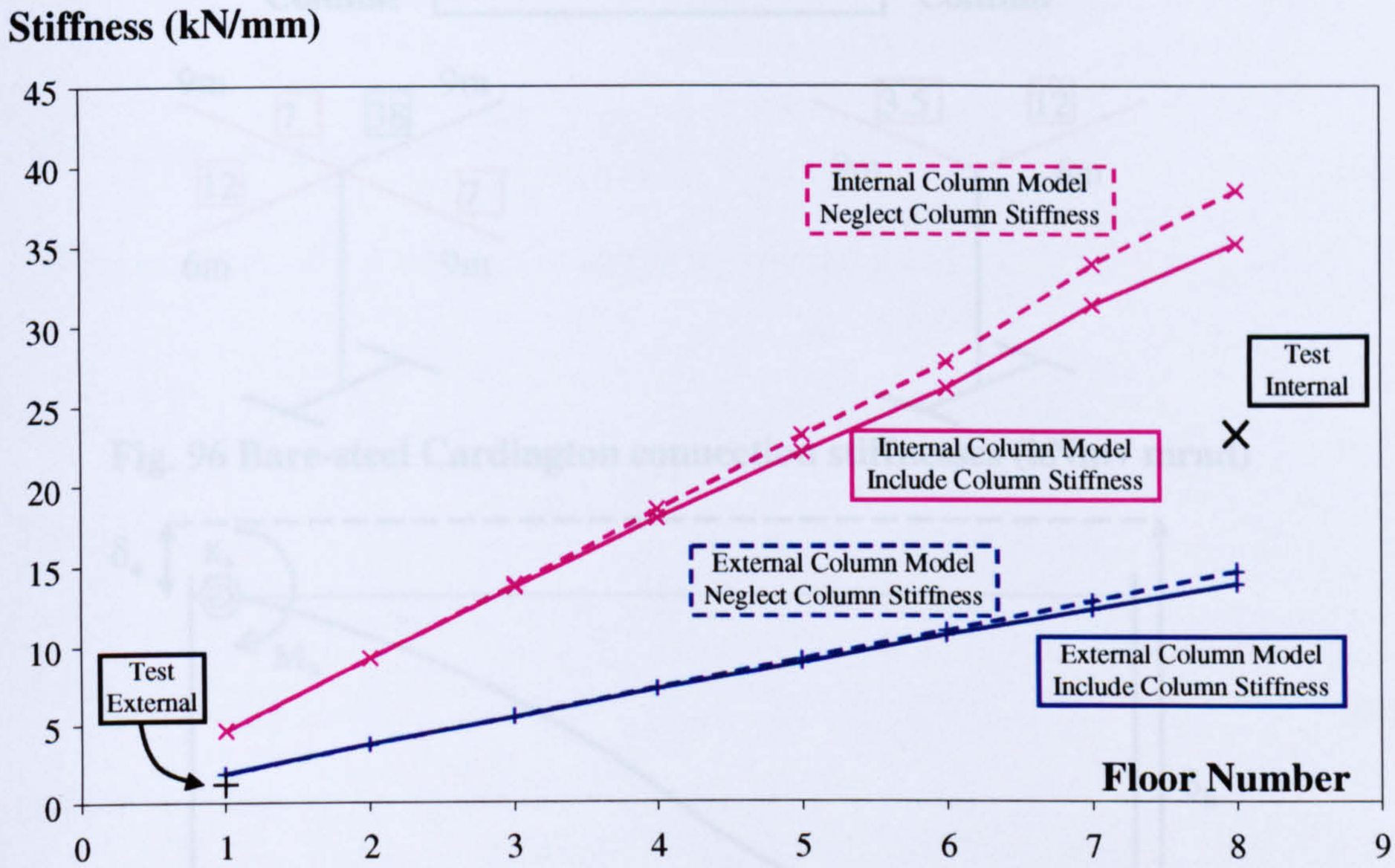

Fig. 95 Comparison of mathematical model and Cardington test

7.4 Semi-Rigid Connections

Realistic values of bare-steel beam-to-column connection stiffnesses will now be incorporated into the model. These stiffnesses, shown in Fig. 96, are taken from previous experimental work performed at the University of Sheffield[50].

7.4.1 Modification Of Lateral Beam Stiffness

The model for calculating the lateral stiffness of the beams which has been used so far assumes that both ends of the beams are completely fixed against rotation. Experiments have shown that this is not the case in a real structure[26,28], and this semi-rigid effect may go some way towards explaining why the Cardington test results show a lower stiffness than the model. Tests on connections of a similar

arrangement to those used in the Cardington frame[28] suggest that, rather than being rigidly connected, the beam-to-column connections have an initial rotational stiffness of the order of tens of kNm / mrad. The model of the lateral stiffness of a beam can therefore be modified as follows:

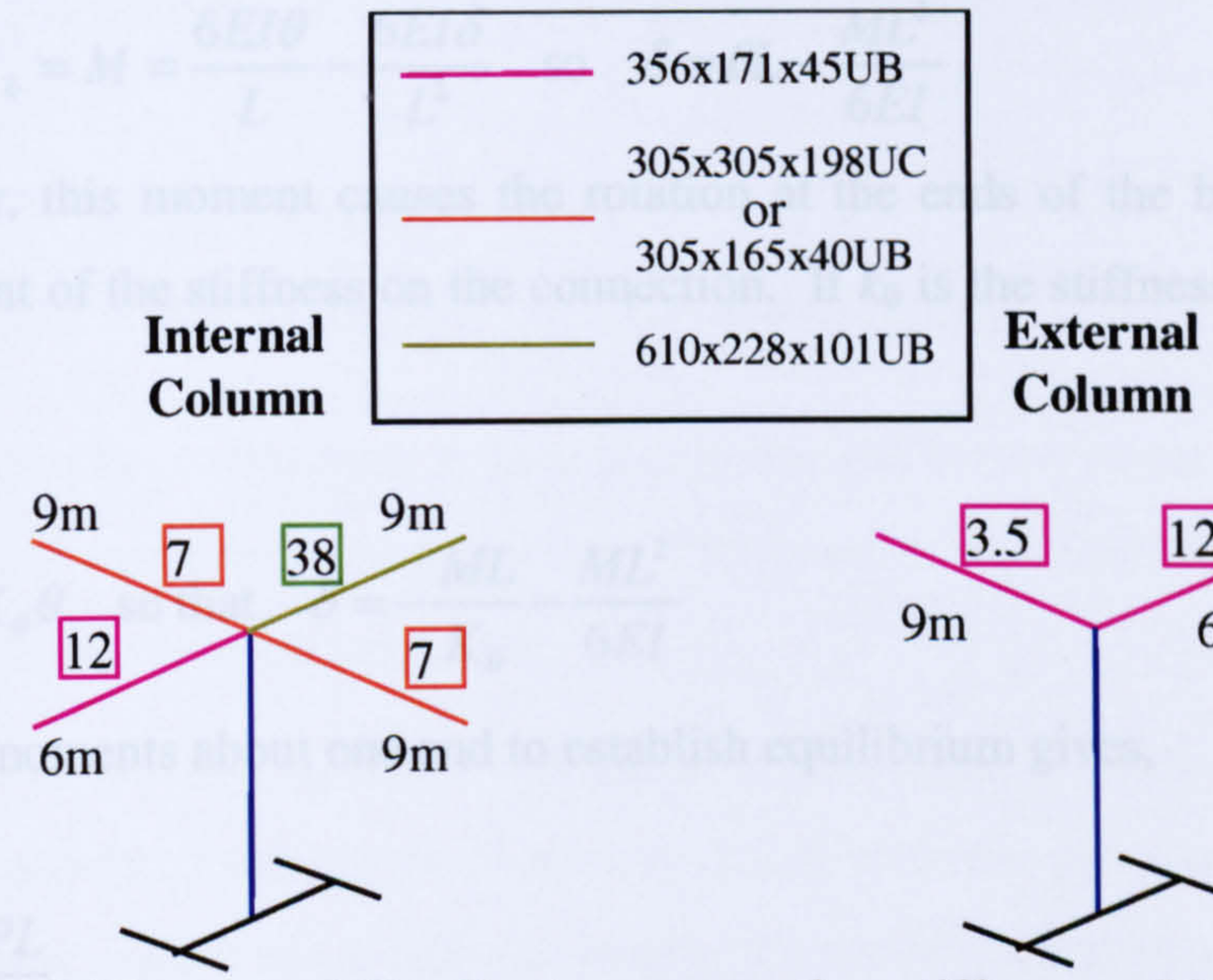

Fig. 96 Bare-steel Cardington connection stiffnesses (kNm / mrad)

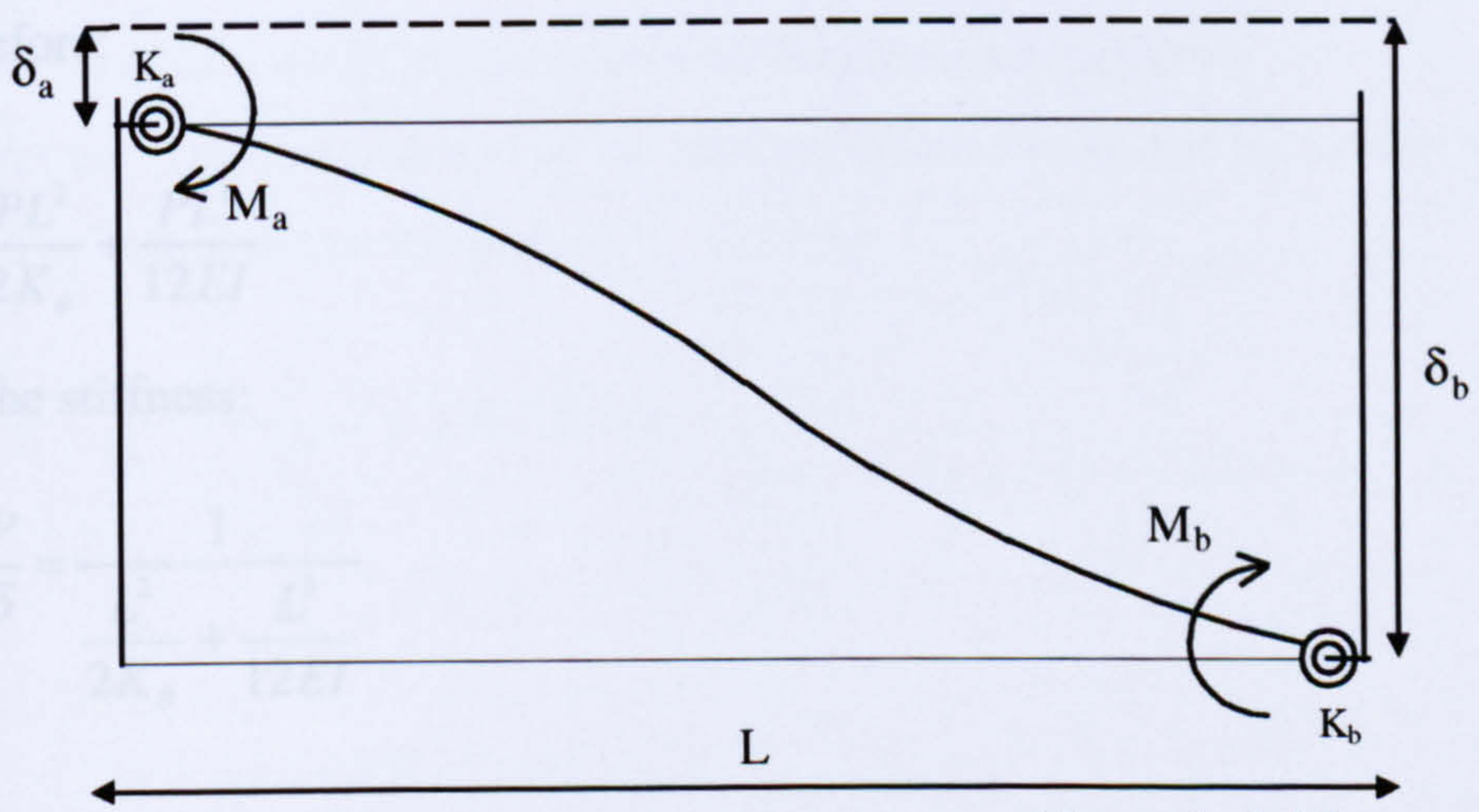

Fig. 97 A deflected beam-column arrangement with semi-rigid connections

Noting that $\theta_a = \theta_b$ (= θ say) the following slope-deflection equation applies:

$$M_a = \frac{2EI}{L}\left[2\theta_a + \theta_b + \frac{3(\delta_a - \delta_b)}{L}\right] = \frac{2EI}{L}\left[2\theta + \theta + \frac{3(0-\delta)}{L}\right]$$

$$= \frac{2EI}{L}\left(3\theta - \frac{3\delta}{L}\right) \qquad \textbf{(60)}$$

It is assumed that the stiffness of the connection at each end of the beam is the same. It can be stated from symmetry that the moments at each end of the beam are the same. The following equation therefore applies.

$$M_a = M_b = M = \frac{6EI\theta}{L} - \frac{6EI\delta}{L^2} \quad \text{so} \quad \delta = \theta L - \frac{ML^2}{6EI} \tag{61}$$

However, this moment causes the rotation at the ends of the beams and so this is dependent of the stiffness on the connection. If k_θ is the stiffness of the connections, then:

$$M = -K_\theta \theta \quad \text{so that} \quad \delta = -\frac{ML}{K_\theta} - \frac{ML^2}{6EI} \tag{62}$$

Taking moments about one end to establish equilibrium gives,

$$M = \frac{-PL}{2} \tag{63}$$

Therefore:

$$\delta = \frac{PL^2}{2K_\theta} + \frac{PL^3}{12EI} \tag{64}$$

and the stiffness:

$$k = \frac{P}{\delta} = \frac{1}{\frac{L^2}{2K_\theta} + \frac{L^3}{12EI}} \tag{65}$$

7.4.2 Comparison With External Cardington Test Column

If the connection stiffness is incorporated into the assumption of the lateral stiffness of the beams in the Cardington frame, the restraint provided by the top floor beams can be re-calculated using the model above.

$$k_b^3 = \frac{1}{\frac{L^2}{2K_\theta} + \frac{L^3}{12EI}} = 452 \text{ N/mm} \tag{66a \& b}$$

$$k_b^6 = \frac{1}{\frac{L^2}{2K_\theta} + \frac{L^3}{12EI}} = 72 \text{ N/mm}$$

So the modified value of k_s, which includes connection stiffness, can be calculated as follows.

$$k_s^1 = k_b^3 + k_b^6 = 524 \text{ N/mm} \quad \text{so} \quad \alpha^1 = \frac{k_r^1}{k_c^1} = \frac{k_s^1}{k_c^1} = 0.00092 \tag{67}$$

This gives a huge reduction in lateral stiffness and results in the model showing half the value of restraint found in the test. The model is obviously highly sensitive to the value of connection stiffness used.

Using these new lateral beam stiffnesses, the restraint from the rest of the structure can be calculated exactly as in section 7.3.4, with the ground floor again being a special case since it has a different length. The results are shown on Fig. 98.

7.4.3 Comparison With Internal Cardington Test Column

In a similar way, the restraint to the internal column provided by the top floor beams can be re-calculated as follows:

$$k_b^{1\&2} = \frac{1}{\frac{L^2}{2K_\theta} + \frac{L^3}{12EI}} = 109 \text{ N/mm}$$

$$k_b^3 = \frac{1}{\frac{L^2}{2K_\theta} + \frac{L^3}{12EI}} = 452 \text{ N/mm}$$

$$k_b^4 = \frac{1}{\frac{L^2}{2K_\theta} + \frac{L^3}{12EI}} = 691 \text{ N/mm} \tag{68a, b \& c}$$

so that

$$k_s^1 = \quad k_b^1 + k_b^2 + k_b^3 + k_b^4 = 1361 \text{ N/mm} \tag{69}$$

and

$$\alpha^1 = \frac{k_s^8}{k_c^8} = 0.0024 \tag{70}$$

It should be noted that the 6m long beam now provides the most lateral restraint. This is because the connection stiffness is much smaller than the lateral bending stiffness of the beam and becomes the dominant effect. The way this stiffness contributes to the overall stiffness of the beam depends upon the length of the beam, making the shorter beams much more significant.

The restraint applied to the floors below can now be calculated as in section 7.3.5 but using these modified beam stiffnesses. Again, since Floor #7 has a different beam section it is necessary to re-calculate the floor stiffness k_b^5.

$$k_b^5 = \frac{1}{\frac{L^2}{2k_\theta} + \frac{L^3}{12EI}} = 157 \text{ N/mm} \tag{71}$$

Column	k_s *(N/mm)*	k_r *(N/mm)*	k_c *(N/mm)*	α
1	1361	1361	567025	0.00240
2	1361	2719	567025	0.00480
3	1361	4067	567025	0.00717
4	1361	5399	567025	0.00952
5	1361	6709	752688	0.00891
6	1361	8011	752688	0.01064
7	1409	9336	1264516	0.00738
8	1361	10629	1229268	0.00865

Table 9 Stiffness of restraint of internal column

These results are compared to the test and shown as the solid pink line on Fig. 98. As with the external column, incorporating the connection stiffness into the model greatly reduces the restraint stiffness. The test result from the Cardington frame indicates that the actual connection stiffnesses in situ may be greater than those assumed for this study.

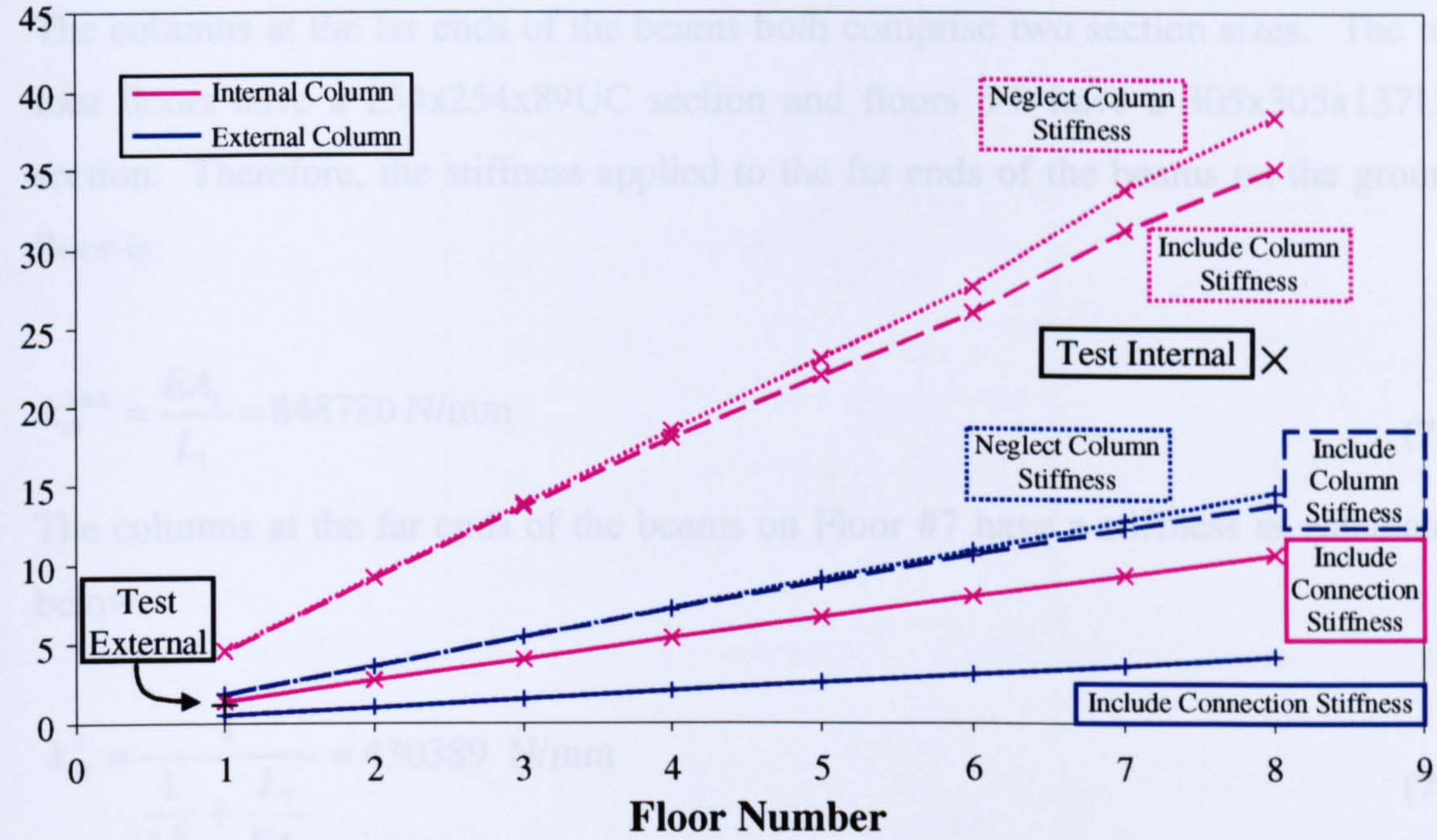

Fig. 98 Comparison of mathematical model and Cardington test

7.5 Columns In Tension

The far ends of the beams are connected to columns, which stretch when resisting the vertical expansion. This effect can have a noticeable effect in some cases, as is shown in this section.

7.5.1 Modification Of Lateral Beam Stiffness

Until now, the model has assumed that the far ends of the beams framing into a heated column are not allowed to move vertically. In fact, they are attached to columns, which may stretch when resisting the vertical expansion of the heated column. This effect can be incorporated into the model by reducing the vertical stiffnesses of the beams accordingly. For example, the equations for the lateral stiffness of the beams on the top floor, given in eqn. (68a) become: -

$$k_b^{1\&2} = \frac{1}{\frac{L^2}{2k_\theta} + \frac{L^3}{12EI} + \frac{1}{k_{t1}^{1\&2}}} \qquad (72)$$

Where:

k_{tn}^{m} = Axial restraint stiffness in tension of the column at the end of beam m on floor n.

7.5.2 Comparison With External Cardington Test Column

The columns at the far ends of the beams both comprise two section sizes. The top four floors have a 254x254x89UC section and floors 5-8 have a 305x305x137UC section. Therefore, the stiffness applied to the far ends of the beams on the ground floor is:

$$k_{t8}^{3\&6} = \frac{EA_1}{L_1} = 848780 \text{ N/mm} \tag{73}$$

The columns at the far ends of the beams on Floor #7 have a stiffness as calculated below:

$$k_{t7}^{3} = \frac{1}{\frac{1}{k_{t8}^{3}} + \frac{L_7}{EA_7}} = 430389 \text{ N/mm} \tag{74}$$

Following this scheme, it is possible to construct the following table of column tension stiffnesses, noting that both columns have identical section sizes all the way up the building.

These tension stiffnesses can then be used to re-calculate the restraint applied to the column on the top floor as follows.

$$k_{b1}^{3} = \frac{1}{\frac{L^2}{2k_\theta} + \frac{L^3}{12EI} + \frac{1}{k_{t1}^{1}}} = 450 \text{ N/mm}$$

$$k_{b1}^{6} = \frac{1}{\frac{L^2}{2k_\theta} + \frac{L^3}{12EI} + \frac{1}{k_{t1}^{1}}} = 72 \text{ N/mm} \tag{75a \& b}$$

Comparison of these new values with the values found when columns in tension are neglected (452 & 72 N/mm) shows that this effect makes a negligible difference. In fact, when α is re-calculated it is found to have changed by less than 1%.

Axial Stiffness	*End of Beams #3&6*
Floor #1	848780
Floor #2	430389
Floor #3	288284
Floor #4	216726
Floor #5	156796
Floor #6	122830
Floor #7	100960
Floor #8	85701

Table 10 Axial stiffnesses of tension columns for external Cardington column

$$k_s^1 = k_b^3 + k_b^6 = 522 \text{ N/mm} \quad \Rightarrow \quad \alpha^1 = \frac{k_r^1}{k_c^1} = \frac{k_s^1}{k_c^1} = 0.00092 \tag{76}$$

The length of the columns in tension is greatest on the top floor and so these have the lowest axial stiffness, as shown in Table 10. This means that these top columns include the largest discrepancy from the earlier model, which assumed the far ends of the beams to be completely restrained from moving vertically. Thus, it can be shown that the restraint factors of the floors below will change by an even smaller margin when column tension effects are included.

7.5.3 Comparison With Internal Cardington Test Column

The same scheme can be used to calculate the stiffnesses in tension of the columns at the far ends of the beams that frame into the internal column, as shown in Table 11. It can be noted that the columns at the ends of beams 1 and 4 are exactly the same as the columns at the ends of beams 3 and 6 as calculated above.

These tension stiffnesses can then be used to re-calculate the restraint applied to the heated internal columns using the new model.

$$k_{b1}^1 = \frac{1}{\frac{L^2}{2k_\theta} + \frac{L^3}{12EI} + \frac{1}{k_{t1}^1}} = 109 \text{ N/mm}$$

$$k_{b1}^2 = \frac{1}{\frac{L^2}{2k_\theta} + \frac{L^3}{12EI} + \frac{1}{k_{t1}^1}} = 109 \text{ N/mm}$$

$$k_{b1}^3 = \frac{1}{\frac{L^2}{2k_\theta} + \frac{L^3}{12EI} + \frac{1}{k_{t1}^1}} = 450 \text{ N/mm}$$

$$k_{b1}^4 = \frac{1}{\frac{L^2}{2k_\theta} + \frac{L^3}{12EI} + \frac{1}{k_{t1}^4}} = 685 \text{ N/mm} \qquad \textbf{(77a, b, c \& d)}$$

Axial Stiffness	*End of Beam #1*	*End of Beam #2*	*End of Beam #3*	*End of Beam #4*
Floor #8	848780	1229268	1229268	848780
Floor #7	430389	623321	623321	430389
Floor #6	288284	363685	363685	288284
Floor #5	216726	256743	256743	216726
Floor #4	156796	198402	176724	156796
Floor #3	122830	146975	134732	122830
Floor #2	100960	116721	108865	100960
Floor #1	85701	96796	91330	85701

Table 11 Axial stiffness of tension columns for internal Cardington column

So

$$k_s^1 = \quad k_b^1 + k_b^2 + k_b^3 + k_b^4 = 1353 \text{ N/mm} \qquad \textbf{(78)}$$

and

$$\alpha^1 = \frac{k_s^1}{k_c^1} = 0.00239 \qquad \textbf{(79)}$$

As can be seen, taking the tension in these eighth storey columns into account has made no noticeable difference to the relative restraint factor. It can therefore be concluded that, in the case of the Cardington frame, we can neglect the effect of tension in the columns. However, we have the model available to take account of this effect should a structure require it. For instance, if the sway- or connection-

stiffness is relatively high. The stretching of the columns is expected to have a greater effect in the rigid case, since the stiffer connections will transfer more load to the supporting columns. For example, when rigid connections are assumed for the internal Cardington frame column, the model shows a reduction in relative restraint factor for the top-floor column from $\alpha^1 = 0.00813$ to $\alpha^1 = 0.00809$. Although more significant than in the semi-rigid case, this is still only a reduction of less than 1%.

7.6 Composite Beams

Up to this point, it has been assumed that the structure that contributes to the restraint is skeletal and constructed from bare steel members. However, there is no reason why this model cannot be extended to structures with composite floors. The basis of the model is that a value for the lateral stiffness of the restraining beams is calculated. Various ways of achieving this, increasing in complexity, have been described above. These methods can all be applied to composite beams if the stiffness of the beam and its connections are modified from the simple assumption of the elastic lateral stiffness of the steel beam.

7.6.1 Modification Of Lateral Beam Stiffness

Many different systems are used to construct concrete flooring on a steel-framed building. Modern systems, such as those which use trapezoidal decking as permanent formwork, have the steel attached to the concrete by shear-studs. The decking does not provide structural strength, but acts as a base on which the concrete is poured. The shear-studs can provide various levels of interaction between decking and beam, depending on their strength and spacing. A number of experiments have been performed to determine typical levels of interaction[33]. For the purpose of this study, full interaction between the decking and steel is assumed.

An equivalent Young's modulus can be calculated assuming a "smeared" stiffness approach. Concrete has a Young's modulus approximately one fifteenth of that of steel. An equivalent section is therefore constructed by reducing the width of the concrete flange to one fifteenth of its real width and then considering it as having the same Young's modulus as steel.

$$k_{beam} = k_{composite} = \frac{12\, E_{composite}\, I_{composite}}{L^3_{composite}} \tag{80}$$

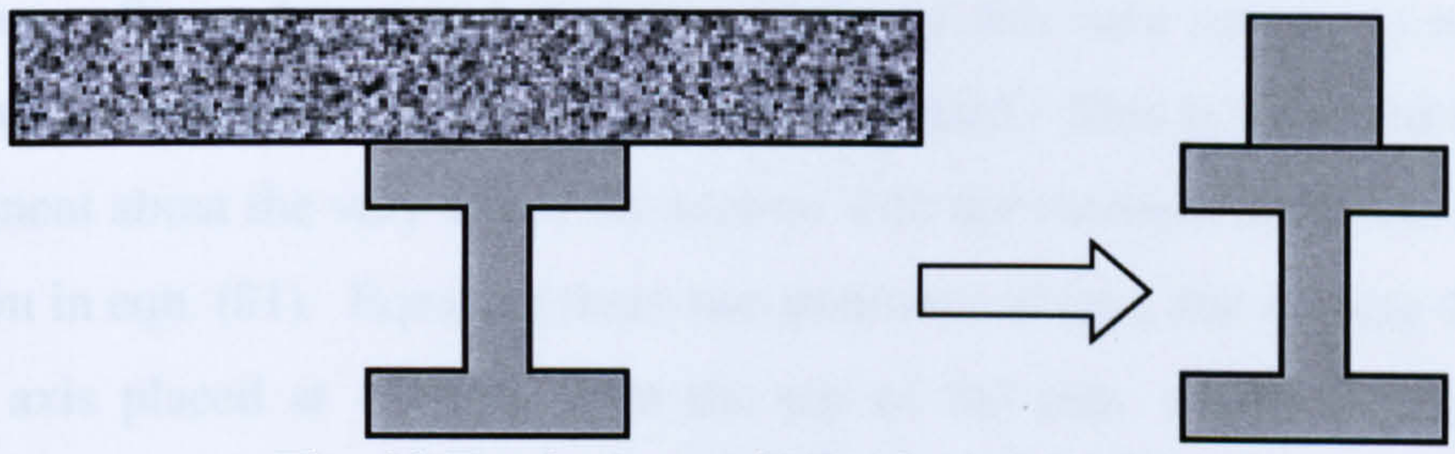

Fig. 99 Equivalent width of steel section

The effective width of the concrete flange used in design to BS5950 is usually one quarter of the length of the beam.

7.6.2 Comparison With External Cardington Test Column

For example, the 6m long beam k_b^3, framing into the corner column, has an effective flange width of 1.5m. The equivalent section comprises a steel beam with a 0.1m wide steel "slab" on top. The concrete slabs in the Cardington frame have a nominally 70mm nominally continuous thickness with a 65mm trapezoidal steel decking below. The ribbed part of the slab has little effect on the strength of the beam, but raises the lever arm of the 70mm-thick solid layer.

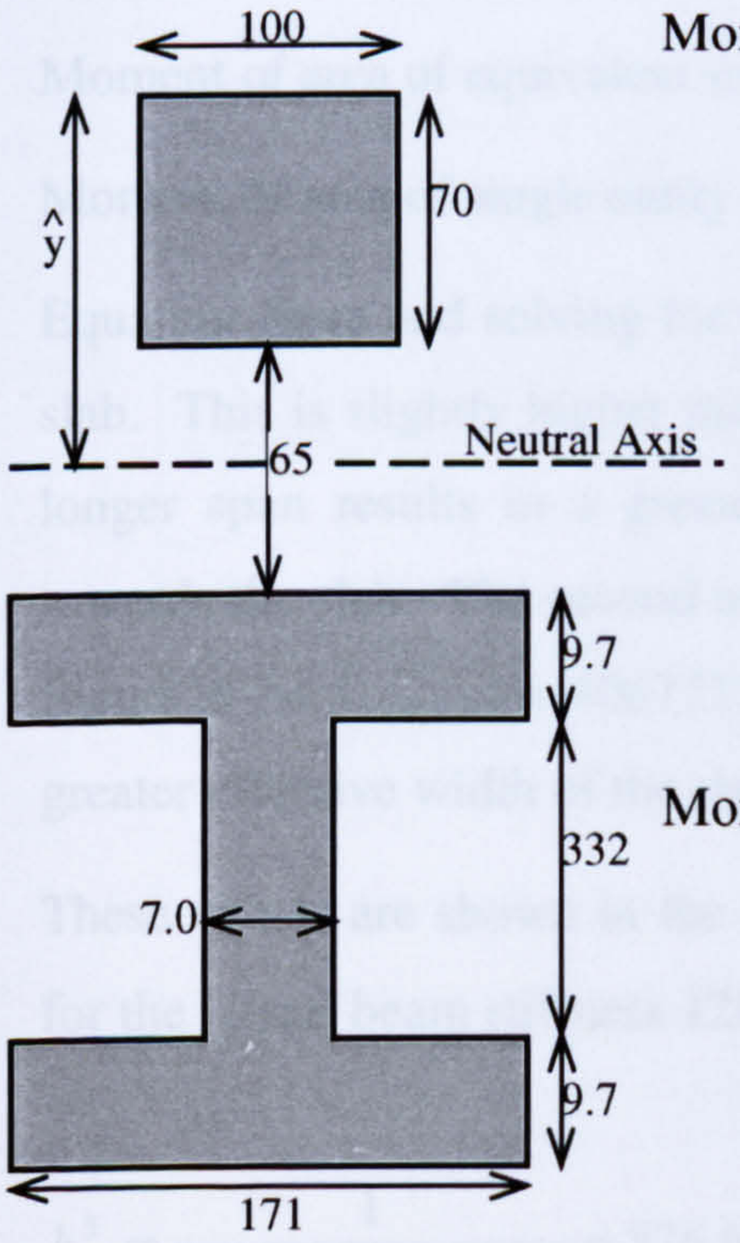

Moment of Area of Equivalent Section About Top

$$= 100\ x\ 70\ x\ 35$$

$$+ 171\ x\ 9.7\ x\ (70 + 65 + \frac{9.7}{2})$$

$$+ 332\ x\ 7.0\ x\ (70 + 65 + 9.7 + \frac{332}{2})$$

$$+ 171\ x\ 9.7\ x\ (70 + 65 + 9.7 + 332 + \frac{9.7}{2})$$

$$= 1997783\ \text{mm}^3$$

Moment of Area of Single Entity About Top

$$= \{(100\ x\ 70) + 2(171\ x\ 9.7) + (332\ x\ 7.0)\}\hat{y}$$

$$= 12641\ \hat{y}\ \text{mm}^3$$

Fig. 100 Moment of area **(81a & b)**

To calculate the equivalent section, the steel "slab" is assumed to be 65mm from the top flange. Since the second moment of area of this new section is required, the position of the elastic neutral axis must be calculated. This is achieved by equating the moment about the very top of the section with the moment about the neutral axis as shown in eqn. (81). Equating these two moments of area and solving for $\hat{y}$ gives a neutral axis placed at 158 mm from the top of the slab, which is roughly in the middle of the trapezoidal decking.

The Second Moment of Area about this neutral axis can now be calculated in the usual way.

$$I_{Composite} = I_{Slab} + I_{Beam} = \left\{\frac{bd^3}{12} + Ay_{slab}^2\right\} + \left\{I_{Beam} + A_{Beam}\, y_{beam}^2\right\} \qquad (82)$$
$$= 363068444 \ \ mm^4$$

Where $y_{slab\,/\,beam}$ = distance of centre of slab / beam to the neutral axis

This is over three times the I-value of the isolated steel beam, which would be a measure of the increase in restraint stiffness given by the beam. If the process is repeated for the 9m long beam, which frames into the external column, a similar increase in stiffness is found:

Moment of area of equivalent section about top $= 2120283 \text{ mm}^3$

Moment of area of single entity about top $= 16141\ \hat{y} \text{ mm}^3$

Equating these and solving for $\hat{y}$ gives the neutral axis 131mm below the top of the slab. This is slightly higher than the position found for the 6m long beam since the longer span results in a greater effective slab width and moves the neutral axis towards the slab. The second moment of area can now be calculated as above and is found to be $I_{composite} = 406775770 \text{ mm}^4$, which is again slightly higher due to the greater effective width of the slab.

These values are shown in the dark shaded rows on Table 12 and can now be used for the lateral beam stiffness $12EI / L^3$ in the re-calculation of k_b[3&6].

$$k_{b1}^3 = \frac{1}{\frac{L^2}{2k_\theta} + \frac{L^3}{12EI} + \frac{1}{k_{t1}^1}} = 576 \text{ N/mm}$$

(83a & b)

$$k_{b1}^{6} = \frac{1}{\frac{L^2}{2k_\theta} + \frac{L^3}{12EI} + \frac{1}{k_{t1}^{1}}} = 81\ \text{N/mm}$$

$$k_s^1 = k_b^3 + k_b^6 = 657\ \text{N/mm} \quad \Rightarrow \quad \alpha^1 = \frac{k_r^1}{k_c^1} = \frac{k_s^1}{k_c^1} = 0.00116 \qquad \textbf{(84)}$$

The presence of the concrete slab therefore increases the restraint due to the beams by over 25%. However, the restraint stiffness is still less than 60% of the value found in the test. This suggests that an extra effect is present which has not yet been included in the model.

7.6.3 Comparison With Internal Cardington Test Column

As a further comparison, the same modification to the beam stiffness can be made for the internal Cardington column. The modified beam stiffnesses for the beams framing into the internal column are shown in the table below. They are shown as the thick line on Fig. 101 and again are about 20% higher than when the concrete slab is neglected. However, this is still only one half of the stiffness found during the Cardington tests.

No.	*Section*	*Neutral Axis(mm)*	I_b *(mm^4)*
$k_b^{1\&2}$	9m long 305x165x40UB	152	85030000
k_b^3	6m long 365x171x45UB	158	363068444
k_b^4	9m long 610x228x101UB	301	757800000
k_b^5	9m long 305x305x198UC	170	509000000
k_b^6	9m long 365x171x45UB	131	406775770

Table 12 Second moments of area including concrete stiffness

Results from the Cardington tests, performed when the concrete was in place, show that the restraint stiffness of the internal column increased by nearly three times and the external column by over eight times.

Column	k_s *(N/mm)*	k_r *(N/mm)*	k_c *(N/mm)*	α
1	1681	1681	567025	0.00296
2	1680	3356	567025	0.00592
3	1679	5015	567025	0.00884
4	1678	6649	567025	0.01173
5	1676	8266	752688	0.01098
6	1674	9850	752688	0.01309
7	1688	11463	1264516	0.00906
8	1670	13027	1229268	0.01060

Table 13 Restraint stiffnesses including concrete stiffness

The inclusion of concrete into the model does increase the stiffness of the restraint provided. However, the stiffness is not increased by as much as found in the tests. The main difference between the tests and the model is that in the tests, the column is in the centre of a large slab, supported on four edges. The model's representation of this by four composite beams that do not interact with each other will therefore underestimate the restraint this provides.

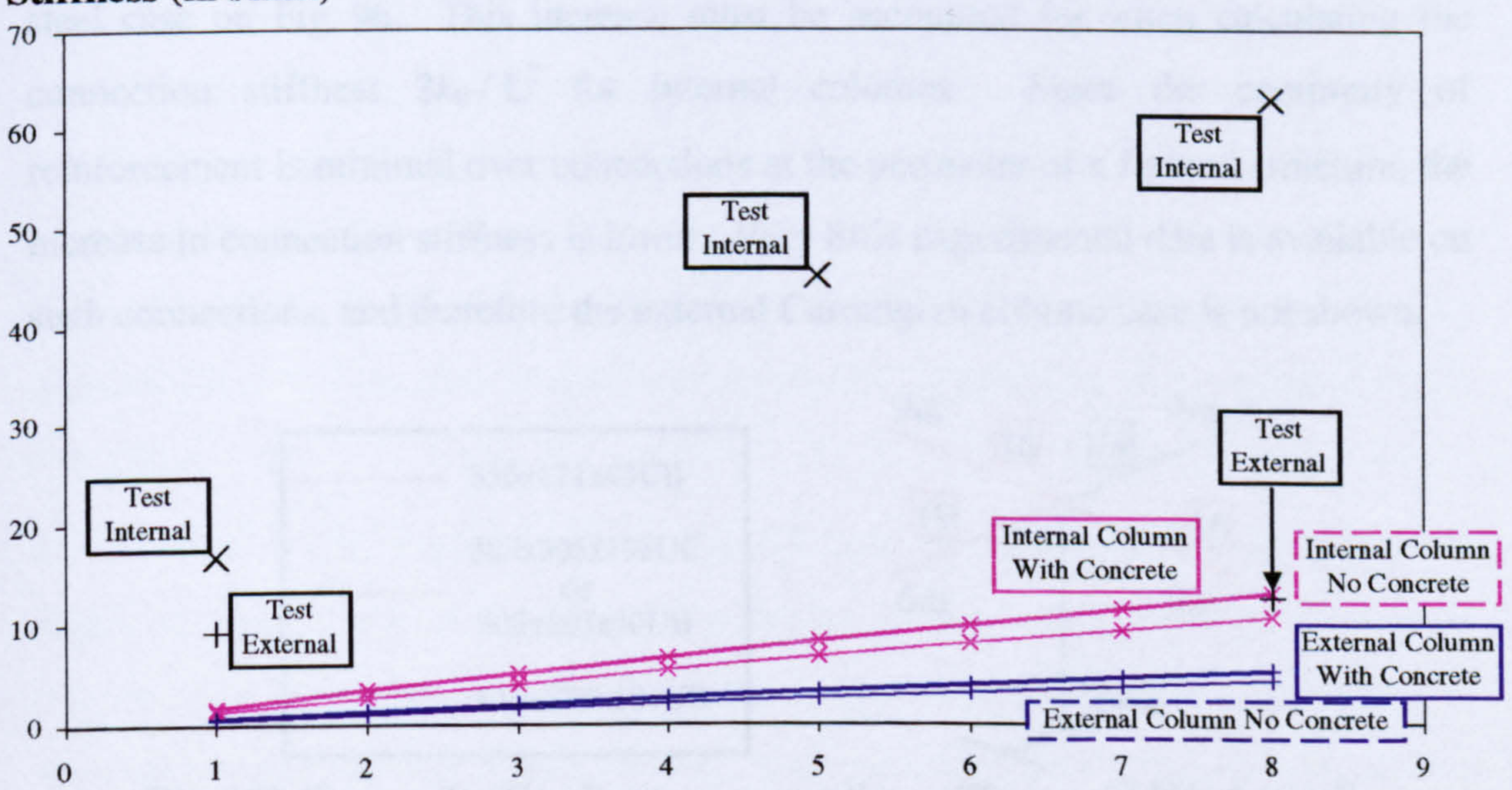

Fig. 101 Comparison where concrete is present

A factor, which increases the restraint applied by each composite beam, by considering this two-way spanning interaction, could be developed and introduced into the model. This would require a great deal of investigation, analysis and validation and is outside the scope of this investigation.

However, there is another difference between the tests and the models, the effects of which are more readily assessed. It has already been shown that the connection stiffness is a dominant effect in assessing the overall restraint applied to the structure. Thus, data for connections where a concrete slab acts compositely with a beam should be used, as discussed in the following section.

7.6.4 Modification Of Connection Stiffness

In addition to increasing the lateral stiffness of a beam, experiments have shown[26,28] that the presence of concrete greatly increases the stiffness of the beam-column connection. A number of more complex but accurate models for modifying the connection stiffness are available[25], based on experimental results and incorporating the exact geometry of the connection details, however these methods are outside the scope of this simple model. As a general guide, the stiffness is increased by between two and three times[25] as shown on Fig. 102, which can be compared with the bare-steel case on Fig. 96. This increase must be accounted for when calculating the connection stiffness $2k_\theta / L^2$ for internal columns. Since the continuity of reinforcement is minimal over connections at the perimeter of a framed structure, the increase in connection stiffness is lower. Very little experimental data is available on such connections, and therefore the external Cardington column case is not shown.

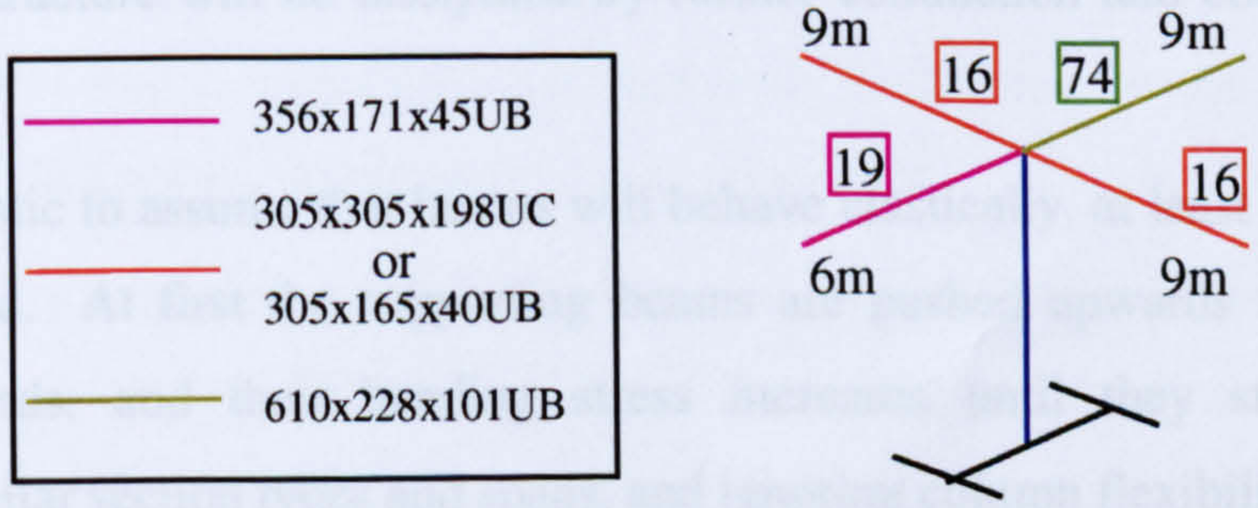

Fig. 102 Composite Cardington connection stiffnesses (kNm / mrad)

If these modified stiffness values are used to calculate the axial stiffness applied to the ground floor, internal Cardington column, the stiffness increases from 13kN/mm to 21.4kN/mm. Although an increase of 64%, this value is still around one third of

the 62.8kN/mm stiffness measured during the relevant test. In fact, these composite stiffness values would have to be ten times higher to give this level of restraint. There is certainly no experimental evidence of connection stiffness values of this magnitude, therefore some other factor must be present in the tests which is not taken into account in this model. For example, apart from the two-way spanning of floor slabs as discussed in section 7.6.3, there is a large tolerance on test results due to experimental errors. There is also evidence to suggest[51] that the assumption of a nominal 70mm thickness for the concrete slab is greatly conservative. This would have the effect of increasing the lateral stiffness of the composite beams as discussed in section 7.6.1.

7.7 Extension of Model

Many more extensions can be made to the model. Each one improves the accuracy of the model but at the same time makes it more complicated. This section explains how a number of effects can be incorporated into the model, but does not give an in-depth analysis of the effects.

7.7.1 Beam Yielding

So far, the model has been used to calculate the restraint applied to a column at ambient temperature, and the restraining structure has been assumed to behave elastically. It is certainly realistic to assume that surrounding structure will remain around ambient temperature, since a fire on the ground floor will not heat beams on higher floors of a structure to any noticeable degree. Most of the heat conducted to surrounding structure will be dissipated by further conduction and cooling through convection.

It is also realistic to assume that beams will behave elastically, at least until they are highly strained. At first the supporting beams are pushed upwards as the heated column expands, and their bending stress increases until they start to yield. Assuming similar section types and spans, and ignoring column flexibility, the beams above a heated column would all yield at the same time, giving a limit to the possible restraint force. If column flexibility is taken into account, the beams just above the heated column take a larger share of the thermal strain and so yield first. Yielding progresses up the building until plastic hinges have formed in every beam.

However, a heated column at high load ratio will be able to support much less extra force before yielding. When it is heated, both its Young's modulus and yield strength will be considerably reduced. In this case, beam yielding is unlikely to occur, since the heated column will yield first and prevent any further increase in restraint force. Only in a situation where the heated column is at a low load ratio will the beams yield, since the column will have lost a large proportion of its strength, but may still be stronger than the beams.

As was seen in Chapter 3, beam yielding is also important in the post-failure stage, where the loads of the structure are supported increasingly by the beams above the heated column. In this case, the yield strength of the beams is the limiting factor in determining how much of this load can be redistributed through the beams. An extreme case is the situation where all the loads on a column can be redirected by beams to alternative load paths, once the column is heated. This means that the column can be heated indefinitely, and could effectively be removed, without causing structural failure.

7.7.2 Multiple Bay Fires

The above investigation assumes that only one column is heated. Although compartmentation in a building can sometimes cause this situation to occur, it is more likely that a number of columns will be engulfed in flame during a fire. It should be noted that, for simplicity, a plane frame is used here for discussion, but the columns could have beams framing in from the third dimension. These beams can be treated in the same way as beams in-plane, and incorporated into the model easily. Similarly, when more than two columns are considered, they are pictorially represented as in-line columns but once again, the model can be used to represent columns which are not in-line without added complexity.

The case when two columns are heated will be considered first, as shown in Fig. 103. It is assumed that columns "a" and "b" are of the same section and are heated at the same rate. Columns "c" and "d" are also of identical section. In other words, the structure is symmetric about the line which passes through the midpoints of beams "5" and "6". This ensures that the columns will expand at the same rate.

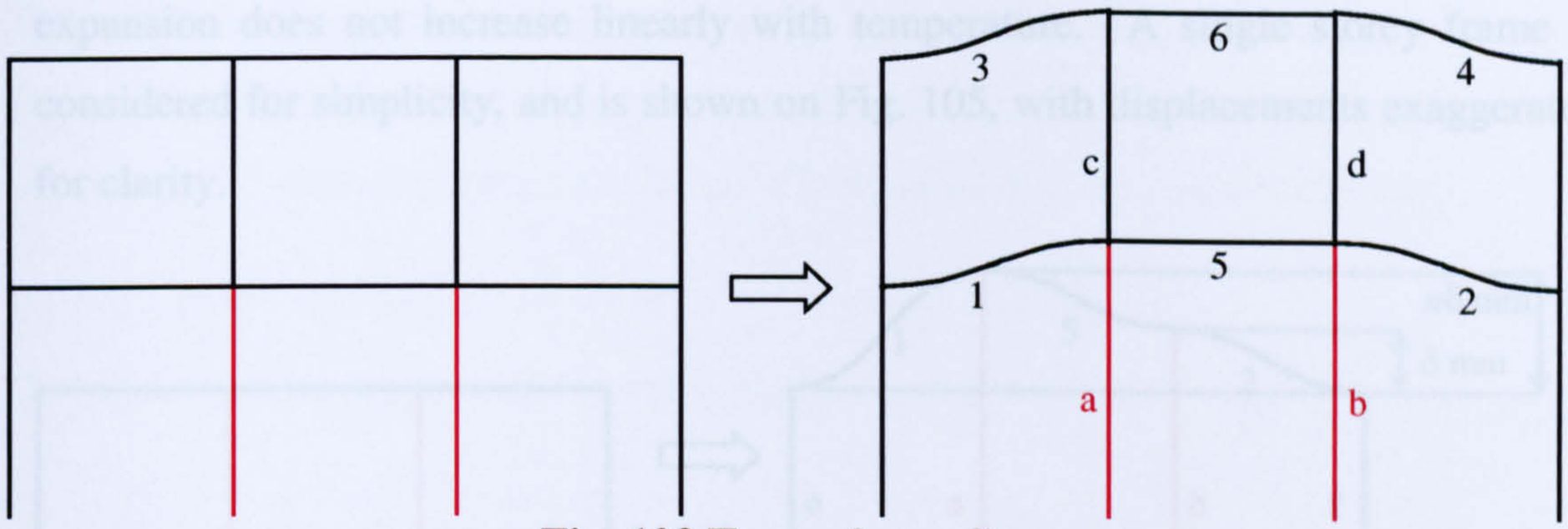

Fig. 103 Two-column fire

It can clearly be seen that beams "5" and "6" in the middle bay do not bend since there is no relative movement between their ends. The only restraint to expansion comes from the beams in the left and right bays numbered 1 to 4. Therefore, the model can be applied to structures of this type by neglecting the stiffnesses of the beams that join two heated columns.

A special case of a multi-floor fire is when an entire floor is heated, as shown in Fig. 104. In this case, the whole of the structure above the fire is pushed upwards as the heated columns expand. There are no cold, unexpanded columns to push against, and as such, the columns are unrestrained. The α factor for such a situation is therefore zero. However, this situation is extremely unlikely to occur, since any natural fire would undoubtedly vary in temperature in different positions throughout the floor. This would lead to different columns having different levels of thermal expansion, and thus introduce restraint as discussed below.

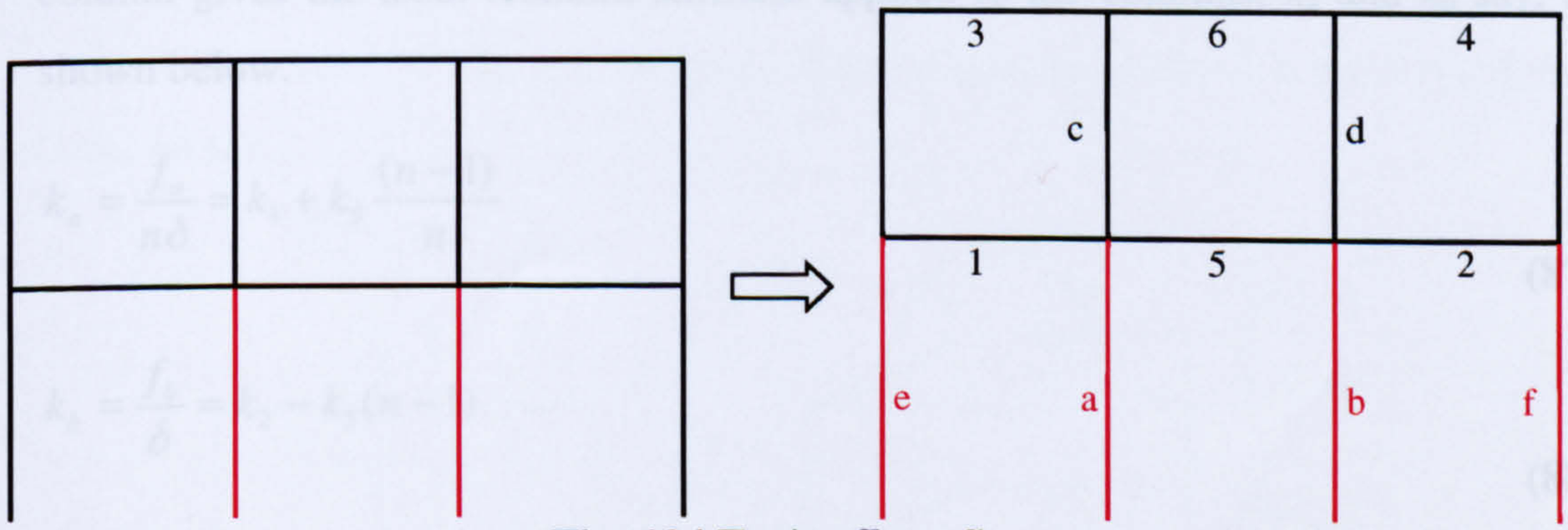

Fig. 104 Entire floor fire

If a frame similar to the one suggested above is considered, the expansion of column "a" can be said to be *n*-times that of the expansion of column "b" for example. It should be noted that this is not the same as column "a" having increased in temperature by *n*-times the amount of column "b", since the coefficient of thermal

expansion does not increase linearly with temperature. A single storey frame is considered for simplicity, and is shown on Fig. 105, with displacements exaggerated for clarity.

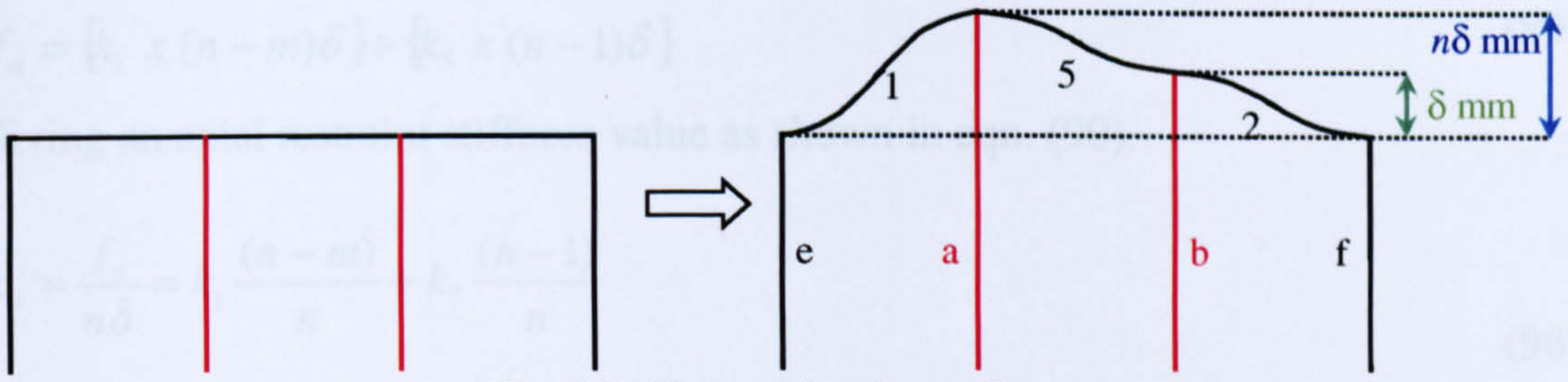

Fig. 105 Unequal column heating

If k_i denotes the stiffness of beam "i", then the increase in the axial force of column "a", f_a say, can be calculated as in eqn. (85).

$$\begin{aligned} f_a &= \{k_1 \ x \text{ Flexure of Beam } 1\} + \{k_5 x \text{ Flexure of Beam } 5\} \\ &= \{k_1 \ x \ n\delta\} + \{k_5 \ x \ (n-1)\delta\} \end{aligned} \tag{85}$$

Similarly, the increase in axial force of column "b" is given by eqn. (86), noting that the force due to beam "5" has the opposite sign to the contribution made by beam "5" to column "a".

$$\begin{aligned} f_b &= \{k_2 \ x \text{ Flexure of Beam } 2\} - \{k_5 x \text{ Flexure of Beam } 5\} \\ &= \{k_2 \ x \ \delta\} - \{k_5 \ x \ (n-1)\delta\} \end{aligned} \tag{86}$$

This increase in axial force divided by the axial displacement of the top of the column gives the axial restraint stiffness applied to the columns, k_a and k_b say, as shown below.

$$k_a = \frac{f_a}{n\delta} = k_1 + k_5 \frac{(n-1)}{n} \tag{87}$$

$$k_b = \frac{f_b}{\delta} = k_2 - k_5(n-1) \tag{88}$$

These two equations can be shown to hold true for the cases already analysed. For example, when the columns expand at equal rates, $n = 1$. Thus eqns. (87) and (88) reduce to $k_a = k_1$ and $k_b = k_2$ respectively, where the stiffness of beam "5" is irrelevant since it undergoes zero flexure, as predicted above.

This method of assessing axial restraint can be extended to give general equations. For example, if column "e" were also heated, and expanded at a rate of *m*-times that of column "b", then the force in column "a" would have to be re-calculated as:

$$f_a = \{k_1 \; x \; (n-m)\delta\} + \{k_5 \; x \; (n-1)\delta\} \tag{89}$$

Giving an axial restraint stiffness value as shown in eqn. (90).

$$k_a = \frac{f_a}{n\delta} = k_1 \frac{(n-m)}{n} + k_5 \frac{(n-1)}{n} \tag{90}$$

Similarly, the stiffness in column "e" could be calculated, as shown in eqn. (91), noting that this expression has only a single term since only one beam frames into the column. As expected, the sign of this stiffness depends upon *n* or *m* is greater, which leads to the column being in either tension or compression.

$$k_e = \frac{f_e}{m\delta} = k_1 \frac{(n-m)}{m} \tag{91}$$

7.7.3 Multiple Floor Fires

There are strict rules[2,52] about maintaining the integrity of fire compartments to stop vertical spread of fire, making multi-floor fires unlikely to occur. Nevertheless, the mathematical model can be extended in a similar way to that which incorporates beam yielding, to study heated columns on more than one floor. Consider a two-storey, two-bay fire as shown in Fig. 106, in which the ground floor column expands by a certain distance, δ say, and the upper floor column expands by a given multiple of this, *n*δ say.

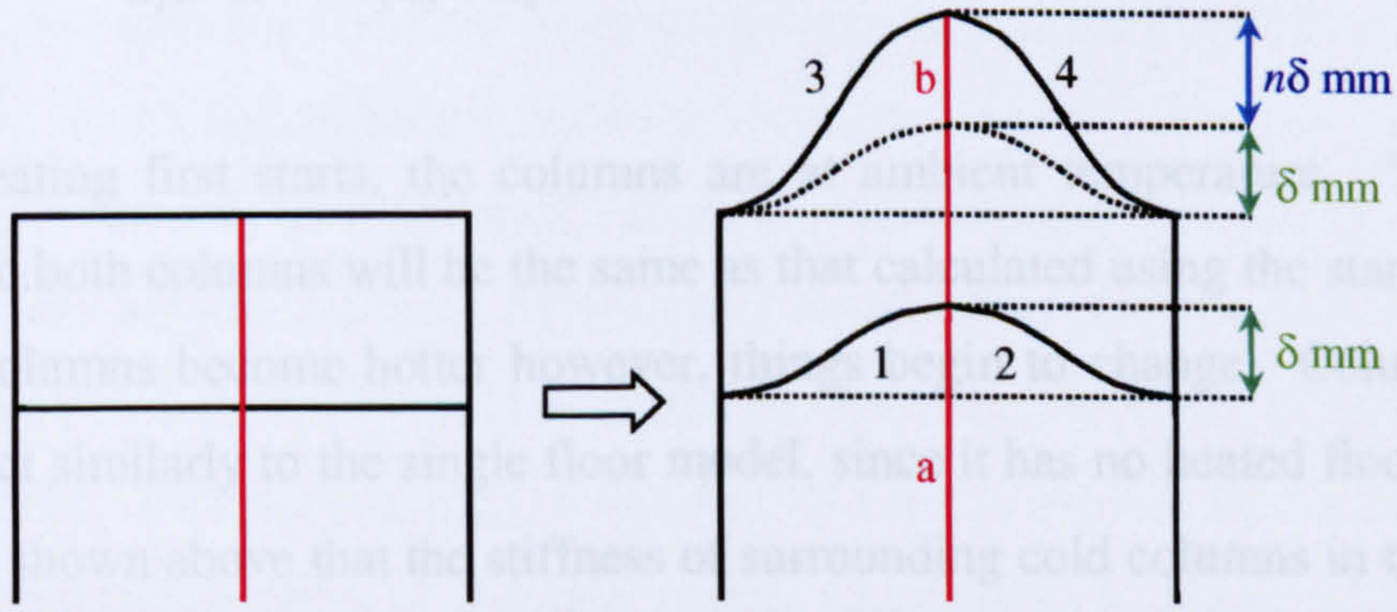

Fig. 106 Two-floor fire

The restraint applied to column "a" can be calculated using the method described above for multiple bay heating, by first calculating the increase in force in column "a" as shown in eqn. (92).

$$f_a = \{k_{floor1}\ x \text{ Flexure of Floor 1}\} + \{k_{floor2} x \text{ Flexure of Floor 2}\}$$

$$= \{(k_1 + k_2)\ x\ \delta\} + \left\{\frac{1}{\frac{1}{k_b} + \frac{1}{k_3 + k_4}}\ x\ (n+1)\delta\right\} \quad \textbf{(92)}$$

Then the axial restraint stiffness is calculated as follows:

$$k_a = \frac{f_a}{\delta} = (k_1 + k_2) + \frac{(n+1)}{\frac{1}{k_c^b} + \frac{1}{k_3 + k_4}} \quad \textbf{(93)}$$

In this case, the stiffness k_c^b of the column above the one being considered will change as its temperature increases. The blue line in Fig. 7 shows a_t, the coefficient in the Ramberg-Osgood Equation which determines how the Young's modulus of steel changes with temperature. The equation used for calculating k_c^b can then be modified, noting that the coefficient a_t is based on a Young's Modulus of 180000N/mm^2. Thus, the restraint stiffness decreases with temperature, which is logical given that the structure above column "a" will soften as it heats up.

$$k_a = (k_1 + k_2) + \frac{1}{\frac{L_t^b}{E_t^b A_t^b} + \frac{1}{(k_3 + k_4)}}$$

$$= (k_1 + k_2) + \frac{1}{\frac{180000 L^b}{a_t E^b A^b} + \frac{1}{(k_3 + k_4)}} \quad \textbf{(94)}$$

When heating first starts, the columns are at ambient temperature. The restraint applied to both columns will be the same as that calculated using the standard model. As the columns become hotter however, things begin to change. Column "b" will always act similarly to the single floor model, since it has no heated floors above. It has been shown above that the stiffness of surrounding cold columns in tension is too great to affect the restraint applied to a column in a typical structure. The cold columns below the heated column have this same stiffness, and as such were neglected in previous models. However in this case, there is a heated column below,

which becomes less stiff as its temperature increases. Therefore, this lower column can squash, and effectively reduces the axial restraint applied to column "b". Equations can be derived for column "b" in a similar way to that above. However, since the floors apply force in series with each other, the equation has a different form, as shown in eqn. (95).

$$f_a = \frac{1}{\frac{1}{k_{floor1}\ x\ \text{Flexure of Floor 1}} + \frac{1}{k_{floor2} x\ \text{Flexure of Floor 2}}}$$

$$= \frac{1}{\frac{1}{(k_c^a + k_1 + k_2)\delta} + \frac{1}{(k_3 + k_4)(n+1)\delta}} \tag{95}$$

The axial restraint stiffness to column "b" can be calculated as before:

$$k_b = \frac{f_b}{n\delta} = \frac{1}{\frac{n}{(k_c^a + k_1 + k_2)} + \frac{n}{(k_3 + k_4)(n+1)}} \tag{96}$$

Where the stiffness k_c^a of the column below is temperature-dependent, and can be derived from the Ramberg-Osgood equations as for k_c^b above.

7.7.4 Conclusions

The purpose of the mathematical model is to provide a method by which the axial restraint applied to a column can be calculated when the column forms part of a multi-storey frame. This then allows the tests performed at Ulster, and the analyses using VULCAN, to be applied to realistic structures. This section shows that as the system becomes more complicated, for example in a multi-storey fire, or as more effects such as beam yielding are taken into account, the model is still applicable. However, the equations become more complicated and there is a limit after which the use of the mathematical model becomes too complicated. Thus, we have the non-linear finite element analysis tool VULCAN to analyse the stiffness of the structure and take into account all these higher-order terms. The mathematical model should be seen as a simple tool to quickly assess the approximate levels of restraint present in a structure. More importantly, it can also be used to explain the mechanics behind the axial restraint process of columns in fire, and leads to a greater understanding of the interactions involved.

8 Numerical Assessment Of The Mathematical Restraint Model

This chapter uses the VULCAN program to validate the previously developed mathematical model. Firstly the Cardington tests are used as a benchmark, and then multiple-floor and multiple-bay fires are investigated.

8.1 Comparison With Cardington Tests

In order to validate further the mathematical model, parallel analyses of the Cardington column tests have been performed using the VULCAN program.

8.1.1 Introduction

The Cardington structure described in Fig. 86 was modelled in VULCAN, using section properties taken from standard section tables for the specified section sizes. A yield strength of 390 kN/mm^2 was used to represent Grade 50 steel and a yield strength of 308 kN/mm^2 for Grade 43 as was indicated by coupon tests on Cardington sections. A Young's modulus of 210kN/mm^2 was assumed throughout. Spring elements were placed on each end of every beam to allow pinned, rigid and semi-rigid connections to be modelled. Where semi-rigid connections are modelled, the rotational stiffness is taken from experiments performed on bare-steel connections at the Building Research Establishment[50,53]. As in the previous chapter, the analyses assume that all steelwork is kept cold except for the specified column, which is heated uniformly on the fire-affected floor. The ambient-temperature axial stiffness is calculated by dividing the increase in the column's axial force (produced by the restraint to thermal expansion) by its axial expansion. For consistency with the previous chapter, the floors are numbered from the top down, and thus a general increase in restraint is expected as we move down from Floor 1 to Floor 8.

8.1.2 External Column Results

The dashed lines on Fig. 107 show the axial restraint stiffnesses indicated by the VULCAN analyses, for various connection stiffnesses, of the external test column. The solid, marked lines show the restraint stiffnesses as calculated by the mathematical model. The actual test result from the Cardington frame is shown for comparison. This is of course, simply a single point, which would only become a

line if the repeat tests on columns at the same grid-point on other storeys had not suffered from experimental problems.

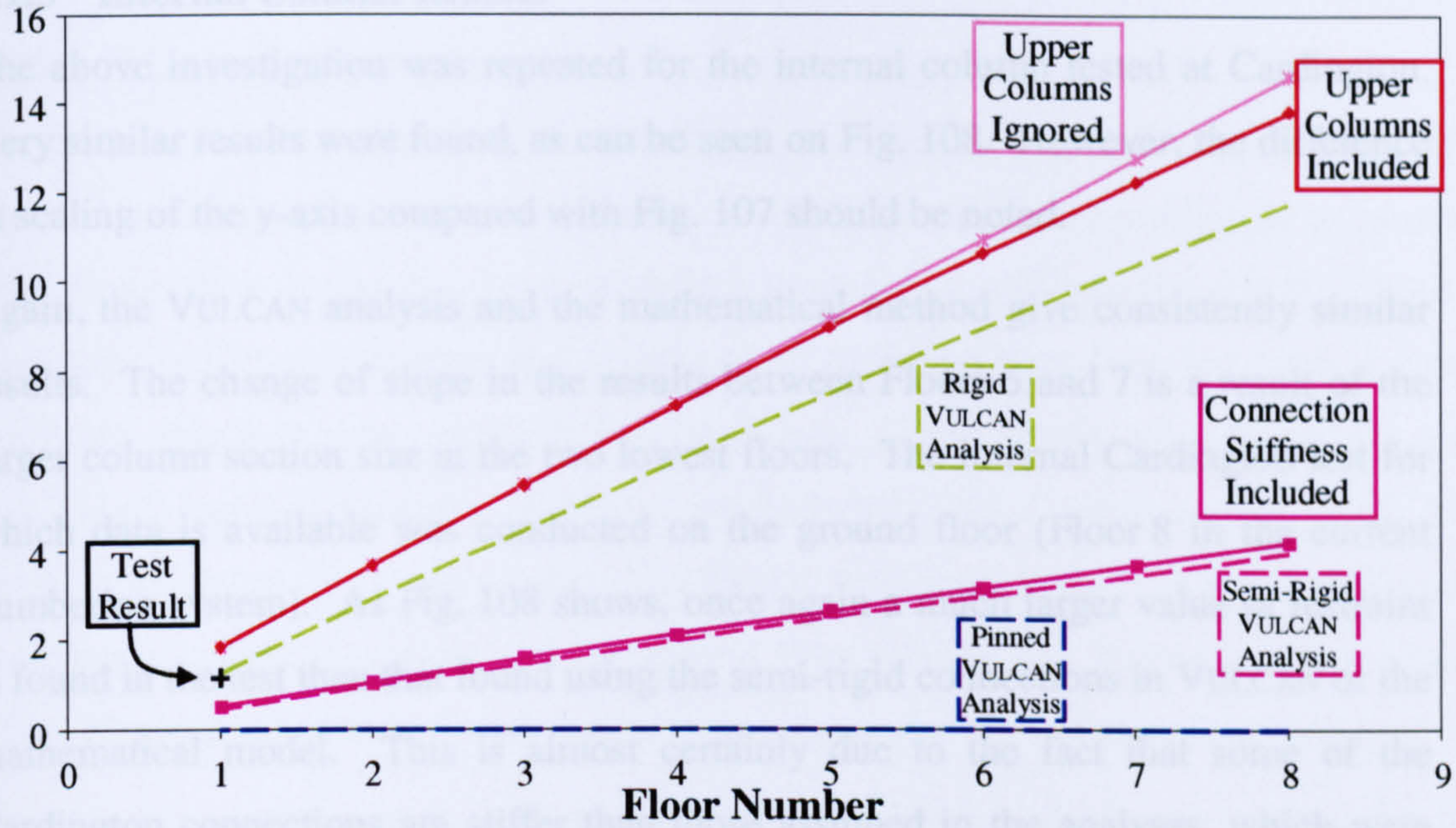

Fig. 107 Axial restraint to external column calculated using mathematical model

The general trend that the level of restraint increases from the upper to the lower storeys of the building can clearly be seen. It is also clear that increasing the beam-to-column connection stiffness directly increases the restraint stiffness.

In addition, we can see the effect on the mathematical model of including the elastic compression stiffness of columns above the test column. The restraint stiffness is progressively relieved as the number of storeys above the test column increases. However, this is a minor effect compared with the inclusion of connection stiffness in the model, which brings the mathematical model results much closer to those found using VULCAN, albeit further from the result found from the Cardington test. However, as discussed in the previous chapter, there is evidence to suggest that the true connection stiffnesses present in the Cardington frame may be higher than assumed here by using results from tests performed on isolated connections. It would be possible to perform a number of analyses and reverse-engineer the calculations to give an indication of the true level of connection stiffness. However, since the beam-to-column connections involve a number of different beam and column section sizes, there would be no way to distribute the newly calculated connection stiffness between the different types of connection. This would make the

exercise of little use, and the resulting values would be based on a single test result of dubious reliability, since it was subject to experimental problems.

8.1.3 Internal Column Results

The above investigation was repeated for the internal column tested at Cardington. Very similar results were found, as can be seen on Fig. 108. However, the difference in scaling of the y-axis compared with Fig. 107 should be noted.

Again, the VULCAN analysis and the mathematical method give consistently similar results. The change of slope in the results between Floors 6 and 7 is a result of the larger column section size at the two lowest floors. The internal Cardington test for which data is available was conducted on the ground floor (Floor 8 in the current numbering system). As Fig. 108 shows, once again a much larger value of restraint is found in the test than that found using the semi-rigid connections in VULCAN or the mathematical model. This is almost certainly due to the fact that some of the Cardington connections are stiffer than those assumed in the analyses, which were derived from experimental data based on tests of isolated connections.

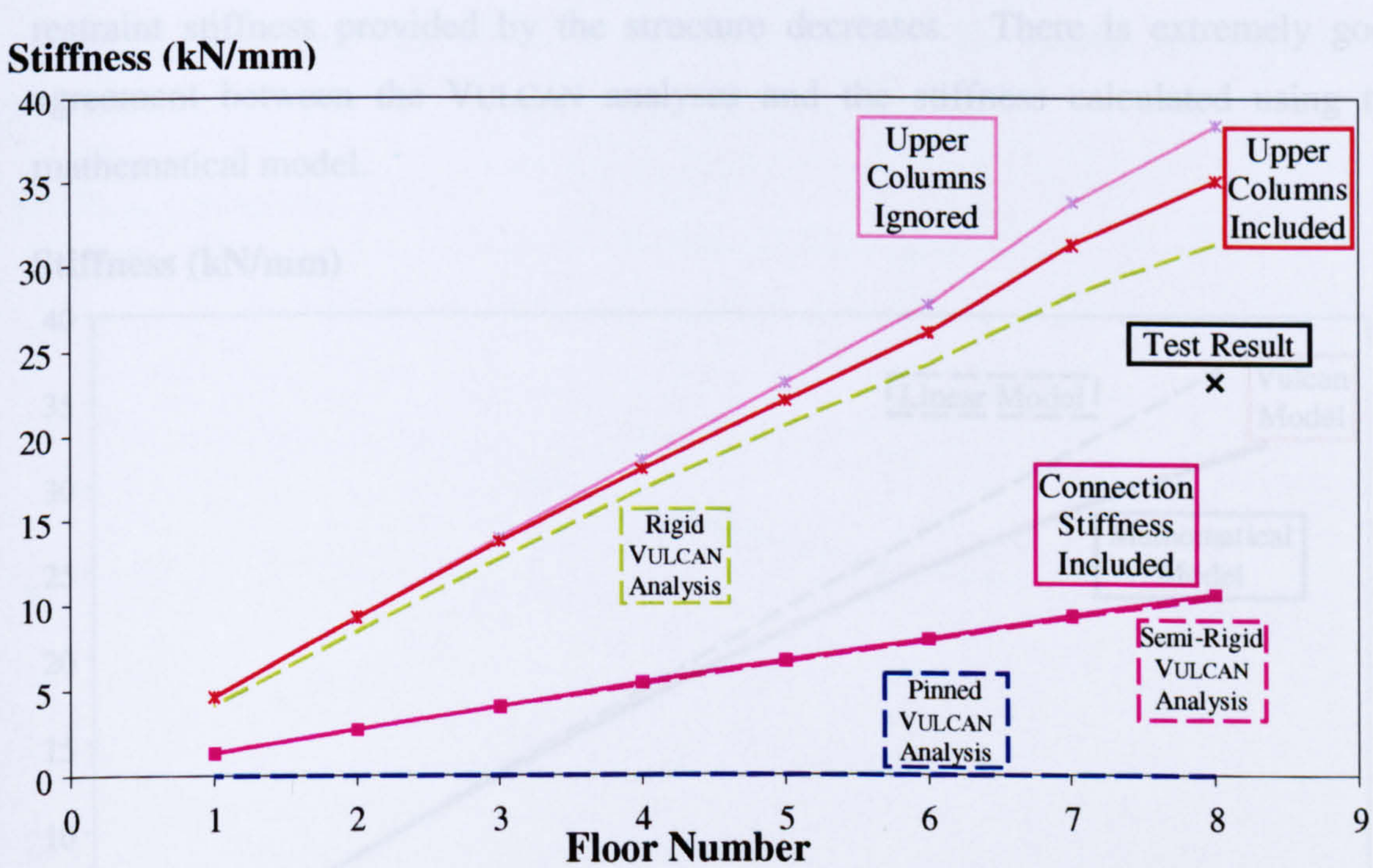

Fig. 108 Axial restraint to internal column calculated using mathematical model

8.2 Single Heated Column

In the previous chapter, a number of suggestions have been made about the behaviour of single heated columns subject to purely elastic restraint stiffness. This

section uses the VULCAN program to provide validation. In order to remove the effects of connections from the investigation, fully rigid connections are assumed throughout.

8.2.1 Effects Of Upper Storeys

In Section 7.3, the effects of the flexibility of columns, within storeys above the heated column, were investigated. A frame similar to that used previously to model the Cardington frame has been modelled in order to validate the effects found. Irregularities in section sizes and lengths of all members have been removed so that only the effects of upper columns will be shown. Consequently, all columns are set as 254x254x89UC sections; all beams are 305x305x118UC sections and Grade 43 steel is used throughout the model. Ten frames were modelled, each with a different number of identical storeys, and the ground floor column was heated in every case. This resulted in a column being heated with various numbers of storeys above it.

As Fig. 109 shows, exactly the same behaviour occurs as was shown in Figure 7.4. As more storeys are added to the structure, the contribution of each to the overall restraint stiffness provided by the structure decreases. There is extremely good agreement between the VULCAN analyses and the stiffness calculated using the mathematical model.

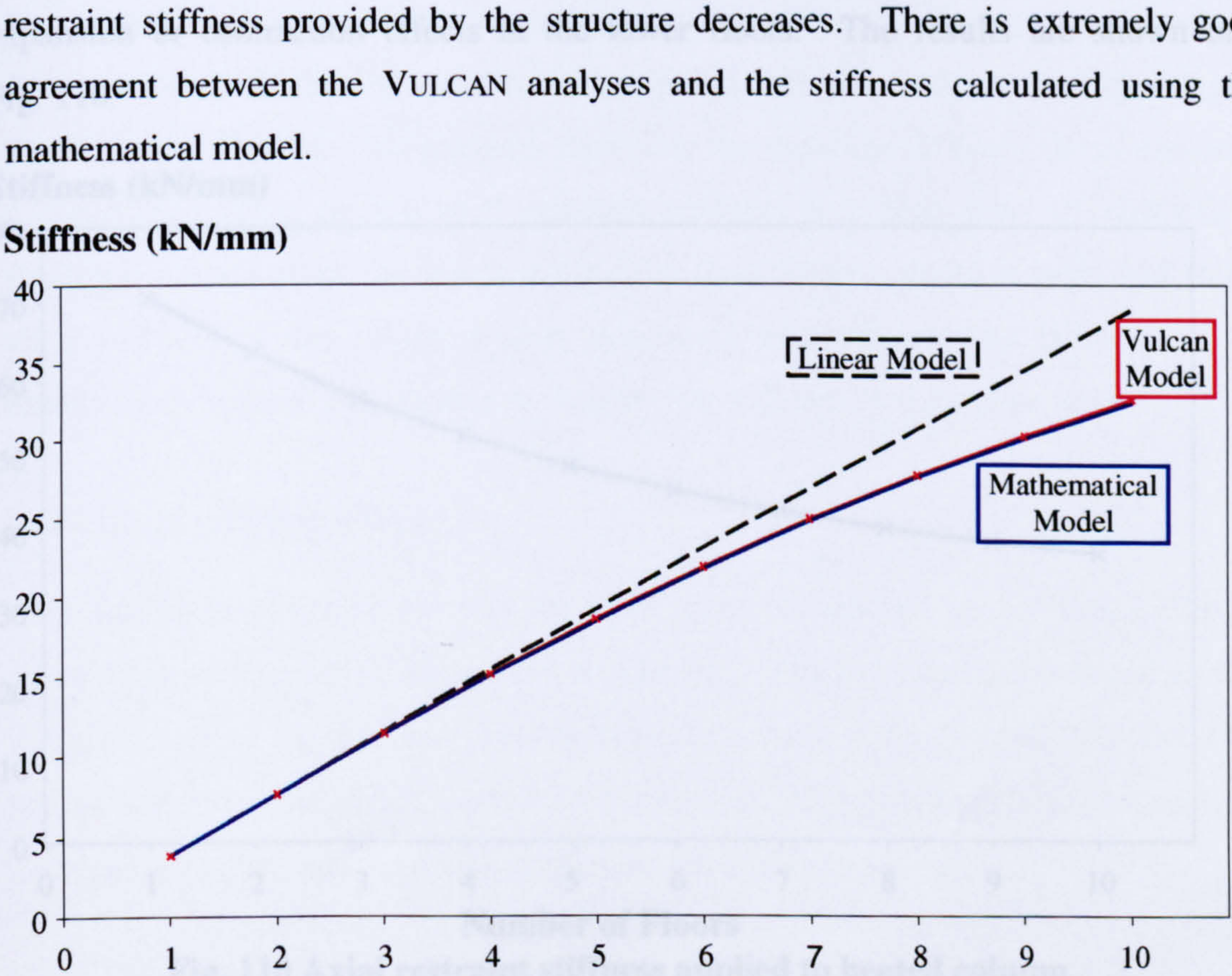

Fig. 109 Axial restraint as more floors are added

8.2.2 Effects Of Lower Storeys

Until now, the effect of lower storeys has been neglected, under the assumption that they will transfer loads directly to the foundations and will not extend or contract in any way. This seems a reasonable assumption in most typical structures, where the roof has no vertical restraint and the foundation provides infinite restraint. The previous section shows that the columns above the heated column can extend or contract, causing a reduction in the restraint provided. There is no reason why the columns below the heated column should not behave similarly. In order to resist the axial force, they are able either to push the rest of the building upwards, or to shorten. A reduction in stiffness is therefore expected, but one of such a small magnitude that neglecting the effect is justifiable.

In order to isolate the effects of lower storeys, a frame identical to that used in the previous section was modelled. However, rather than always heating the ground floor, the top column of a structure with various numbers of floors was heated. Since there are no floors above the heated column, the roof beams were changed to 914x419x388UB sections to increase the applied axial restraint and thus amplify any expansion or contraction effects in the lower floors. The results are shown on Fig. 110.

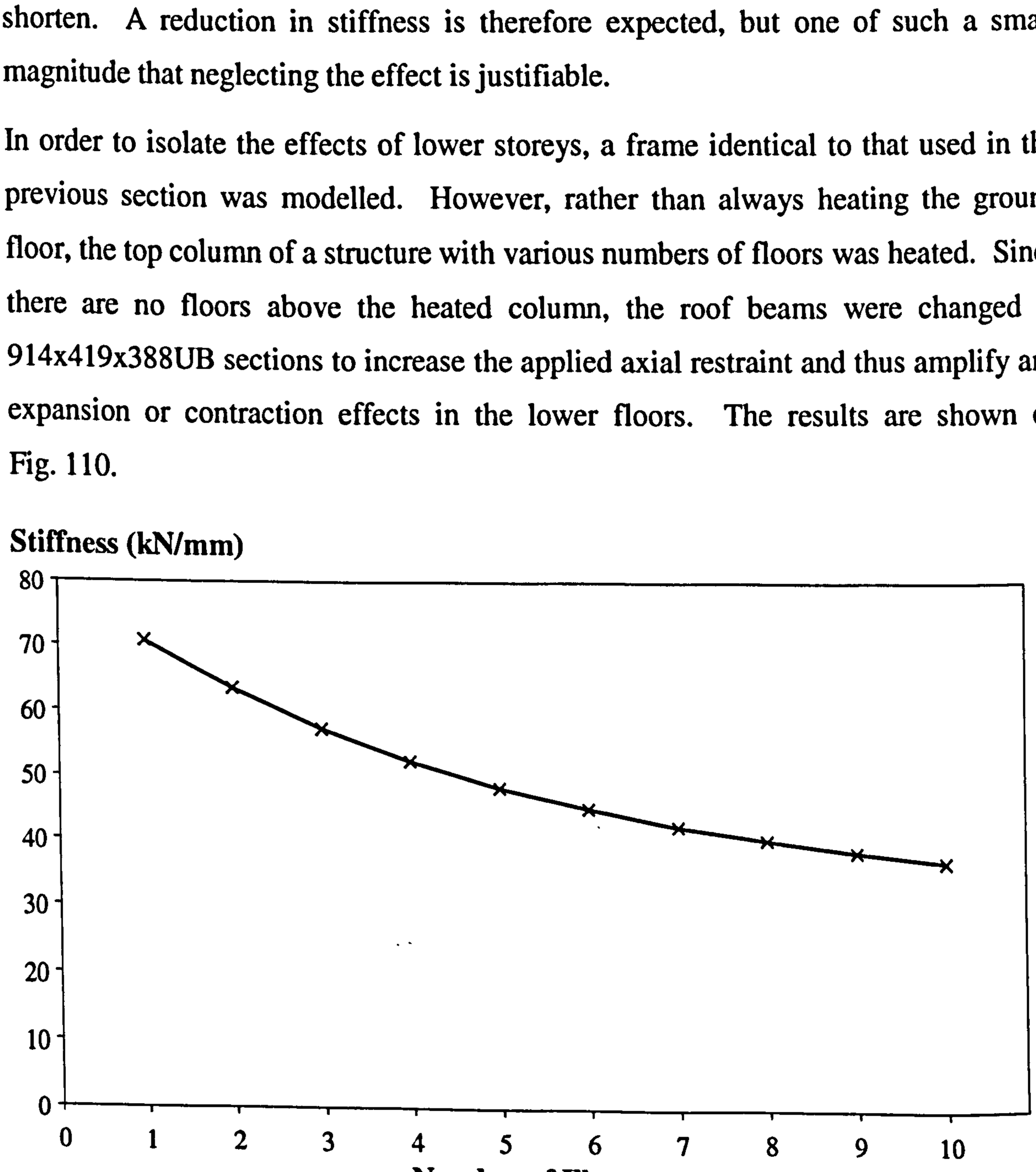

Fig. 110 Axial restraint stiffness applied to heated column

It can be seen from the single-storey case that the roof beams apply an axial restraint of 71kN/mm to the heated column, the bottom of which is fixed in position as it

represents the connection to the foundation. The column that forms the top of a two-storey structure experiences an axial restraint stiffness of 63kN/mm. The only difference between this and the single-storey set-up is that the bottom of the heated column can move downwards by contracting the column underneath. With the addition of further floors below the heated column, the applied axial restraint decreases since the flexibilites for a longer series of columns are being added together. However, each additional column makes less difference, in much the same way that adding columns above the heated column eventually converges on a behaviour where adding further columns makes negligible difference.

8.2.3 Conclusions

The VULCAN investigation into the effect of upper storeys on the axial restraint applied to heated columns follows extremely closely the results obtained using the mathematical model. This shows that the assumptions made in the mathematical model are sensible and take into account the dominant parameters influencing the behaviour.

The presence of lower floors is analogous to the presence of upper floors and the effects of their flexibility could be incorporated into the mathematical model in a similar way. The VULCAN analyses show that the presence of lower floors can have a significant effect on the axial restraint stiffness if a high level of stiffness is provided by the beams. In this case the axial force in the column is high, and so the axial stiffness of the column below, combined with the bending stiffness of the beams below, can be comparable to the bending stiffness of the beams above.

8.3 Multiple-Bay Fires

This section investigates the way the axial restraint imposed on a column changes when other surrounding columns are also heated. The investigation is based around the behaviour of the structure used in Chapter 3, with 305x164x54UB sections for beams and 254x254x167UC sections for columns. All beam-to-column connections are rigid, and UDL and superstructure loads are as shown in Fig. 111.

8.3.1 Single Column

For the basic comparison, the heating of the single, internal column labelled A in Fig. 111 was modelled using VULCAN. The displacement of the top of the lower element of the heated column has been recorded and is shown in light blue, related to the secondary axis of Fig. 112. Also shown, in dark blue, and related to on the primary axis, is the internal force in the column. Since they are plotted on separately scaled axes, these two curves lie on top of each other, showing that the column stiffness remains constant throughout the analysis. Any change in the displacement results in an exactly similar change in axial force. The change in force can be divided by a corresponding change in displacement to give the stiffness applied to the column and this is found to be 30kN/mm.

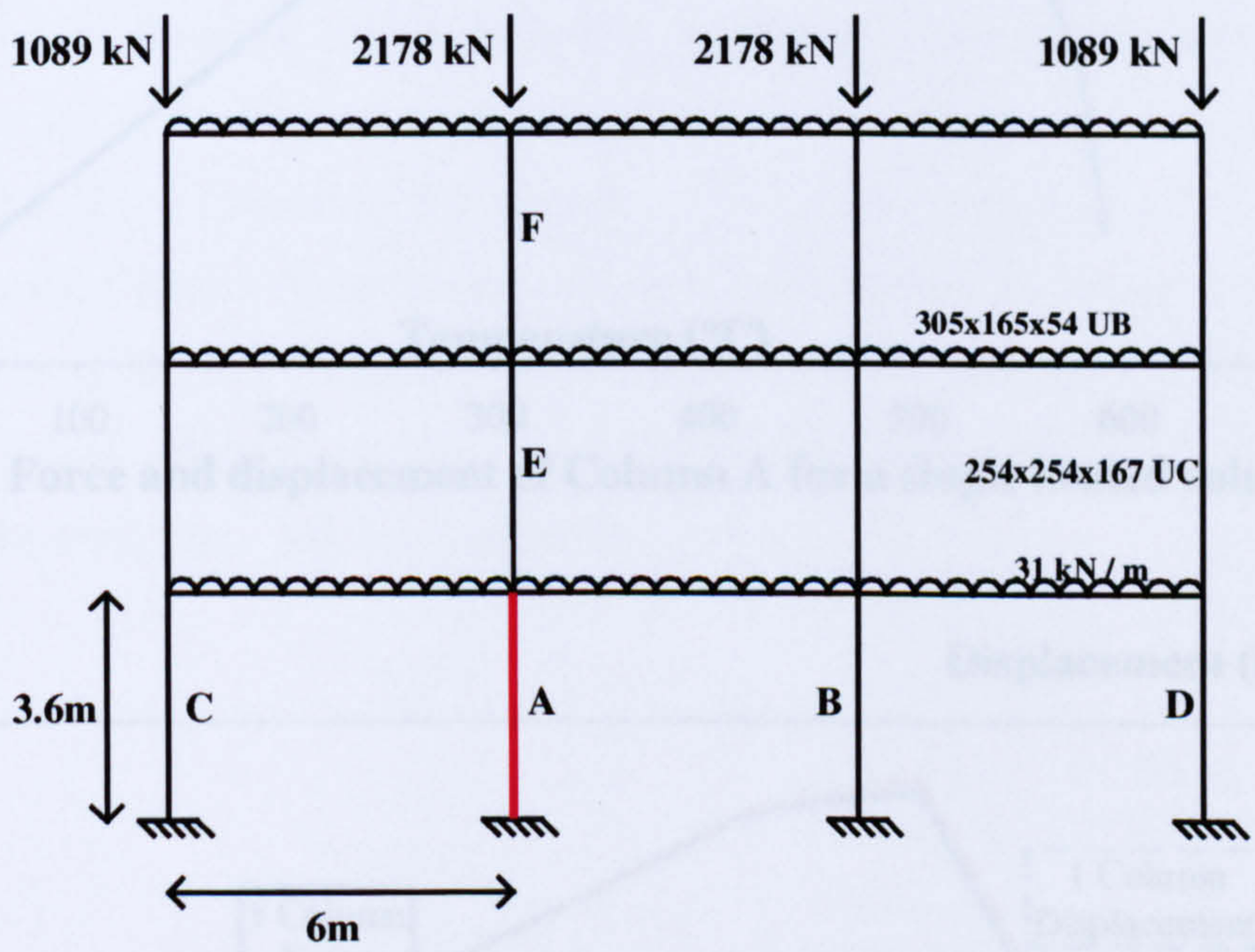

Fig. 111 Structure used for investigation

8.3.2 Two Columns Heated

The same structure was modelled with both internal columns (A & B) heated at the same rate. The results are shown in red on Fig. 113, with the single heated column results shown in blue for comparison. It can clearly be seen that the axial displacement behaviour of the columns changes little, since this is largely due to thermal expansion, which is the same in either case. However, the axial force in each column increases less when two columns are heated. The increase in axial force is due largely to the lateral bending stiffness of the beams that frame in to the column top. As discussed in the previous chapter, when two adjacent columns are heated, the beam connecting the heated columns, both directly and in upper storeys,

contribute little restraint stiffness to the heated columns, since their ends are being pushed upwards at equal rates. Using the results as before a restraint stiffness of 14kN/mm applied to each column can be calculated. It should be noted that due to symmetry the restraint applied to each column is equal.

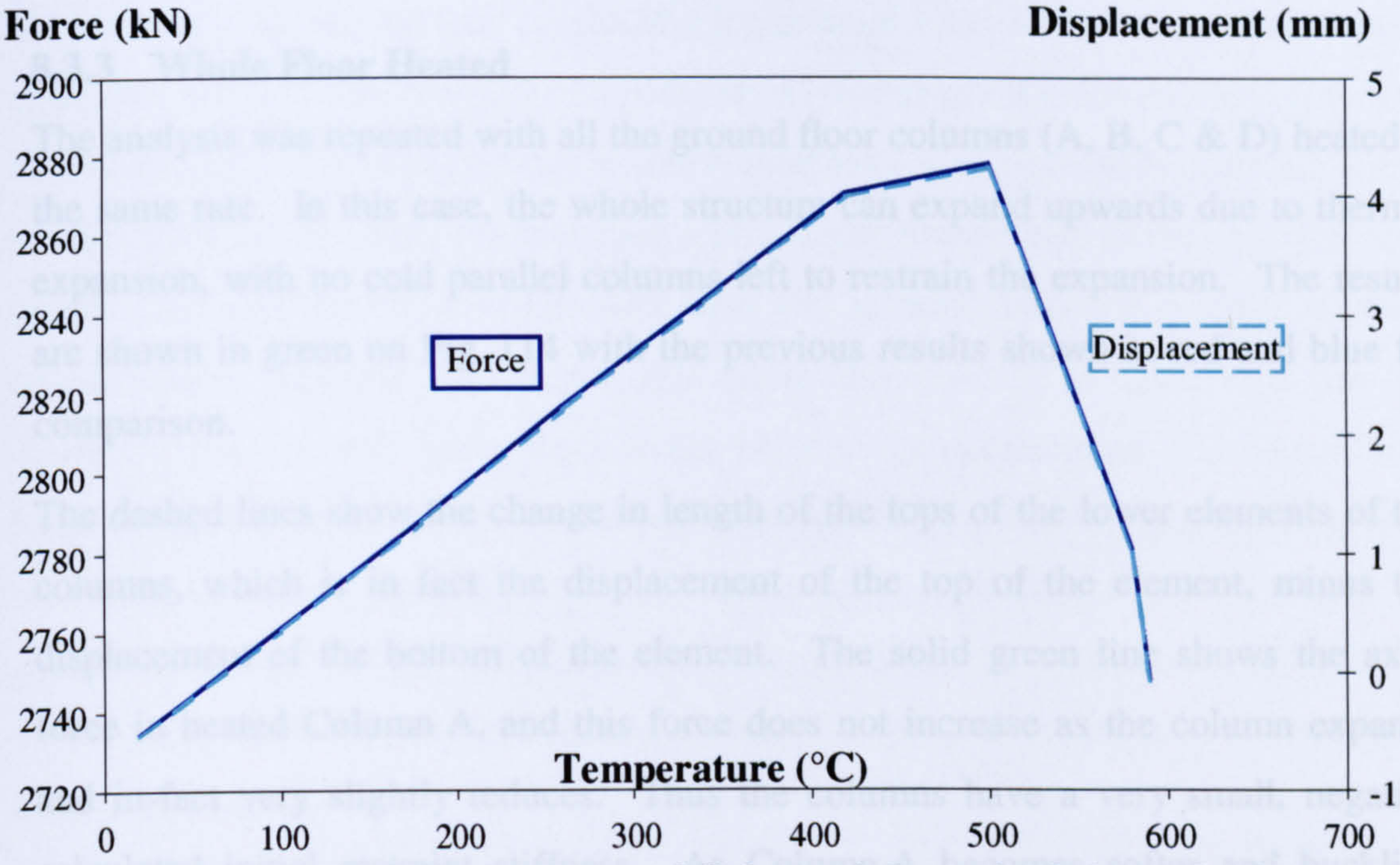

Fig. 112 Force and displacement of Column A for a single heated column

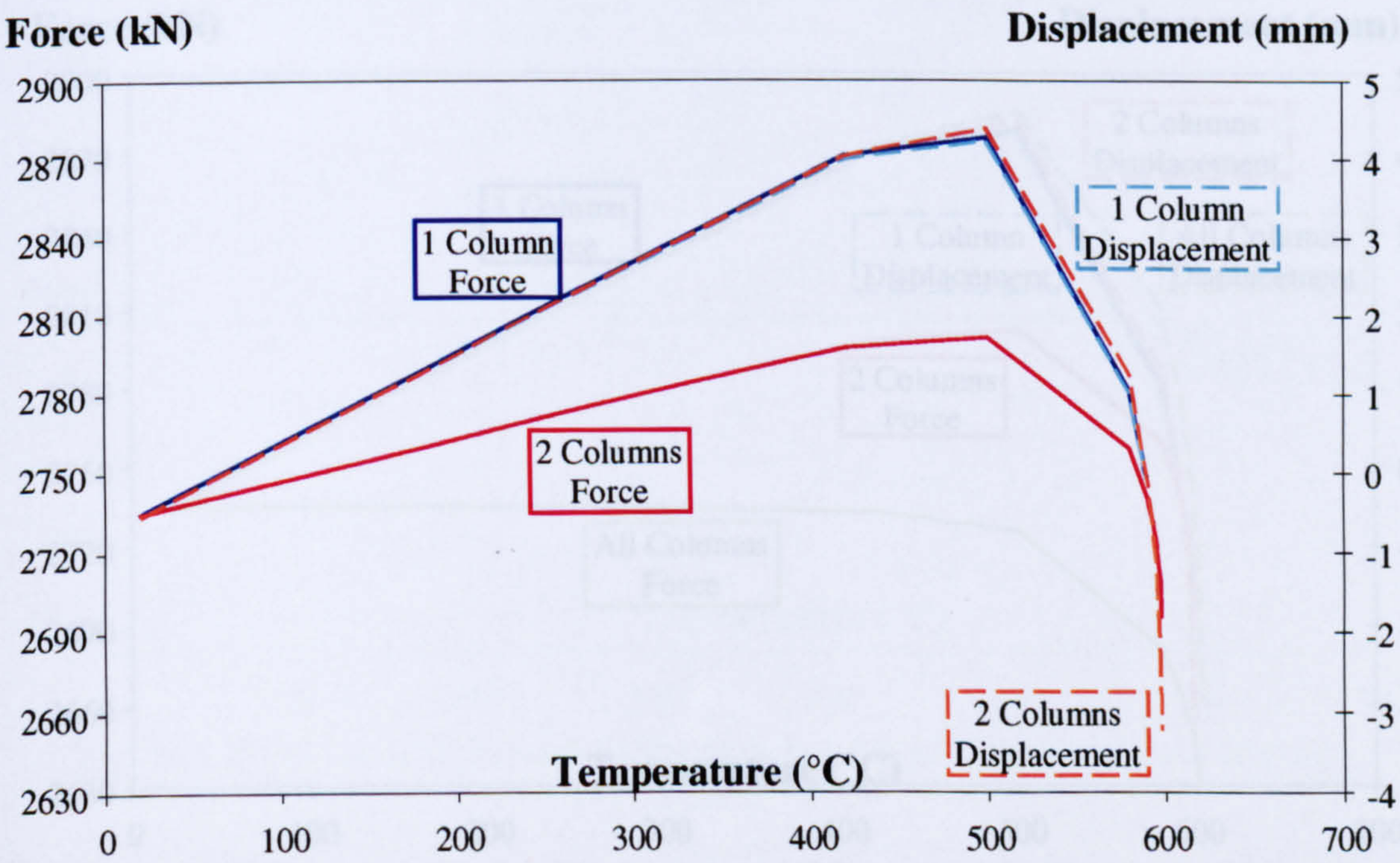

Fig. 113 Force and axial displacement of frame with two heated columns

After the column has contracted below its original length, its axial force reduces below the level of force initially supported. This is possible, since the load is then carried by the cold columns at either edge of the structure. In essence, an alternative load-path is used to carry the load away from the heated columns.

8.3.3 Whole Floor Heated

The analysis was repeated with all the ground floor columns (A, B, C & D) heated at the same rate. In this case, the whole structure can expand upwards due to thermal expansion, with no cold parallel columns left to restrain the expansion. The results are shown in green on Fig. 114 with the previous results shown in red and blue for comparison.

The dashed lines show the change in length of the tops of the lower elements of the columns, which is in fact the displacement of the top of the element, minus the displacement of the bottom of the element. The solid green line shows the axial force in heated Column A, and this force does not increase as the column expands and in-fact very slightly reduces. Thus the columns have a very small, negative calculated initial restraint stiffness. As Column A becomes softer and buckling develops, the axial force reduces further.

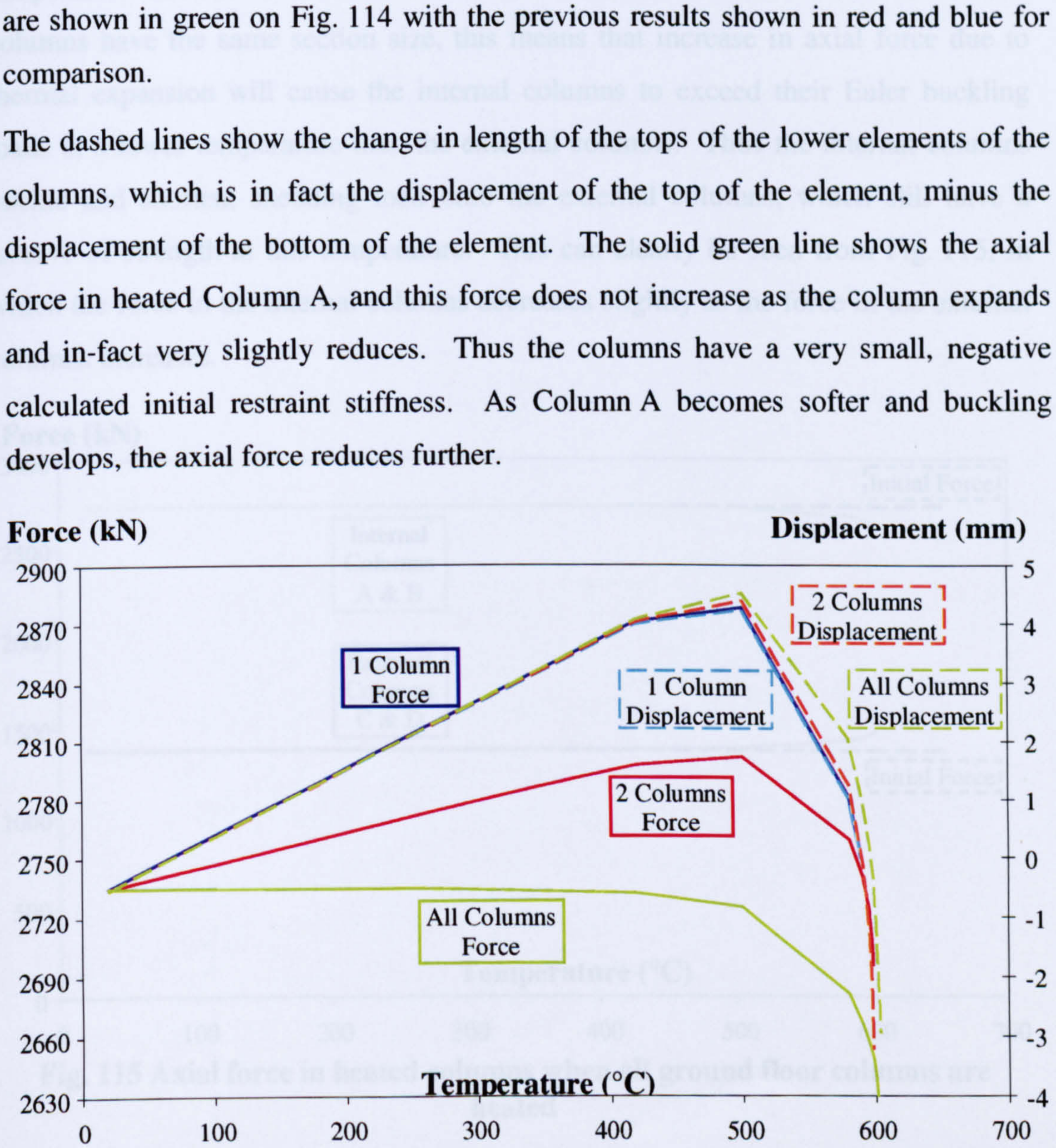

Fig. 114 Force and axial displacement of frame with all columns heated

This seems surprising, since all columns are heated so there should not be an alternative load path along which to carry the loads. However, this can be explained by plotting the axial force in all ground floor columns as shown in Fig. 115.

Although the external columns are heated at the same rate as the internal columns, the uniformly distributed load results in a lower axial force in the external columns, since they support only one half of a beam span. The internal columns support twice this beam length and so have twice as much axial load as the external columns. They are therefore considerably further along a non-linear stress-strain curve at any given temperature and therefore strain more than the external columns. Since all the columns have the same section size, this means that increase in axial force due to thermal expansion will cause the internal columns to exceed their Euler buckling loads at a lower temperature than the external columns. Thus the internal columns buckle and shorten, shedding load onto the external columns, which still have a reserve of strength at this temperature. This can clearly be seen from Fig. 115, in which the force in the internal columns decreases slightly as the force in the external columns increases.

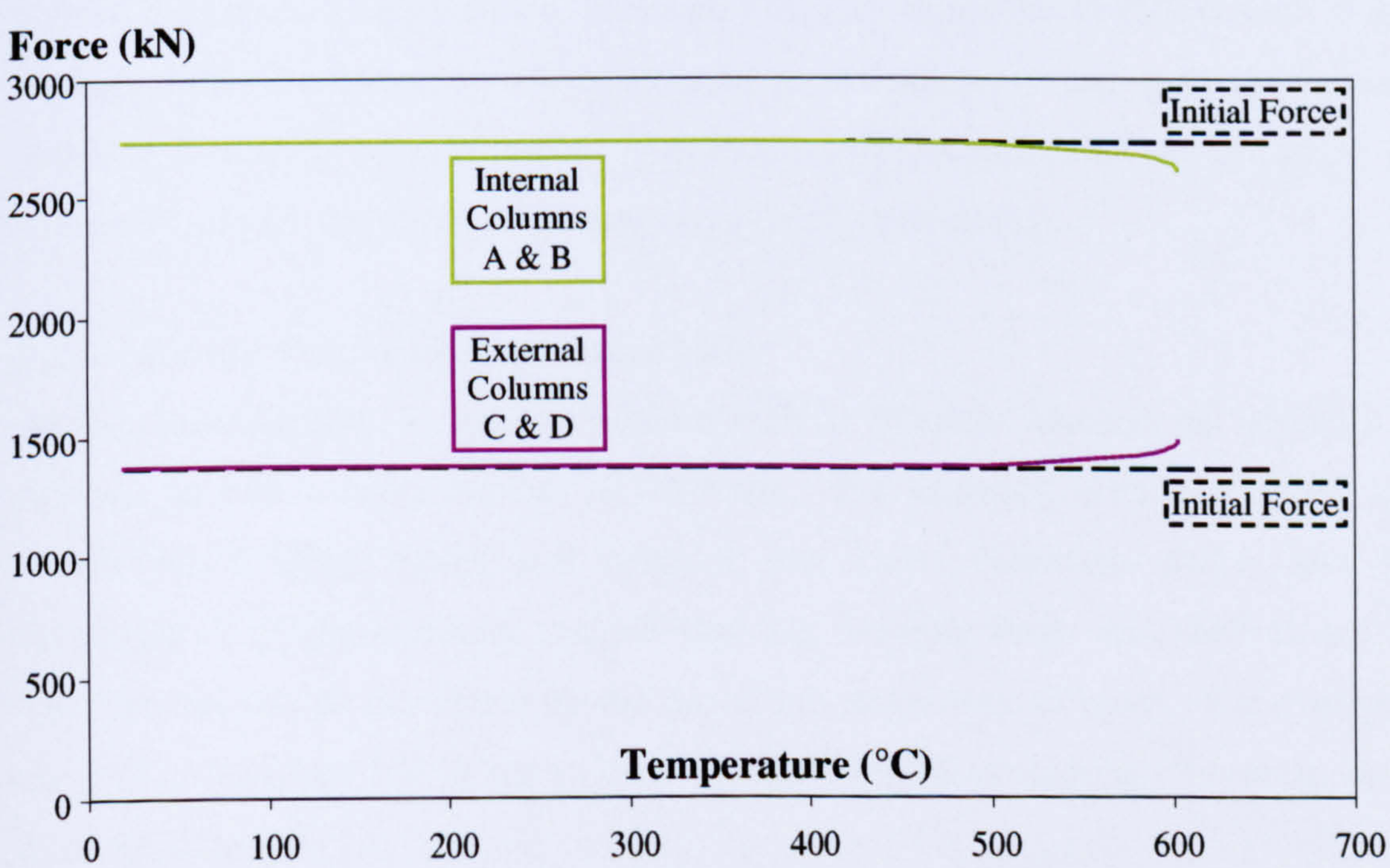

Fig. 115 Axial force in heated columns when all ground floor columns are heated

8.3.4 Conclusions

The assumption of all columns being heated at exactly the same rate is rather simplistic. However, under these circumstances, the results using VULCAN behave as

predicted by the mathematical model. In terms of the temperature at which initial buckling takes place it could actually be beneficial to have two columns engulfed in fire rather than just one. Each would have an increased axial force due to the lateral restraint from one beam per storey, rather than the higher force experienced by a single column being restrained by two beams per storey.

This is of course not ultimately beneficial when the Euler buckling load has been surpassed and the heated columns become shorter than their original length. Under these circumstances, the load has to be shed to columns outside the fire compartment, and twice as much load has to be shed if two columns have "failed".

9 Solution Procedures

This chapter describes an investigation into the way the solution procedures of the finite element method are used to find the displacements of a multi-degree-of-freedom problem resulting from the effects of a set of imposed loads.

9.1 General Introduction

As seen in Chapter 3, steel columns, especially when modelled as part of a larger frame, can exhibit a "snap-through" behaviour. This occurs when part of a structure becomes unstable and the frame's deflections suddenly snap from one stable set of equilibrium solutions to another, via a path which at least in part represents unstable equilibrium. The numerical stability of the solution procedure (as distinct from the structural stability of the equilibrium paths being investigated) can be highly influential on whether the analysis can follow this kind of behaviour. If this is not the case, then a set of stable solutions can be missed and the structure can be said to have "failed" when this is not actually the case. VULCAN currently uses the Newton-Raphson solution method which, although efficient, is unable to follow such snap-through behaviour properly. A number of modifications to the general Newton-Raphson formulation can be made[54,55] to rectify this. A study into the suitability of these methods for the VULCAN program was clearly desirable.

9.1.1 Linear Ambient Temperature Case

As the name suggests, in order to perform a Finite Element Analysis the structure is divided up into a finite number of elements. For example, within VULCAN this means sub-dividing beams and columns into beam elements, which may be connected by spring elements, and sub-dividing concrete floors into shell elements. This process can be automated by the use of pre-processing software. For example, the INSTAF Interface can be used along with the MAKEDAT translator to create input files for VULCAN.

The general process[56] for determining the deflection of the structure can be described in six steps as follows:

1. The properties of each element are compiled to give its relationship between nodal loads and nodal displacements. This is the elemental stiffness at each

node with respect to the nodal degrees of freedom (d.o.f.). Each element has a "shape function" to determine how deflections represented by the degrees of freedom change between nodes. This is used to assemble an Elemental Stiffness Matrix K_{elem} for each element in the structure.

2. Each elemental stiffness matrix is assembled into the global stiffness matrix K, into which are added the contributions to the nodal stiffness of every element present at each node. This square matrix has as many rows and columns as there are degrees of freedom in the problem, therefore representing as many linear equations as there are possibilities for load components.

3. The applied load components are incorporated into a load vector p.

4. The boundary conditions are imposed by setting the appropriate degrees of freedom to zero leaving a reduced stiffness matrix K_{red}. The number of boundary conditions imposed should be more than the number of linearly independent equations represented by K, so that the reduced matrix K_{red} is non-singular.

5. The simultaneous equations represented by $\mathbf{p} = K_{red}\,\mathbf{d}$ (where d is the vector of displacements for each d.o.f.) is solved for **d**.

6. Further calculations can be performed on these displacements, for example to determine the strains, and therefore stresses present within the structure.

Some kind of post-processing software is usually used to analyse the output, either as a pictorial representation of the deflected shape (for example using SHOWGRID) or as mathematical graphs of the deflections (for example using DATAMOD).

Consider an extremely simple problem of a vertically hanging cable with an axial force imposing tension at one end. Since it is a linear problem, the cable could be represented by a single element with a node at either end. Step 1 of the solution algorithm would simply determine the stiffness (i.e. Young's Modulus) of the material then form this value into a matrix. Step 2 is trivial in this case since there is only one element present. Step 3 formulates the applied load at the end node into a load matrix and Step 4 takes into account the fact that the upper node is fixed in position. Step 5 then uses the stiffness and applied force to determine the displacement of the lower end and Step 6 can be used to turn this displacement into an internal stress or force.

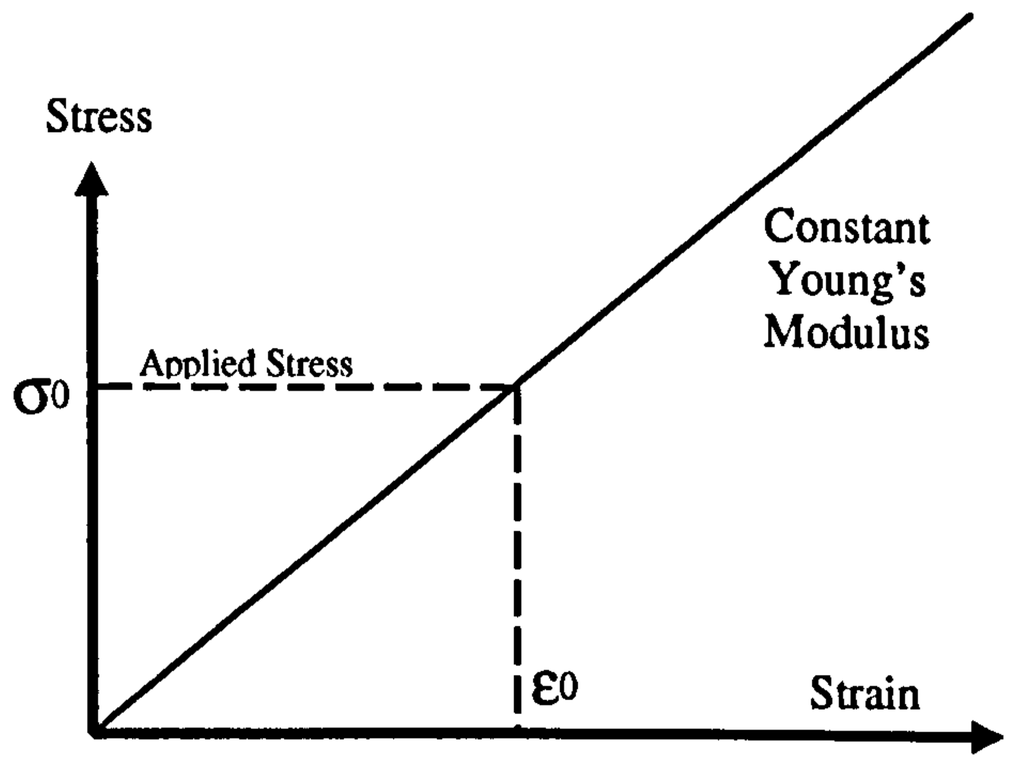

Fig. 116 Stress-strain curve for a linear material

As Fig. 116 shows, in a linear system, the stress σ_0 determined by the strain ε_0, will be equal to the externally applied stress.

9.1.2 Non-linear Ambient Temperature Case

Finite element analysis would not normally be used to solve a linear problem like the one described above since a more direct analysis is simpler to perform and yields the same results. The finite element method is, however, ideal for solving non-linear problems. In the context of VULCAN, the term non-linear refers to both geometric and material non-linearity. The former is caused by large changes of geometry and the latter by the curvilinear relationship between stress and strain in high-temperature steel and concrete.

If the above simple example were re-analysed using a non-linear material, the finite element process could be used in a similar way. In this case, the initial stiffness of the cable would be used in forming the stiffness matrix. The solution from Step 6 for the strain ε_1 would be the applied stress σ divided by the Young's modulus. However, applying this value of strain to the actual stress-strain curve, the solution for the stresses from Step 6 would actually be σ_1 as shown in Fig. 117.

The difference between σ and σ_1 is known as the "out-of-balance force" (o.b.f.). Several, well established procedures have been developed in order to find an acceptable approximation to the correct nodal strains for a given applied stress. Most of these involve going from Step 6 where the o.b.f. is determined back to Step 2 and re-forming the stiffness matrix using updated values for the tangent stiffness of each element at this new level of strain. Each loop from Steps 2 to 6 is known as an

iteration. These iterations are repeated until the o.b.f. is reduced below a tolerance limit. In addition, the load may be applied in several steps, with the stiffness being re-evaluated at each stage. This can also increase the stability of the final solution. However, each of these kinds of iteration takes time to compute, and so it can be important to choose the appropriate method to solve a particular problem.

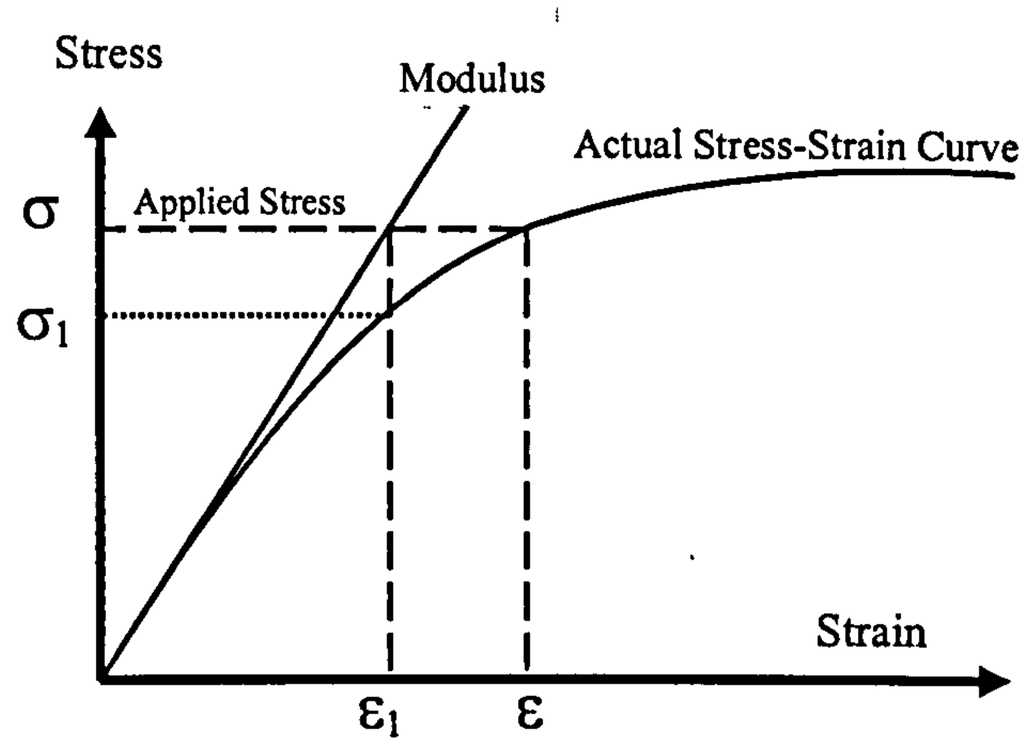

Fig. 117 Stress-strain curve for a simple tension member of non-linear material

9.1.3 Non-linear Elevated Temperature Case

One of the main features of VULCAN is that it is a non-linear F.E.A. program capable of analysis at elevated temperature. The presence of the extra temperature variable in the calculations adds another aspect of non-linearity to the problem. Once the above algorithm has been used to converge on an ambient-temperature solution for the structure, the whole process is repeated at another (usually higher) temperature. At this higher temperature, the stress-strain curve changes shape to reflect the change in material properties. The yield stress and Young's modulus become lower in a non-linear fashion, as has been shown in Chapter 2. Although a more complex method could be applied, the current implementation of VULCAN increases the temperature in pre-set steps, performing a non-linear analysis at each stage. If a solution is not found at a specific temperature, the temperature step size is bisected and the process attempts to continue. It is often possible for this method to manage progressive increase in temperature until the material stress-strain curve becomes ill-defined. For instance, the highly restrained columns of Fig. 25 are analysed up to the melting temperature of steel. However, the analysis may come across a point where the behaviour of the structure changes rapidly and the solution procedure cannot converge on a solution past a certain temperature, as is the case with the columns with low-restraint in Fig. 25.

9.2 Description Of Iteration Schemes

This section introduces a number of iteration schemes commonly used in non-linear finite element analysis. The remainder of this chapter looks at the advantages and disadvantages of these schemes for performing iterations at a single temperature step to converge on a solution. Their suitability to the VULCAN program is also discussed.

9.2.1 Simple Incremental Method

As its name suggests, the simple incremental method is the most basic of the non-linear solution procedures, since it involves no iterations. If the solution algorithm were followed, as in Steps 1-6 above, the calculated solution for the strain ε_0 would be some way from the true solution ε, as shown in Fig. 117. The simple incremental method applies the load as a large number of small but equal increments, and performs Steps 1-6 at each stage. In this way, the elemental stiffness is re-evaluated a number of times, leading to a reasonably accurate approximation to the actual stress-strain curve of the material, but allowing a progressive divergence from the true solution.

An example of a single d.o.f. problem is shown in Fig. 118, where the load is applied in five equal steps, each of which computes a strain increment based on the local tangent stiffness. At the final step, the solution ε_5 is closer to the true solution ε than would have been the case if the load had been applied in a single step, giving ε^* as the solution.

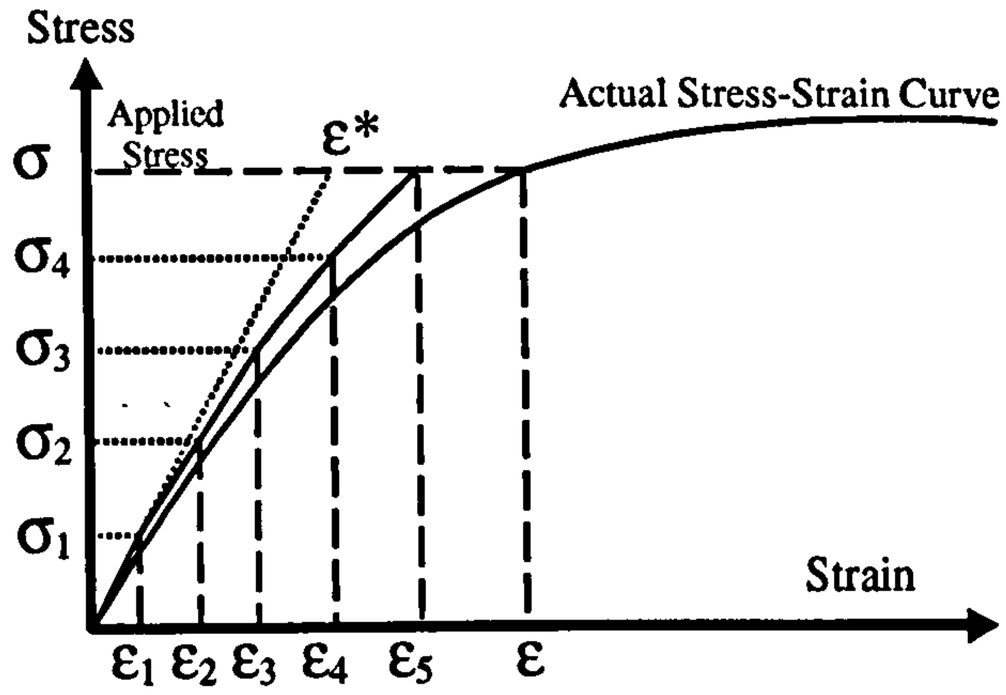

Fig. 118 Simple incremental method

The drawback with this method is that there is a certain level of o.b.f. at each step. This inaccuracy is never corrected, and thus the errors can compound with each step leading to what is known as "drift-off". After many steps, the error can be such that

the method becomes unusable. This drift-off can be minimised by increasing the load in very small steps, so that the o.b.f. is minimal each time. However, this increases the time taken to perform the algorithm to a certain load level, and accuracy is traded off in favour of speed.

9.2.2 Newton-Raphson Method

A variety of iteration schemes have been developed[55] to be performed before further increases in load are applied, in order to ensure that the o.b.f. is minimised at each load step. The Newton-Raphson method is often favoured due to its relative simplicity and high accuracy within a specific set of problem types. This is the solution method currently adopted in the VULCAN program.

As Fig. 119 shows, the applied stress at which we require the strain is indicated by σ. The strain is calculated using Steps 1-6 as above. This results in a strain ε_1 as before, and the o.b.f. is given by $(\sigma - \sigma_1)$. Thus the point with strain ε_1 and stress σ_1 is used as a starting point the next iteration of Steps 1-6 with the tangent stiffness matrix being calculated for this new initial point. This process is repeated until the o.b.f. has been reduced to within a certain pre-set tolerance limit.

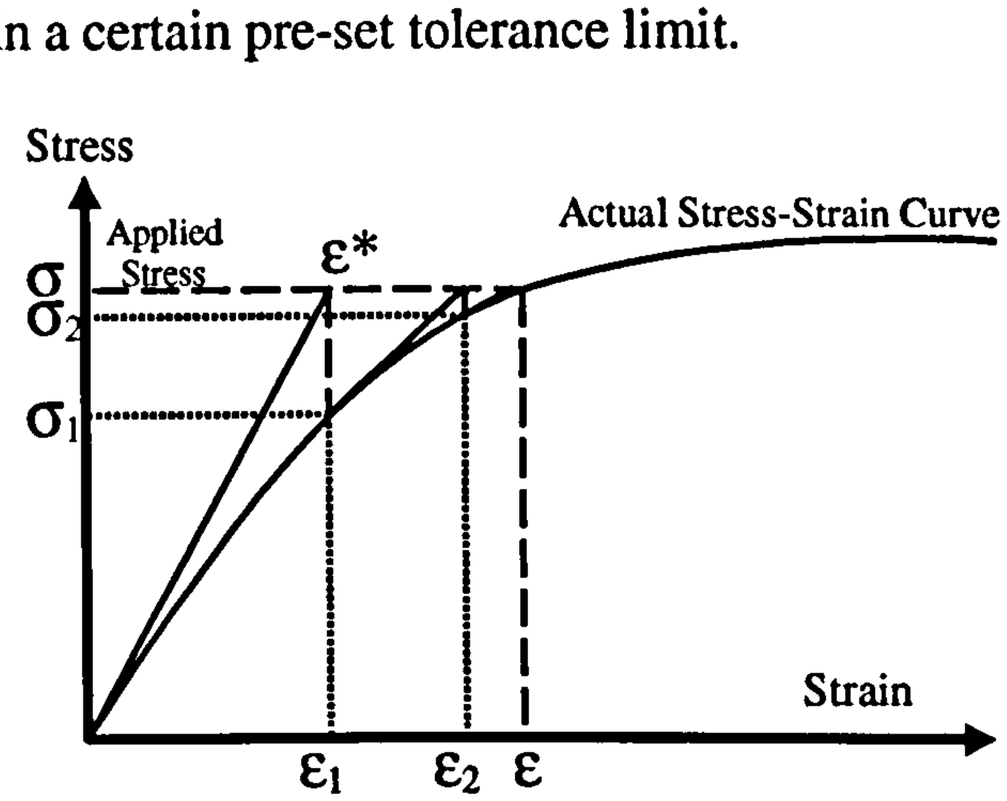

Fig. 119 Newton-Raphson method

The major problem with this method is its instability around areas of zero stiffness (limit-points or run-away) and unloading curves (snap-through). As Fig. 120 shows, since the method is controlled by making steps of load (stress) and calculating the resulting strain, systems with low tangent stiffness result in very large changes in strain for a given change in stress. If the solution process passes from a positive stiffness to a negative stiffness for example, the iteration scheme diverges and a solution cannot be found beyond the limit point.

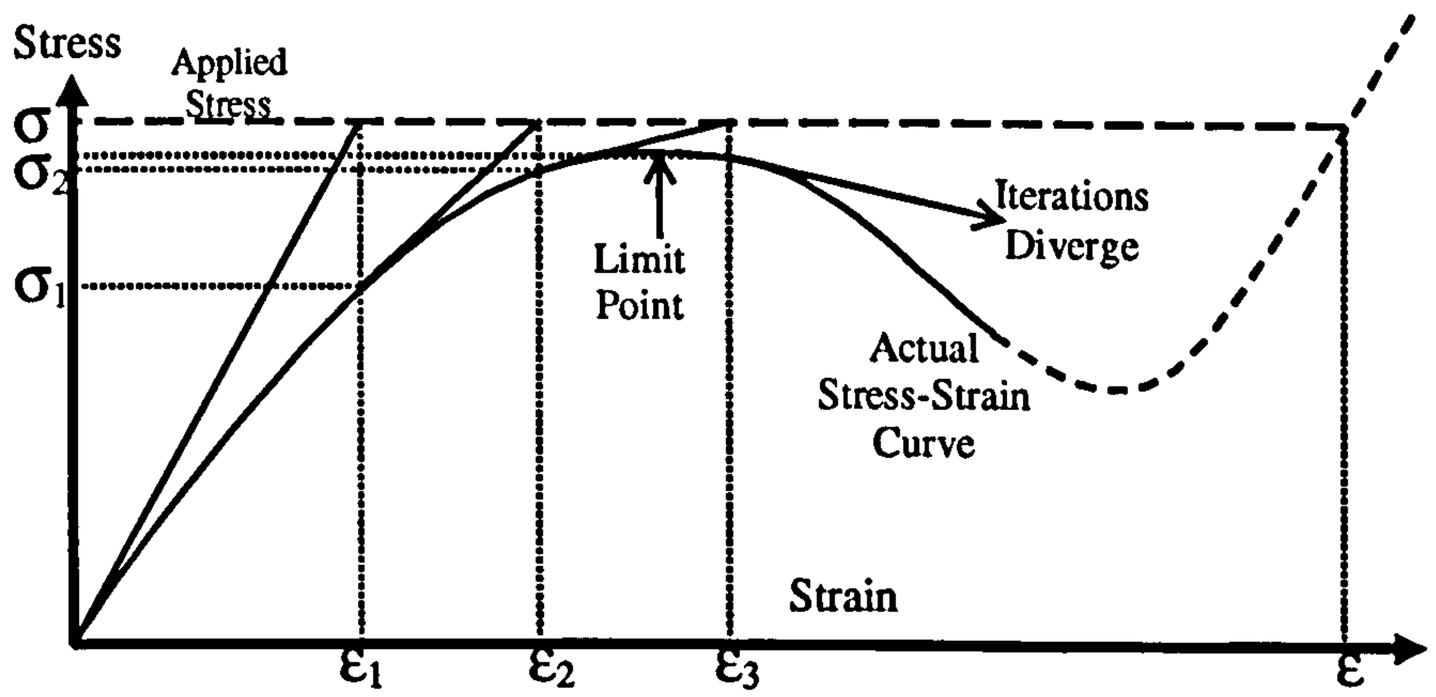

Fig. 120 Snap-through divergence

9.2.3 Modified Newton-Raphson Method

As explained above, when using the Newton-Raphson method the stiffness matrix has to be re-calculated at the start of each iteration. This can prove to be time-consuming, especially for very large structures with a large number of elements. An alternative method is known as the Modified Newton-Raphson method, which simply re-uses the initial stiffness matrix at each iteration as shown in Fig. 121.

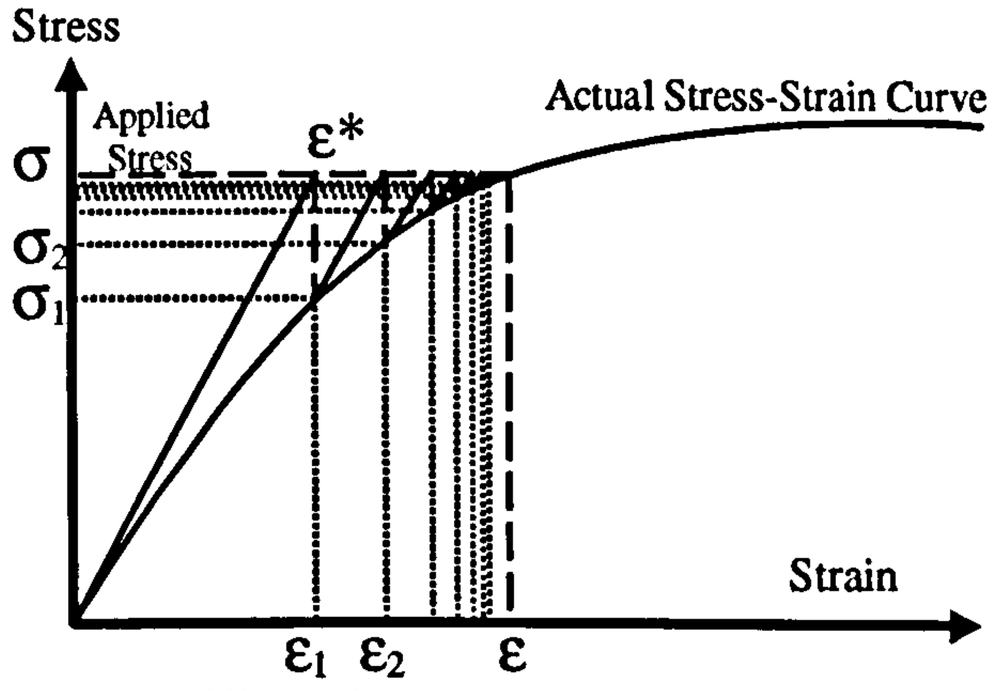

Fig. 121 Modified Newton-Raphson method

However, as can be seen from Fig. 121 the tangent stiffness matrix does not accurately represent the stiffness of the structure at each step. This increases the number of iterations required to reduce the o.b.f. below a certain tolerance. Therefore, this modification introduces a trade-off between the speed of each iteration and the number of iterations required. Thus, this method is especially useful when the structure has a low level of non-linearity, and as such the initial stiffness matrix is somewhat similar to the stiffness matrix that would otherwise have been calculated.

This method is slightly more stable on the approach to limit points than the standard Newton-Raphson method. However, load steps that start close to the limit point use

increments of the degrees of freedom which are based on conditions at zero load. These conditions may no longer be of any relevance, and the method still has an inherent inaccuracy problem in such cases.

9.2.4 Displacement Control Method

One way to overcome these limit-point problems is to make steps of displacements, rather than loads. The displacement control method uses this system, in which a pre-determined d.o.f. is changed in steps, and the other d.o.f.'s are calculated accordingly. The simple, one-dimensional case is shown in Fig. 122, where ε is the pre-defined change in strain and σ is the final calculated stress. A scheme of iterations is performed at each constrained strain level to determine intermediate stresses and strains in the other d.o.f.'s.

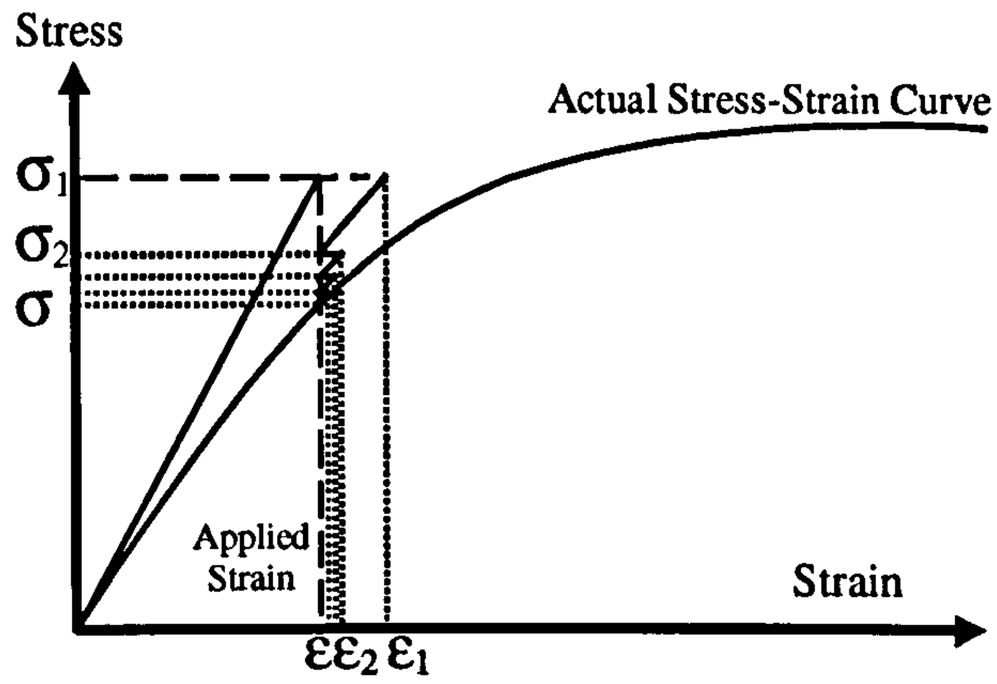

Fig. 122 Displacement control method

Since iterations are performed at a constant strain level, solutions are available at and beyond limit points. The analogous problem to the limit-point of the Newton-Raphson method is that the displacement control method is unstable around areas of infinite stiffness. Thus divergence can occur in systems which show "snap-back" behaviour, as shown in Fig. 123.

Since the solution procedure is led by controlling steps of a particular d.o.f., the stability of the method is highly sensitive to the choice of the d.o.f. that is used. In addition, since this is not a load-controlled method, the final solution occurs at a pre-determined strain rather than stress. Therefore, further iterations will be required to find a solution within a certain tolerance of the applied load.

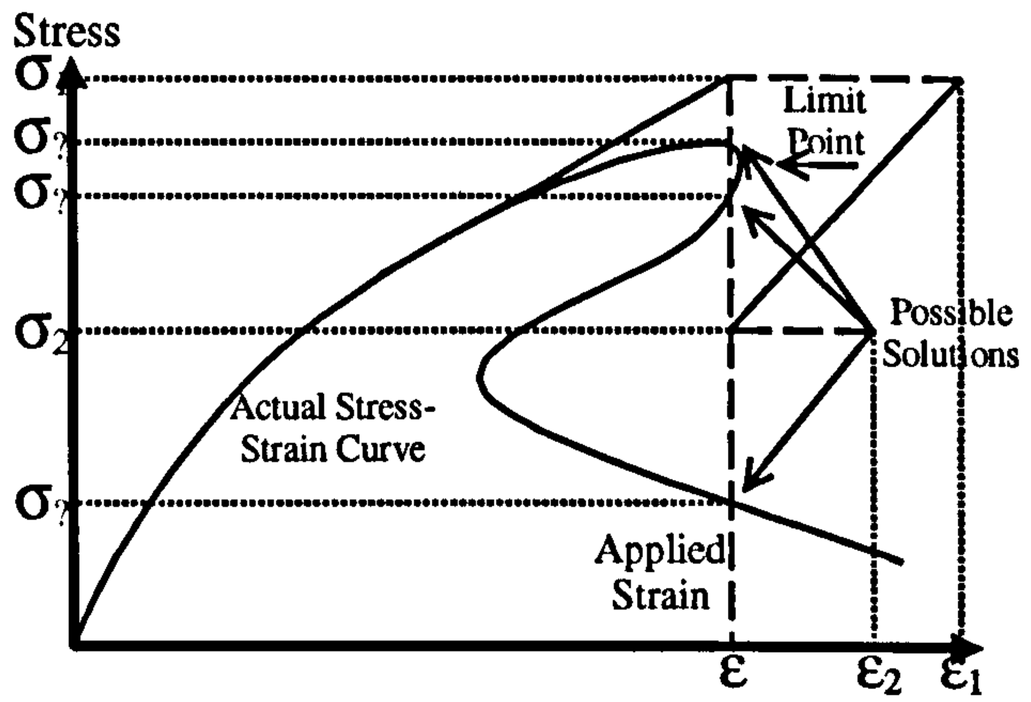

Fig. 123 Snap-back behaviour

9.2.5 Arc-Length Method

In order to overcome the sensitivity to a particular d.o.f., the arc-length method[57] controls a norm of all d.o.f.'s. The "length" of this norm is determined by the level of o.b.f. at a particular iteration and the direction of the norm is prescribed by applying an orthogonal constraint to the displacements. This method is illustrated in Fig. 124.

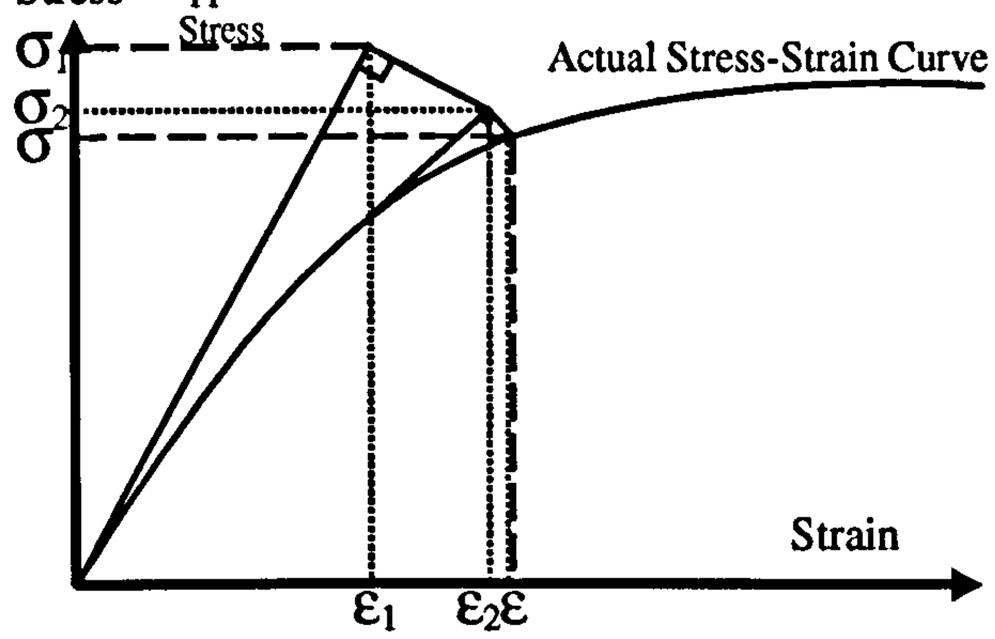

Fig. 124 Arc-length method

The way in which the change in every d.o.f. is taken into account when determining iteration steps makes this method much more stable than the displacement control method. Therefore, snap-through, and a range of snap-back, situations can be handled using this method. Again, the final solution is not generally at the applied load level and further load steps will be required to find a solution at this level.

9.2.6 Work Control Method

The work control method is similar to the arc-length method in that it takes a scaling of all the d.o.f's to control the iterations. The difference is that this method incorporates the stress level in this scaling, so that the concept of a constant change in work (force x distance) is conserved, rather than simply a constant change in

"distance" along the equilibrium curve (the arc-length). This is illustrated in Fig. 125. Again, no one d.o.f. is any more significant than another in controlling the iteration scheme and so this method can also follow snap-through and snap-back behaviour.

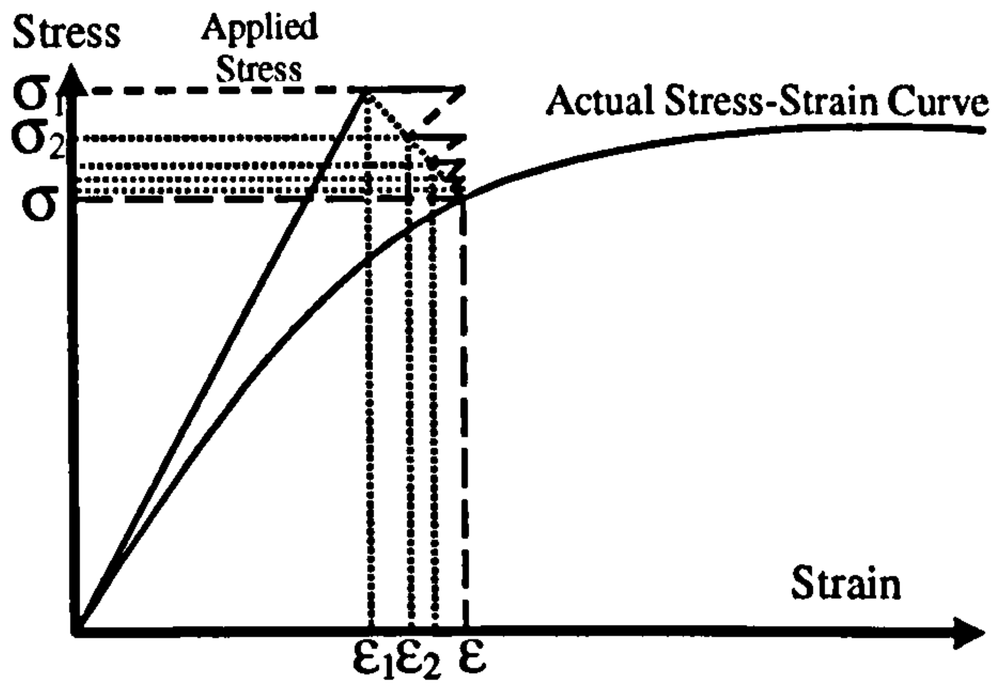

Fig. 125 Work control method

9.3 Investigative Computer Programs

It is far too complicated to study these methods from within the VULCAN program itself, since many degrees of freedom are associated with each node and many different physical effects are considered. This would make an isolated study of the solution procedures far too difficult. Therefore a number of QuickBasic programs to solve one- and two-degrees of freedom problems were written completely independent of VULCAN in order to gain a full understanding of the processes involved in using each method.

Computer graphics were used to present the output so that the processes involved in the solution procedures could easily be followed and compared.

9.3.1 Single Degree Of Freedom Investigation

As an introduction to the problems of solving non-linear equations, a trivial single degree of freedom problem was constructed within a QuickBasic program. A particular mathematical function, which is shown as eqn. (97) below, was chosen to represent the problem. This is a purely mathematical exercise and so the equation has no physical significance. A cubic equation was chosen since it allows investigation of the behaviour of the solution procedures around a limit-point. In this case, the limit-points, where the gradient dy/dx is zero, are shown in eqn. (98) to be at $x = 2$ and $x = 4$.

$$y = (x-1)(x-3)(x-5)+15 = x^3 - 9x^2 + 24x - 20 \tag{97}$$

$$\frac{dy}{dx} = 3x^2 - 18x + 24 = (x-2)(3x-12) \qquad \frac{dy}{dx} = 0 \Rightarrow x = 2,4 \tag{98}$$

9.3.2 Single Degree Of Freedom Results

Below is a collection of screen-shots from the suite of QuickBasic programs used to investigate the different solution procedures for non-linear analysis. These can be compared with the relevant schematic representations of Fig. 116 – Fig. 125 above.

For example, the displacement-control method is shown in Fig. 129, which identifies the initial displacement along the tangent stiffness in dark-blue and subsequent iterations at a constant displacement level in alternating light- and dark-blue lines.

The work-control method shown in Fig. 131 looks quite similar to the displacement-control method, in this single d.o.f. case. This is due to the nature of the specific problem and work increment chosen, and results in the concept of constant work being achieved by a reduction in load being counteracted by what seems to be a very small increase in displacement. This is just an anomaly of this particular example, and it can be seen that the methods give very different results in other cases, such as the two d.o.f. example described in the following section.

It should be noted that the post-limit-point solutions for the arc-length and work-control methods do not completely represent the true algorithm process. In these cases, where the initial tangent stiffness is negative, the absolute value of the gradient has been used, which ensures that the solution path progresses in a positive direction with respect to displacement. This has been used to show that the methods are capable of converging to post-limit-point solutions, even when their initial step is far from the final converged solution. If this switching of sign had not been performed, the subsequent load-step after the first post-limit-point solution would have been in a negative displacement sense. This would reverse the direction of the solution path and the final solution would again be near to the limit point.

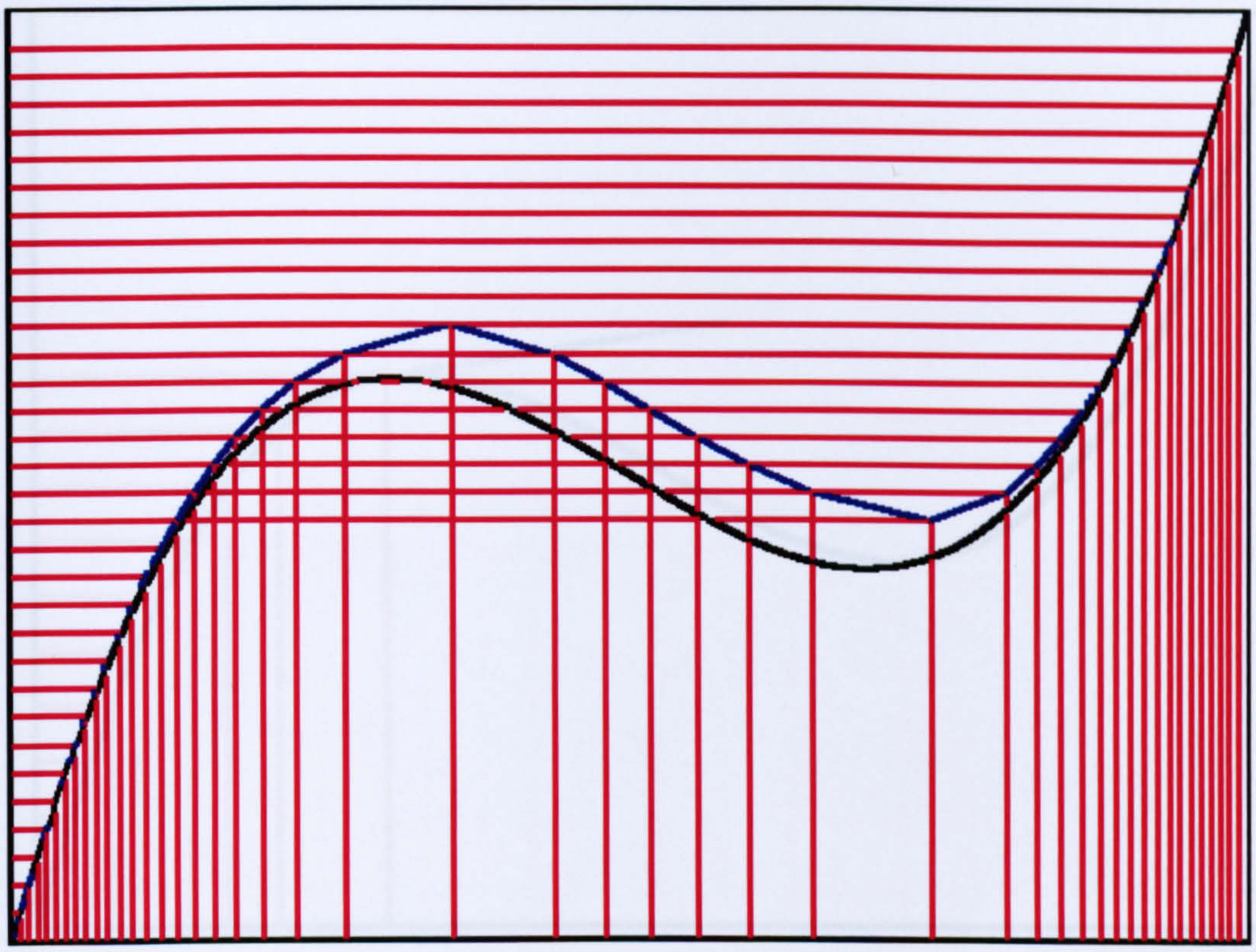

Fig. 126 Simple incremental method

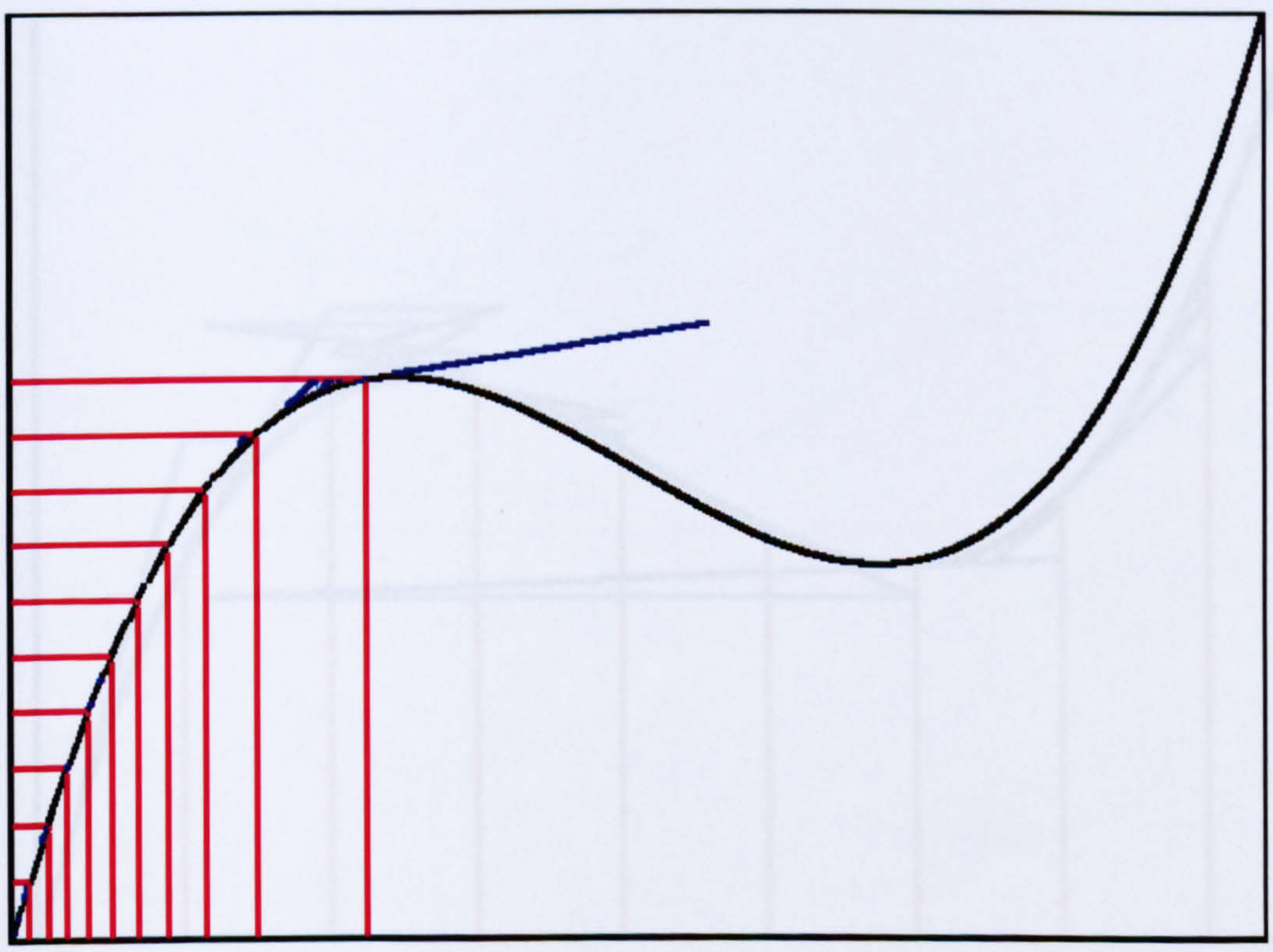

Fig. 127 Newton-Raphson method

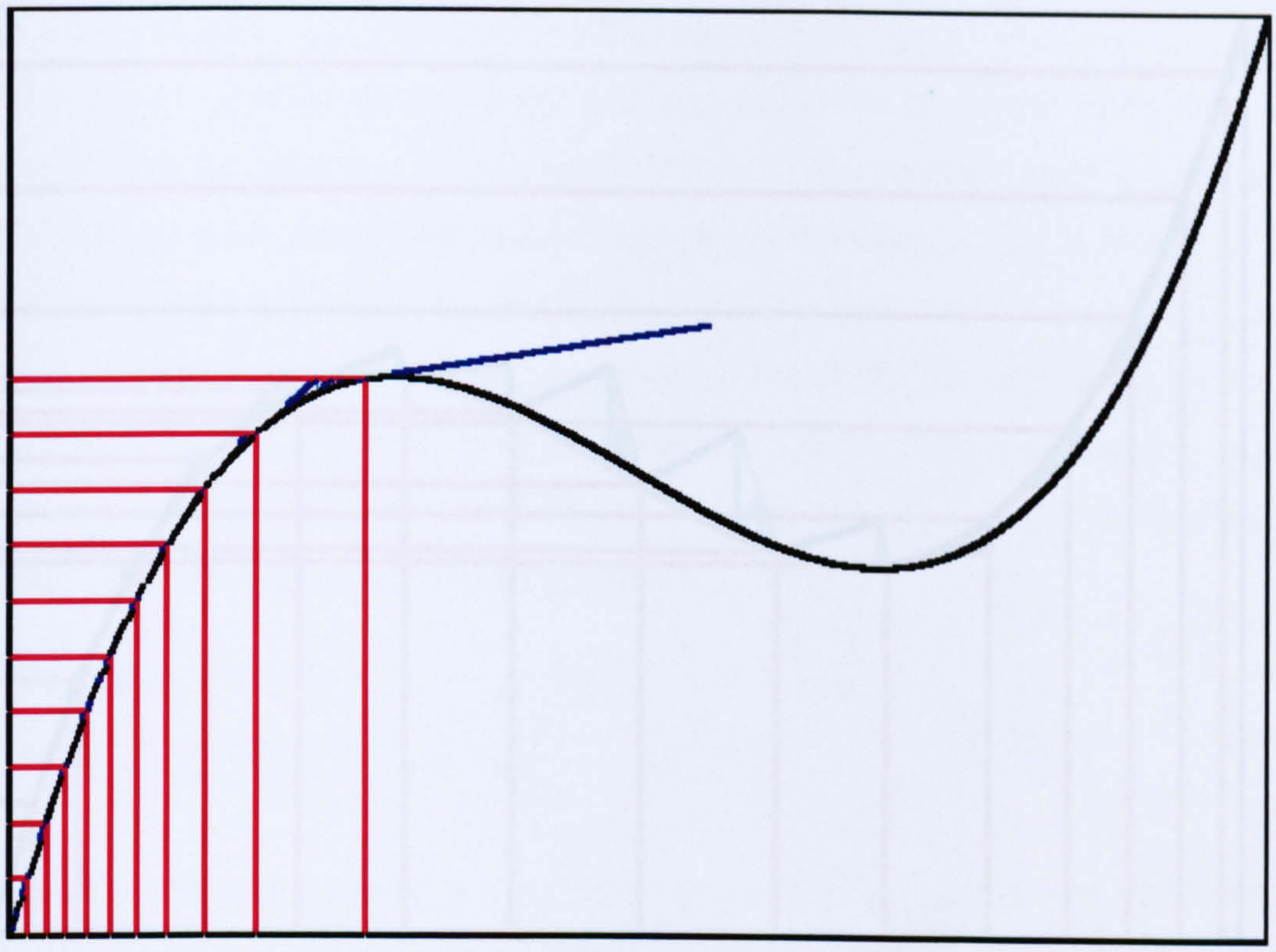

Fig. 128 Modified Newton-Raphson method

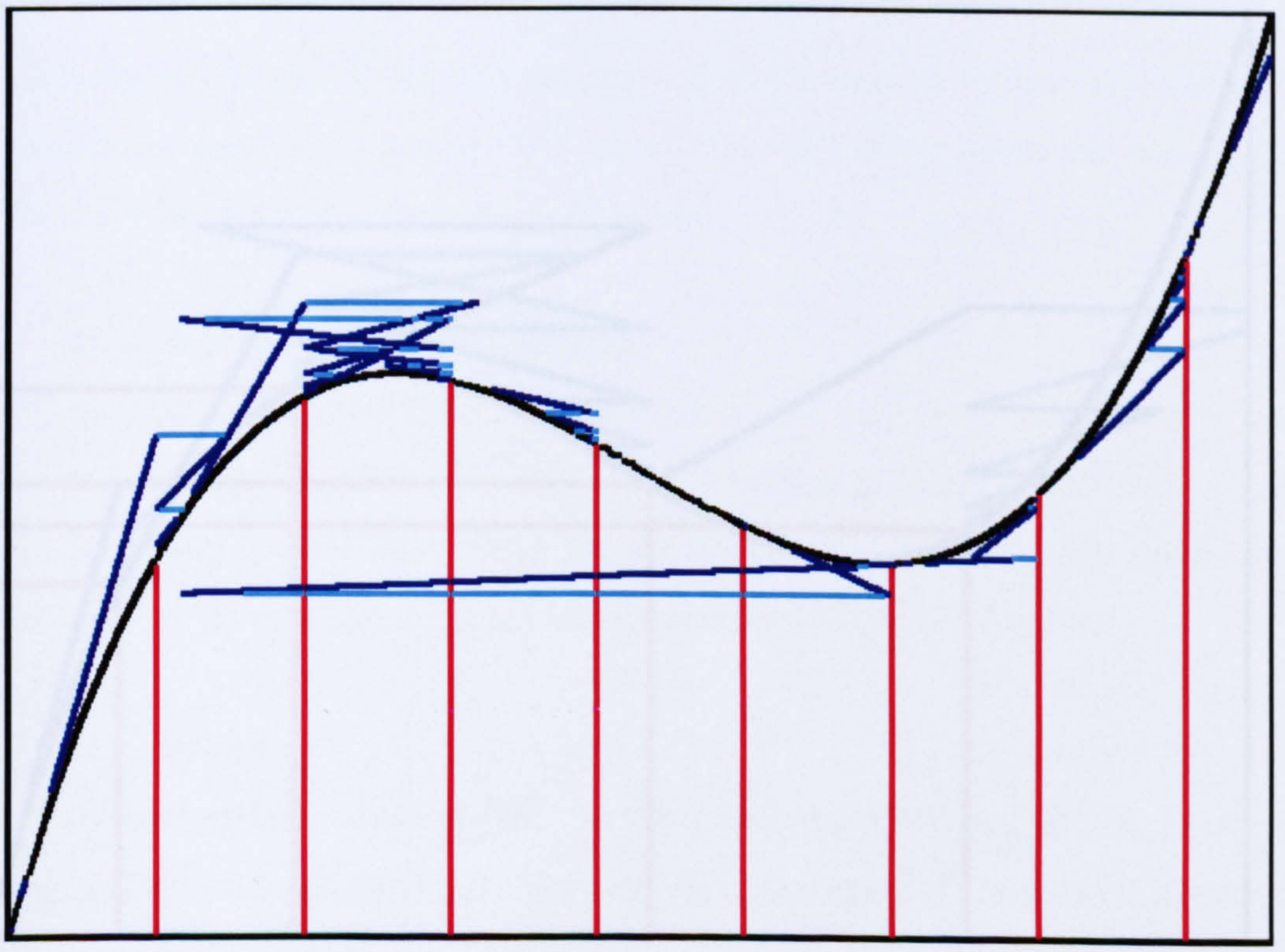

Fig. 129 Displacement control method

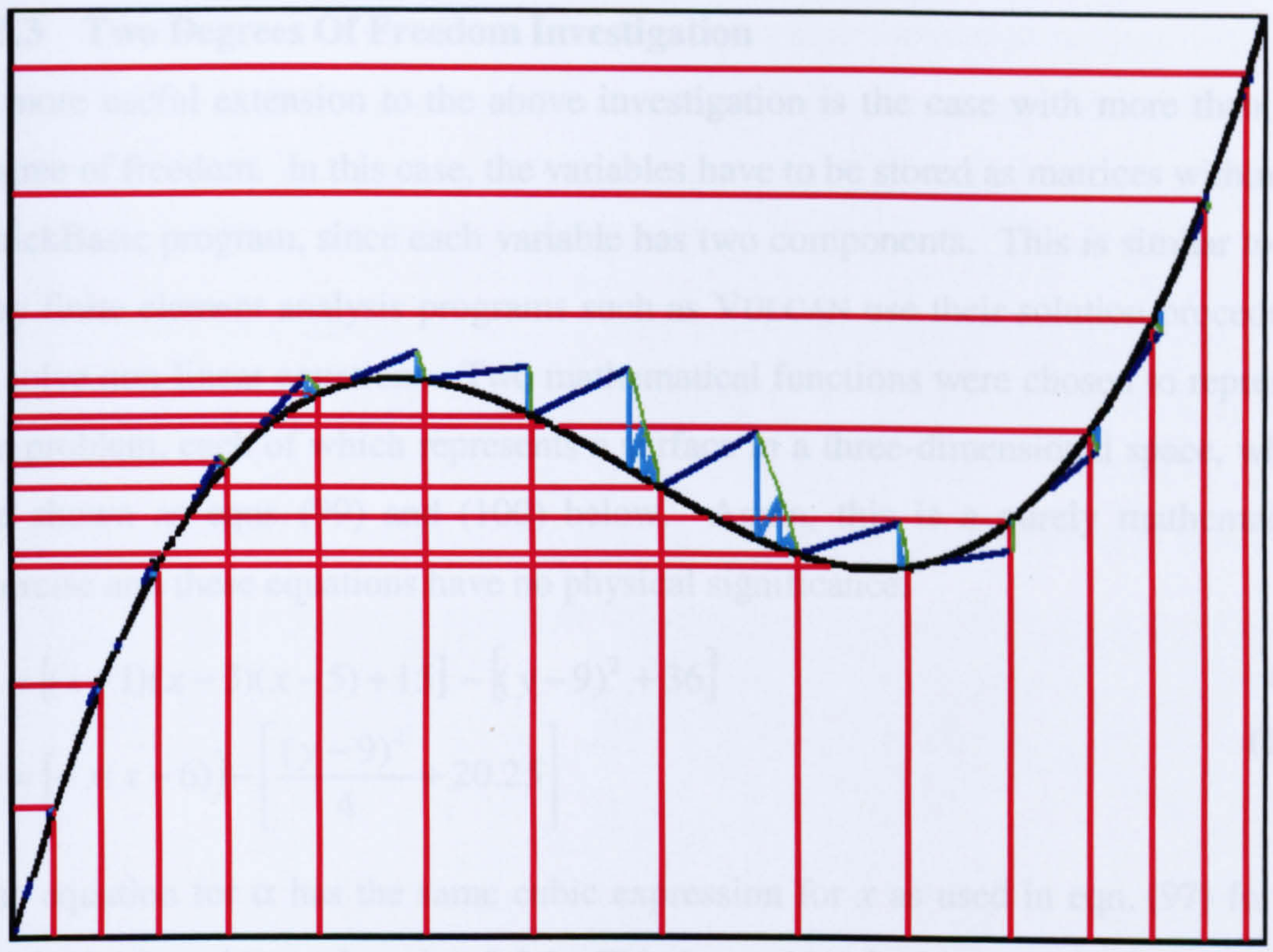

Fig. 130 Arc-length method

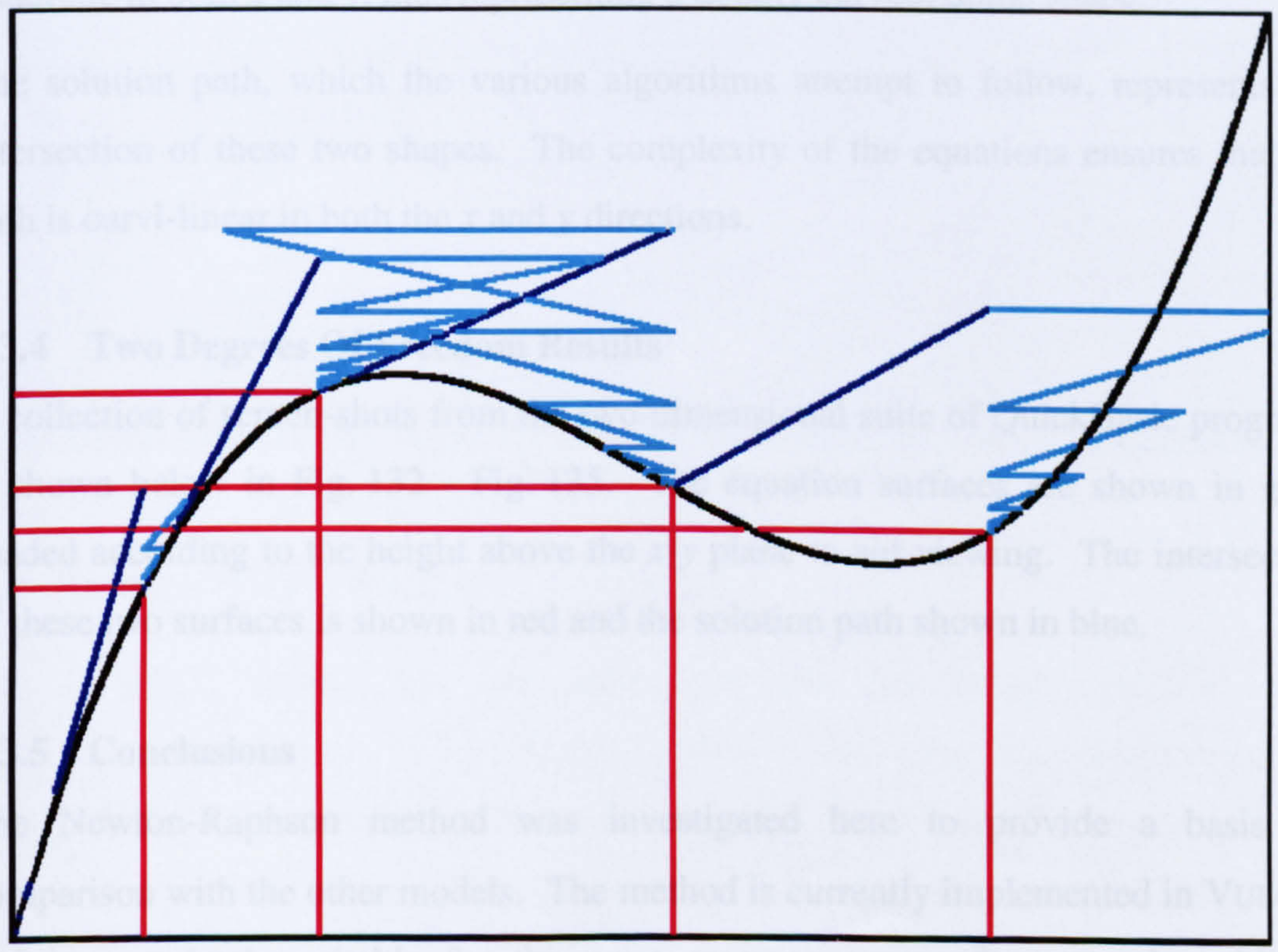

Fig. 131 Work control method

This need for a small amount of intelligence to be used in choosing which direction to travel along the solution path is inherent in post-limit-point algorithms and is discussed in more detail at the end of this chapter.

9.3.3 Two Degrees Of Freedom Investigation

A more useful extension to the above investigation is the case with more than one degree of freedom. In this case, the variables have to be stored as matrices within the QuickBasic program, since each variable has two components. This is similar to the way finite element analysis programs such as VULCAN use their solution procedures to solve non-linear equations. Two mathematical functions were chosen to represent the problem, each of which represents a surface in a three-dimensional space, which are shown as eqns. (99) and (100) below. Again, this is a purely mathematical exercise and these equations have no physical significance.

$$\alpha = [(x-1)(x-3)(x-5)+15] - [(y-9)^2 + 36] \tag{99}$$

$$\beta = [-x(x-6)] - \left[\frac{(y-9)^2}{4} + 20.25\right] \tag{100}$$

The equation for α has the same cubic expression for x as used in eqn. (97) for the single d.o.f. problem of section 9.3.1. This is combined with a quadratic expression for y such that a cubically curved sheet is bent in an arc. The equation for β is quadratic in both x and y, thus representing a doubly curved, dome shape.

The solution path, which the various algorithms attempt to follow, represents the intersection of these two shapes. The complexity of the equations ensures that the path is curvi-linear in both the x and y directions.

9.3.4 Two Degrees Of Freedom Results

A collection of screen-shots from the two-dimensional suite of QuickBasic programs is shown below in Fig. 132 - Fig. 135. The equation surfaces are shown in grey, shaded according to the height above the x-y plane to aid viewing. The intersection of these two surfaces is shown in red and the solution path shown in blue.

9.3.5 Conclusions

The Newton-Raphson method was investigated here to provide a basis for comparison with the other models. The method is currently implemented in VULCAN and is completely suitable for the most common types of structural problems. However, as shown in Chapter 3, some types of problems that exhibit snap-back behaviour can be of interest in the context of this work. Therefore, there is motivation to include a choice in the solution methods available within VULCAN.

The displacement control method was relatively straightforward to program and gave fast, stable convergence onto a solution even in the two-dimensional case. However, its unsuitability to snap-back problems suggests that, although it could be a future development of VULCAN, priority should be given to other solution procedures.

The choice between the arc-length and work control methods seems an arbitrary one, since they are similar in the way that a scaling of all degrees of freedom is used. When using the work control method to solve the two-degrees-of-freedom problem above, some instability occurred; and thus, the arc-length method has been favoured.

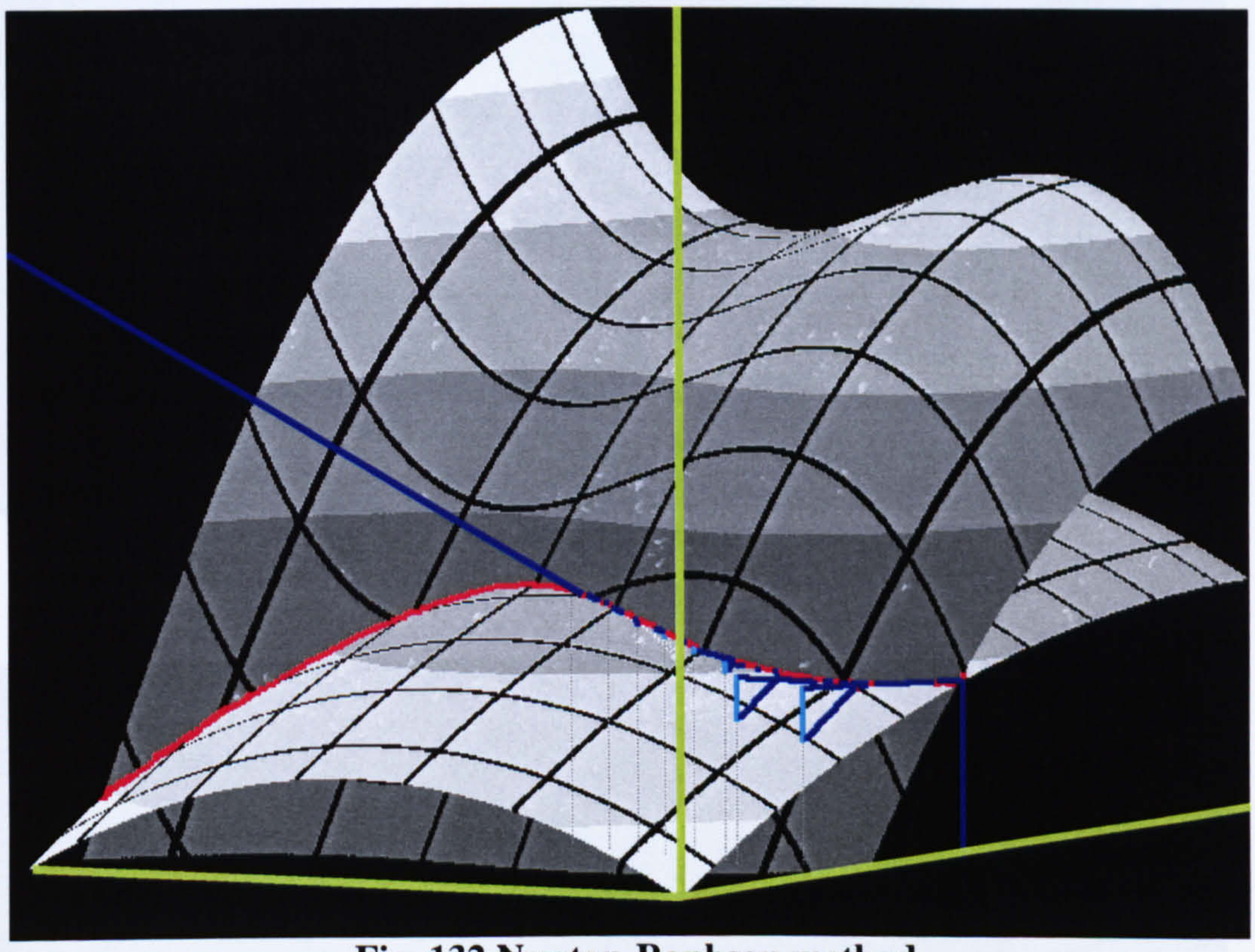

Fig. 132 Newton-Raphson method

9.4 Inclusion Into VULCAN

The arc-length method has been introduced into the VULCAN program as a preliminary modification of the solution procedure. However, time did not permit a fully robust implementation of the method and further work is required to allow generic problems to be solvable using this method, as described in the conclusions sub-section.

The purpose of this section is to use a simple structural example to show that the new code for the arc-length method is working correctly. It will be shown that this method is at least as capable as the Newton-Raphson method of solving elevated-

temperature non-linear analyses. Further studies can later be performed to show the advantages of the arc-length method over load-controlled methods.

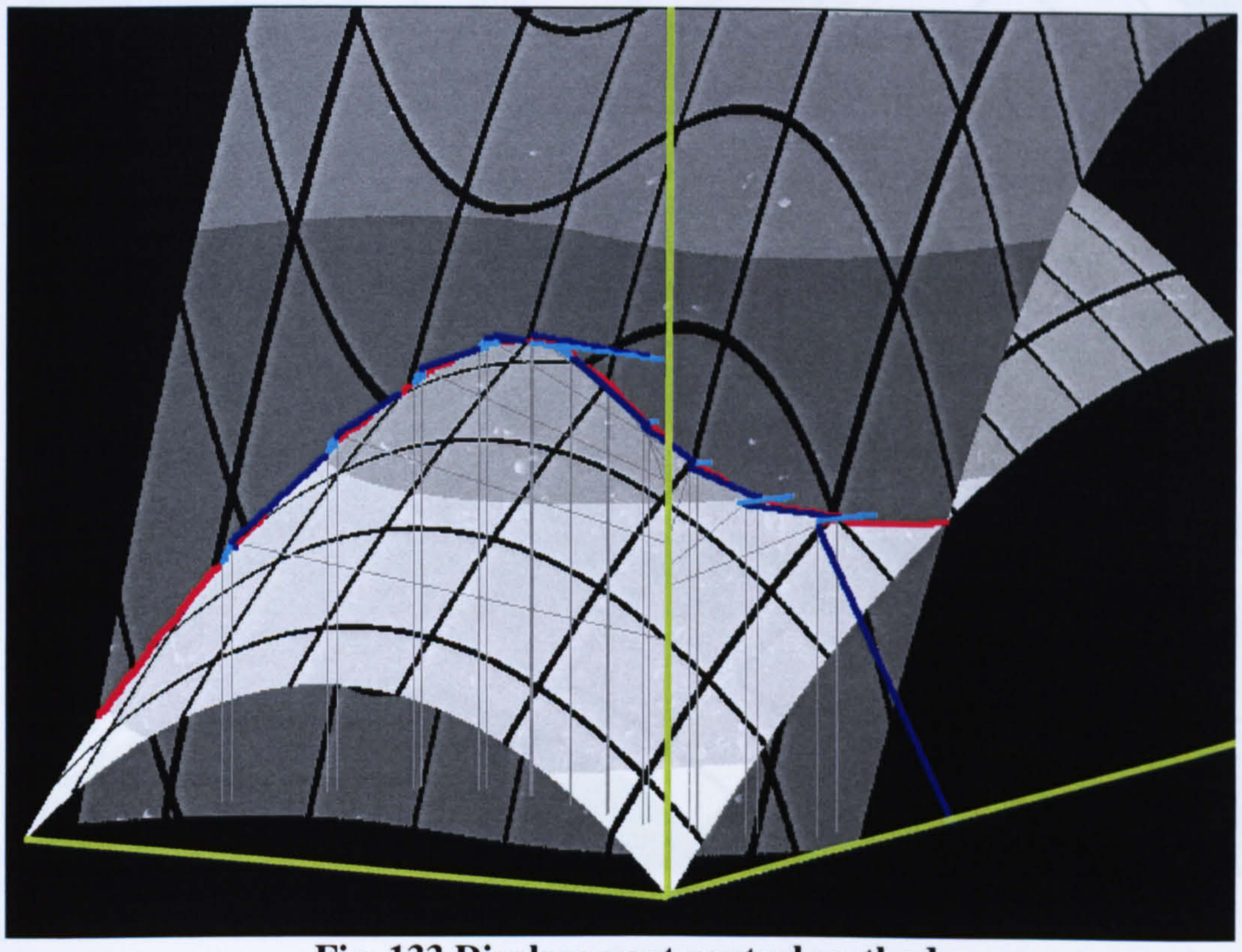

Fig. 133 Displacement control method

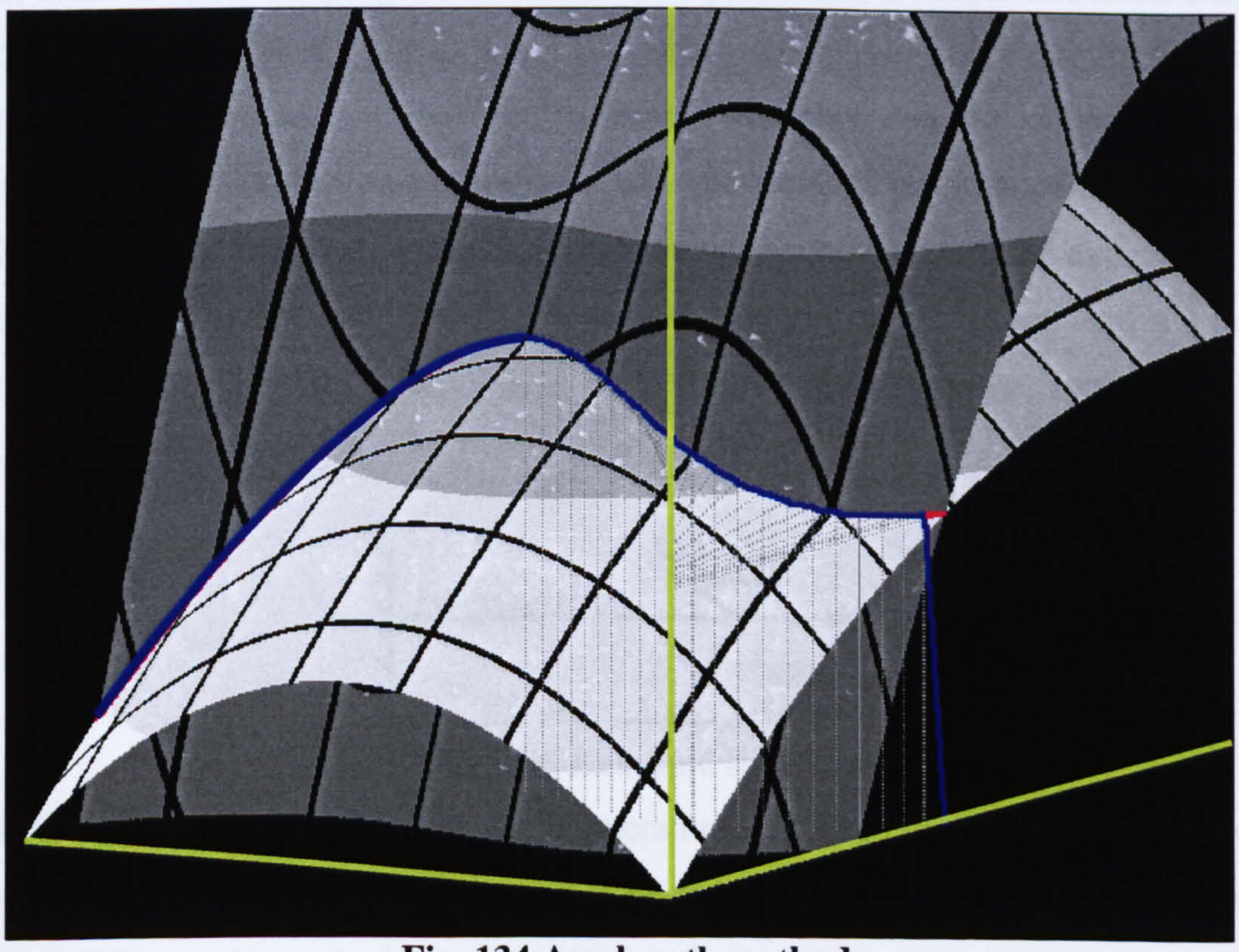

Fig. 134 Arc-length method

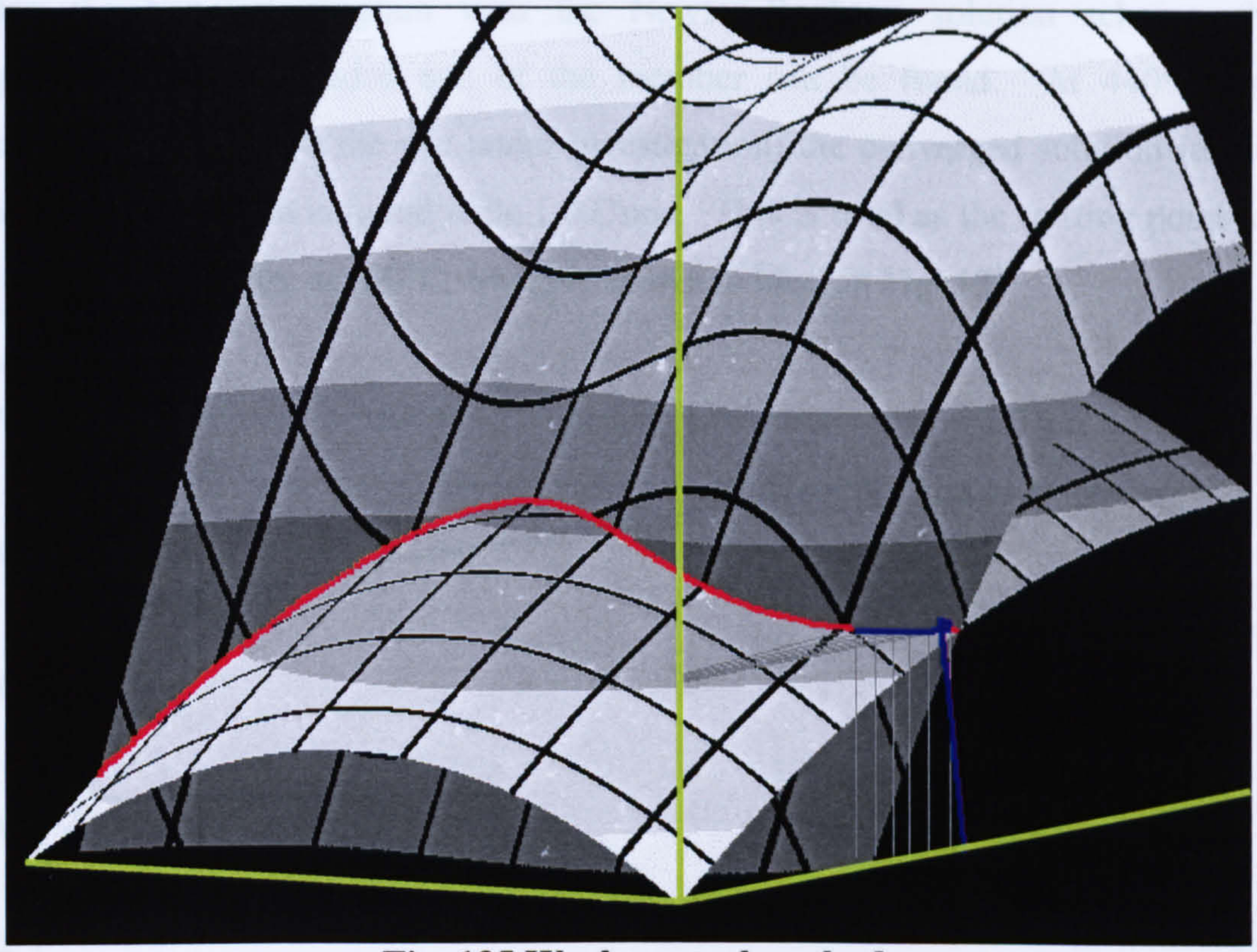

Fig. 135 Work control method

9.4.1 Description Of Simple Structural Example

In order to show the progress of the solution procedure, a simple structural example has been created as a VULCAN input file. This example has only one unconstrained degree of freedom, so that the solution variables can be followed without complication. The chosen example is a single-element problem of a 100mm long 254x254x73UC section, in which every boundary condition is fixed except the axial displacement at one end. Steel with a yield strength of 355N/mm^2 and a Young's modulus of 210kN/mm^2 was used. A tension force of 2253kN was applied axially at one end as shown in Fig. 136.

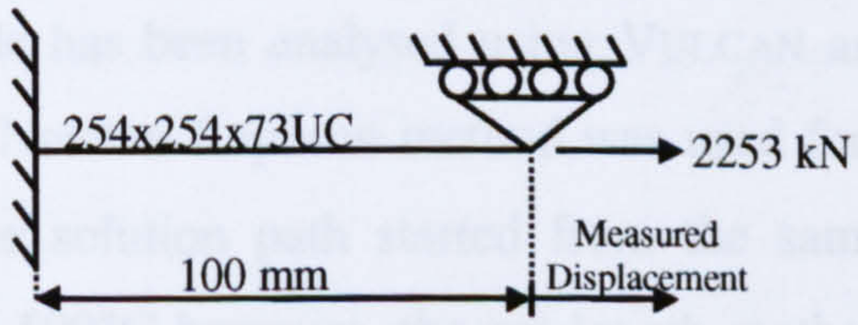

Fig. 136 Example structure

This problem is linear at ambient temperature, but becomes non-linear at elevated temperatures due to the non-linearity of material stress-strain curves. A temperature of 500°C was chosen for basic comparison of solution methods.

9.4.2 Initial Load Step Using Simple Example With Newton-Raphson Method

Using the VULCAN program with the Newton-Raphson solution scheme, the displacement of the loaded end of the member can be found. At 440°C (the temperature step before the one under investigation) the converged solution for the extension of the beam is found to be 1.003mm. This is used as the starting point for the solution procedure at 500°C, which is shown in blue on Fig. 137.

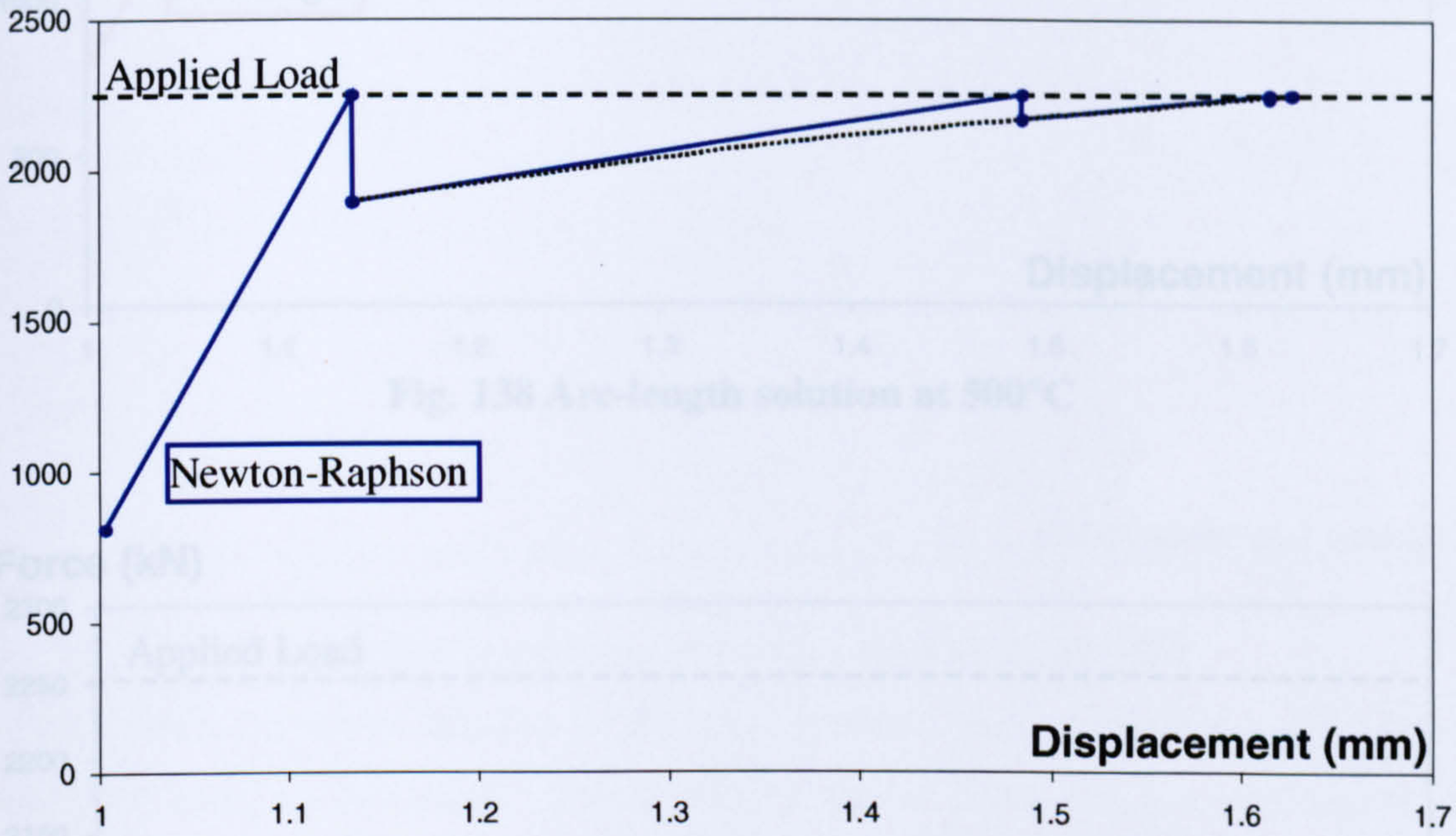

Fig. 137 Newton-Raphson solution at 500°C

It can be seen that the Newton-Raphson solution procedure follows its path up until the applied load and the internal forces are within their specified tolerance. At this point, the extension of the member is 1.626mm. This solution path can be compared with the idealised path shown in Fig. 119 and shows that the method is behaving as expected.

9.4.3 Initial Load Step Using Simple Example With Arc-length Method

The same simple example has been analysed using VULCAN and implementing the arc-length method. The Newton-Raphson method was used for temperatures below 500°C to ensure that the solution path started from the same point as with the previous analysis. After 500°C however, the arc-length method was used, and the results can be seen on Fig. 138. This should be compared to Fig. 137 which uses the Newton-Raphson method. A detailed view of the convergence of the solution path can be seen on Fig. 139.

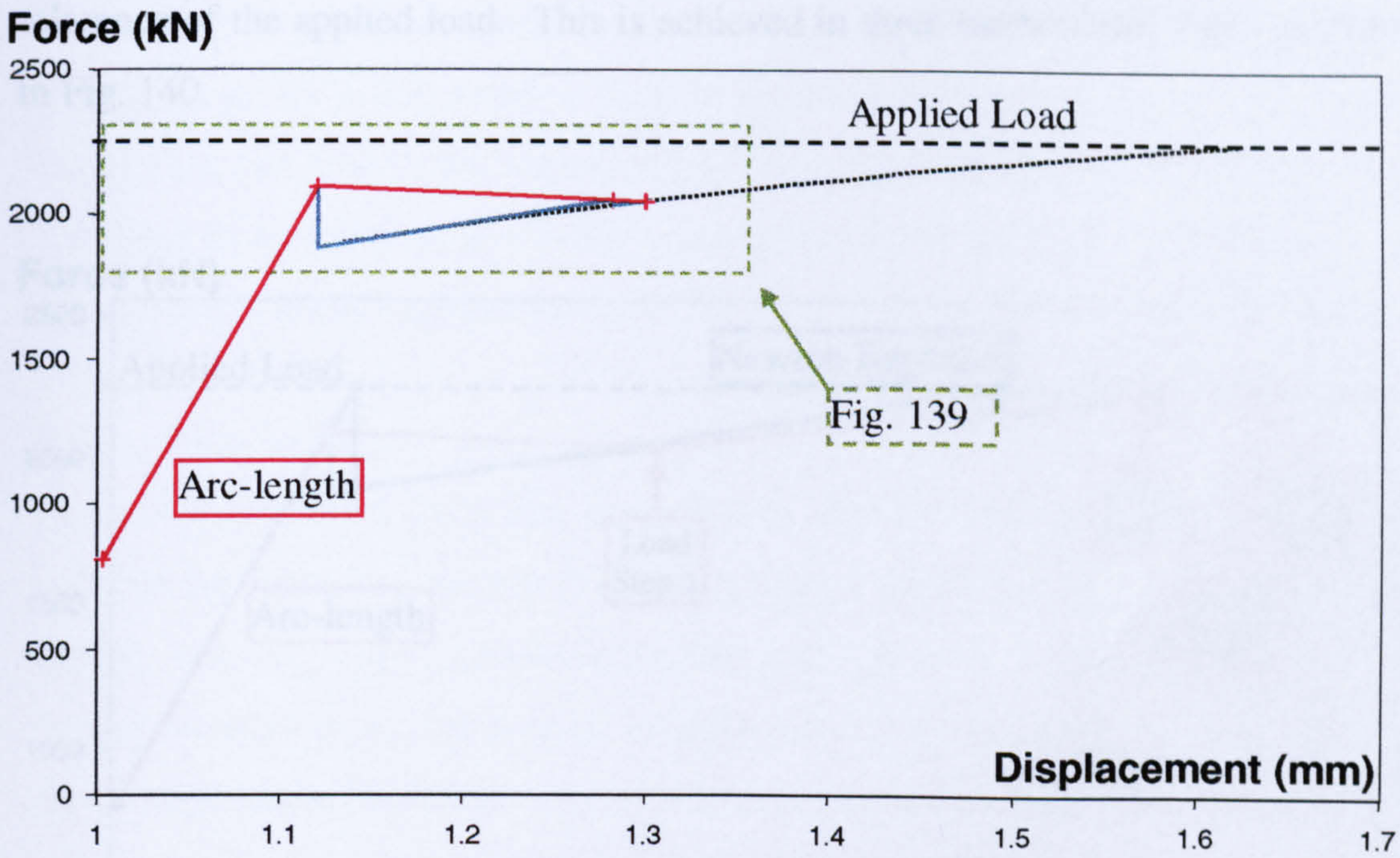

Fig. 138 Arc-length solution at 500°C

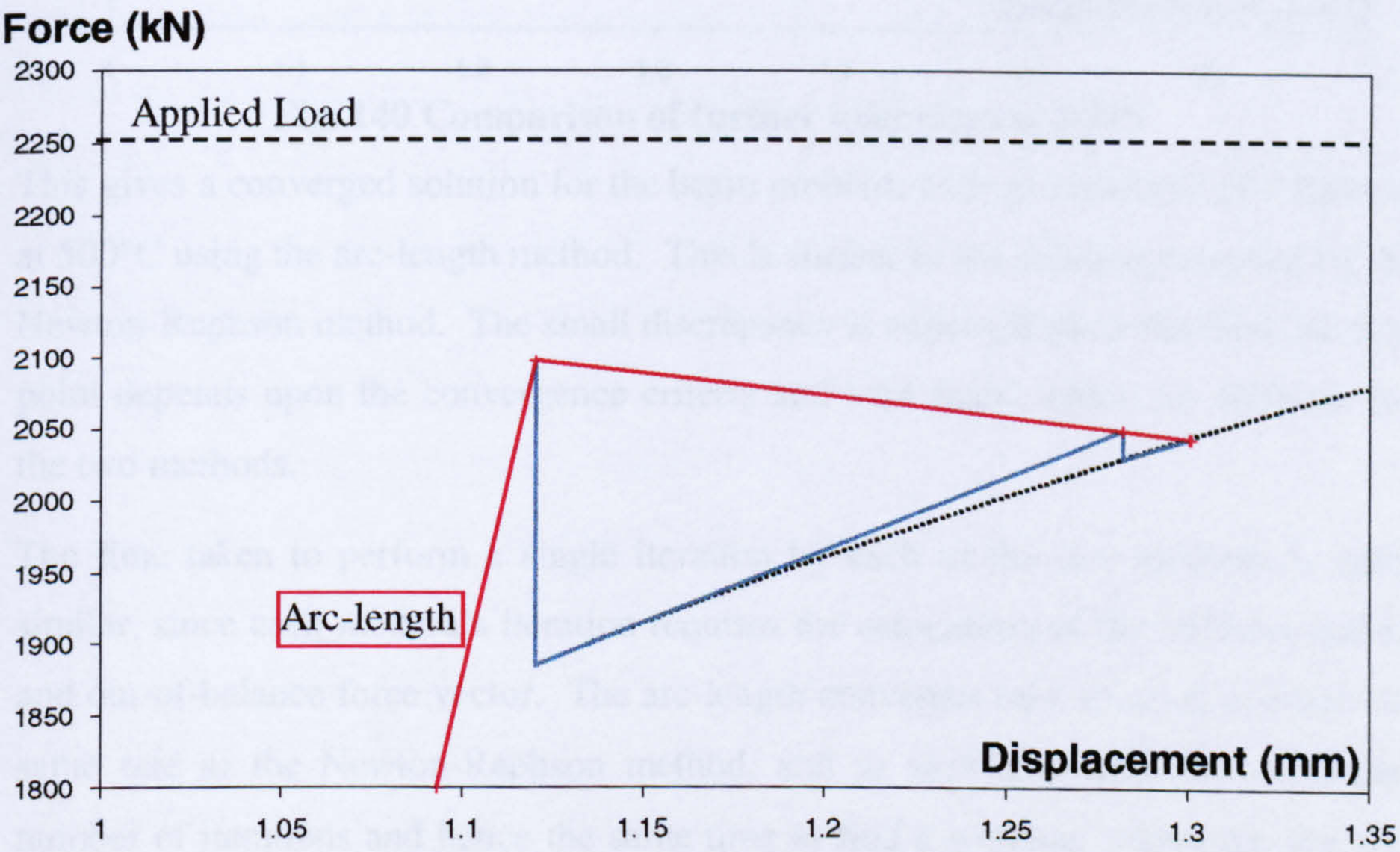

Fig. 139 Arc-length solution at 500°C in detail

9.4.4 Further Load Steps

As explained in the previous section, the arc-length method changes both the load and displacement applied to the problem in order to converge on a stable solution. In order to find the displacement of the simple tension member problem at the applied load, further load steps must be performed until the solution converges to within a

tolerance of the applied load. This is achieved in three further load steps, as shown in Fig. 140.

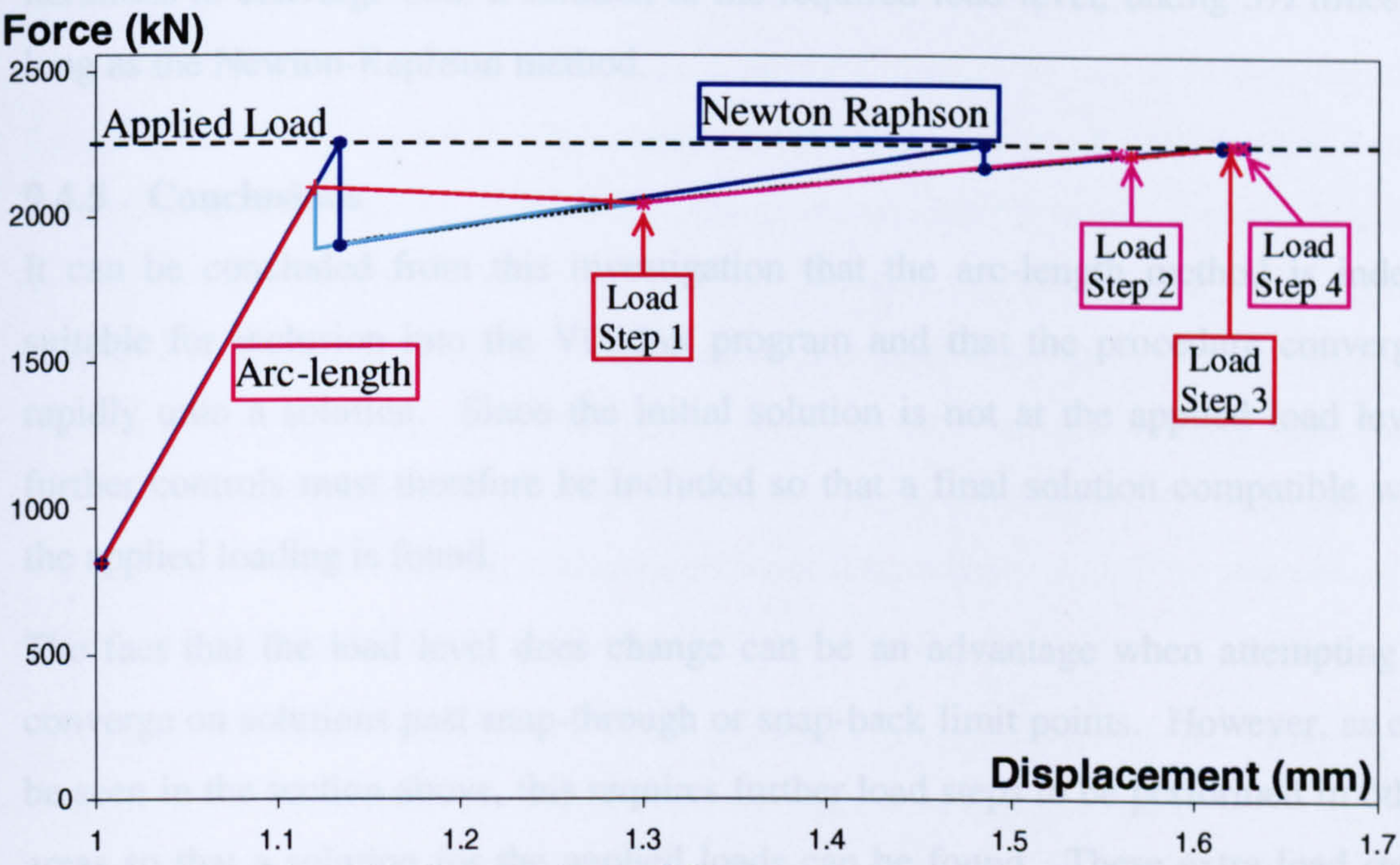

Fig. 140 Comparison of further load steps at 500°C

This gives a converged solution for the beam problem with an extension of 1.628mm at 500°C using the arc-length method. This is similar to the solution provided by the Newton-Raphson method. The small discrepancy is expected since the final solution point depends upon the convergence criteria and load steps, which are different for the two methods.

The time taken to perform a single iteration by each of the two methods is quite similar, since each method's iteration requires the calculation of the stiffness matrix and out-of-balance force vector. The arc-length converges on a solution at much the same rate as the Newton-Raphson method, and as such generally uses a similar number of iterations and hence the same time to find a solution. However, the arc-length solution is not necessarily at the desired load-level, and therefore further sets of iterations are required. This increases the overall time to find a desired solution, by a factor, which depends on the specific problem, such as its degree of non-linearity and the parameter chosen for the "arc length".

For example, the Newton-Raphson solution to the problem shown above in Fig. 140 required 6 iterations to converge within a tolerance of the true solution at the required load level. The first load-step of the arc-length method required 7 iterations

to converge to within the same tolerance of the solution path. However, since this solution was not at the required load level, three further load-steps were required, taking 5, 4 and 5 iterations respectively. Thus, the arc-length procedure required 21 iterations to converge onto a solution at the required load-level, taking 3½ times as long as the Newton-Raphson method.

9.4.5 Conclusions

It can be concluded from this investigation that the arc-length method is indeed suitable for inclusion into the VULCAN program and that the procedure converges rapidly onto a solution. Since the initial solution is not at the applied load level, further controls must therefore be included so that a final solution compatible with the applied loading is found.

The fact that the load level does change can be an advantage when attempting to converge on solutions past snap-through or snap-back limit points. However, as can be seen in the section above, this requires further load steps to be performed in other areas so that a solution for the applied loads can be found. These extra load steps take time to perform; meaning the program will usually take longer to run than when using the Newton-Raphson method. The extra time taken will depend upon the specific problem and solution parameters, but can be a price worth paying for the ability to follow snap-through and snap-back solution paths.

It is therefore suggested that any modification to the solution procedures used in the VULCAN program is done whilst maintaining the Newton-Raphson capability. The default method chosen to perform iterations should be the Newton-Raphson method, with the arc-length method being switched on in areas close to limit-points of the problem. This is, in effect, what was done in the previous section, where the Newton-Raphson iteration scheme was used for temperatures below 500°C.

At the time of writing, the program retains the ability to use the Newton-Raphson method, and the arc-length method is switched on when the lower-flange of temperature profile #1 is at or above 500°C. The size of the arc-length used for each iteration is constant and fixed inside the program. However, it would be a relatively simple task for this to be changed so that the arc-length method was used whenever the Newton-Raphson method had failed, and a sensible arc-length could be chosen or entered by the user.

In this instance, the routine was developed to show that the arc-length method is at least capable of following the same solution paths as the Newton-Raphson method. Therefore, it is assumed that the solution curve has a positive tangent stiffness, as in the simple example structure investigated above. Once the procedure has converged on a solution, the next load-step is in a positive direction, and a further solution found at a higher load level. Obviously, the power of the arc-length method lies in its ability to converge on post-limit-point solutions, which would involve negative load-steps. Consequently, some further work is needed to make the solution routine able to follow more general solution paths that exhibit snap-through and snap-back behaviour. A certain level of intelligence, based on the previous solution path, could be introduced, allowing post-limit-point solution paths to be followed. Alternatively, a simple graphical output, combined with user-interactivity, could be introduced to guide the solution process across complex solution surfaces.

The suggested improvements, to expand the solution capability from the very limited and trivial set of problems investigated here, require a fair amount of work and are outside the time-scope of this project.

10 Conclusions

This chapter describes the conclusions drawn from this work and contains the author's recommendations for future work.

10.1 Conclusions

A preliminary investigation into the parameters effecting the behaviour of axially restrained of steel columns has been performed using the VULCAN software developed at the University of Sheffield. The results from this study were used to guide the analysis of results from the partner project, consisting of series of axially restrained column tests performed at the University of Ulster. The analysis of this series of tests has been extended by using VULCAN to investigate the effects of parameters too extreme to be seen in the Ulster test rig.

A mathematical model of restraint to steel columns as part of a larger, framed structure has been developed. This method enables different levels of complexity to be incorporated into the model, depending on the accuracy required.

The code for the VULCAN program and the format of the associated data files has been tidied to aid future development, whilst at all times retaining backwards compatibility. A separate graphical program has been created to make input-file creation and output-file visualisation more straightforward.

A detailed investigation into the solution procedure used within VULCAN has been conducted. The most suitable method of following snap-through and snap-back solution paths has been selected, which has been shown to be important in the investigation of axially restrained columns. In addition, a framework for the method has been incorporated into the VULCAN code.

From the results of this work, a number of important conclusions can be inferred, and these deductions are described in the following sub-sections.

10.1.1 General Behaviour

Axially restrained steel columns of low slenderness fail due to yielding of the cross-section and as such, their failure temperature is governed by the material yield strength of the steel. Initial geometric imperfection is a relatively unimportant factor

and design codes such as EC3 give only nominal values of imperfection for stocky columns. Slender columns fail by flexural buckling and therefore their failure temperatures are sensitive to initial geometrical imperfections.

Initial axial load level affects the failure temperatures of columns of all slendernesses, with an increase in axial load resulting in a decrease in failure temperature.

Under constant load, an increase in slenderness causes a decrease in failure temperature. However, the EC3 design-load for columns decreases rapidly as slenderness increases. Therefore, at a constant multiple of the design-load, failure temperature can be seen to increase as slenderness increases in cases with low levels of initial geometric imperfection.

Thermal gradients introduce thermal bowing, reducing the failure temperature of slender columns, in which the failure mode is flexural buckling.

The temperature at which an axially restrained column returns to its original length after an initial expansion is independent of the level of imposed axial restraint.

10.1.2 Finite Element Modelling Considerations

Finite element analysis of axially restrained steel columns is extremely sensitive to the stress-strain model used. The Ramberg-Osgood model incorporated in the VULCAN program contains parameters that change in a multi-linear fashion with temperature, introducing artificially sudden changes in results. A smoothed model has been developed which should be used in preference to the standard model. However, due to its acceptance in the engineering community and its computationally faster calculation time, the EC3 method is preferred.

Linear spring elements can be successfully used to model isolated, axially restrained column tests, which represent columns as part of a framed structure. However, when the columns become shorter than their original length, columns in the Ulster test rig are no longer axially restrained. Columns that form part of a frame would be supported by the surrounding structure, and would be supported until the surrounding structure begins to yield. A linear spring model using the VULCAN program continues to support the column until no further stress-strain data is available for calculation. Therefore, the spring model and Ulster test column data are only

applicable to a column in a framed structure whilst the column is longer than its original, ambient temperature length.

The ability of structures to utilise alternative load paths to carry loads has been highlighted once an isolated column member has undergone what could be called failure. In this case, the structure can have a significant reserve of strength, and in no way can the structure as a whole be said to have failed.

10.1.3 Modelling Of Ulster Tests

Analyses of the axially restrained column tests performed at Ulster are affected by the yield stress of the steel used. The column failure temperatures increase with yield stress, and so tensile testing of test specimens is required to allow accurate modelling.

Since the behaviour of axially restrained columns at elevated temperatures is dominated by thermal expansion effects, the results are highly sensitive to the thermal expansion coefficient of the steel. The Ulster columns have a thermal expansion coefficient of approximately 93% of that assumed by EC3.

The Ulster test rig undergoes considerable bedding-in as the test column begins to expand. This can be incorporated into the spring model used in VULCAN, but is almost impossible to predict.

The VULCAN models show good agreement with the test data before the columns have become shorter than their original length. In particular, the maximum supported axial force is accurately predicted. However, the temperature at which this peak force occurs is consistently lower in the model than in the test. This is attributed to a combination of bedding-in, inaccuracies in stress-strain and thermal expansion data, and with the presence of rotational restraint in the test bearings in the form of friction.

The column tests are highly sensitive to longitudinal and sectional temperature distributions, which were quite variable in the Ulster furnace, making predictive analyses difficult.

VULCAN analyses are more accurate when rotational restraint is present in the test rig, since buckling takes place more slowly, and therefore dynamic effects are minimised.

As column eccentricity increases, the maximum supported axial force, and hence the failure temperature decreases. The VULCAN program can model the presence of eccentricity in a stable fashion and lends weight to the observation that the levels of eccentricity present in the Ulster test were extremely low.

10.1.4 Assessment Of Axial Restraint

A method of assessing the level of axial restraint present in a multi-storey framed structure has been developed. A number of levels of complexity are possible, each involving more detailed calculations, but resulting in a more realistic estimate of the restraint. The effects of beam yielding, and multiple floor / bay fires can also be assessed.

A simple method for the accurate estimation of the level of restraint present in a given structure is important in making the other conclusions and test results from this work applicable to a more general situation.

The axial stiffness of columns above the fire compartment have an effect on the restraint stiffness to the heated columns. However, columns outside the fire compartment, which are pushed upwards by the heated column, have a negligible effect.

The presence of concrete floor-slabs has the effect of increasing axial restraint to a heated column, both by forming composite beams and by acting as a fully interactive two-dimensional plate. The latter has not been addressed in this report.

The stiffness of beam-column connections dominates the level of imposed axial restraint.

This mathematical method compares well with VULCAN analyses. However, validation against test results is difficult due to the lack of reliable tests.

10.1.5 VULCAN Program

The VULCAN program provides a stable and accurate basis for non-linear analysis of steel and composite structures at elevated temperatures. As such, it is an ideal platform for future developments.

The currently implemented Newton-Raphson solution procedure is fast and effective for non-linear problems up to "limit-points", where the tangent stiffness vanishes

before becoming negative. However, a post-limit-point solution can generally be found in these problems, and the temperature steps reversed to trace snap-back behaviour down to the lower limit-point.

The arc-length method is the preferred method to trace snap-through and snap-back situations. However, its implementation is computationally slower, and as such should only be used in areas close to limit-points. Some degree of control is needed to guide the solution process past these regions.

The new format for data files makes the creation of input files and the extraction of output data much easier, resulting in a time saving and easier debugging. Correspondingly, the ShowGrid program is an extremely valuable tool with a huge potential for further development.

10.2 Recommendations For Further Work

As a result of the work carried out during this project, the following recommendations for further work can be made.

10.2.1 Further Testing

Since the thermal expansion of steel has been shown to have a great effect on the behaviour of axially restrained steel columns, the data for thermal expansion of steel collated by British Steel should be validated and extended. The values assumed in EC3 have been shown to be too conservative for research purposes, and more accurate values based on experimental data should be found.

Further tests on isolated steel columns in fire would be useful. In particular, the effects of rotational restraint should be investigated in more detail, with a number of accurately assessed levels of connection stiffness. In addition, the effect of eccentric loading should be investigated, with a parallel study using finite element analysis for mutual validation.

The stiffness of beam-column connections has a great influence in the level of restraint applied to columns when part of a framed structure. Thus, an accurate but simplistic method of assessing connection stiffness should be devised. The "component method" of deducing the rotational stiffness of composite connections,

currently being developed by experiment at the University of Sheffield, is one such way of addressing this problem.

A significant reserve of strength has been shown to be present in framed structures, which can extend the life of a fire compartment. Consequently, further testing on the effects of heating columns within sub-frames is desirable to evaluate the capacity of a general framed structure to redistribute loads. The completion of the programme of column tests on the LBTF at Cardington would provide valuable information.

10.2.2 Software Development

Since the behaviour of steel columns in fire has been shown to be highly sensitive to thermal gradients, further VULCAN analyses of furnace tests should be paralleled with some level of CFD type analysis. This would allow predictions of the thermal assault on the test specimen, and validate the CFD models to provide thermal data for VULCAN allowing it to be used as a design tool by practising engineers. The process of information exchange between CFD software and VULCAN could be automated. In addition, an investigation into the applicability of statistical methods, such as the Monte-Carlo approach, to the problem of the lack of consistency of thermal assault should be performed.

The arc-length method should be fully integrated into the VULCAN code, so that post-limit-point behaviour can be followed. This should be done in a way that allows the method to be switched on when needed and controlled by user-interaction or by the use of an "intelligent" algorithm, to minimise run-times.

The ShowGrid program is a valuable tool so long as it is constantly updated in line with future developments of the VULCAN data-files. The tagged-block format of the input- and output-files goes some way to facilitate this, and this should be maintained with consideration given to future changes.

10.3 Concluding Remark

It is apparent that, as the level of axial restraint applied to a column increases, the temperature at which the maximum axial force is supported decreases. However, for columns that form part of a larger, framed building, the very members which provide this restraint also provide support for the column once it has become shorter than its original length. The column's axial load can be redistributed along alternative load

paths, and consequently, this should not be seen as a "failure" of the structure as a whole.

It has also been demonstrated that the VULCAN program is capable of accurately simulating complex behaviour shown by the Ulster test programme. Moreover, with the development of solution algorithms like the arc-length method, the number of problems to which this program is applicable will increase even further.

REFERENCES

[1] Eurofer, "Steel and fire safety – A global approach", (1990).

[2] Department of the Environment and The Welsh Office, "Approved document B, B/2/3/4 Fire Spread", HMSO, (1985).

[3] European Convention for Constructional Steelwork, "European recommendations for the fire safety of steel structures", Elsevier, Amsterdam, (1982).

[4] Ramberg, W. and Osgood, W., "Description of stress-strain curves by three parameters", National Advisory Committee for Aeronautics, Technical Note 902, (1942).

[5] Eurocode 3 Part 1.2, "Design of steel structures : General rules for structural fire design", Commission of the European Communities, (1993).

[6] Kirby, B.R. and Preston, R.R., "High temperature properties of hot-rolled structural steel for use in fire engineering design Studies", *Fire Safety Journal*, **13**, (1988), pp27-37.

[7] Mäkeläinen, P. & Outinen, J., "Results of the high-temperature tests on structural steels S235, S355, S350GD+Z and S420M", Compilation of Research Reports TeRT-95-03, TeRT-95-07 and TeRT-96-02, Helsinki University of Technology, (1998).

[8] International Iron and Steel Institute, "International Fire Engineering Design for Steel Structures : State of the Art", (1993).

[9] Sakumoto, Y., Yamaguchi, T., Ohashi, M. & Saito, H., "High temperature properties of fire-resistant steel for buildings", J. Struct. Engng., ASCE, **118 (2)**, (1992), pp392-407.

[10] Euler, L., "De curvis elastic - Appendix to 'Methodus inveniendi lineas curvas maximi minimive proprietate gaudentes'", Lausanne and Geneva, (1744).

[11] British Standards Institution, "BS5950 : Structural use of steelwork in buildings : Part 1 : Code of practice for design in simple and continuous construction", BSI, (1992).

[12] Eurocode 3, "Design of Steel Structures : Part 1.1 : General rules and rules for buildings", Commission of the European Communities, (1993)

[13] Wang, Y.C., Lennon, T. & Moore, D.B., "The behaviour of steel frames subject to fire", *J. Const. Steel Research*, (1994).

[14] Swanson, J., "Keynote Address", The eighth international ANSYS conference and exhibition, Pittsburgh, (1998).

[15] Hendriks, M.A.N., "On DIANA's software development environment", Proceedings of the second DIANA conference on computational mechanics, Amsterdam, (1997).

[16] El Zanaty, M.H. and Murray, D.W. "Non-linear finite element analysis of steel frames". *ASCE, J. Struct. Div.*, **109 (ST2)**, (1983), pp353-368.

[17] Saab, H.A. "Non-linear finite element analysis of steel frames in fire", PhD Thesis, University of Sheffield, (1990).

[18] Saab, H.A., & Nethercot, D.A., "Modelling steel frame behaviour under fire conditions", *Engineering Structures*, **13**, (1991), pp371-382.

[19] Najjar, S.R. "Three dimensional analysis of steel frames and sub-frames in fire", PhD Thesis, University of Sheffield, (1994).

[20] Najjar, S.R. & Burgess, I.W., "A non-linear analysis for three-dimensional steel frames in fire conditions", *Engineering Structures*, **18 (1)**, (1996), pp77-89.

[21] Bailey, C.G. "Simulation of the Structural Behaviour of Steel-framed Buildings in Fire", PhD Thesis, University of Sheffield, (1995).

[22] Bailey, C.G., Burgess, I.W. & Plank, R.J., "The lateral-torsional buckling of unrestrained steel beams in fire", *J. Const. Steel Research*, **36 (2)**, (1996), pp101-119.

[23] Bailey, C.G., Burgess, I.W. & Plank, R.J., "Structural simulation of fire tests on a full-scale composite building frame", SSRC IC/Brazil'96 - 5th Colloquium on Structural Stability, Rio de Janeiro, (1996).

[24] Bailey, C.G., Burgess, I.W. & Plank, R.J., "Analyses of the effects of cooling and fire spread on steel framed buildings", *Fire Safety Journal*, **26**, (1996), pp273-293.

[25] Leston-Jones, L.C. "The influence of semi-rigid connections on the performance of steel framed structures in fire", PhD Thesis, University of Sheffield, (1997).

[26] Leston-Jones, L.C., Burgess, I.W. & Plank, R.J., "The behaviour of real connections in steel framed construction in fire conditions", SSRC IC/Brazil'96 - 5th Colloquium on Structural Stability, Rio de Janeiro, (1996).

[27] Al Jabri, K. In Publication, PhD Thesis, University of Sheffield, (1999).

[28] Al Jabri, K., Lennon, T., Burgess, I.W. & Plank, R.J., "The behaviour of steel and composite beam-column connections in fire", Second World Conference on Structural Steel Design, San Sebastian, *J. Const. Steel Research*, **46 (1-3)**, (1998), Paper No. 180.

[29] Rose, P.S. In Publication, PhD Thesis, University of Sheffield, (1999).

[30] Rose, P.S., Bailey, C.G., Burgess, I.W. & Plank, R.J., "The influence of floor slabs on the structural performance of the Cardington frame in fire", Second World Conference on Structural Steel Design, San Sebastian, *J. Const. Steel Research*, **46 (1-3)**, (1998), Paper No. 181.

[31] Rose, P.S., Burgess, I.W., Plank, R.J., & Bailey, C.G., "The influence of floor slabs on the structural performance of composite frames in fire", Kerensky International Conference, Hong Kong, (1997), pp511-520.

[32] Huang, Z., Burgess, I.W. & Plank, R.J., "Layered slab elements in the modelling of composite frame behaviour in fire", Second International Conference on Concrete Under Severe Conditions, Tromsö, (1998), pp785-794.

[33] Huang, Z., Burgess, I.W. & Plank, R.J., "Influence of shear connectors on the behaviour of composite steel-framed buildings in fire", *J. Construct. Steel Research*, (in press).

[34] Huang, Z., Burgess, I.W. & Plank, R.J., "Non-linear analysis of reinforced concrete slabs subject to fire", *A.C.I. Structural J.*, **96 (1)**, (1999), pp127-135.

[35] Allam, A.M., Green, M.G., Burgess, I.W. & Plank, R.J., "Fire engineering design of steel framed structures - Integration of design and research", Second World Conference on Structural Steel Design, San Sebastian, *J. Const. Steel Research*, **46 (1-3)**, (1998), Paper No. 170.

[36] Franssen, J-M., & Dotreppe, J.C., "Fire resistance of columns in steel frames", *Fire Safety Journal*, **19**, (1992), pp159-175.

[37] "Structural Fire Engineering Investigation of Broadgate Phase 8 Fire, Steel Construction Institute, (1991).

[38] First Cardington Conference, "First results from the Large Building Test Facility", 16-17 November (1994).

[39] Second Cardington Conference, "Fire, static & dynamic tests at the Large Building Test Facility", 12-14 March, (1996).

[40] Simms, W.I., "An experimental investigation of axially restrained steel columns in fire", PhD Thesis, University of Ulster, (1997).

[41] Randall, M.J. "The effects of axial restraint on the behaviour of steel columns in fire" , PhD Thesis, University of Ulster, (1998).

[42] Shanley, F.R., "Inelastic Column Theory", *J. Aero. Sci.*, **14 (5)**, (1947), pp261-268.

[43] Shepherd, P.G., Burgess, I.W., Plank, R.J. & O'Connor, D.J., "The performance in fore of restrained steel columns in multi-storey construction", Kerensky International Conference, Hong Kong, (1997), pp333-342

[44] Ali, F., O'Connor, D.J., Simms, W.I., Randall, M.J., Shepherd, P.G. & Burgess, I.W., "The effect of axial restraint on the fire resistance of steel columns", Second World Conference on Structural Steel Design, San Sebastian, *J. Const. Steel Research*, **46 (1-3)**, (1998), Paper No. 71.

[45] Randall, M.J., Ali, F.A., O'Connor, D.J., "Experimental reports on axially restrained columns", Internal Report, University of Ulster, (1998).

[46] Ayrton, W.E. & Perry, J., "On Struts", *The Engineer*, **62**, (1886), pp464.

[47] Robertson, A., "The strength of struts", *I.C.E. Selected Engineering Papers*, **28**, (1925).

[48] Lennon, T. & Simm, C., "Elevated temperature column tests : Results from Phase 1", Building Research Establishment Internal Note N201/93, (1993).

[49] Lennon, T. & Simm, C., "Elevated temperature column tests : Results from Phase 2", Building Research Establishment Internal Note N201/93, (1993).

[50] Liu, X.R., "The effect of semi-rigid connections on the performance of non-sway steel-framed structures", MPhil Thesis, University of Sheffield, (1998).

[51] Rose, P.S., Burgess, I.W. & Plank, R.J., "A slab thickness survey of the Cardington test frame", Research Report DCSE/96/F/7, University of Sheffield, (1996).

[52] British Standards Institution, "BS476 : Method for determination of the fire resistance of elements of construction : Part 20", BSI, (1987).

[53] Al-Jabri, K.A., Burgess, I.W. & Plank, R.J., "Behaviour of steel and composite beam-to-column connections in fire", Research Report DCSE/98/F/7, University of Sheffield, 1998.

[54] Chen W. F. & Lui E. M., "Stability design of steel frames : 3.7 Solution algorithms for non-linear analysis", (1971).

[55] Crisfield, M.A., "Iterative solution procedures for linear and non-linear structural analysis", Transport and Road Research Laboratory Report 900, (1979).

[56] Hinton, E & Owen, D.R.J., "A simple guide to finite elements", Pineridge Press, (1980).

[57] Crisfield, M.A., "Variable step lengths for non-linear structural analysis", Transport and Road Research Laboratory Report 1049, (1979).

[58] Furumura, F. and Shinohara, Y., "Inelastic behaviour of protected steel beams and frames in fire", Report of the Research Laboratory of Engineering Materials, **3**, (1978), pp1-14.

[59] Lawson, R.M., "Behaviour of steel beam-to-column connections in fire", *The Structural Engineer*, **68 (14)**, (1990), pp263-271.

COMPUTER SOFTWARE REFERENCE

Below is a list of computer software previously referenced in this thesis. Each program has been developed at the Department of Civil & Structural Engineering of the University of Sheffield, UK.

VULCAN Various, 1988 - Present

VULCAN is the non-linear finite element analysis code developed at the University of Sheffield and based on the INSTAF program. It is used to analyse the effects of elevated temperatures on three-dimensional steel and composite structures.

INSTAF Interface Emberey, C. & Swallow, S., 1996

A pre-processor to create VULCAN input files, especially those representing multi-storey framed structures with grid-like beam-column arrangements.

MAKEDAT Shepherd, P.G., 1996

A conversion program initiated from the INSTAF Interface, which takes the output from the INSTAF Interface program and converts this into a VULCAN input file.

DATAMOD Plank, M., 1996

A post processor program, written in Visual Basic, which takes a VULCAN output file and plots graphs of specified nodal displacements or internal forces.

SHOWGRID Shepherd, P.G., 1996 - Present

A graphical tool, written in Visual Basic, which displays and amends both VULCAN input- and output-files. This is mainly used for validation of data-files and graphical presentation of results. An in-depth description of this program is given in Appendix B.

A Appendix A – Input- And Output-File Format

The input file used by the VULCAN program is an ASCII text file named "s.dat", which is read by the program to define the geometry, material properties and temperature profiles on which to perform analysis. This appendix describes the new format for this file, introduced by the author, in order to incorporate future developments to the VULCAN program.

A.1 General Description

Due to the origins of the VULCAN code and the nature of academic software development, the format of the input file was unstructured and undocumented. This made preparation of input files difficult, and more importantly, errors were extremely difficult to locate. It was therefore decided to completely change the format of the input file to separate out the different kinds of information into manageable blocks of data. In this way, a problem with member connectivity, for example, could more easily be located in the member connectivity data-block.

In addition, a separate, graphical interface program called SHOWGRID has been created to read an input file and display the corresponding structure on the screen. In this way, a wrongly defined input file, which may still be possible to analyse, but represents the desired structure incorrectly, can usually be identified and the error corrected. The operation of this graphical interface is described in Appendix B.

Similarly, the output file created by VULCAN, which contains the results of analysis, has been re-formatted to reflect the changes in input file format. Output files are often very large, and the newly formatted version allows specific results to be located quickly. Information about the structure on which the analysis has been performed is now included in the output file. In this way, only the output file needs to be archived on disk in order to allow further analyses at a later date. This also allows the SHOWGRID program to read these new output files and to display displacement results as a series of animated pictures. This can be a very powerful tool in understanding the behaviour of the structure.

In order to maintain backwards compatibility, both the VULCAN and SHOWGRID programs have the ability to identify and read old-style input files, so archived data files can still be used for research.

A.1.1 Input File Format

The general format of the input file is a series of blocks of text and is loosely based on the tagging system used successfully in HTML. The start of each block is identified by a header tag in angled brackets "<>" containing descriptive text. Then follow a number of lines of data, the format of which is specific to that particular block. As an error-check, the end of the block is identified by the same identifying word used as a footer tag enclosed in curly brackets "{}". In this way, if the input data is not as expected, the end-of-block marker may not be read when expected and an error is identified by the VULCAN (or SHOWGRID) program. This prohibits a corrupt data file from being analysed and removes the possibility of erroneous results being accepted as valid.

A.1.2 Output File Format

When the VULCAN program performs an analysis, an output file is generated, usually named "s.1". The format of this file is much the same as that of the input file. In fact, the whole of the input file, except the temperature data, is copied straight to the initial section of the output file. In this way, an output file contains sufficient information to reconstruct the corresponding input file, allowing archived output files to be re-analysed.

After the repeat of the input blocks, the output file contains sets of three output blocks, each stating the calculated temperatures, displacements and forces. Before each displacement block there is some informative text, giving details of the achievement of the convergence criteria for that particular temperature step. If no convergence was achieved, the displacements and forces are not printed, and the next temperature step is displayed.

In this way, future developments to the program can be incorporated, by defining a new output block, containing slab-cracking information for example, without causing other programs like SHOWGRID to fail. It is also important to give the output blocks, which contain analysis results, different names from any input file blocks, which contain different information. This ensures that no confusion will ever arise, and no third-party programs, like SHOWGRID, will have problems distinguishing the type of data held in a block.

A.1.3 Remarks For Future Development

The blocks may occur in the data file in any order, with the exception of the <HEADER> block, which must occur on the first line of the data file in order to identify the file as a newly formatted VULCAN input file. However, it is recommended that the blocks be defined in a sensible order, so that anyone reading the file is able to follow the development of the structure from definition of size, through geometry and material properties, to loading and temperature data. It is also recommended that the data within each block be indented from the left edge of the file and that blank lines are placed between blocks. In this way, the separate blocks are easily distinguishable from each other.

Since data is only stored between the header and footer tags of each block, any amount of text can be placed between blocks. This gives the opportunity for inclusion of further descriptive text or comments, which may be of use in identifying and annotating the file at a later date. For instance, the line before the start of a block could be used to describe the form of the data held within the block. The obvious exception to this is the <HEADER> block, which must be the first line of the file.

It is intended that backwards compatibility be maintained at all times. Therefore, if some future development leads to, for example, to the inclusion of layered slab elements, these elements should be placed in a newly defined data block. In this way, the VULCAN program can search for the layered slab block, and if it is not found, can assume the input file is of an older type and consequently search for the standard slab block. If this system is followed, both the VULCAN and SHOWGRID programs will always be able to use data files created for any version of the program.

A.2 Required Blocks

A number of blocks need to be present in order for an analysis to be computable. This section contains a sub-section for each required block with the actual names of the variables shown in the blocks, and a description below. The text that occurs as part of a data file is shown in Italics, with descriptive text in normal style.

A.2.1 Header

<HEADER>

Head(1) *Head(2)* ... *Head(9)*

{HEADER}

This block simply holds a single-line text description of the input file. This descriptive text is echoed into the output file and can help to identify old files stored on disk. The text description must not contain mathematical operators such as "+" and must be less than 72 characters long.

Within the program the header is stored as an array of nine elements, each containing eight text characters (hence 9 x 8 = 72 characters maximum). This was done to maintain compatibility with the old program code but does not affect the way the text should look in the data file; it should be treated simply as a line of text.

One special consideration is that the <HEADER> section is also used to identify the file as a *new* input file type. If it is not present, the program assumes an <u>old</u> type of input file is present and reads the rest of the file as such, using the first line of the file as header text.

A.2.2 Program Control

<PROGRAM CONTROL>

iref	*irco*	*ic*		
fl1	*fl2*			
lincr	*flinc*	*tolinc*	*tol*	*unit*

{PROGRAM CONTROL}

These variables are a remnant of the original INSTAF program, which control loading increments. Although they are still used in the program, their compatibility with recent developments to the program has not been checked. As such, they should be regarded as obsolete and their default values shown below should always be used.

iref	= flag to give results in local co-ordinates if non-zero	= 0
irco	= load increment counter	= 0
ic	= load counter	= 0
fl1	= joint load factor	= 1.0
fl2	= member load factor	= 1.0
linrc	= load increment	= 1

fl1 = joint load increment factor = 0.0

tolinc = tolerance increment = 1

tol = tolerance = 0.005

unit = unit multiplication factor = 1.0

A.2.3 Structure Information

<STRUCTURE INFORMATION>

nj	*nfe*	*ne*	*nfj*
itlim	*expand*	*ntemp*	*ieq*
ndxst	*ndmt*	*ndrt*	*ndtemp*

{STRUCTURE INFORMATION}

The first line specifies the number of joints (nodes) present in the structure, the number of flexural elements (steel + spring elements), the total number of elements and the number of flexible joints (springs).

The second line specifies the maximum number of iterations to be used and the expansion coefficient. If the expansion coefficient is set to zero, the EC3 quadratic equation is used to specify how the expansion coefficient for steel changes with temperature. If a negative value is set, then the material is assumed to have no thermal expansion. This is illogical, but is done in this way to retain compatibility with old data files.

The second line also specifies which temperature profile is to be used. This is an integer between 1 and 13. Profiles 1-6 use a corresponding number of temperatures in the <TEMPERATURE DATA> block and map those temperatures to levels on the major-axis cross-section using linear interpolation as shown in Fig. 141. Profile 10 takes three values and specifies stepped temperatures for the top flange, web and bottom flange respectively. Temperature profile 13 allows the temperature of each segment of the cross-section to be specified exactly and is usually used for matching test data to analyses. The remaining profiles 7, 8, 9, 11, 12 and any higher integer are currently unassigned and can be used for future development.

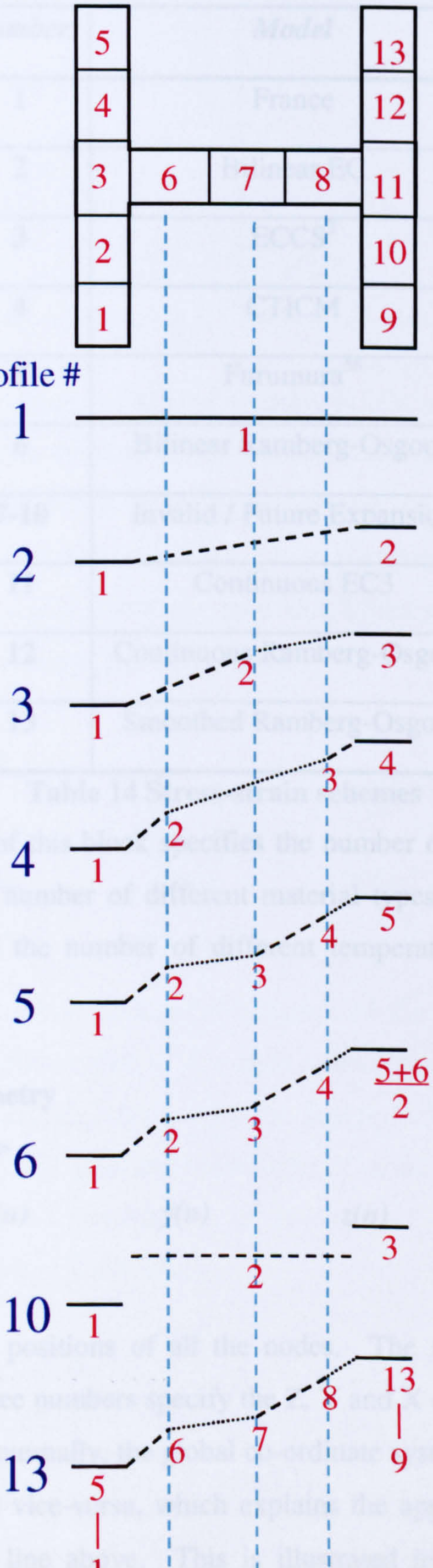

Fig. 141 Temperature profile

The last number on the second line specifies which stress-strain model is to be used for steel at elevated temperatures according to the scheme shown in Table 14.

Number	*Model*
1	France
2	Bilinear EC
3	ECCS[3]
4	CTICM
5	Furumura[58]
6	Bilinear Ramberg-Osgood
7-10	Invalid / Future Expansion
11	Continuous EC3
12	Continuous Ramberg-Osgood
13	Smoothed Ramberg-Osgood

Table 14 Stress-strain schemes

The third and last line of this block specifies the number of different beam-column cross-section sizes, the number of different material types, the number of residual stress distributions and the number of different temperature profiles of the type previously specified.

A.2.4 Nodal Geometry

<NODAL GEOMETRY>

n *x(n)* *y(n)* *z(n)*

{NODAL GEOMETRY}

This block defines the positions of all the nodes. The first number is the node number and the next three numbers specify the Z, Y and X co-ordinates of that node. It should be noted that internally, the global co-ordinate system stores the Z-values in an array called X() and vice-versa, which explains the apparent mismatch between this statement and the line above. This is illustrated in the manifold shown in Fig. 142.

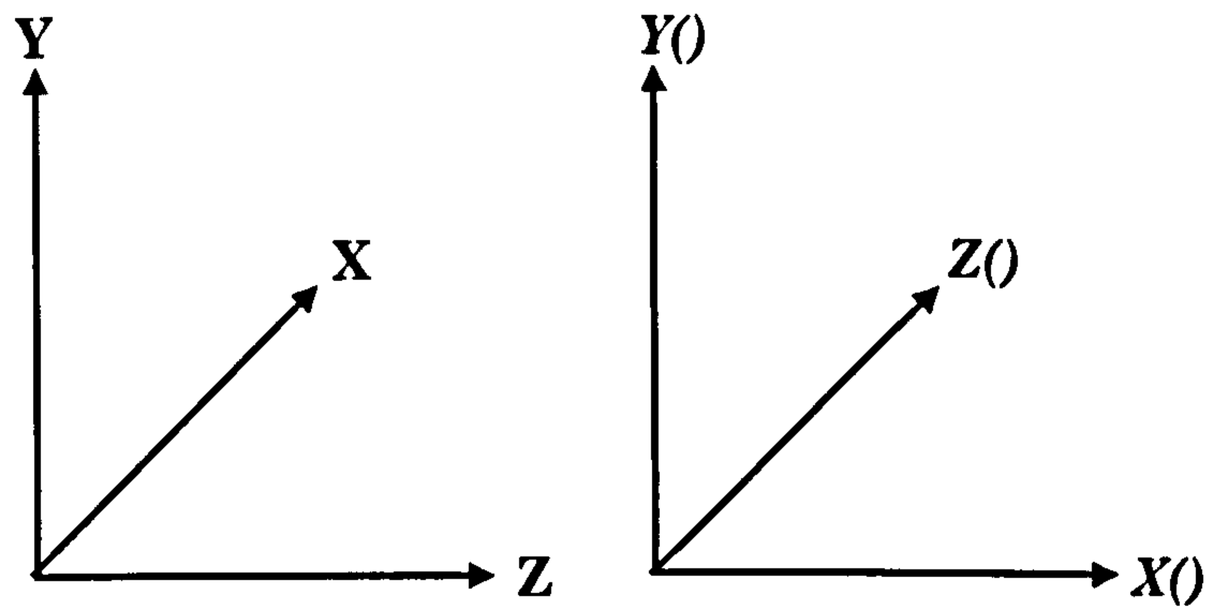

Global Axes **Internal Arrays**

Fig. 142 Co-ordinate system of structure, and program arrays

The number of co-ordinates must match up with the number of nodes specified in the <PROGRAM CONTROL> block. If this is not the case, an "ERROR : {PROGRAM CONTROL} block not found}" will occur. It is also preferable for readability to number the nodes sequentially, although since each triplet of co-ordinates is labelled with its node number, this is not strictly necessary.

A.2.5 Section Sizes

<SECTION SIZES>

n	*h(n)*	*w(n)*	*tf(n)*	*tw(n)*

{SECTION SIZES}

This block specifies the cross-sectional dimensions of the beam elements. Each is identified by a section type number *n*. For each *n* the depth, *h(n)* and the width *w(n)* of the I-Section are specified, followed by the flange and web thicknesses. Each definition must be on a single line, and the number of definitions must be equal to the number of different section types *ndxst* specified in the <STRUCTURE INFORMATION> block.

A.2.6 Material Properties

<MATERIAL PROPERTIES>

n	*ey(n)*	*ep(n)*	*eult(n)*	*ys(n)*	*yps(n)*	*ults(n)*

{MATERIAL PROPERTIES}

This block specifies the ambient temperature stress-strain curve for steel in a similar fashion to the section sizes. Each line specifies one material type and the total number of material types must equal *ndmt* as specified in the

<STRUCTURE INFORMATION> block. Each material is defined by a tri-linear stress-strain curve in the manner shown in Fig. 143.

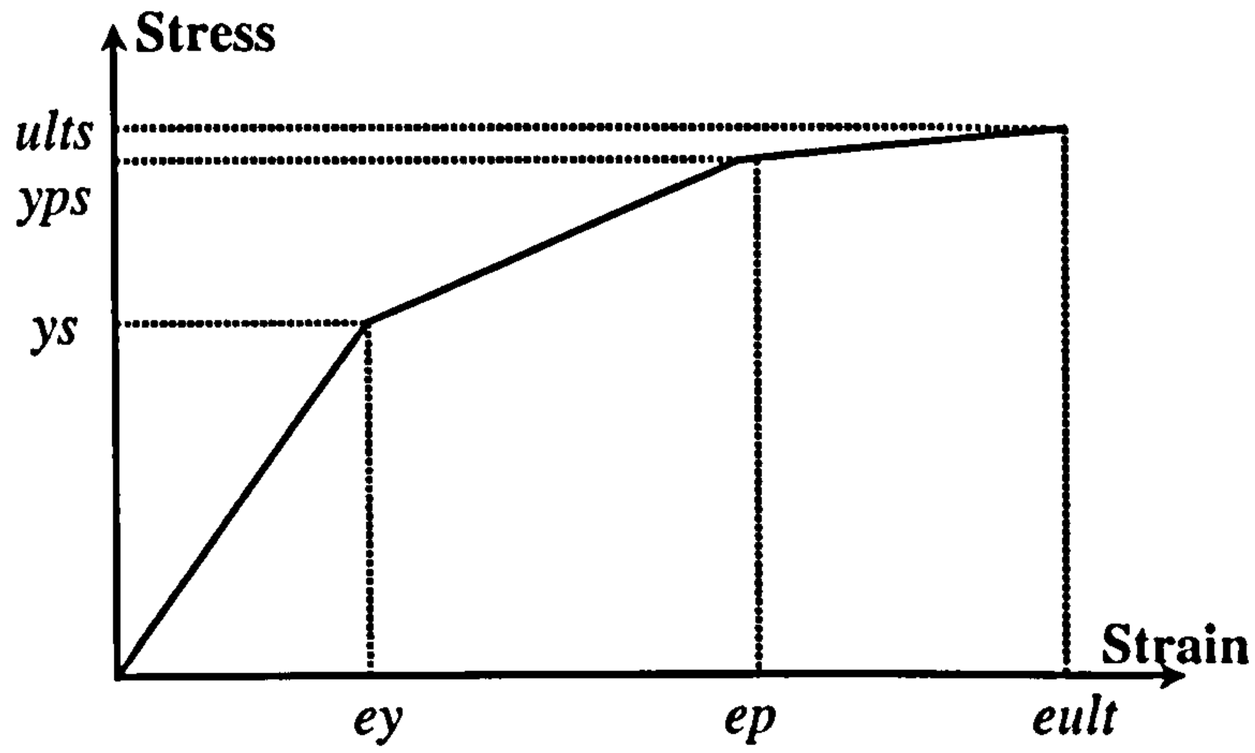

Fig. 143 Definition of ambient temperature stress / strain curve

A.2.7 Residual Stresses

<RESIDUAL STRESSES>

n epr(n,1) epr(n,2) epr(n,3) epr(n,4) epr(n,5)

{RESIDUAL STRESSES}

This block specifies the ambient temperature residual stress pattern for steel in a similar fashion to the section sizes. Each line specifies one residual stress pattern and the total number of patterns must equal *ndrt* as specified in the <STRUCTURE INFORMATION> block.

Each material is defined by five stress values in the manner shown on Fig. 144, with linear interpolation used to define values within the section. In reality, the residual stress pattern must be self-equilibrating in terms of axial force and bending moment about both principle axes, and should be symmetric about both axes. The usual way of guaranteeing this is for *epr(1)=epr(5)=epr(3)=-epr(2)=-epr(4)*.

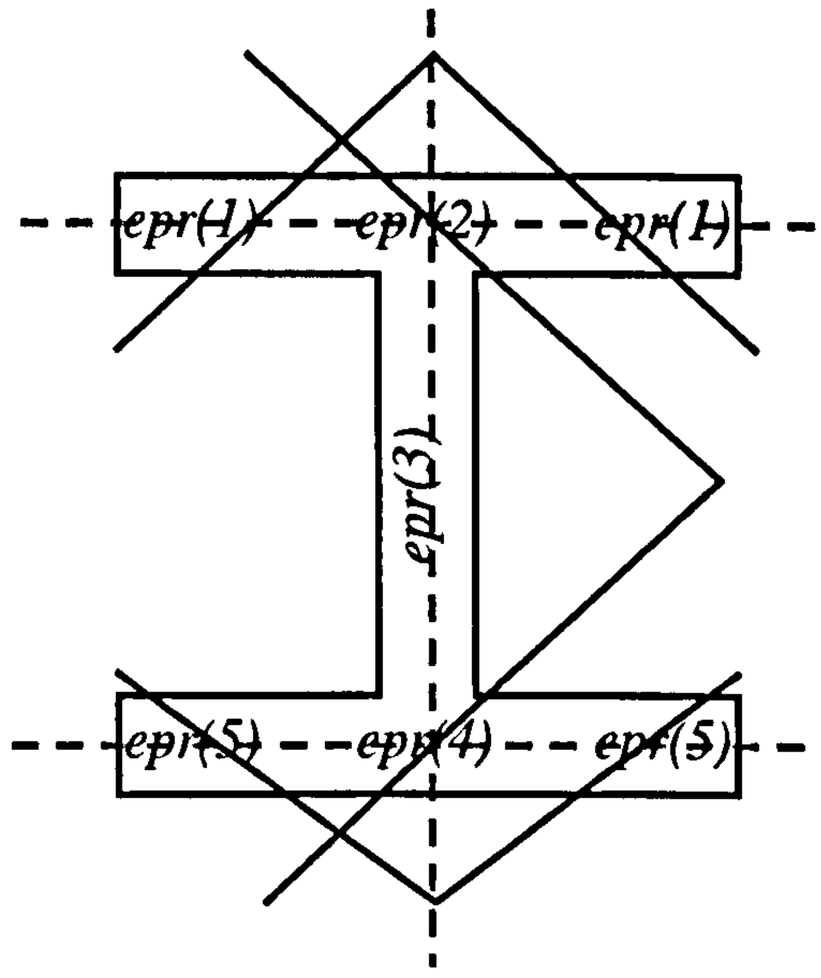

Fig. 144 Residual stress definition

A.2.8 Member Data

<MEMBER DATA>

m itype(m) ypoint(m)

m nod(1,m) nod(2,m) nsr(m) mxst(m) mt(m) mrt(m) mtemp(m) g(m)

m itype(m) ypoint(m)

m nodp(1,m) nodp(2,m) nodp(3,m) nodp(4,m)

{MEMBER DATA}

This block defines the steel and concrete members. Each member has two lines of data.

The first line defines the element number, the type of element as shown in Table 15 and the offset distance normal to the major axis of the connecting nodes from the element centroid. For elements in beam members, the *ypoint* value is usually given as half the depth of the beam section plus half the thickness of the slab plus the depth of any decking. Thus, the node is placed at the centre of the slab.

If a member is defined as a column, then it is treated exactly like a beam, except that extra care is taken in applying twist along its length, because of an anomaly in the transformation matrices. A heated slab element is similarly the same as a standard slab element, except that its Young's modulus value is reduced in a crude simulation of the effects of heating. In the current version of the program, at the time of writing, the slab elements are layered and this is no longer necessary.

itype	*Member*
1	Beam
2	Slab
3	Column
4	Hot Slab

Table 15 Member type values

The second line of data defines the element number and the start and end node numbers of the element. The next number is zero if the element is part of a beam or column. If non-zero, the element is defined as a spring element of a given type selected from those shown in Table 16. It should be noted that types 1 and 2 are specific connections based on some tests conducted by the SCI[59], and should not be used for other connections.

Number	*Spring Type*
1	Extended End-plate
2	Flush End-plate
3	Pinned
4	Rigid
5	Semi-Rigid
6	Pinned Axial
7	Rigid Axial
8	Semi-Rigid Axial

Table 16 Spring element type definition

Next, the cross-section, stress-strain and residual stress profiles of the element are defined, in terms of the reference numbers defined in the relevant blocks as described above. Then the temperature profile number of the element is defined, along with the rotation of the element about its axis in degrees. This rotation angle is defined as the angle between the plane of the web and the Y-axis. In this way, a column can be

orientated such that an adjoining beam meets either the flange or the web. However, if a column's axis lies along the Y-axis, this definition is ambiguous. Therefore, in this case, the angle is measured between the plane of the web and the Z-axis. Thus, if a column lies along the Y-axis, and a beam lies along the Z-axis, a rotation value of zero will result in the beam connecting to the flange. Conversely, a rotation value of 90° will result in the beam framing in to the column's web.

For slab elements, the *ypoint* value defines the thickness of the slab. The second line of data simply defines the element number and the four corner nodes, which must be defined anticlockwise when viewed from above.

A.2.9 Boundary Conditions

<BOUNDARY CONDITIONS>

n	*kode(n)*	*kode1(n)*

{BOUNDARY CONDITIONS}

In this block, the boundary conditions for each node are defined for each of the eleven degrees of freedom. First the node number is stated, followed by two blocks of 0's or 1's, which define the degree of freedom as free, or fixed, respectively. The degrees of freedom are stated in the order shown in Table 17 for historical, and not logical reasons.

A.2.10 Joint Loads

<JOINT LOADS>

node	*u*	*v*	*w*	*ry*	*rx*	*rz*	*rzz*
0	*0*	*0*	*0*	*0*	*0*	*0*	*0*

{JOINT LOADS}

This block defines the joint loads present in a structure. The first number states the node, the following numbers define the load in the Z, Y and X directions, the moments about the Y, X and Z axes and a warping bi-moment about the length of the member.

Any number of lines of load data may be defined, and since the number is not specified elsewhere in the input file, the program continues to read load data until a line of zeros is found.

Degree Of Freedom	*Description*
1	Strain along Y axis
2	Strain along X axis
3	Rotation about Z axis
4	Twisting along length
5	Warping
6	Displacement in Z axis
7	Displacement in Y axis
8	Displacement in X axis
9	Rotation about X axis
10	Rotation about Y axis
11	Strain along Z axis

Table 17 Degrees of freedom

A.2.11 Temperature Data

<TEMPERATURE DATA>

n	*tem2(n,1)*	*tem2(n,2)*	*tem2(n,3)*	...
0	*0*	*0*	*0*	...

{TEMPERATURE DATA}

This block specifies the temperature data for a specific profile number *n*. The number of temperature values that must be specified depends on the chosen profile type as shown in .

After entries for the correct number of profiles (*ndtemp*) have been read, an analysis is performed, and the process is then repeated. When a line containing *ndtemp* zeros

is read, automatic temperature increments are calculated from that point on, using linear interpolation.

A.2.12 End Of File

{END OF FILE}

Due to differences in the handling of disk files between versions of FORTRAN, this end-of-file block must be present, with a new-line character at the end. This indicates that the search for a specific block has failed, and the program can act accordingly. Any text after this marker is ignored by the program.

Certain DOS-based text editors (such as MultiEdit) may strip the final new-line character from the end of a file. Therefore, it is recommended that a character such as a period ".", or some descriptive text is placed on the line after the end-of-block marker. In this way, the text editor can strip the final new-line character from the file without causing the program to fail.

A.3 Optional Blocks

This section defines blocks that can be present in a data file to further specify the analysis. However, these blocks are not compulsory, since each has a default specification, which is used if the blocks are not present.

A.3.1 Rotational Stiffness

<ROTATIONAL STIFFNESS>

semirigd

{ROTATIONAL STIFFNESS}

This specifies the rotational spring stiffness of a semi-rigid spring in the current units, if a spring of type 5 or 8 is chosen, as defined in Table 16. If this block is not present, a value of 10^{12} is assumed.

A.3.2 Axial Stiffness

<AXIAL STIFFNESS>

axisrigd

{AXIAL STIFFNESS}

This specifies the axial stiffness of a spring, if a spring of type 6, 7 or 8 is chosen, as defined in Table 16. If this block is not present, a value of 13000 is assumed.

A.3.3 Display Temperatures

<DISPLAY TEMPERATURES>

ishowtem(1)

ishowtem(2) ishowtem(3) ...

{DISPLAY TEMPERATURES}

As an analysis progresses, current reference temperatures are displayed on the screen. This block allows specific temperatures to be displayed. The first line contains the number of temperatures to be displayed. The second line then contains that number of pairs of values. The first number in each pair defines the profile number and the second defines which of the 13 segment temperatures within the cross section is to be displayed. If this block is not present, the middle of the bottom flange of the highest numbered temperature profile is used.

A.3.4 Display Deflections

<DISPLAY DEFLECTIONS>

ishowdef(1)

ishowdef(2) ishowdef(3) ...

{DISPLAY DEFLECTIONS}

This block allows the displacements of various nodes to be displayed on the screen as the analysis progresses. The first number specifies how many displacements are to be shown. The second line contains the numbers of nodes whose displacements are to be displayed.

In adition to being displayed on the screen, a separate output file is created named "NODExxxx.def", which contains the temperature and displacement values for the relevant node, where *xxxx* indicates the node number. The reference temperature used in this file is the first display temperature defined in the previous section.

This block should be used to create output files which contain the displacements of nodes of interest. These files can easily be imported into a spreadsheet program to

plot temperature-displacement graphs. If this block is not present, no displacements are displayed and no files are created.

A.3.5 Display Forces

<DISPLAY FORCES>

ishowfrc(1)

ishowfrc(2) *ishowfrc(3)* ...

{DISPLAY FORCES}

This block is similar to the *<DISPLAY DEFLECTIONS>* block, except that element numbers are specified and their internal forces are displayed. If this block is present, corresponding output files are created, named "MEMBxxxx.frc".

A.4 Output Blocks

This section describes the blocks that appear only in the output file, which have not been described above.

A.4.1 Header

<HEADER>OUTPUT

Head(1) *Head(2)* ... *Head(9)*

{HEADER}

This block simply holds the single-line text description of the input file. The only difference between this and the input file <HEADER> block is the word "OUTPUT" after the block. This is used to signal to SHOWGRID that the file contains displacement data in addition to the structure data.

A.4.2 Temperatures

<TEMPERATURES>

n *tem2(n,1)* *tem2(n,2)* *tem2(n,3)* ... *tem2(n,13)*

{TEMPERATURES}

This block defines the temperatures comprising each temperature profile, to which the following nodal displacement and internal force blocks relate. The first number

is the number of the temperature profile and the next thirteen numbers are the temperatures. The temperatures of all thirteen positions on the cross-section are always displayed, allowing the automatic linear interpolation of temperatures, for example across a flange, to be checked.

A.4.3 Nodal Displacements

<NODAL DISPLACEMENTS>

n	*disp(1)*	*disp(2)*	*disp(3)*	...	*disp(11)*

{NODAL DISPLACEMENTS}

The first number states the node number and the next eleven numbers show the displacement of that node in each of the eleven degrees of freedom. The degrees of freedom are in the order Numbers 6 – 11 and then 1 – 5 according to Table 17. This ensures that the Z, Y and X displacements are easily found at the start of the line of data.

A.4.4 Internal Forces

<INTERNAL FORCES>

m	*iii*	*d(1)*	*d(2)*	*d(3)*	*d(4)*	...	*d(11)*
	jjj	*d(12)*	*d(13)*	*d(14)*	*d(15)*	...	*d(22)*

{INTERNAL FORCES}

For each steel beam-column or spring element, two lines of output data are generated to show the internal force resultants for each node. The variable *m* indicates the element number, and *iii* indicates the number of the start node. The next eleven numbers show the internal force resultants at that node, in each of the eleven degrees-of-freedom. The order of these degrees of freedom are as for the *<NODAL DISPLACEMENTS>* block. The next line contains the same data (without the element number) for the end node, numbered *jjj*.

After writing this block, the analysis moves on to the next temperature step. Thus the next block present in the file is the *<TEMPERATURES>* block for the next step.

A.5 Example Files

Section A.5.1 presents a listing of an example input file. This particular file represents an 18-element steel column with a spring element at either end, which was used to model the 152x152x23UC Ulster test column. The applied load is 396kN (load ratio 0.6) and the axial restraint stiffness is 34kN/mm (α= 0.1).

The only difference between the text shown here and the data file actually used is that the temperature data has been reduced to save space. The notes that appear outside some blocks (e.g. the <AXIAL STIFFNESS> block) actually occur in the data file to aid readability.

Section A.5.2 contains an example of the blocks which occur in output files. This example is taken from an Ulster test column with full rotational restraint. Again, the file has been reduced to save space, and the edits have been clearly indicated.

A.5.1 S.Dat

```
<HEADER>
     Ulster Test Column 152x152x23UC with load ratio 0.6 and alpha value 0.1
{HEADER}

<PROGRAM CONTROL>
     0    0    0
     1.0      1.0
     1      0.0     0.005     0.00001     1.0
{PROGRAM CONTROL}

<STRUCTURE INFORMATION>
     21   20   20    2
     100      0.0      13      12
     1    1    1    9
{STRUCTURE INFORMATION}

<NODAL GEOMETRY>
     1          0.00       0.000       0.000
     2          1.00       0.000       0.000
     3        100.00       0.000       0.347
     4        200.00       0.000       0.684
     5        300.00       0.000       1.000
     6        400.00       0.000       1.286
     7        500.00       0.000       1.532
     8        600.00       0.000       1.732
     9        700.00       0.000       1.879
    10        800.00       0.000       1.970
    11        900.00       0.000       2.000
    12       1000.00       0.000       1.970
```

```
    13      1100.00      0.000      1.879
    14      1200.00      0.000      1.732
    15      1300.00      0.000      1.532
    16      1400.00      0.000      1.286
    17      1500.00      0.000      1.000
    18      1600.00      0.000      0.684
    19      1700.00      0.000      0.347
    20      1799.00      0.000      0.000
    21      1800.00      0.000      0.000
{NODAL GEOMETRY}

<SECTION SIZES>
     1     155.1     154.7      7.8     4.2
{SECTION SIZES}
Taken from measured data

<MATERIAL PROPERTIES>
     1     0.001528571     0.5     0.9     321.0     321.0     321.0
{MATERIAL PROPERTIES}
Taken from coupon test

<RESIDUAL STRESSES>
     1     0.0     0.0     0.0     0.0     0.0
{RESIDUAL STRESSES}

<MEMBER DATA>
     1    1     0.0
     1    1    2    3    1    1    1    1     0.0
     2    1     0.0
     2    2    3    0    1    1    1    1     0.0
     3    1     0.0
     3    3    4    0    1    1    1    1     0.0
     4    1     0.0
     4    4    5    0    1    1    1    2     0.0
     5    1     0.0
     5    5    6    0    1    1    1    2     0.0
     6    1     0.0
     6    6    7    0    1    1    1    3     0.0
     7    1     0.0
     7    7    8    0    1    1    1    3     0.0
     8    1     0.0
     8    8    9    0    1    1    1    4     0.0
     9    1     0.0
     9    9   10    0    1    1    1    4     0.0
    10    1     0.0
    10   10   11    0    1    1    1    5     0.0
    11    1     0.0
    11   11   12    0    1    1    1    5     0.0
    12    1     0.0
    12   12   13    0    1    1    1    6     0.0
    13    1     0.0
```

```
13   13   14    0    1    1    1    6    0.0
14    1     0.0
14   14   15    0    1    1    1    7    0.0
15    1     0.0
15   15   16    0    1    1    1    7    0.0
16    1     0.0
16   16   17    0    1    1    1    8    0.0
17    1     0.0
17   17   18    0    1    1    1    8    0.0
18    1     0.0
18   18   19    0    1    1    1    9    0.0
19    1     0.0
    19   19   20    0    1    1    1    9    0.0
    20    1     0.0
    20   20   21    6    1    1    1    9    0.0
{MEMBER DATA}

<AXIAL STIFFNESS>
     3.4D4
{AXIAL STIFFNESS}
This represents an alpha value of 01

<BOUNDARY CONDITIONS>
     1    11111    111111
     2    11111    010000
     3    11100    010000
     4    11100    010000
     5    11100    010000
     6    11100    010000
     7    11100    010000
     8    11100    010000
     9    11100    010000
    10    11100    010000
    11    11100    010000
    12    11100    010000
    13    11100    010000
    14    11100    010000
    15    11100    010000
    16    11100    010000
    17    11100    010000
    18    11100    010000
    19    11100    010000
    20    11111    010000
    21    11111    111111
{BOUNDARY CONDITIONS}

<JOINT LOADS>
    20    -396000.0     0.0     0.0     0.0     0.0     0.0     0.0
     0          0          0       0       0       0       0       0
{JOINT LOADS}
This represents a load ratio of 0.6
```

```
<DISPLAY TEMPERATURES>
     1
     2     7
{DISPLAY TEMPERATURES}

<DISPLAY DEFLECTIONS>
     2
     11    20
{DISPLAY DEFLECTIONS}

<DISPLAY FORCES>
     1
     20
{DISPLAY FORCES}



<TEMPERATURE DATA>
    1          20.308     20.034     23.759     as such for all thirteen positions
    2          22.058     24.658     27.259     as such for all thirteen positions
    3          27.807     29.282     30.758     as such for all thirteen positions
    4          34.471     34.062     33.653     as such for all thirteen positions
    5          29.636     29.593     29.550     as such for all thirteen positions
    6          24.801     25.124     25.447     as such for all thirteen positions
    7          20.983     21.979     22.975     as such for all thirteen positions
    8          23.015     24.627     26.239     as such for all thirteen positions
    9          24.032     25.951     27.870     as such for all thirteen positions
```

These nine profiles are defined many times, each with higher temperature values taken from the test results as the column is heated. The data continues up to around 600°C at which point linear interpolation is initiated by the following line:

```
    0          0.0        0.0        0.0        as such for all thirteen positions
{TEMPERATURE DATA}

{END OF FILE}
.
```

A.5.2 S.1

```
<HEADER>OUTPUT
          Ulster Test Column 127x76x13UB (14UB13) with RIGID Connections
{HEADER}
```

The input file is echoed exactly, with the blocks in the order in which the program reads them.

Then the file outputs sets of the three results blocks, an example of which can be seen below:

```
<TEMPERATURES>  Load Increment # 17
      1   114.056 122.007 129.958 137.909 as such for all thirteen positions
      2   123.028 126.527 130.025 133.523 as such for all thirteen positions
      3   132.000 131.046 130.091 129.137 as such for all thirteen positions
      4   157.916 145.266 132.617 119.968 as such for all thirteen positions
      5   165.888 150.449 135.010 119.570 as such for all thirteen positions
      6   173.860 155.631 137.402 119.173 as such for all thirteen positions
      7   156.031 146.811 137.590 128.370 as such for all thirteen positions
      8   104.430 118.806 133.182 147.558 as such for all thirteen positions
      9    78.629 104.804 130.978 157.153 as such for all thirteen positions
{TEMPERATURES}


     ITERATION NO.    7    LOAD TOLERANCE = 0.000008    DISPL. TOLERANCE  =  0.000000

<NODAL DISPLACEMENTS>  Load Inc # 17  Iteration #  8
    1      0.0000      0.0000      0.0000      as such for all 11 degrees of freedom
    2      0.0000      0.0000      0.0000      as such for all 11 degrees of freedom
    3      0.0773      0.0000     -0.0257      as such for all 11 degrees of freedom
    4      0.1565      0.0000     -0.1086      as such for all 11 degrees of freedom
    5      0.2406      0.0000     -0.2408      as such for all 11 degrees of freedom
    6      0.3248      0.0000     -0.4135      as such for all 11 degrees of freedom
    7      0.4138      0.0000     -0.6161      as such for all 11 degrees of freedom
    8      0.5028      0.0000     -0.8372      as such for all 11 degrees of freedom
    9      0.5995      0.0000     -1.0420      as such for all 11 degrees of freedom
   10      0.6962      0.0000     -1.1950      as such for all 11 degrees of freedom
   11      0.7910      0.0000     -1.2911      as such for all 11 degrees of freedom
   12      0.8858      0.0000     -1.3249      as such for all 11 degrees of freedom
   13      0.9787      0.0000     -1.2914      as such for all 11 degrees of freedom
   14      1.0717      0.0000     -1.1852      as such for all 11 degrees of freedom
   15      1.1779      0.0000     -1.0045      as such for all 11 degrees of freedom
   16      1.2838      0.0000     -0.7503      as such for all 11 degrees of freedom
   17      1.4094      0.0000     -0.4701      as such for all 11 degrees of freedom
   18      1.5311      0.0000     -0.2264      as such for all 11 degrees of freedom
   19      1.6580      0.0000     -0.0576      as such for all 11 degrees of freedom
   20      1.7807      0.0000      0.0000      as such for all 11 degrees of freedom
   21      0.0000      0.0000      0.0000      as such for all 11 degrees of freedom
{NODAL DISPLACEMENTS}

<INTERNAL FORCES>  Load Inc # 17  Iteration #  8
      1   1  -198500.746885     -0.000022     as such for all 11 degrees of freedom
          2   198500.746885      0.000022     as such for all 11 degrees of freedom
      2   2  -198500.746885  -1634.615540     as such for all 11 degrees of freedom
          3   198500.746885   1634.615540     as such for all 11 degrees of freedom
      3   3  -198500.746885   4971.869106     as such for all 11 degrees of freedom
          4   198500.746885  -4971.869106     as such for all 11 degrees of freedom
      4   4  -198500.746885   3158.094864     as such for all 11 degrees of freedom
```

	5	198500.746885	-3158.094864	as such for all 11 degrees of freedom
5	5	-198500.746885	3779.244664	as such for all 11 degrees of freedom
	6	198500.746885	-3779.244664	as such for all 11 degrees of freedom
6	6	-198500.746885	3055.595990	as such for all 11 degrees of freedom
	7	198500.746885	-3055.595990	as such for all 11 degrees of freedom
7	7	-198500.746885	5128.779456	as such for all 11 degrees of freedom
	8	198500.746885	-5128.779456	as such for all 11 degrees of freedom
8	8	-198500.746885	7391.537523	as such for all 11 degrees of freedom
	9	198500.746885	-7391.537523	as such for all 11 degrees of freedom
9	9	-198500.746885	-4285.002083	as such for all 11 degrees of freedom
	10	198500.746885	4285.002083	as such for all 11 degrees of freedom
10	10	-198500.746885	-1636.863977	as such for all 11 degrees of freedom
	11	198500.746885	1636.863977	as such for all 11 degrees of freedom
11	11	-198500.746885	-520.294089	as such for all 11 degrees of freedom
	12	198500.746885	520.294089	as such for all 11 degrees of freedom
12	12	-198500.746885	-7430.361577	as such for all 11 degrees of freedom
	13	198500.746885	7430.361577	as such for all 11 degrees of freedom
13	13	-198500.746885	19487.390198	as such for all 11 degrees of freedom
	14	198500.746885	-19487.390198	as such for all 11 degrees of freedom
14	14	-198500.746885	8296.285821	as such for all 11 degrees of freedom
	15	198500.746885	-8296.285821	as such for all 11 degrees of freedom
15	15	-198500.746885	22208.851273	as such for all 11 degrees of freedom
	16	198500.746885	-22208.851273	as such for all 11 degrees of freedom
16	16	-198500.746885	12862.457253	as such for all 11 degrees of freedom
	17	198500.746885	-12862.457253	as such for all 11 degrees of freedom
17	17	-198500.746887	-2070.031164	as such for all 11 degrees of freedom
	18	198500.746887	2070.031164	as such for all 11 degrees of freedom
18	18	-198500.746885	4767.054815	as such for all 11 degrees of freedom
	19	198500.746885	-4767.054815	as such for all 11 degrees of freedom
19	19	-198499.420109	-8276.590857	as such for all 11 degrees of freedom
	20	198499.420109	8276.590857	as such for all 11 degrees of freedom
20	20	-101500.746885	-0.000068	as such for all 11 degrees of freedom
	21	101500.746885	0.000068	as such for all 11 degrees of freedom

{INTERNAL FORCES}

B Appendix B – SHOWGRID Graphical Interface

B.1 General Description

SHOWGRID is a computer program which reads a VULCAN input or output file and represents the data as a picture of the relevant structure on the computer screen. It is written in Visual Basic for use on a PC running Windows95/98 or NT. This allows instant identification of many types of error within the data file, which would be difficult to spot by reading the files as text.

A number of tools are available within SHOWGRID to change the view of the structure and identify certain elements and properties. In this way, discrepancies between the intended model and the structure represented by the data file can easily be discovered.

In addition, SHOWGRID can display the displacement results from a VULCAN analysis. This can be extremely useful in understanding the behaviour of the structure in fire, and allows the results to be instantly appreciated by someone unfamiliar with the intricacies of finite element analysis.

B.1.1 Graphical Conventions

Fig. 145 shows a typical screenshot from SHOWGRID. In this case, the represented structure is one quarter of a typical floor of the Cardington LBTF, in which one beam has been heated to simulate the restrained beam test. Each type of element is shown in a different colour to distinguish, for example, between heated and cold slab elements. The colour convention used is shown in Table 18.

The window title shows the file name of the current model and the text from the <HEADER> block of the data file, as described in Appendix A. This indicates the benefits of including a sensible description in the input file.

The arrow buttons in the top right-hand corner of the screen allow the view of the structure to be rotated about the current axis, indicated on the menu bar. Otherwise, the majority of the commands are available through selection of the relevant menu option. These commands are described in the following section.

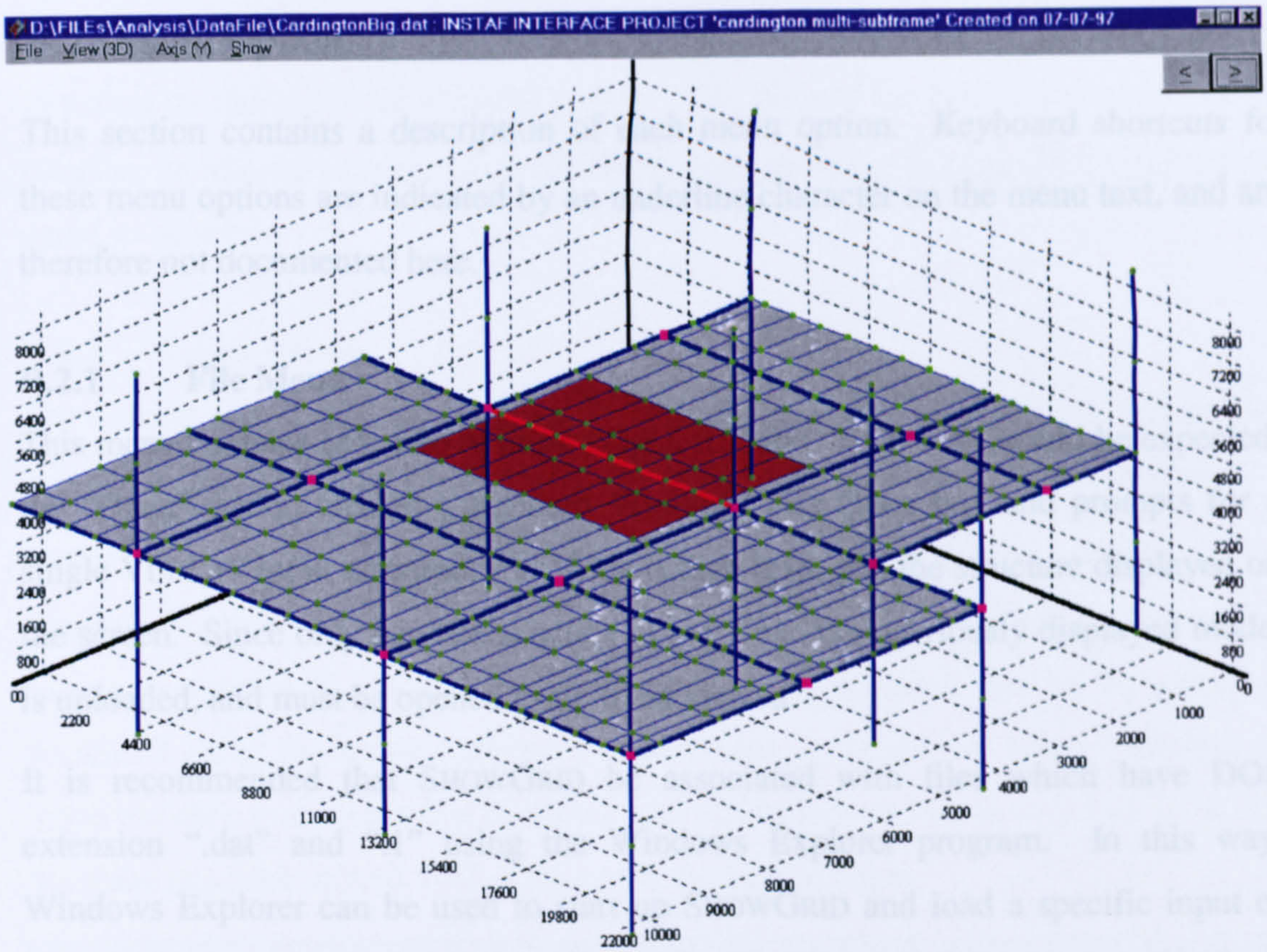

Fig. 145 Example screenshot

Colour	*Element Type*
Green	Loaded Node
Dark-Green	Unloaded Node
Blue	Cold Beam / Column
Red	Hot Beam / Column
Pink	Spring
Grey	Cold Slab
Brown	Hot Slab
Cyan	Cut-away Plane
Yellow	Highlighted Property

Table 18 Colour convention

B.2 Menu Options

This section contains a description of each menu option. Keyboard shortcuts for these menu options are indicated by an underline character on the menu text, and are therefore not documented here.

B.2.1 File Menu

This menu contains only two options, "Open ..." and "Exit". As would be expected, the "Open" option created a standard Windows File Open box and prompts for a single VULCAN input or output file. This is then read, and the structure displayed on the screen. Since only one file is active at any time, the previously displayed model is unloaded, and must be opened again to be viewed.

It is recommended that SHOWGRID be associated with files which have DOS extension ".dat" and ".1" using the Windows Explorer program. In this way, Windows Explorer can be used to start up SHOWGRID and load a specific input or output file in a single action. This renders the File-Open option redundant; however the facility has been retained in order to save time when viewing a number of files sequentially.

The "Exit" option closes the SHOWGRID program and returns control of the mouse and keyboard to the previously active program. Pressing the "Escape" key also closes the program, except when an animation is being displayed, as described in section B.2.5.

B.2.2 View Menu

As the name suggests, this menu is used to change the type of view presented on the screen. The user chooses one of three views; a "3D" view, a "2D" view or a 2D "Cut" view. This "Cut" view displays a section through a 3D structure, allowing elevations of internal beam gridlines to be shown.

In addition to choosing one of the three view types, this menu allows the user to print the contents of the screen, or to copy it to the clipboard as a bitmap image. The clipboard can then be pasted into other windows applications, such as a word processor, for inclusion in reports.

There is also the option to "Keep Aspect Ratio", which would display a square structure on the screen as a square picture. The default for this option is off, so the structure is normally stretched to fill the screen, allowing the maximum amount of detail to be seen.

B.2.3 Axis Menu

The current axis can be set as X, Y or Z using this menu. In 3D view, the current axis is the one about which the structure is rotated when the arrow buttons are used. In Cut view, the structure is displayed as a 3D picture, and a plane is overlaid. If, for example, the current axis is chosen to be the Z-axis, the plane will be defined as having a constant Z value. The constant value in question can be increased or decreased using the arrow buttons, the increment or decrement being sufficient to move the slice to the next line of nodes. An example is shown in Fig. 146, in which the plane has been moved until it lies along the heated beam.

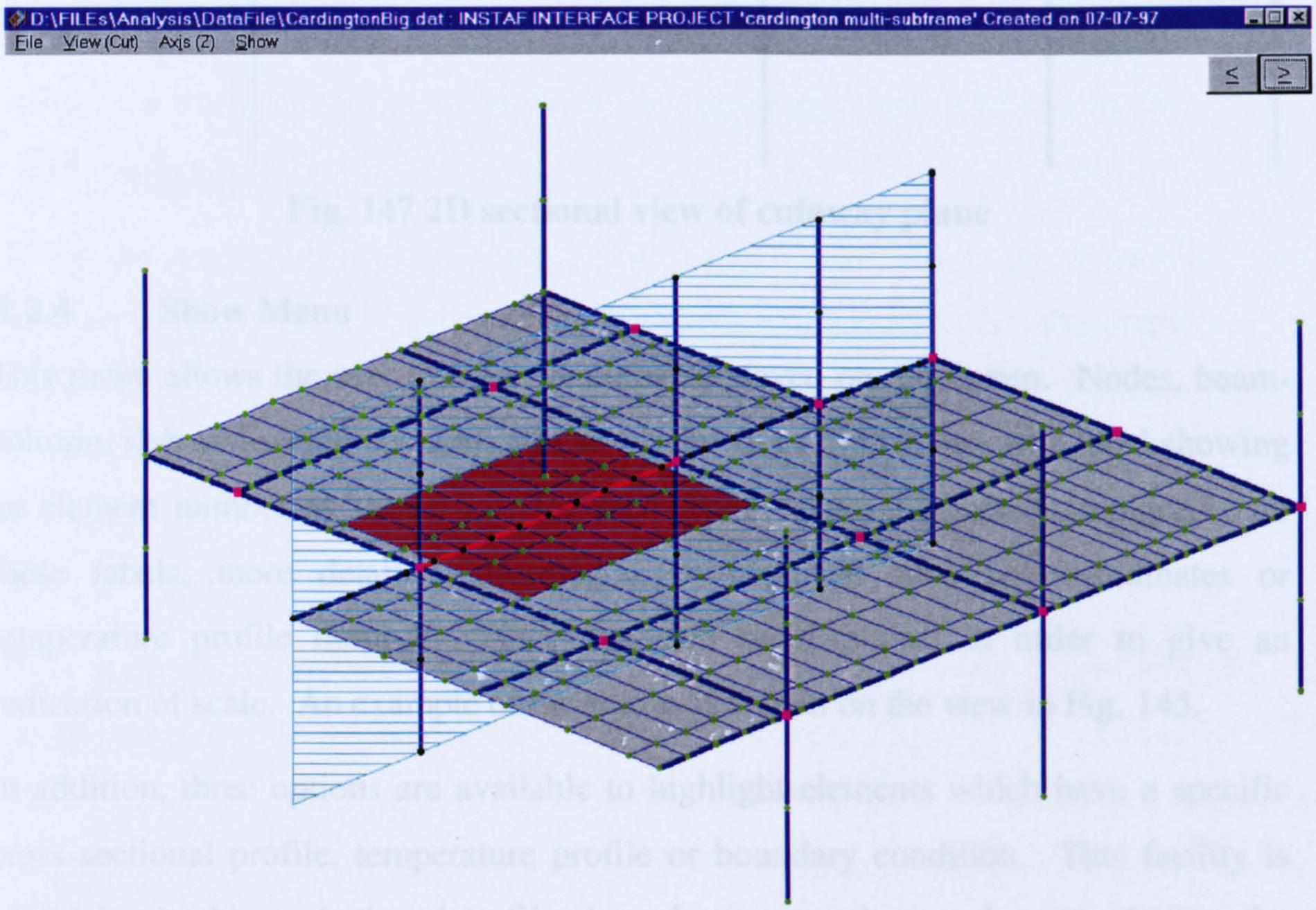

Fig. 146 Cutaway plane

If the view is then shifted into 2D mode, this cutaway plane is redrawn, with all out-of-plane elements ignored. The 2D view of the plane defined in Fig. 146 is shown in

Fig. 147. The window title in 2D view displays the global co-ordinates of the mouse pointer.

Fig. 147 2D sectional view of cutaway plane

B.2.4 Show Menu

This menu allows the user to select features displayed on the screen. Nodes, beam-column, slab and spring elements can all be shown or hidden, as can a label showing an element number as shown in , for each type. When the pointer is placed over these labels, more detailed information is displayed such as co-ordinates or temperature profile number. Axes can also be displayed in order to give an indication of scale. An example of these axes is shown on the view in Fig. 145.

In addition, three options are available to highlight elements which have a specific cross-sectional profile, temperature profile or boundary condition. This facility is useful in checking whether data files have been created properly and whether, for instance, all the nodes along a line of symmetry have been given correct and consistent boundary conditions.

B.2.5 Animate Menu

This menu is only visible for new-format data files, since there is not enough information in the old-style files to deduce structure and displacement details. The menu is not selectable if the current data file is an input file, since obviously no displacement information is available in an input file.

The first menu option initiates an animation of the structure according to the calculated displacement results. There is also the option to step through the animation frame by frame, allowing any particular screen-shot to be extracted using the "Copy" or "Print" options.

Animation can be time consuming, especially with very large structures or with many temperature steps. Therefore, the Escape key can be pressed at any time to stop the animation. In this case, just the animation, and not the program is terminated. There is also an option to begin the animation at a particular temperature. This can skip through low temperature results where there may not be a noticeable displacement. This can be particularly useful when test data has been used to form the basis of an analysis, and contains many readings as the furnace slowly begins to heat up.

Since the calculated displacements are often small compared to the overall structure geometry, a scale factor can be defined from this menu, by which the displacements are multiplied before they are displayed. In the example shown in for example, the displacements have been magnified by 10 times in each direction.

B.3 Remarks For Future Development

This program is an extremely valuable tool in creating valid input files and in understanding the corresponding results. However, if its use is not taken into account when developing the format of VULCAN data files, it could rapidly become redundant. SHOWGRID has been written to embrace the practice of enclosing known formatted data in uniquely labelled blocks. Since it ignores data that is not inside a recognised block, it allows for the future expansion of the VULCAN program, without losing any functionality. Therefore, any newly developed element types, or output results, should be placed within a new data block, allowing SHOWGRID to continue to access the currently defined geometrical data and display it correctly. The

SHOWGRID code could then be updated at a later date, to take these new developments into account, and display the extra information accordingly.

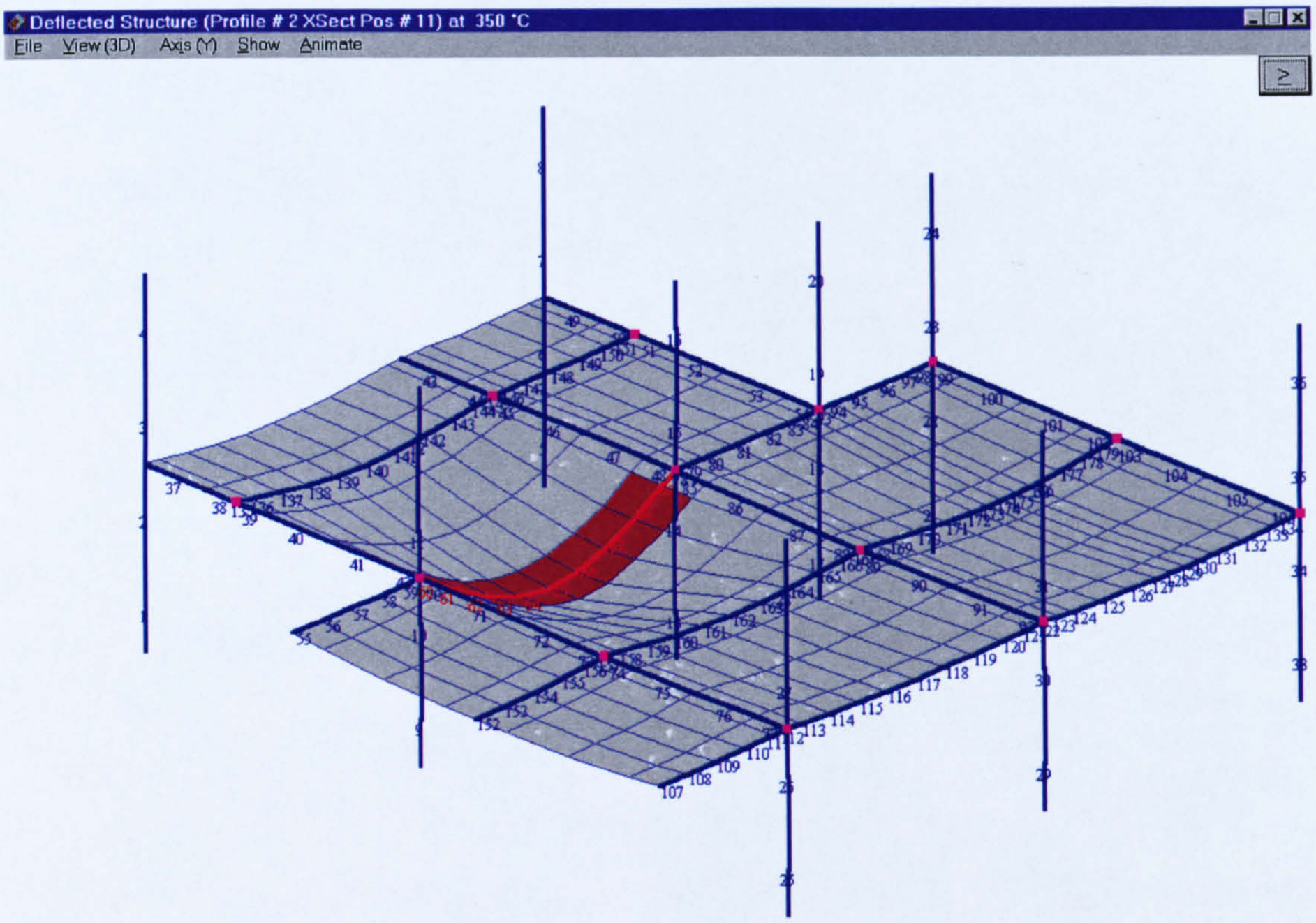

Fig. 148 Animated output file